UNIVERSIDAD AUTÓNOMA DE MADRID
DEPARTAMENTO DE BIOQUÍMICA

Tesis Doctoral

La colaboración entre los linfocitos T $CD8^+$ de memoria residente y circulante mejora la inmunidad antitumoral

Neris Michel Enamorado Escalona

Madrid, 2017

Departamento de Bioquímica

Facultad de Medicina

Universidad Autónoma de Madrid

Tesis Doctoral

La colaboración entre los linfocitos T $CD8^+$ de memoria residente y circulante mejora la inmunidad antitumoral

Memoria presentada por el Licenciado en Bioquímica:

Neris Michel Enamorado Escalona

Para optar al grado de Doctor en Bioquímica, Biología Molecular, Biomedicina y Biotecnología por la Universidad Autónoma de Madrid

Director de tesis: Dr. David Sancho Madrid

Este trabajo se ha realizado en el laboratorio de Inmunobiología de la Fundación-Centro Nacional de Investigaciones Cardiovasculares Carlos III.

El Doctor David Sancho Madrid, líder del grupo de investigación "Inmunobiología" de la Fundación-Centro Nacional de Investigaciones Cardiovasculares Carlos III (CNIC),

CERTIFICA

que **Neris Michel Enamorado Escalona**, Licenciado en Bioquímica por la Universidad de La Habana y Máster en Biomedicina Molecular por la Universidad Autónoma de Madrid, ha realizado bajo su supervisión el trabajo de Tesis Doctoral: **La colaboración entre los linfocitos T CD8$^+$ de memoria residente y circulante mejora la inmunidad antitumoral.**

Para la realización de esta Tesis Doctoral se contó con la financiación de: Contratos para investigadores predoctorales Fundación La Caixa-Severo Ochoa (OSLC-CNIC-2013-04), los proyectos de investigación de la Unión Europea (635122 PROCROP H2020), del Consejo Europeo de Investigación (ERC-2010-StG 260414), de la Fundación ACTERIA y del Ministerio de Economía y Competitividad (SAF2010-15120, SAF2013-42920R y SAF2016-79040-R).

Revisado el presente trabajo, expresa su conformidad para la presentación del mismo en el Departamento de Bioquímica de la Universidad Autónoma de Madrid, por considerar que reúne los requisitos necesarios para ser sometido a su evaluación ante el tribunal correspondiente para optar al grado de **Doctor en Bioquímica, Biología Molecular, Biomedicina y Biotecnología por la Universidad Autónoma de Madrid.**

David Sancho
Director de tesis

A mi hija Laura

Resumen

1. Resumen

La vacunación antitumoral se realiza con el objetivo de desencadenar una protección por el sistema inmunitario que impida las recaídas y la metástasis. La infiltración de tumores humanos con linfocitos T $CD8^+$, que expresan marcadores fenotípicos asociados a la memoria residente (Trm) correlaciona con el aumento de la supervivencia. Sin embargo, la interrelación de los linfocitos T $CD8^+$ de memoria residente y circulante en la inmunología tumoral no se ha explorado previamente.

En el presente estudio analizamos la contribución a la inmunidad antitumoral de las subpoblaciones de linfocitos T $CD8^+$ de memoria residente y circulante, generadas mediante diferentes vías de inmunización con el virus vaccinia. Mientras que las dos poblaciones de memoria, por sí solas, fueron suficientes para retrasar el crecimiento del tumor, la Trm aumentó la inmunidad antitumoral en presencia de la memoria circulante. La transferencia adoptiva de memoria central (Tcm) generó respuesta Trm en procesos de infección viral o tras la inoculación de un tumor. Asimismo, la combinación de la transferencia adoptiva de Tcm con la administración del anticuerpo anti-PD-1 aumentó la infiltración de linfocitos T en el tumor, que expresaron marcadores fenotípicos asociados a la Trm, y redujo en el crecimiento tumoral. Además, la reactivación de linfocitos Tcm contra el tumor dependió de células dendríticas que requieren la expresión del factor de transcripción Batf3.

Nuestros resultados muestran la plasticidad y colaboración entre linfocitos Tcm y Trm, así como los requerimientos para la reactivación de linfocitos Tcm en un contexto antitumoral. Este conjunto de observaciones contribuye a mejorar las estrategias de vacunación antitumoral y la inmunoterapia.

Abstract

2. Abstract

The goal of successful antitumoral immunity is the development of long term protective immunity to prevent relapse. Infiltration of tumors by $CD8^+$ T cells with a resident memory (Trm) phenotype correlates with improved survival. However, the interplay of circulating $CD8^+$ T cells and Trm cells remains poorly explored in tumor immunity.

Using different vaccination strategies that fine-tune the generation of Trm cells or circulating memory T cells, here we show that, while both subsets are sufficient for anti-tumor immunity, the presence of Trm cells improves anti-tumor efficacy. Transferred central memory T cells (Tcm) generate Trm cells following viral infection or tumor challenge. Anti-PD-1 treatment promotes infiltration of transferred Tcm cells within tumors, improving anti-tumor immunity. Moreover, Batf3-dependent dendritic cells are essential for reactivation of circulating memory anti-tumor response. Our findings show the plasticity, collaboration and requirements for reactivation of memory $CD8^+$ T cells subsets needed for optimal tumor vaccination and immunotherapy.

Índice

3. Índice

Abreviaturas

4. Abreviaturas

Abreviatura	Español	English
ACT	transferencia adoptiva	*adoptive cell transfer*
APC	células presentadoras de antígeno	*antigen presenting cells*
B16-OVA	línea tumoral de melanoma de ratón que expresa ovoalbúmina	
Batf3	factor de transcripción 3 tipo ATF con dominio de cremallera de leucina	*basic leucine zipper ATF-like transcription factor 3*
Bcl-2	linfoma 2 de las células B	*B-cell lymphoma 2*
BDCA-3	CD141, antígeno 3 de las células dendríticas de sangre	*blood DC antigen 3*
BLIMP1	proteína 1 con dedos de zinc que contiene dominios PR	*PR domain zinc finger protein 1*
BRAF	Oncogen B-Raf con actividad serina-treonina quinasa	*B-Raf proto-oncogene, serine/threonine kinase*
CAR	células con receptor de antígenos quimérico	*chimeric antigen receptor*
CCR	receptor de quimiocinas	*C-C chemokine receptor*
CD	cúmulo de diferenciación	*cluster of differentiation*
CDP	progenitor común de células dendríticas	*common* dendritic cell *progenitors*
CDR3	región determinante de la complementariedad	*complementarity-determining regions*
CLA	antígenos asociados a los linfocitos cutáneos	*cutaneous lymphocyte-associated antigen*
CLEC9A		*C-type lectin domain family 9, member A*
CSF-1	factor 1 estimulador de colonias	*colony-stimulating factor-1*
CTL	linfocito T citotóxico	*citotoxic T lymphocyte*
CTLA-4	antígeno 4 de los linfocitos T citotóxicos	*cytotoxic T-lymphocyte antigen 4*
CXCR	receptores de quimiocinas tipo C-X-C	*C-X-C chemokine receptor*
CXCL	ligando de la familia de quimiocinas C-X-C	chemokine (C-X-C motif) ligand
d.p.i	días post-infección	*days post-infection*
DC	células dendríticas	*dendritic cells*
DNFB	1-flúor-2,4-dinitrobenzeno	1-Fluoro-2,4-dinitrobenzene
DNGR-1	Proteína codificada por el gen *Clec9a*	*DC NK group receptor type-1*
dLN	ganglio linfático drenante	*draining lymph node*
EDTA	ácido etilendiaminotetracético	*ethylenediaminetetraacetic acid*
Eomes	Eomesodermina	*eomesodermin*
FACS	citometría de flujo	*fluorescence-activated cell sorting*
FBS	suero fetal bovino	*fetal bovine serum*

Abreviatura	Español	English
FLT3-L	ligando 3 de la tirosina quinasa tipo Fsm	*Fms-like tyrosine kinase 3 ligand*
FMO	fluorescencia menos una	*fluorescence minus one*
FSC-A	Tamaño	*forward scatter-area*
FTY720		*2-Amino-2-[2- (4-octyl-phenyl)-ethyl]-propane-1,3-diol hydrochloride*
GMFI	media geométrica de la intensidad de la fluorescencia	*geometric mean of fluorescence intensity*
GMCSF	factor estimulador de colonias de monocitos y macrófagos	*granulocyte-macrophage colony-stimulating factor*
HEV	venas endoteliales altas	*high endothelial venules*
HIV	virus de la inmunodeficiencia humana	*human immunodeficiency virus*
HSV	virus del herpes simple	*herpes simple virus*
i.d.	intradérmico	*intradermal*
i.n.	intranasal	*intranasal*
i.p.	intraperitoneal	*intraperitoneal*
i.v.	intravenoso	*intravenous*
ICAM-1	molécula 1 de adhesión intercelular	*intercellular adhesion molecule 1*
ID2	proteína inhibidora de la unión al DNA	*DNA-binding protein inhibitor*
IFITM-3	proteína 3 de transmembrana inducida por interferón	*interferon-induced transmembrane protein 3*
IL	interleuquina	*interleukin*
Irf8	factor 8 de regulación del interferón	*interferon regulatory factor 8*
Klf2	factor 2 tipo *Kruppel*	*Kruppel-like factor 2*
LAG-3	gen 3 de activación de linfocitos	*lymphocyte-activation gene 3*
LN	ganglio linfático	*lymph node*
LCMV	virus de la coriomeningitis linfocítica	*lymphocytic choriomeningitis virus*
MC38-OVA	línea tumoral de adenocarcinoma de colon que expresa ovoalbúmina	
MCMV	virus del moteado clorótico del maíz	*Maize chlorotic mottle virus*
MHC	complejo mayor de histocompatibilidad	*major histocompatibility complex*
mTOR	diana de mamíferos para rapamicina	*mammaliam target for rapamycin*
Nfil3	factor nuclear regulado por IL-3	*nuclear factor, interleukin 3 regulated*
NK	células asesinas naturales	*natural killer*
Notch2		*neurogenic locus notch homolog protein 2*
NS	no significativo	*no significant*
OT-I	Células T $CD8^+$ específicas para el péptido 257-264 de la ovoalbúmina restringidas al MHC-I	

Abreviatura	Español	English
OVA	ovoalbúmina	*ovalbumin*
p.f.u	partículas virales formadoras de placas	*plaque-forming units*
PBS	solución tampón salina de fosfato	*phosphate buffered saline*
PD-1	proteína 1 de la programación de la muerte	*programmed cell death protein 1*
PDL-1	ligando de PD-1	*programmed cell death protein 1 ligand*
Post	posterior a	*post*
rVACV-OVA	virus vaccinia que expresa ovoalbúmina	*recombinant vaccinia virus-ovalbumin*
s.c.	subcutáneo	*subcutaneous*
s.e.m.	error estándar de la media	*standard error of the mean*
s.s.	escarificación en la piel	*skin scarification*
S1P	esfingosina-1 fosfato	*sphingosine-1 phosphate*
S1P1	receptor de S1P	*sphingosine-1-phosphate receptor 1*
Sca-1	antígeno 1 de células madre	*stem cells antigen-1*
SHP-1	Fosfatasa 1 que contiene el dominio de la región de homología 2 de Src	*Src homology region 2 domain-containing phosphatase-1*
SMAD4	Proteína homóloga de la proteína de mosca MAD y de la proteína SMA de *Caenorhabditis elegans*	
SSC-A	complejidad	*size scatter-area*
T-bet	factor de transcripción asociado a linfocitos T	*T-box transcription factor*
TCR	receptor de células T	*T cell receptor*
Tcm	memoria T central	*T central memory*
TdLN	nódulo linfático drenante del tumor	*tumor draining lymph node*
Tem	memoria T efectora	*T efector memory*
TGF-β	factor *β* de transformación y crecimiento	*transforming growth factor-β*
Th17	linfocitos T colaboradores tipo 17	*T-helper 17*
TIL	linfocitos que infiltran el tumor	*tumor-infiltrating lymphocytes*
TLR	receptores tipo Toll	*Toll-like receptor*
TNF-α	factor de necrosis tumoral	*tumor necrosis factor*
Trm	memoria T residente de tejido	*tissue T resident memory*
Tscm	células madre de memoria T	*T stem cell-like memory*
VCAM-1	molécula de adhesión a las células vasculares	*vascular cell adhesión molecule 1*
VSV	virus de la estomatitis vesicular	*vesicular stomatitis virus*
WT	Tipo silvestre	*wild type*

Introducción

5. Introducción

5.1 Sistema inmunitario y microambiente tumoral

Los **tumores** son agrupaciones de varios tipos celulares: las células tumorales que le dan origen, fibroblastos, células endoteliales y una gran variedad de células del sistema inmunitario. Inicialmente, la infiltración del tumor con células del sistema inmunitario es pobre. Sin embargo, a medida que el tumor progresa hay una mayor infiltración de células NK (del inglés, *natural killer*), macrófagos, células dendríticas (DC del inglés, *dendritic cells*), células mieloides supresoras y linfocitos T reguladores. También hay que destacar a los linfocitos T efectores, por su papel en la terapia antitumoral (Fox *et al*. 2011).

La cirugía y la quimioterapia son métodos clásicos para tratar a los pacientes con cáncer, aunque no totalmente resolutivos. Las células tumorales tienen una gran inestabilidad genética y epigenética. Por esta razón, los tratamientos farmacológicos se encuentran con mecanismos de resistencia que inhabilitan su efecto. Además, la cirugía está limitada a la extracción de tumores primarios en estadios tempranos (Sharma *et al.* 2015a).

Los estudios recientes colocan el tratamiento con **linfocitos T** como una estrategia terapéutica con suficiente diversidad y capacidad de adaptación para eliminar tumores (Rosenberg *et al.* 2015; Sharma *et al.* 2015a). Estas células expresan receptores de antígenos generados al azar por recombinación genética. El gran repertorio de clones de linfocitos T probablemente es suficiente para cubrir no solo a los antígenos tumorales clásicos, sino también a los nuevos antígenos tumorales que resultan de la inestabilidad del genoma. Aparte de su especificidad, la generación de células T de memoria constituye otra ventaja respecto al resto de terapias antitumorales. La **memoria T** se caracteriza por una larga supervivencia y una mayor capacidad efectora ante el reencuentro con el antígeno (Kaech *et al.* 2012; Youngblood *et al.* 2015). Esto aumentaría la eficiencia de una vacunación antitumoral basada en la generación de memoria T, con muchas posibilidades para evitar metástasis.

Para que los linfocitos T, tanto *naive* como de memoria, monten una respuesta inmunitaria correcta, deben encontrar los antígenos en el contexto de **células presentadoras** (APC del inglés, *antigen presenting cells*) como las DC. Las DC proveen el resto de señales coestimulatorias (Satpathy *et al.* 2012; Pfirschke *et al.* 2017). Después

del encuentro con las **APC**, probablemente en el TdLN (del inglés, *tumor draining lymph node*), los linfocitos T *naive* adquieren, y los de memoria restablecen, sus funciones citotóxicas. Ambos tipos celulares migran hacia el tumor para generar una respuesta efectora (Pfirschke *et al.* 2017). Cuando los linfocitos T están dentro del tumor, el éxito de "la batalla" depende de su capacidad para superar el gran número de barreras reguladoras. Dentro de estas barreras se destacan la expresión de moléculas de inhibición, las citoquinas inhibidoras, las células mieloides supresoras, las células T reguladoras y otros mecanismos que mitigan la respuesta inmunitaria en el ambiente tumoral (Sharma *et al.* 2015b).

5.2 Memoria T

El estudio de los **linfocitos T CD8$^+$ de memoria** ha revelado el extraordinario potencial de diversificación de la inmunidad adaptativa. Cuando los linfocitos T CD8$^+$ *naive* encuentran a su antígeno, cognado presentado en el contexto del complejo mayor de histocompatibilidad de clase I (MHC-I, del inglés, *major histocompatibility complex class I*) junto a las señales de coestimulación y las citoquinas apropiadas se inicia un programa de proliferación y diferenciación (Kaech *et al.* 2012; Böttcher *et al.* 2015). Se producen cambios en las moléculas de adhesión y en la expresión de receptores de quimiocinas en la superficie de los linfocitos T, que les permiten salir de los órganos linfoides secundarios (Kaech *et al.* 2012). Después de varios días de expansión, la población específica por el patógeno se reduce en número, lo que se conoce como fase de **contracción de la memoria**. Aproximadamente el 90% de los linfocitos muere por apoptosis, mientras que el 10% que sobrevive; lo hace largos períodos de tiempo y en algunos casos para toda la vida (Mueller *et al.* 2013). Si el proceso de infección se elimina, estas células se convierten en linfocitos de memoria con función protectora (**Figura I1**).

La memoria T se caracteriza por tener una vida larga, alta capacidad proliferativa y readquiere su función efectora después del reencuentro con el antígeno (Chang *et al.* 2014). La población de memoria T CD8$^+$ se mantiene mediante la renovación homeostática dependiente de la interleuquina 15 (IL-15) (Surh *et al.* 2006).

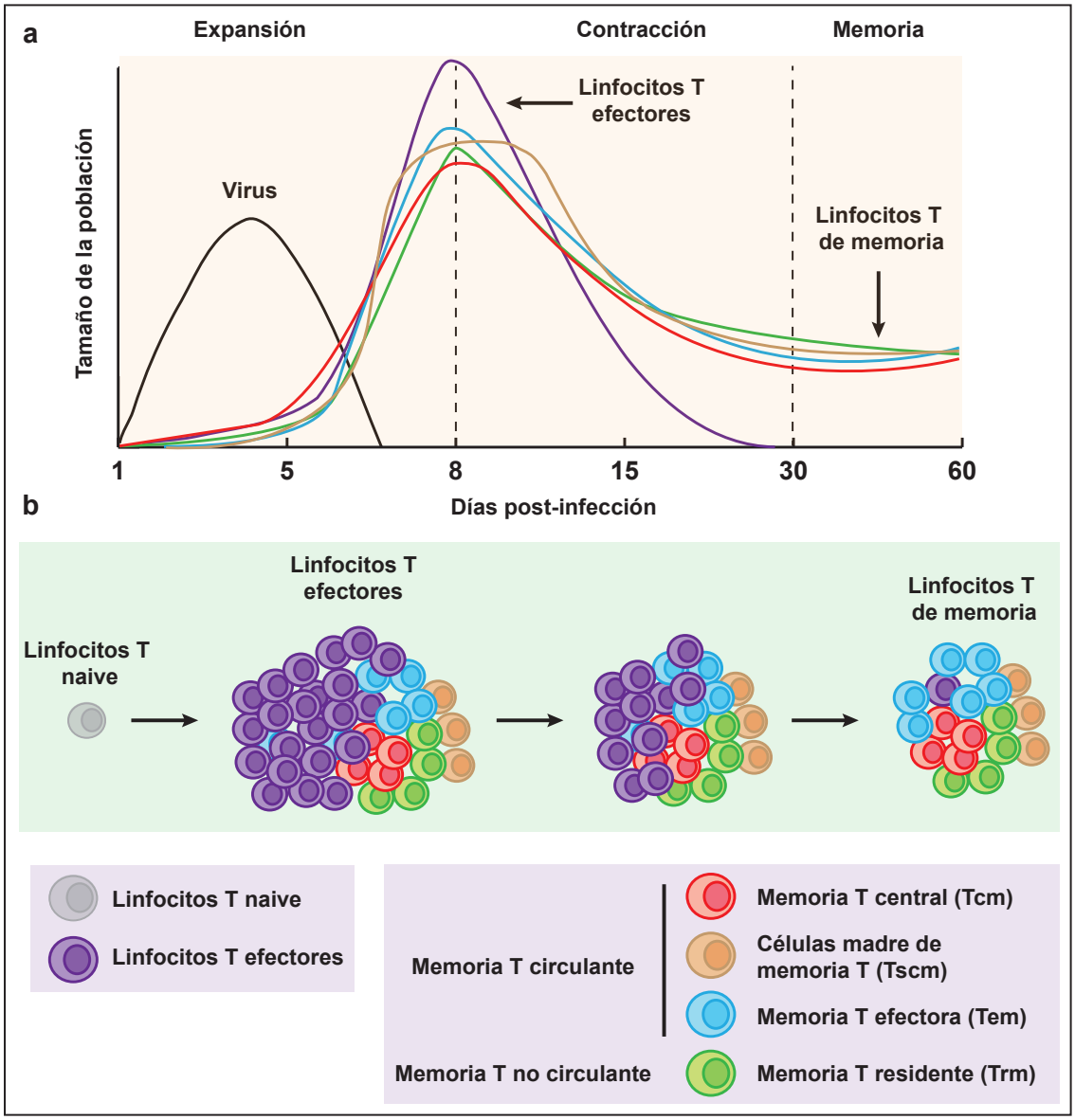

Figura I1. Cinética de la respuesta T CD8$^+$ tras una infección viral
(**a**) Durante una infección viral aguda los linfocitos T específicos por el antígeno proliferan rápidamente (fase de expansión) y se diferencian en linfocitos T citotóxicos que median la eliminación del virus. La mayoría de estas células muere en las próximas semanas durante la fase de contracción de la respuesta. Solamente un número muy bajo de linfocitos T efectores (5–10%) sobrevive y se convierte en memoria T CD8$^+$ funcional y madura. (**b**) El conjunto de linfocitos T efectores se puede clasificar en distintas subpoblaciones en dependencia de la expresión génica y las proteínas de superficie, las funciones efectoras, los patrones de migración y la capacidad de proliferación. Por ejemplo, la memoria T circulante, que incluye la memoria T central (Tcm, del inglés *T central memory*), la memoria T efectora (Tem, del inglés *T effector memory*) y las células madre de la memoria T (Tscm, del inglés *T stem cell-like memory*) y la memoria T no circulante, que incluye la memoria T residente de tejido (Trm, del inglés, *Tissue resident memory*).

La heterogeneidad de los linfocitos T CD8$^+$ de memoria en la expresión de receptores de superficie, la función efectora, la localización y las propiedades de migración, han llevado a su clasificación en dos grandes poblaciones (Tabla 1) (Sallusto *et al.* 1999; Hamann *et al.* 1997): la **memoria circulante**, compuesta por la memoria central (Tcm del inglés, *T central memory*), las células madre de la memoria (Tscm del

inglés, *T stem cell-like memory*) (Lugli *et al.* 2013; Klebanoff *et al.* 2016) y la memoria efectora (Tem del inglés, *T efector memory*), y la **memoria residente** (Trm del inglés, *tissue resident memory*) (Chang *et al.* 2014).

Tabla 1. Poblaciones de linfocitos T CD8$^+$ de memoria

Población	Marcadores fenotípicos	Localización
Tcm	CD44^{hi}, CD62L$^+$, CCR7$^+$, CD127$^+$, CD69$^-$, CD103$^-$	Ganglios linfáticos, bazo, sangre y médula ósea
Tem	CD44^{hi}, CD62L$^-$, CCR7$^-$, CD127$^+$, CD69$^-$, CD103$^-$	Bazo, ganglios linfáticos, sangre, pulmones, hígado, tracto intestinal, tracto reproductivo, riñones, tejido adiposo y corazón
Tscm	CD44^{lo}, CD62L$^+$, CD122$^+$, Sca-1$^+$	Ganglios linfáticos y bazo
Trm	CD44^{hi}, CD62L$^-$, CCR7$^-$, CD69$^+$, CD103$^+$	Epitelio de la piel, intestinos, vagina, glándulas salivales, pulmones, cerebro y ganglios linfáticos

Tcm, memoria T central; Tem, memoria T efectora; Tscm, células madre de memoria T; Trm, memoria residente de tejido

5.2.1 Memoria T circulante

La primera descripción funcional de los **subtipos de memoria T circulante** proviene de Sallusto y colaboradores (Sallusto *et al.* 1999), cuando dividieron los linfocitos de memoria en subpoblaciones con distintas características fenotípicas. A partir de varios estudios en ratones (Masopust *et al.* 2001) se adoptó un modelo en el que la memoria T CD8$^+$ circulante se divide en dos subpoblaciones: Tcm y Tem (Tabla 1). En la **Tem** la disminución de la expresión de las moléculas de retención CD62L y CCR7 limita su habilidad para residir en los ganglios linfáticos (LN del inglés, *lymph node*), permitiéndole circular y establecerse en los tejidos periféricos. Además, preserva la función efectora para responder rápidamente ante un estímulo. Por el contrario, la Tcm expresa **CD62L** y **CCR7**, restringiendo su ubicación anatómica a los tejidos linfáticos. En los órganos linfoides secundarios la Tcm tienen mayor potencial proliferativo que la Tem, sin embargo, las células Tem tienen mayor potencial efector (Masopust *et al.* 2001; Klebanoff *et al.* 2016).

Las células T de memoria circulante migran constantemente por todo el cuerpo. Algunos experimentos pioneros siguieron el recorrido de los linfocitos T desde la sangre hacia los órganos linfáticos mediante las **venas endoteliales altas** (HEV del inglés, *high endothelial venules*) especializadas y de ahí a los vasos linfáticos eferentes. Los linfocitos T también pueden entran al LN mediante los vasos linfáticos aferentes (Carbone *et al.* 2015). La memoria circulante llega a los LN donde permanece por aproximadamente 6-18 horas escaneando antígenos antes de retornar a la circulación mediante la linfa (Tomura *et al.* 2008; Grigorova *et al.* 2010). Este **patrón de migración** se ve alterado por la exposición a antígenos, que aumentan la entrada y retienen las células T en los LN (Hall *et al.* 1965).

Los estudios sobre los cambios en el fenotipo y la función de la memoria T en reposo donde se utilizan varias rondas de estimulación con una infección aguda, han contribuido a la comprensión de su regulación genética (Joshi *et al.* 2011; Nolz *et al.* 2011). Mediante el uso de una estrategia de ***prime-boost*** Masopust y colaboradores demostraron que en comparación con la respuesta primaria de la memoria T $CD8^+$, la respuesta secundaria y terciaria se enriquece en cualidades efectoras y se localiza principalmente en los tejidos no linfáticos (Masopust *et al.* 2006a). La exposición reiterada al antígeno enriquece progresivamente la memoria efectora, con células que tienen una menor expresión de **CD62L** y CD127 y una mayor expresión de granzima B (Masopust *et al.* 2006a). Desde el punto de vista genético, con cada estimulación adicional se modifica un programa de genes en las poblaciones de memoria T $CD8^+$ (Wirth *et al.* 2010). Si se compara con células de memoria primaria, en la memoria secundaria y terciaria aumentan los niveles de mRNA (del inglés, *messenger ribonucleic acid*) que codifican para granzima B, CCR5, IL-2Rα, T-bet (del inglés, *T-box transcription factor*), BLIMP1 (del inglés, *PR domain zinc finger protein 1*) e ID2 (del inglés, *DNA-binding protein inhibitor 2*), y disminuyen los niveles de mRNA que codifican para **CCR7**, CD62L, TCF1, ID3 y MYC (Wirth *et al.* 2010). Los estudios de *prime-boost* sugieren que la cantidad de células T de memoria se puede aumentar, lo cual tiene una gran implicación para la generación de nuevas vacunas (Youngblood *et al.* 2015). Teniendo en cuenta que las diferencias fenotípicas utilizadas para clasificar las diferentes poblaciones se modifican progresivamente con nuevas reestimulaciones, se genera la pregunta de si las subpoblaciones están comprometidas a su respectivo estadio tras la estimulación inicial o retienen cierto nivel de plasticidad transcripcional

(Youngblood *et al.* 2015).

5.2.1.1 Células madre de memoria T o Tscm

Recientemente se ha identificado una nueva subpoblación de memoria T. Este subtipo celular con propiedades y características fenotípicas de un linfocito *naive*, expresa un programa de genes muy parecido, pero posee la habilidad de proliferar homeostáticamente en presencia de IL-7 e IL-15 (Tabla 1). Se conocen como las **células madre de memoria T**, debido a que poseen muchas características de las células madre. Además, tienen el potencial de producir diferentes subpoblaciones de memoria T con una eficiente respuesta efectora (Gattinoni *et al.* 2011; Lugli *et al.* 2013).

El **modelo de células madre inmunológicas** se apoya, en parte, en la existencia de células madre de memoria T. Este modelo propone que una célula de memoria que se reencuentre con el antígeno es capaz de dividirse y generar dos grupos celulares, uno con una diferenciación terminal y otro con habilidad para autorenovarse (Fearon *et al.* 2001). En un modelo de transferencia adoptiva de una única célula Tcm se demostró la habilidad de autorenovación y multipotencia, a través de transferencias adoptivas en serie y varias rondas de infección (Graef *et al.* 2014). La población de linfocitos humanos Tcm y Tem con alta expresión de IL-18R y el receptor de NK CD161 se parece a las células madre hematopoyéticas, ya que sobrevive a las exposiciones con drogas durante la quimioterapia (Turtle *et al.* 2009). Otra población distinta de células T $CD8^+$ que expresa $CD44^{lo}$, $CD62L^{hi}$ y altos niveles de Sca-1 (del inglés, *stem cells antigen-1*), CD122 y Bcl-2 (del inglés, *B-cell lymphoma 2*) (Gattinoni *et al.* 2009)' (Zhang *et al.* 2005), tiene una capacidad proliferativa y funciones superiores al resto de Tcm en experimentos de cáncer e injerto contra huésped.

5.2.2 Transferencia adoptiva de linfocitos T

La **transferencia adoptiva** (ACT del inglés, *adoptive cell transfer*) consiste en la expansión *ex vivo* y la reinfusión de linfocitos T (antígeno específico) a los pacientes. La ACT es un método potencialmente curativo para el tratamiento de pacientes con cáncer (Sadelain *et al.* 2009; Jensen *et al.* 2014; Maus *et al.* 2014; Rosenberg *et al.* 2015) y síndromes de reactivación viral (Bollard *et al.* 2012; Leen *et al.* 2014; Maus *et al.* 2014). La habilidad de modificar genéticamente linfocitos T de sangre periférica de pacientes y redirigirlos contra el tumor y los antígenos asociados a los virus, mediante la

modificación del TCR (del inglés, *T cell receptor*) o la utilización de la tecnología CAR (del inglés, *chimeric antigen receptor*) ha simplificado mucho la generación de células T para la ACT (June *et al.* 2009; Jena *et al.* 2010; Kershaw *et al.* 2013; Dotti *et al.* 2014).

En varios modelos preclínicos las **poblaciones mínimamente diferenciadas** como las células T *naive,* la Tscm, y la Tcm tienen mayor supervivencia (Klebanoff *et al.* 2005; Gattinoni *et al.* 2009, 2011; Wang *et al.* 2011; Cieri *et al.* 2013; Graef *et al.* 2014), actividad antitumoral (Klebanoff *et al.* 2005; Gattinoni *et al.* 2009, 2011), actividad antibacteriana (Graef *et al.* 2014) y actividad antiviral después de una ACT; si se compara con la Tem y las células T efectoras. A pesar de estos datos, la mayoría de las terapias con linfocitos T no utiliza una población definida de células T. Por el contrario, utilizan poblaciones de células T sin fraccionar (Jensen *et al.* 2014). Las células T derivadas de la transferencia de linfocitos T de memoria efectora modifican directamente a las células T *naive*, formando grupos de interacción durante la estimulación. Este proceso se llama diferenciación precoz (Klebanoff *et al.* 2016), y sincroniza el desarrollo de células T *naive* con el de células Tem. Como resultado, aumenta el proceso de diferenciación funcional, transcripcional y metabólico, que disminuye la actividad antitumoral de las células T (Klebanoff *et al.* 2016).

5.2.3 Memoria T residente

La **Trm** se describió por primera vez en el año 2001 (Masopust *et al.* 2001). Posteriormente, el mismo grupo de investigación demostró que la Trm del intestino no recircula en el bazo ni en los LN de ratones parabiontes, como lo hace el resto de células T (Klonowski *et al.* 2004). En condiciones fisiológicas la Trm se encuentra en las barreras protectoras como el tracto gastrointestinal, el tracto respiratorio, el aparato reproductivo y la piel. También se han encontrado en el cerebro, los riñones, las articulaciones y otros tejidos que no son barreras biológicas (Tabla 1). La Trm que aparece en los tejidos que no son barreras tiene un programa transcripcional similar a la de los tejidos que constituyen las barreras (Wakim *et al.* 2012).

5.2.3.1 Generación de Trm

Los linfocitos *naive* recirculan entre la sangre y los LN, donde permanecen entre 12 y 24 horas antes de retornar a la sangre y migrar hacia otro LN (von Andrian *et al.* 2003). La **localización anatómica de los LN** influye en el tipo de moléculas de

residencia que expresan los linfocitos *naive,* cuando se activan en un determinado microambiente (Liu *et al.* 2006; Sallusto *et al.* 2009). Los linfocitos vírgenes que se activan en los dLN (del inglés, *draining lymph node*) de la piel expresan CLA (del inglés, *cutaneous lymphocyte-associated antigen*), una variante glicosilada del ligando de la glicoproteína selectina-P (Picker *et al.* 1993; Sallusto et al 2009) y un ligando para la E-selectina, así como un conjunto de receptores de quimiocinas que facilitan la migración a la piel (CCR4, CCR8 y CCR10) (Campbell *et al.* 1999; Campbell *et al.* 1999; Homey *et al.* 2002). Después que las células T efectoras salen del dLN de la piel hacia la sangre, aquellas con **marcadores de retención en piel** se quedan atrapadas preferencialmente por los vasos inflamados de la piel y se extravasan a la dermis (Chong *et al.* 2004). Esta secuencia de eventos se repite una y otra vez en las diferentes barreras protectoras durante toda la vida de un organismo. Como resultado, se acumula una población Trm diversa, abundante, cuya especificidad no se superpone con otras poblaciones en cada uno de los tejidos de las barreras protectoras (Jiang *et al.* 2012; Clark *et al.* 2015). De esta forma, el pulmón contiene Trm específicas para el virus de la influenza (Hogan *et al.* 2001; Wei *et al.* 2005; Wu *et al.* 2014), los intestinos contienen Trm específicas para el rotavirus (Kuklin *et al.* 2000), la piel está enriquecida en Trm específicas para *Cándida* (Seneschal *et al.* 2012; Schlapbach *et al.* 2014), y la mucosa del tracto reproductivo contiene Trm específicas para el virus del herpes simple (HSV del inglés, *herpes simple virus*) (Nakanishi *et al.* 2009; Mackay *et al.* 2012; Shin *et al.* 2012; Iijima y Iwasaki *et al.* 2014).

Recientemente se demostró que un linfocito T *naive* puede generar simultáneamente un linfocito Trm y otro Tcm con la misma especificidad. La Trm de la piel y la Tcm de los LN comparten la misma secuencia variable (CDR3 del inglés, *complementarity-determining regions*) del TCR (del inglés, *T cell receptor*). Lo cual sugiere que las células Trm y Tcm tienen un **precursor común** (Park *et al.* 2015). La Trm de tejidos periféricos está duplicada en especificidad de antígenos por una población de memoria Tcm (Gaide *et al.* 2015).

La infección de la piel de ratones mediante escarificación con el virus vaccinia (VACV del inglés, *vaccinia virus*) induce la **acumulación de Trm**, tanto en la zona infectada como en los sitios alejados por toda la piel (Jiang *et al.* 2012). Este fenómeno también se describió durante la inmunización de la piel con proteínas y haptenos (Gaide *et al.* 2015). La piel no inflamada contiene venas post-capilares que expresan bajos

niveles de E-selectina, quimiocinas e ICAM-1 (del inglés, *intercellular adhesion molecule 1*), moléculas requeridas para que las células T se extravasen (Chong *et al.* 2004) y se establezcan en las zonas no infectadas. Además, los **encuentros repetidos** con un mismo patógeno en distintos sitios de la piel conllevan a la acumulación de la Trm específica por el patógeno en toda la superficie epitelial. Por esta razón, se pueden encontrar con más frecuencia un mayor número de Trm específicas por un patógeno determinado (Jiang *et al.* 2012; Gaide *et al.* 2015).

En los modelos de infección con VACV las DC dependientes de Batf3 (del inglés, *basic leucine zipper transcription factor, ATF-like 3*) se requieren para la **generación óptima de Trm**, pero no para su diferenciación en la piel o la formación de memoria circulante. Las **DC DNGR-1$^+$** (del inglés, *DC NK group receptor type 1*, también conocido como CLEC9A, del inglés, *C-type lectin domain family 9 member A*) promueven la inducción de T-bet y la retención de los linfocitos T CD8$^+$ en los LN, lo cual contribuye a la formación de precursores de Trm. La retención de linfocitos T en el LN aumenta la generación de Trm, mientras que la deficiencia genética o el bloqueo con anticuerpos anti-DNGR-1 inhiben el *priming* de la Trm. El bloqueo de las señales específicas provistas por las DC DNGR-1$^+$ durante el *priming*, tales como IL-12, IL-15, o CD24, también reproduce el fenotipo anterior (Iborra *et al.* 2016).

5.2.3.2 Señales para el desarrollo de Trm

El desarrollo de Trm involucra muchos puntos críticos como la entrada al tejido, la retención en el tejido, y la consiguiente respuesta local a las señales que contribuyen al desarrollo y supervivencia de la Trm en el tejido. La vía de **señalización mTOR** (del inglés, *mammaliam target for rapamycin*) permite la migración y acumulación de linfocitos T en la mucosa (Cyster *et al.* 2012). En la piel, algunos receptores de quimiocinas como **CXCR3** (del inglés, *C-X-C chemokine receptor*) dirigen la localización de linfocitos T en la epidermis y la subsecuente formación de Trm (Iwata *et al.* 2004). Asimismo, CXCR3 dirige la localización de linfocitos T en el epitelio pulmonar (Bromley *et al.* 2005; Mackay *et al.* 2015). La velocidad de salida desde los tejidos es también un factor determinante en la formación de Trm. Por ejemplo, los linfocitos T que carecen de **CCR7**, requerido para la salida de los linfocitos T desde los tejidos periféricos (Zabel *et al.* 1999), muestran un aumento en la conversión local y formación de Trm en piel (Iwata *et al.* 2004).

Existe un gradiente en los niveles de **S1P** (del inglés, *sphingosine 1 phosphate*) en el cuerpo de humanos y ratones. Los niveles más bajos se encuentran en los tejidos periféricos, los niveles intermedios en los dLN, y los más altos en la sangre (Cyster *et al.* 2012; Skon *et al.* 2013; Turner *et al.* 2014). Este gradiente de S1P guía a los linfocitos T desde los tejidos hasta los dLN y desde los dLN hacia la sangre. La expresión de **CD69** en la Trm interfiere con la expresión y función de S1P1 (del inglés, *sphingosine-1-phosphate receptor 1*). De esta forma bloquea la capacidad de estas células para seguir el gradiente de S1P, lo que contribuye a su residencia en el tejido (Turner *et al.* 2014). Los linfocitos T $CD8^{+}CD69^{-/-}$ forman menos Trm en la piel (Bromley *et al.* 2013) y en los pulmones (Watanabe *et al.* 2015), pero no en las placas de Peyer (Hadley *et al.* 2014). S1P1 también parece ser importante para la regulación del desarrollo de la Trm. Los niveles de expresión de S1P1 son bajos como parte del programa transcripcional de la Trm (Iwata *et al.* 2004). La expresión forzada de esta molécula inhibe la formación de Trm (Briskin *et al.* 1997). La disminución en los niveles de expresión del factor de transcripción **Klf2** (del inglés, *Kruppel-like factor 2*) en los precursores de Trm es muy relevante para el desarrollo de Trm, ya que disminuye la expresión de S1P1 (Briskin *et al.* 1997).

Aunque las señales que programan la Trm *in situ* son diferentes en dependencia del tejido, la citoquina **TGF-β** (del inglés, *transforming growth factor-β*) tiene un papel único en este proceso, al menos para el desarrollo de Trm $CD69^{+}CD103^{+}$ en piel, intestinos y pulmones (Iwata *et al.* 2004; Nestle *et al.* 2009; Piet *et al.* 2011; Mackay *et al.* 2015). El desarrollo de Trm mediado por TGF-β en pulmones es independiente de la vía de señalización SMAD4, que es el primer mediador de la vía TGF-β (Shimamura *et al.* 1992). Dado el amplio pero regulado proceso de expresión de TGF-β en los tejidos, se podría especular que esta citoquina tiene un papel no redundante en el desarrollo de Trm. Sin embargo, se ha demostrado que la Trm $CD103^{-}$ se puede desarrollar de una manera independiente a la señalización de TGF-β en la lámina propia de los intestinos, después de una infección con *Yersinia pseudotuberculosis* (Campbell *et al.* 1999) . Además, la citoquina IL-33 y el factor de necrosis tumoral (TNF-α del inglés, *tumor necrosis factor α*) en combinación con TGF-β pueden inducir un fenotipo asociado a la Trm ($CD69^{+}$, $CD103^{+}$) (Mackay *et al.* 2001), e incluso disminuir la expresión de Klf2 en linfocitos T $CD8^{+}$ (Briskin *et al.* 1997). Las señales inducidas por TGF-β también regulan la expresión de T-bet en linfocitos T $CD8^{+}$. T-bet regula negativamente la diferenciación

de Trm y la expresión de CD103 (Mackay *et al.* 2015).

La **IL-15** que participa en el mantenimiento de la Tcm y Tem, podría ser un factor decisivo para la diferenciación y supervivencia de la Trm. En ausencia de IL-15 la Trm no permanece en la piel tras la infección con HSV (Iwata *et al.* 2004). Sin embargo, los linfocitos $CD69^+$ en los dLN no requieren la expresión de IL-15 para su mantenimiento (Iwata *et al.* 2004), lo cual sugiere que ambas poblaciones son controladas por señales diferentes (Kupper *et al.* 2004).

La integrina **CD103** es otro marcador de Trm, aunque se expresa más en Trm $CD8^+$ que en Trm $CD4^+$. Es un ligando de E-cadherina, una molécula de adhesión expresada por células epiteliales de tejidos barreras (Watanabe *et al.* 2015). En modelos de ratón las células T $CD8^+$ específicas para HSV-1 no expresan CD103 antes de entrar a la piel, pero su expresión aumenta cuando entran a la epidermis en respuesta a TGF-β (Mackay *et al.* 2013). CD103 también se expresa en la Trm de pulmones, intestino, y en la Trm de cerebro tras una infección viral (Piet *et al.* 2011; Wakim *et al.* 2012; Laidlaw *et al.* 2014), (Sheridan *et al.* 2014). Se cree que la expresión de CD103 permite la interacción con E-cadherina. Sin embargo, la memoria residente no requiere la adhesión a E-cadherina. La Trm $CD8^+$ y $CD4^+$ se puede localizar en la dermis. Las DC $CD103^+$ también se encuentran en la dermis sin haber entrado nunca en la epidermis (Nestle *et al.* 2009). Aunque no se conoce completamente el papel de la expresión de CD103, se cree que es un marcador fenotípico de diferenciación, más que un requerimiento para la residencia en el tejido. En muchos modelos de ratón y en humanos, la Trm $CD103^+$ tiene menor potencial proliferativo y mayor capacidad efectora y productora de citoquinas que la Trm $CD103^-$ (Masopust *et al.* 2001; Reinhardt *et al.* 2001; Gebhardt *et al.* 2009; Piet *et al.* 2011; Wakim *et al.* 2012; Laidlaw *et al.* 2014; Sheridan *et al.* 2014).

5.2.3.3 Migración y supervivencia de Trm

Aunque los linfocitos de memoria que permanecen en los tejidos no recirculan en el organismo, tienen la habilidad de migrar dentro de zonas limitadas de forma longitudinal. Por ejemplo, las células Trm $CD8^+$ en la epidermis son capaces de migrar con una morfología dinámica, extendiendo las proyecciones de su membrana en varias direcciones (Hijnen *et al.* 2013; Mueller *et al.* 2013; Ariotti *et al.* 2014). Estas células Trm son considerablemente mucho más lentas que otras células T en la dermis de la piel. La forma ameboidea de estas células T se parece a la morfología de los linfocitos de los

dLN con una migración clásica. El ambiente de la epidermis induce una forma de **migración astringente** en las células T, la cual aumenta con la disminución de la inflamación una vez que la Trm se ha formado (Liu *et al.* 2010; Ariotti *et al.* 2014).

La migración lenta promueve una mayor retención de Trm en los sitios donde hubo infección. Además, podría aumentar su eficiencia ante una nueva infección, debido a que la Trm puede explorar mejor su microambiente. Sin embargo, para que la Trm explore los sitios cercanos y otros sitios más alejados, debe cubrir un área lo suficientemente grande como para detectar la replicación de los patógenos. Debido a la lentitud de la migración de la Trm debe existir una alta densidad de Trm para cubrir toda el área completamente (Hijnen *et al.* 2013).

5.2.3.4 Mecanismos efectores de Trm

La Trm que protege a los tejidos tiene la **habilidad de detectar y responder con mayor rapidez** ante una infección con un patógeno que las células T de la circulación. Sin embargo, la Trm está numéricamente en desventaja respecto a la replicación rápida de un patógeno. Además, no está totalmente demostrada la capacidad proliferativa de la Trm ante las diferentes infecciones (Kaech *et al.* 2012). Aunque los CTL (del inglés, *citotoxic T lymphocyte*) pueden lisar directamente células dianas infectadas mediante la expresión de perforinas y granzimas, y las células Trm pueden expresar granzima B (Mackay *et al.* 2001; Jiang *et al.* 2012; Hu *et al.* 2015), no se conoce bien si las células Trm son capaces de lisar directamente con eficiencia. Se ha visto que la Trm del cerebro es capaz de lisar células dianas cargadas con péptidos *in situ* (Wei *et al.* 2005). Por el contrario, la Trm (von Andrian *et al.* 2003) de pulmón protege contra el virus de la influenza a través de un proceso que involucra la producción de IFN-γ y otras citoquinas en ausencia de proliferación o función citotóxica (Purwar *et al.* 2011).

Los experimentos recientes demuestran que la Trm realiza su función efectora utilizando **mecanismos distintos a la lisis directa** de la célula diana. La Trm encuentra y responde a los antígenos *in situ* y puede producir citoquinas como el **IFN-γ**, lo cual aumenta el **reclutamiento de la memoria circulante** desde la sangre (Borowitz *et al.* 1993; Sallusto *et al.* 2009). En el aparato reproductor femenino de ratones, la producción temprana de citoquinas de la Trm en respuesta a los antígenos induce la expresión de la molécula de residencia VCAM-1 (del inglés, *vascular cell adhesión molecule 1*) en las células endoteliales de los vasos sanguíneos. Esto contribuye a estimular y reclutar

células NK, DC y células B al aparato reproductor (Hu *et al.* 2015). Asimismo, la reestimulación de la Trm induce un **estado de alerta en los tejidos**, que se caracteriza por un aumento en la expresión de muchos genes de la inmunidad innata, por ejemplo IFITM-3 (del inglés, *interferon-induced transmembrane protein 3*) (Kupper *et al*. 2012). Debido a este mecanismo de alerta, la activación local de la Trm y la consiguiente cascada inmunológica, se eliminan casi completamente los patógenos no relacionados antigénicamente (Kupper *et al.* 2012; Hu *et al.* 2015). La protección concomitante de la Trm es inesperada, y sugiere que estas células tienen un papel en la conexión de la inmunidad innata con la inmunidad adaptativa.

5.2.3.5 Trm en tumores

La infiltración de linfocitos T en tumores y en la zona peritumoral se asocia con una **mejor respuesta antitumoral** a largo plazo (Rao *et al.* 2010). Un estudio reciente sugiere que esa infiltración puede predecir si va a haber o no respuesta a una inmunoterapia con el anticuerpo anti-PD-1 (del inglés, *programmed cell death protein 1*) (Tumeh *et al.* 2014). La expresión de moléculas inhibidoras en el estroma tumoral como PD-L1, o la producción de otros factores inmunosupresores impiden la función efectora de la Trm específica para los antígenos tumorales (Park *et al.* 2015). La expresión de CD103 en las células Trm de cáncer de ovario es un marcador de un buen pronóstico (Webb, *et al.* 2014), y los mismos resultados se encontraron en pacientes con cáncer de pulmón (Djenidi *et al.* 2015).

5.3 Plasticidad de linfocitos T

Las poblaciones de memoria mayoritarias en los diferentes tejidos tienen diferencias funcionales. Sin embargo, no está claro si estas diferencias son un reflejo de las **señales que se reciben del ambiente** (linfático o no linfático), o si son dirigidas por **señales y programas genéticos intrínsecos a las células**, adquiridos durante el encuentro con el antígeno y dependientes de las condiciones inflamatorias previas. Para abordar el papel del ambiente proporcionado por el tejido en el mantenimiento de las funciones de la memoria, Wakim y colaboradores realizaron una serie de experimentos de transferencia adoptiva (Wakim *et al.* 2010). Las células Trm tomadas del cerebro, transferidas al bazo por vía intravenosa y expuestas al antígeno, tienen una capacidad de proliferación muy limitada (Wakim *et al.* 2010). Por el contrario, la memoria T circulante tomada del bazo y

trasplantada al cerebro mantiene un alto potencial proliferativo (Wakim *et al.* 2012). Estos datos sugieren que la diferenciación de Trm en el cerebro está ligada a un programa genético intrínseco, que restringe su capacidad proliferativa. En oposición a estos estudios en el cerebro, Masopust y colaboradores demostraron que la Trm tomada del intestino y transferida de nuevo al mismo organismo por vía intravenosa produce células efectoras y varias subpoblaciones de memoria, después del reencuentro con el antígeno (Masopust *et al.* 2006b). Estos datos por su parte, sugieren que las señales extrínsecas a la célula también contribuyen a las características específicas de cada subpoblación.

Para entender mejor la influencia sobre la **regulación transcripcional de la Trm**, Wakim y colaboradores analizaron el perfil de expresión genética de Trm y lo compararon con las subpoblaciones convencionales de memoria (Wakim *et al.* 2012). Las células Trm del cerebro adquieren varios programas de expresión génica, previamente descritos para controlar la diferenciación de la memoria, como Tcf1 y Eomes (del inglés, *eomesodermin*) (Wakim *et al.* 2012). Del mismo modo, Skon y colaboradores describieron que la disminución en la expresión de Klf2 es crítica para la expresión de señales de retención en células $CD8^+$ específicas, y de esta forma controlar la habilidad de entrar en la circulación o de mantenerse en los tejidos no linfáticos (Skon *et al.* 2013). Estos datos indican que los programas de expresión génica están acoplados a cambios intrínsecos en los factores de transcripción. Además, la relativa plasticidad de los programas es sensible a la duración de la estimulación por el TCR y a la estimulación por correceptores (Youngblood *et al.* 2015).

Los esfuerzos por entender la estabilidad de los programas génicos expresados en células de memoria se centran en factores de transcripción asociados a diferentes estados de diferenciación. Recientemente los estudios se enfocan en la investigación de **modificaciones epigenéticas de histonas y DNA** (del inglés, *deoxyribonucleic acid*), como mecanismos que regulan la accesibilidad a la cromatina (Youngblood *et al.* 2015). En un modelo de infección aguda, durante la estimulación se observó una demetilación del promotor de PD-1 consistente con un aumento en los niveles de expresión de PD-1. Tras la eliminación del virus las células adquirieron progresivamente la metilación del promotor durante la diferenciación a memoria (Youngblood *et al.* 2011). Sin embargo, después de una exposición crónica al antígeno, las células fueron incapaces de readquirir la metilación en el locus PD-1 (Youngblood *et al.* 2011, 2013).

5.4 Células dendríticas tipo 1 (cDC-1)

Las **DC son células presentadoras de antígenos por excelencia**, que median la respuesta inmunitaria innata y adaptativa (Schraml *et al.* 2015). Se identificaron por primera vez en el bazo de ratones, debido a su morfología que las distinguía de los macrófagos (Steinman *et al.* 1973). Son células móviles, con morfología estelar, que expresan altos niveles de CD11c y MHC-II (Nussenzweig *et al.* 1981, 1982). Tienen la capacidad de migrar desde los tejidos no linfoides hacia los tejidos linfoides y una habilidad superior para estimular a los linfocitos T *naive* (Heath *et al.* 2009; Steinman *et al.* 2010; Idoyaga *et al.* 2013). No obstante, en circunstancias de inflamación o de infección, los monocitos y los macrófagos también pueden estimular a los linfocitos T. Además, las DC regulan la respuesta inmunitaria innata sin necesidad de activar linfocitos T o migrar a los órganos linfoides secundarios (Reis e Sousa *et al.* 1997; Mashayekhi *et al.* 2011; Whitney *et al.* 2014). Estas anormalidades dificultan una definición única de marcadores fenotípicos, que permita conceptualizar inequívocamente a las DC y a la vez distinguirlas de monocitos y macrófagos (Hume *et al.* 2002; Hume 2006, 2008). Los estudios recientes en la caracterización de los precursores de DC en ratones en paralelo con los estudios de ontogenia en monocitos y macrófagos (Doulatov *et al.* 2010; Hashimoto *et al.* 2013; Hettinger *et al.* 2013; Naik *et al.* 2013; Onai *et al.* 2013; Schraml *et al.* 2013; Massoud *et al.* 2014; Sathe *et al.* 2014), sugieren que las DC se generan a partir del progenitor común de las DC (CDP, del inglés *common DC progenitor*) y son dependientes de la citoquina FLT3-L (del inglés, *Fms-like tyrosine kinase 3 ligand*).

Se pueden distinguir **4 tipos distintos de DC**: las DC clásicas o convencionales (cDC) (Steinman *et al.* 1973), las DC plasmacitoides (Cella *et al.* 1999; Siegal *et al.* 1999), las DC derivadas de monocitos (Randolph *et al.* 1999; Geissmann *et al.* 2003; Serbina *et al.* 2003) y las DC de Langerhans (Schuler *et al.* 1985). Las **cDC** se conocen por su eficiencia en la iniciación y dirección de la respuesta T (Heath *et al.* 2009; Steinman *et al.* 2010; Hashimoto *et al.* 2011). En ratones, las cDC se pueden dividir en subpoblaciones $CD11b^-$ y $CD11b^+$. La subpoblación **cDC-1** también conocida como "CD8α-*like*" está compuesta por las DC $CD8\alpha^+$ $CD11b^-$ en los órganos linfoides secundarios, y sus homólogas $CD103^+CD11b^-$ en los tejidos periféricos. Estas últimas migran hacia el dLN tanto en homeostasis como en condiciones inflamatorias. Todas las DC "CD8α-like" de ratón comparten un patrón de expresión de genes que depende de los

factores de transcripción **Irf8** (del inglés, *interferon regulatory factor 8*) y **Batf3**. Además, realizan la presentación cruzada de antígenos exógenos a linfocitos T $CD8^+$, particularmente aquellos antígenos asociados a células muertas (Heath *et al.* 2009; Edelson *et al.* 2010; Steinman *et al.* 2010; Hashimoto *et al.* 2011; Miller *et al.* 2012). Las **cDC-2** o $CD11b^+$ son dependientes de **Irf4**. Son más heterogéneas y se componen de subtipos celulares dependientes de los factores de transcripción Notch2 (del inglés, *neurogenic locus notch homolog protein 2*) o Klf4, e inducen las respuestas Th17 (del inglés, *T-helper 17*) y Th2 respectivamente (Persson *et al.* 2013; Schlitzer *et al.* 2013; Bedoui *et al.* 2015).

5.4.1 cDC-1 dependientes de Batf3 dirigen la respuesta inmunitaria Th1

La regulación transcripcional de las DC $CD8\alpha^+$ se ha estudiado extensivamente. El desarrollo de las DC $CD8\alpha^+$ es dependiente de los factores de transcripción Irf8, ID2, Nfil3 (del inglés, *nuclear factor, interleukin 3 regulated*), Batf3 y Bcl-6 (del inglés, *B-cell lymphoma 6 protein*) (Schiavoni *et al.* 2002; Hacker *et al.* 2003; Tamura *et al.* 2005; Hildner *et al.* 2008; Kashiwada *et al.* 2011; Watchmaker *et al.* 2014). La **ausencia de Batf3 inhibe el desarrollo de DC $CD8\alpha^+$**. Sin embargo, la interacción de Irf8 con Batf y Batf2 (Tussiwand *et al.* 2012) compensa esta deficiencia (Murphy *et al.* 2013). Aunque las DC humanas no expresan CD8α, los estudios de expresión génica sugieren que las DC equivalentes son una población que expresa BDCA-3 (del inglés, *blood DC antigen 3*, también conocido como CD141), identificadas en la sangre periférica (Robbins *et al.* 2008). Las DC $CD141^+$ humanas expresan los factores de transcripción Irf8, Batf3 y DNGR-1. Este último receptor potencia la presentación cruzada de antígenos derivados de células necróticas (Sancho *et al.* 2009). Además, secretan IL-12 induciendo una polarización Th1 (Maldonado-López *et al.* 1999; Mashayekhi *et al.* 2011).

La función específica de Batf3 en el desarrollo de DC $CD8\alpha^+$ no está clara. Sin embargo, el estudio de **ratones *Batf3*$^{-/-}$** ha demostrado el papel crítico que las DC $CD8\alpha^+$ realizan en la modulación de la respuesta inmunitaria. Las DC dependientes de Batf3 son necesarias para la inducción de una respuesta tipo 1 ante la infección con *Toxoplasma gondii*. Esto se debe a su función no redundante de ser las **principales productoras de IL-12**, que promueve la activación de NK y la producción de IFN-γ (Gazzinelli *et al.* 1993, 1994; Sher *et al.* 1993; Reis e Sousa *et al.* 1997; Hou *et al.* 2011; Mashayekhi *et al.*

2011). La respuesta local Th1 frente a *Leishmania major* también está disminuida en ratones *Batf3*$^{-/-}$. Estos ratones tienen un número menor de DC CD103^{+} en la piel y una consiguiente disminución en la producción de IL-12 (Martínez-López *et al.* 2015). Asimismo, la ausencia de DC CD103^{+} en el pulmón y la disminución en la producción de IL-12 generan una respuesta Th1 deficiente, después de la exposición aguda o crónica al ácaro del polvo doméstico (Conejero *et al.* 2017). Como los animales *Batf3*$^{-/-}$ tienen una deficiencia en la generación de Trm en los modelos de vacunación con VACV e influenza, los ratones vacunados no se protegen frente a un segundo estímulo con el virus (Iborra *et al.* 2016).

Recientemente las cDC-1 han despertado un gran interés en la inmunología tumoral. El **papel crítico de las DC dependientes de Batf3 en la inmunidad antitumoral** es evidente en los ratones *Batf3*$^{-/-}$, los cuales no rechazan eficientemente los tumores inmunogénicos (Hildner *et al.* 2008). Mediante el uso de quimeras y modelos de deficiencia condicional en ratón, se demostró que la señalización de los IFN tipo 1 en las DC dependientes de Batf3 se requiere para el control inmunológico del crecimiento tumoral (Diamond *et al.* 2011; Fuertes *et al.* 2011).

El tratamiento previo con IL-12 restablece la habilidad de ratones *Batf3*$^{-/-}$ para estimular una respuesta T CD8^{+} antitumoral y rechazar tumores inmunogénicos, lo cual se debe probablemente al restablecimiento de la función de las DC dependientes de Batf3 (Tussiwand *et al.* 2012).

Recientemente se demostró que las **DC CD103^{+}** son las únicas capaces de transportar antígenos tumorales al TdLN. En el TdLN estas DC estimulan y activan la respuesta T CD8^{+} específica por el tumor (Roberts *et al.* 2016; Salmon *et al.* 2016). Asimismo, se demostró que las DC CD103^{+} aparte de activar directamente células T CD8^{+}, transfieren antígenos a otras células mieloides residentes en el LN con otras funciones. Todos los procesos anteriores son **dependientes de CCR7** (Roberts *et al.* 2016).

La ventaja de las DC CD103^{+} para regular la respuesta antitumoral se ha utilizado en diferentes modelos animales de cáncer. Por ejemplo, en un modelo murino de cáncer de mama, el bloqueo de CSF-1 (del inglés, *colony-stimulating factor-1*) combinado con paclitaxel aumenta la fracción de DC CD103^{+} y la infiltración de linfocitos T en el tumor (Ruffell *et al.* 2014). Las quimioterapias inmunogénicas que aumentan la expresión de

TLR4 (del inglés, *toll like-receptor 4*) en DC CD103$^+$ residentes del pulmón promueven la infiltración de linfocitos T, y un aumento en la actividad antitumoral (Pfirschke *et al.* 2016). Además, la citoquina FLT3-L expande la población de DC CD103$^+$ mientras que la citoquina GM-CSF (del inglés, *granulocyte-macrophage colony-stimulating factor*) promueve las DC CD103$^-$ (Broz *et al.* 2014). La respuesta antitumoral débil e ineficiente de linfocitos T se puede rescatar con anticuerpos inmunomoduladores contra PD-1 (CD279) o CD137. Las DC dependientes de Batf3 son esenciales para las terapias con anticuerpos monoclonales anti-CD137 o anti–PD-1. Los ratones *Batf3*$^{-/-}$ no activan la respuesta antitumoral mediada por CTL contra los antígenos tumorales, incluyendo los neoantígenos (Sanchez-Paulete *et al.* 2016). La administración sistémica de FLT3-L, seguida de una inyección intratumoral con poly (I:C) expande y activa la población de progenitores de DC CD103$^+$ en el tumor, lo cual aumenta la respuesta a BRAF, el bloqueo de PD-L1 y protege a los ratones contra los tumores (Salmon *et al.* 2016).

Un estudio reciente demostró que las DC CD103$^+$ en los pulmones internalizan el material citoplasmático unido a las membranas, liberado por células tumorales en la vasculatura del pulmón (Headley *et al.* 2016). Después de la inyección con células tumorales que expresan OVA (del inglés, *ovalbumin*) se detectan DC CD103$^+$ cargadas con este antígeno en los ganglios linfáticos mediastinales tres días más tarde. Las DC y los linfocitos T OT-I (linfocitos T CD8$^+$ transgénicos con el TCR específico para el péptido SIINFEKL de OVA presentado en H2-Kb) que fueron previamente transferidos forman asociaciones en forma de grumos. Estos linfocitos tienen una morfología consistente con la de linfocitos T activados. La habilidad de las DC CD103$^+$ para activar linfocitos T OT-I se confirmó *ex vivo* y utilizando ratones quimeras (Headley *et al.* 2016).

La infiltración de linfocitos T en el tumor no ocurre siempre, y los mecanismos que explican este comportamiento no están completamente claros. Las DC CD103$^+$ intratumorales son las mayores productoras de dos quimiocinas, **CXCL9 y CXCL10**, que promueven el reclutamiento de linfocitos T efectores reactivos contra el tumor (Spranger *et al.* 2017). Un trabajo anterior había mostrado que la activación de la vía de señalización de β-catenina, una vía pro-tumoral intrínseca de melanoma, reduce el número de DC CD103$^+$ y previene la activación de linfocitos T específicos para el tumor (Spranger *et al.* 2015). En conjunto, los resultados sugieren que las DC CD103$^+$ no solamente promueven la inmunidad antitumoral, sino que pueden ser suprimidas por células tumorales para evadir el reconocimiento inmunológico.

5.5 Inmunoterapias con anti-PD-1

La molécula **PD-1** es una proteína de inhibición que se encuentra en la superficie de linfocitos B y T activados (Nishimura *et al.* 1998). PD-1 es miembro de la superfamilia de inmunoglobulinas CD28 y CTLA-4 (del inglés, *cytotoxic T-lymphocyte antigen 4*), e interacciona con dos ligandos de la familia B7, PD-L1 (CD274) y PD-L2 (CD273) (Keir *et al.* 2008). PD-L1 está ampliamente distribuido entre los leucocitos y células no hematopoyéticas de tejidos linfoides y no linfoides como las células y el estroma tumoral. PD-L2 se expresa exclusivamente en las **DC y monocitos** (Ishida *et al.* 2002; Yamazaki *et al.* 2002). En las infecciones crónicas, por ejemplo con HIV (del inglés, *human immunodeficiency virus*), hepatitis B y C en humanos y con LCMV (del inglés, *lymphocytic choriomeningitis virus*) clon 13 en ratones, la exposición prolongada al antígeno altera la función y expresión de genes de linfocitos T $CD8^+$ (Virgin *et al.* 2009; Wherry *et al.* 2011). Estos cambios se conocen como agotamiento (*exhaustion*) de las células T, porque las células específicas para el antígeno muestran una pérdida jerárquica en la producción de IL-2, TNF-α, e IFN-γ, menor proliferación, y hasta pérdida de citotoxicidad (Virgin *et al.* 2009; Wherry *et al.* 2011). Esos cambios funcionales se han asociado con la expresión de receptores de inhibición como PD-1, LAG-3 (del inglés, *lymphocyte-activation gene 3*), CD244 y CD160 (Wherry *et al.* 2011).

No fue hasta el 2000, cuando se estableció la función de **PD-1 como punto de control (*checkpoint*)** de la respuesta inmunitaria, después del descubrimiento de sus ligandos (Freeman *et al.* 2000). PD-L1 protege a las células tumorales mediante la inducción de apoptosis en células T (Dong *et al.* 2002). Los ensayos clínicos en fase I con un anticuerpo monoclonal contra PD-1 demostraron respuesta clínica en muchos tipos de tumores: melanoma, carcinoma de riñón, cáncer de células no pequeñas de pulmón (Brahmer *et al.* 2012) y linfoma de Hodgkin (Ansell *et al.* 2015). Un estudio clínico en fase III, donde se trataron pacientes con melanoma metastásico con un anticuerpo diferente contra PD-1 (nivolumab, Bristol-Myers Squibb, BMS) también demostró mejores respuestas clínicas y un beneficio de supervivencia global, si se compara con otros tratamiento de quimioterapia (Robert *et al.* 2014).

Muchas teorías tratan de explicar los mecanismos mediante los cuales PD-1 inhibe la activación de células T. Una posibilidad es que PD-1 compita pasivamente con CD28 por la unión con B7-1 (Butte *et al.* 2007). Además, PD-1 recluta directamente las

fosfatasas SHP-1 y SHP-2 que interfieren con la señalización por el TCR (Yokosuka *et al.* 2012). Las moléculas de PD-1 que se expresan en células T efectoras forman microagrupaciones con el TCR y se acumulan por la señalización de s-SMAC. SHP-2 se recluta inmediatamente asociándose con PD-1 mediante los motivos ITSM, e induce la desfosforilación de las moléculas de señalización del TCR dentro de las microagrupaciones PD-1-TCR (Yokosuka *et al.* 2012). Por otra parte, la unión del TCR con las DC resulta en señales de parada que disminuyen la movilidad de las células T, requerida para la interacción T-DC y el desarrollo de la sinapsis inmunológica (Dustin *et al.* 1997; Mempel *et al.* 2004). PD-1 inhibe las señales de parada inducidas por el TCR. El bloqueo de PD-1 o PD-L1 inhibe la unión prolongada durante la sinapsis entre linfocitos T y DC, aumenta la producción de citoquinas de células T, estimula la señalización por el TCR y elimina la tolerancia periférica en un modelo autoinmune de páncreas (Fife *et al.* 2009).

Objetivos

6. Objetivos

El objetivo general de este trabajo es analizar la interrelación de las subpoblaciones de linfocitos T $CD8^+$ de memoria residente y circulante en la inmunidad antitumoral.

Los objetivos específicos son:

1. Estudiar la contribución relativa de la memoria T $CD8^+$ residente y circulante en la respuesta antitumoral.

2. Analizar la plasticidad de la memoria T $CD8^+$ circulante en procesos inflamatorios.

3. Evaluar el papel de las células dendríticas tipo 1 en la respuesta antitumoral de los linfocitos T $CD8^+$ de memoria.

Materiales y métodos

7. Materiales y métodos

7.1 Ratones

Los ratones se cruzaron y se mantuvieron en la zona SPF (del inglés, *specific pathogen free*) del animalario de la Fundación-Centro Nacional de Investigaciones Cardiovasculares Carlos III de Madrid. Los ratones *Batf3*$^{-/-}$ con el fondo genético C57BL/6 se donaron amablemente por el Dr. K. M. Murphy (Washington University, St. Louis, MO) (Hildner *et al.* 2008). Los ratones transgénicos OT-I (C57BL/6-Tg (TcraTcrb)1100Mjb/J) se cruzaron con los ratones B6-SJL (Ptprca Pepcb/BoyJ) que expresan el alelo CD45.1 para la molécula CD45, ambos provenientes de los laboratorios "The Jackson Laboratory" (Bar Harbor, ME). Se utilizaron ratones machos o hembras indistintamente, entre 7 y 10 semanas de edad, para todos los ensayos. El comité de ética local aprobó todos los estudios con animales. Todos los procedimientos se realizaron teniendo en cuenta las directivas de la Unión Europea 2010/63EU, la ley 2007/526/EC de protección de animales que se usan para experimentación y con otros fines científicos y el Real Decreto español 1201/2005.

7.2 Inmunización con rVACV-OVA

El virus recombinante vaccinia que expresa ovoalbúmina (rVACV-OVA) fue donado por J. Y. Yewdell y J. R. Bennink (NIH, Bethesda, MD) y amablemente proporcionado por M. del Val (CBMSO, Madrid). El crecimiento y la titulación de los lotes virales de trabajo se realizaron en la línea celular CV1 (Iborra *et al.* 2012). A no ser que se indique lo contrario, los ratones fueron inmunizados con rVACV-OVA mediante las siguientes vías: escarificación de la piel (s.s. del inglés, *skin scarification*) en la base de la cola (1-2×10^6 p.f.u.) o en la espalda (10^6 p.f.u.), intradérmica (i.d.) en la oreja (5×10^4 o 10^6 p.f.u.), intranasal (i.n.) (5x10^4 p.f.u.) o intraperitoneal (i.p.) (5×10^4 o 1-2×10^6 p.f.u.). Las células T, se consideraron de memoria 30 días después de la infección (Jiang *et al.* 2012).

7.3 Inoculación de tumores

Las líneas celulares de melanoma que expresa ovoalbúmina (B16-OVA) (Sanchez-Paulete *et al.* 2016) y de adenocarcinoma que expresa ovoalbúmina (MC38-OVA) (Sanchez-Paulete *et al.* 2016) se inocularon a partir de cultivos celulares en fase

exponencial. El tumor B16-OVA se inoculó (i.d.) en un flanco (10^6 células) y el seguimiento del tumor se realizó durante 20-30 días. Alternativamente, el tumor B16-OVA (3×10^5 células) se inoculó intravenoso (i.v.) y los ratones se sacrificaron 20 días después para contar el número de nódulos metastásicos en el pulmón. Los pulmones se fijaron en solución de Fekete (100 ml de etanol al 70%, 10 ml de formaldehido al 4% y 5 ml de ácido acético glaciar al 100%). El tumor MC38-OVA (2×10^6 células) se inoculó subcutáneo (s.c.) en un flanco y el seguimiento del tumor se realizó durante 20-60 días. El volumen del tumor se estimó mediante la fórmula: $V=D\times d^2/2$, donde V es el volumen (mm^3), D es el diámetro mayor (mm) y d es el diámetro menor (mm). Todas las líneas celulares se evaluaron para el contenido de micoplasma rutinariamente.

7.4 Otros reactivos

FTY720 (Cayman Chemical) en solución acuosa se administró (i.p.) cada 4 días a una dosis de 2.5 mg/kg de peso.

7.5 Generación de linfocitos de memoria central

Para la generación de linfocitos T OT-I de memoria central (Tcm), los ratones se transfirieron (i.v.) con linfocitos OT-I *naive* ($1\text{-}3\times10^5$) un día antes de la inmunización (i.d.) con rVACV-OVA (5×10^4 p.f.u.) en la oreja. Los linfocitos Tcm se purificaron mediante un clasificador de células activadas por fluorescencia (FACS Sy3200, Sony), a partir de las suspensiones celulares de dLN y bazos 30 días después de la infección. Los linfocitos $CD8^+CD45.1^+$ se clasificaron en linfocitos *naive* ($CD44^{lo}CD62L^{hi}$), linfocitos Tcm ($CD44^{hi}CD62L^{hi}$) y linfocitos de memoria efectora ($CD44^{hi}CD62L^{lo}$).

7.6 Plasticidad de linfocitos Tcm en un modelo viral

Los ratones se transfirieron (i.v.) con 10^4 linfocitos OT-I *naive* o $1\text{-}2\times10^4$ linfocitos OT-I Tcm, un día antes de la inmunización (i.d.) con rVACV-OVA (5×10^4 p.f.u.) en la oreja. La respuesta de memoria se analizó en las orejas y en los órganos linfoides secundarios de interés según el experimento, 30 o 60 días después de la infección. Se utilizaron CD69 y CD103, como marcadores fenotípicos de los linfocitos residentes (Trm).

7.7 Plasticidad de linfocitos Tcm en un modelo de tumores

Los ratones se transfirieron (i.v.) con $2x10^4$ linfocitos OT-I Tcm un día antes de la inoculación (i.d.) del tumor B16-OVA (10^6 células) o $3x10^3$ o $2x10^4$ linfocitos OT-I Tcm un día antes de la inoculación (s.c.) del tumor MC38-OVA ($2x10^6$ células). Se analizaron los linfocitos que infiltraron el tumor B16-OVA, 20-23 días después de la inoculación del tumor. Asimismo, se analizaron los linfocitos que permanecieron en la piel de los animales que rechazaron el tumor MC38-OVA, 20 o 45 días después de la inoculación del tumor.

Los ratones con tumores palpables de entre 100-150 mm^2 (día 7, para el B16-OVA; día 15-18, para MC38-OVA) se transfirieron con $1-2x10^4$ linfocitos OT-I Tcm. A continuación, los ratones recibieron (i.p.) dos dosis del anticuerpo anti-PD-1 (100 µg, Clon RMP1-14, BioXcell). La primera dosis se inoculó simultáneamente a la transferencia adoptiva y la segunda dosis tres días después. A continuación, se analizaron los marcadores fenotípicos de los linfocitos Trm, CD69 y CD103, 7 días después de la transferencia adoptiva.

7.8 Parabiosis

La parabiosis es el procedimiento experimental por el cual 2 organismos se conectan quirúrgicamente para permitir la anastomosis y compartición del sistema circulatorio. La parabiosis se realizó como se describió previamente (Jiang *et al.* 2012). Brevemente, se rasuró el dorso lateral de los animales y se hicieron incisiones en la piel desde el olecranon hasta la articulación de la rodilla de cada ratón. Se retiró la fascia subcutánea para crear una superficie de aproximadamente 0,5 cm de piel libre. El olecranon y la articulación de la rodilla se cosieron con una sutura de polipropileno (calibre 5.0). La piel dorsal y ventral se cosieron con puntos continuos con sutura de seda (calibre 7.0). Los parabiontes recibieron una dosis única de flunixina-meglumina como antiinflamatorio (1 mg/kg, subcutáneo) y se dejaron recuperar en cabina a una temperatura y pO2 controlados tras la operación. Un mes después de la cirugía, se extrajeron muestras de sangre y otros tejidos de cada pareja para el análisis de los niveles de linfocitos T de memoria.

7.8.1 Parabiosis en el modelo tumoral

Los ratones WT se inmunizaron (s.s.) con rVACV-OVA (10^6 p.f.u.) en la cola, la espalda y la oreja (i.d.) simultáneamente. Posteriormente (30 días después), los ratones inmunizados se unieron quirúrgicamente con ratones sin inmunizar para crear los parabiontes. A continuación (30 días después), los ratones se separaron y se mantuvieron en recuperación durante 30 días. Finalmente, los parabiontes individualizados se inocularon (i.d.) con B16-OVA (10^6 células).

7.8.2 Parabiosis en el modelo de plasticidad en un contexto viral

Los ratones WT se transfirieron (i.v.) con $2x10^4$ linfocitos OT-I Tcm un día antes de la inmunización (i.d.) con rVACV-OVA ($5x10^4$ p.f.u.) en la oreja. Los ratones transferidos e inmunizados se unieron quirúrgicamente 30 días después con ratones sin inmunizar para crear los parabiontes. Se mantuvieron unidos durante otros 30 días. Finalmente, se analizaron los infiltrados de la oreja y el bazo de ambos parabiontes mediante citometría de flujo, y se utilizaron los marcadores fenotípicos asociados a Trm, CD69 y CD103.

7.9 Citometría de flujo

Los dextrámeros marcados con aloficocianina específicos para OVA H-2Kb (257-SIINFEKL-264) se obtuvieron de Immudex (Copenhagen, Denmark). Las muestras se tiñeron en una solución tampón de PBS frío suplementada con 2 mM EDTA y 1% FBS, con la mezcla de anticuerpos deseada durante 15-20 minutos en hielo. Los anticuerpos anti-ratón CD45 (clon 30F11), CD8α (clon 53-6.7), CD103 (clon 2E7), CD44 (clon IM7), CD45.1 (clon A20) y CD45.2 (clon 104) se obtuvieron de *eBioscience*. Los anticuerpos anti-ratón CD62L (clon MEL-14) y CD69 (clon H1.2F3) se obtuvieron de *BD Biosciences*. El anticuerpo anti-ratón CD279 (PD-1, clon 29F.1A12) se obtuvo de *Biolegend*. Las células se analizaron en los citómetros de flujo, *LSRFortessa SORP* (*Becton Dickinson*) o *Spectral Cell Analyzer SP6800* (*Sony*) y los datos se procesaron mediante el programa *FlowJo*, versión 10 (*Tree Star*).

7.10 Análisis estadístico

El análisis estadístico se realizó con el programa *Prism v6* (*GraphPad Software Inc*., La Jolla, CA). La varianza entre los grupos se determinó mediante el test estadístico F. La significación estadística para la comparación entre dos grupos con una distribución normal (evaluada mediante un test estadístico de Shapiro-Wilk), se determinó mediante el test estadístico de la t de Student, con dos colas y sin parear. La comparación entre dos grupos sin una distribución normal, se realizó mediante el test estadístico no paramétrico de Mann-Whitney, con dos colas. Las comparaciones entre más de dos grupos se realizaron mediante el test estadístico one-way o two-way ANOVA, aplicando una corrección de Bonferroni *a posteriori*. Para la **Figura R6d**, se utilizó un modelo de regresión de Cox de efectos mixtos para comparar la incidencia del tumor entre los dos grupos, manteniendo la información de cada uno de los grupos por separado. Se utilizó la función coxme del paquete R, para la cohorte entre el día 0 y el día 17, donde el 50% de los ratones de ambos grupos de parabiontes tenían tumores palpables. El p-valor <0.05 se consideró significativo. Los experimentos se repitieron entre 2 y 3 veces. No se utilizaron estrategias de experimentación a ciegas, ni tampoco se excluyeron ratones de los análisis.

Resultados

8. Resultados

8.1 Tanto la memoria T CD8$^+$ residente como circulante promueven la inmunidad antitumoral

Se estudió el papel de los linfocitos T CD8$^+$ de memoria residente (Trm) y circulante durante la respuesta inmunitaria contra tumores. Para ello, se generaron selectivamente diferentes tipos de linfocitos T de memoria, mediante diferentes vías de inmunización con el virus recombinante vaccinia que expresa ovoalbúmina (rVACV-OVA). Los linfocitos de memoria circulante y Trm se analizaron 30 días después de la infección.

La frecuencia de linfocitos T CD8$^+$CD44$^+$ (memoria T circulante) endógenos, específicos para OVA en los dLN fue igual, independientemente de la vía de inmunización, con una media aritmética alrededor del 0.4% (**Figura R1a-b**).

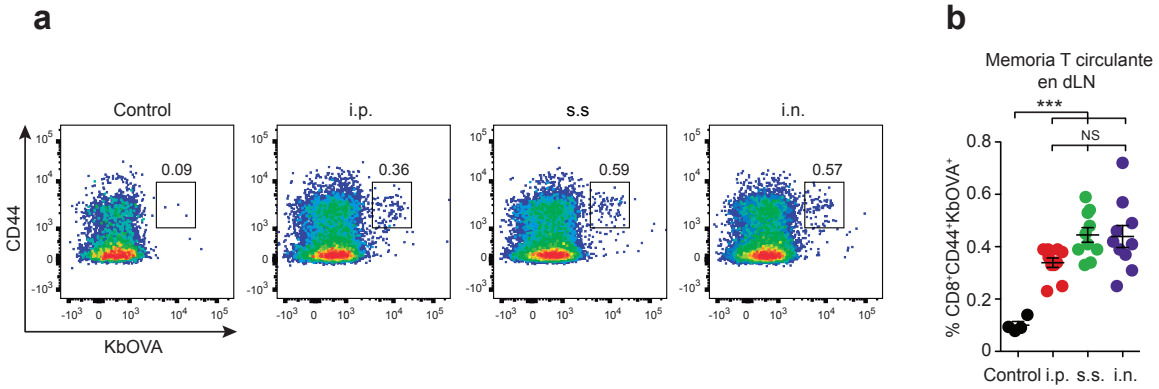

Figura R1. Generación de memoria T CD8$^+$ circulante mediante diferentes vías de infección con rVACV-OVA

(**a**) Gráficos de puntos representativos del análisis por citometría de flujo, que muestran linfocitos T CD8$^+$ de memoria, endógenos, circulantes y específicos para OVA, en dLN de ratones 30 días después de la infección i.p. (5×10^4 p.f.u.), s.s. (2×10^6 p.f.u.) o i.n. (5×10^4 p.f.u.) con rVACV-OVA. (**b**) Frecuencia de linfocitos T CD8$^+$ de memoria, endógenos, circulantes y específicos para OVA en dLN. Combinación de dos experimentos independientes, donde cada punto es un ratón. Se representa la media ± s.e.m (n=4-5/grupo). NS, no significativo; ***, p<0.001; mediante el test estadístico one-way ANOVA, aplicando un test de Bonferroni *a posteriori*.

La inmunización intraperitoneal (i.p.) con rVACV-OVA no generó eficientemente linfocitos Trm CD8$^+$CD69$^+$ en la piel. Sin embargo, la inmunización (s.s.) en la cola generó linfocitos Trm en el propio sitio de la infección (piel de la cola) y en menor medida en un sitio distante como la oreja. (**Figura R2a-d**).

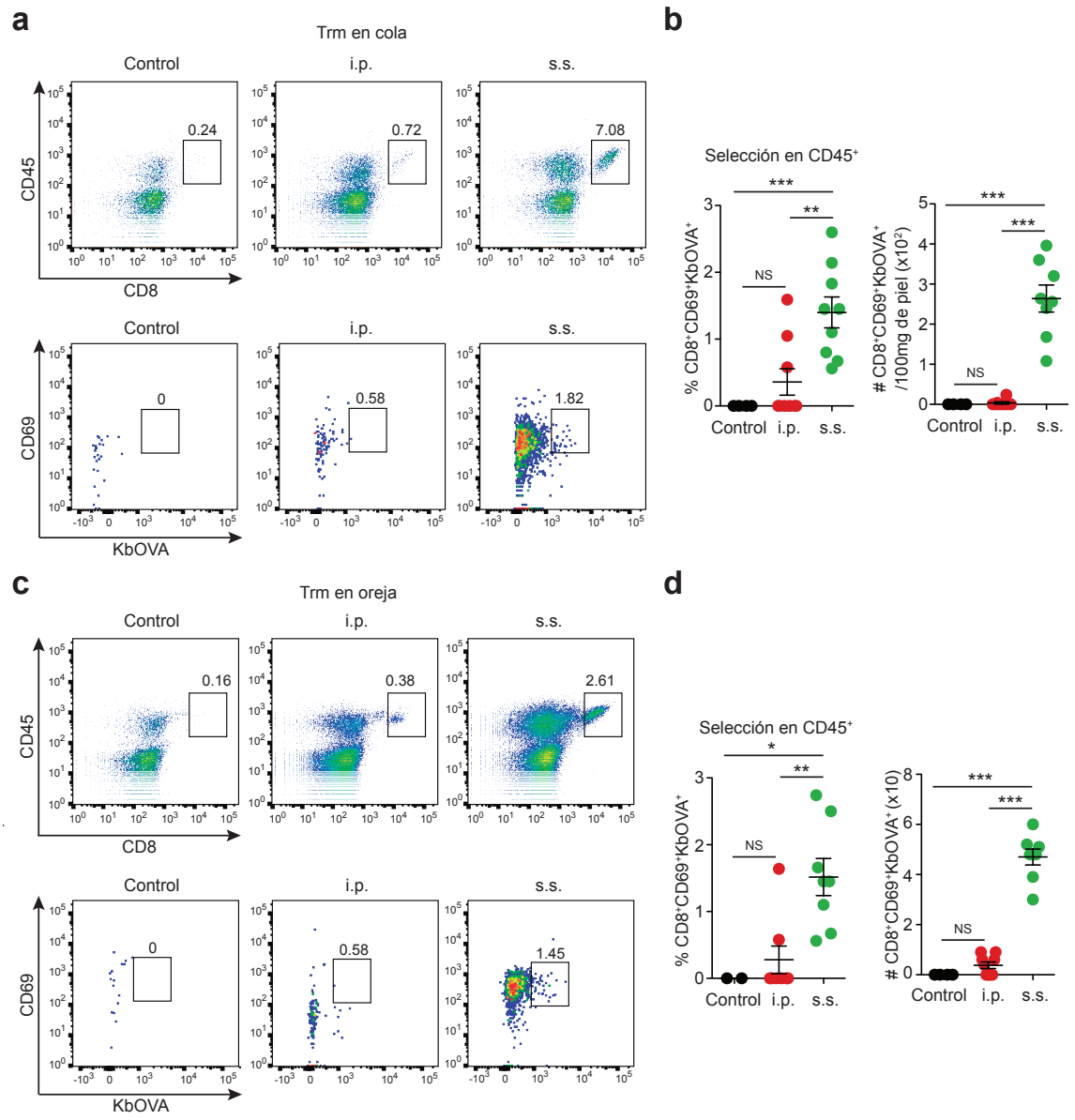

Figura R2. Generación de memoria T CD8$^+$ residente en piel mediante escarificación de la cola con rVACV-OVA

(**a, c**) Gráficos de puntos representativos del análisis por citometría de flujo, que muestran linfocitos T CD8$^+$ de memoria residente (Trm) CD69$^+$, endógenos y específicos para OVA (paneles inferiores), seleccionados previamente en la población CD45$^+$CD8$^+$ (paneles superiores), en la cola (**a**) y en la oreja (**c**), 30 días después de la s.s. en la cola. (**b, d**) Frecuencia (panel izquierdo) y número (panel derecho) de linfocitos Trm específicos para OVA en la cola (**b**) y en la oreja (**d**) 30 días después de la s.s. en la cola. (**b, d**) Combinación de dos experimentos independientes, donde cada punto es un ratón. Se representa la media ± s.e.m (n=4-5/grupo). NS, no significativo; ***, p<0.001; **, p<0.01; *, p<0.05; mediante el test estadístico one-way ANOVA, aplicando un test de Bonferroni *a posteriori*.

Asimismo, la inmunización intranasal (i.n.) generó linfocitos Trm en pulmón, mientras que la inmunización i.p no (**Figura R3a-b**).

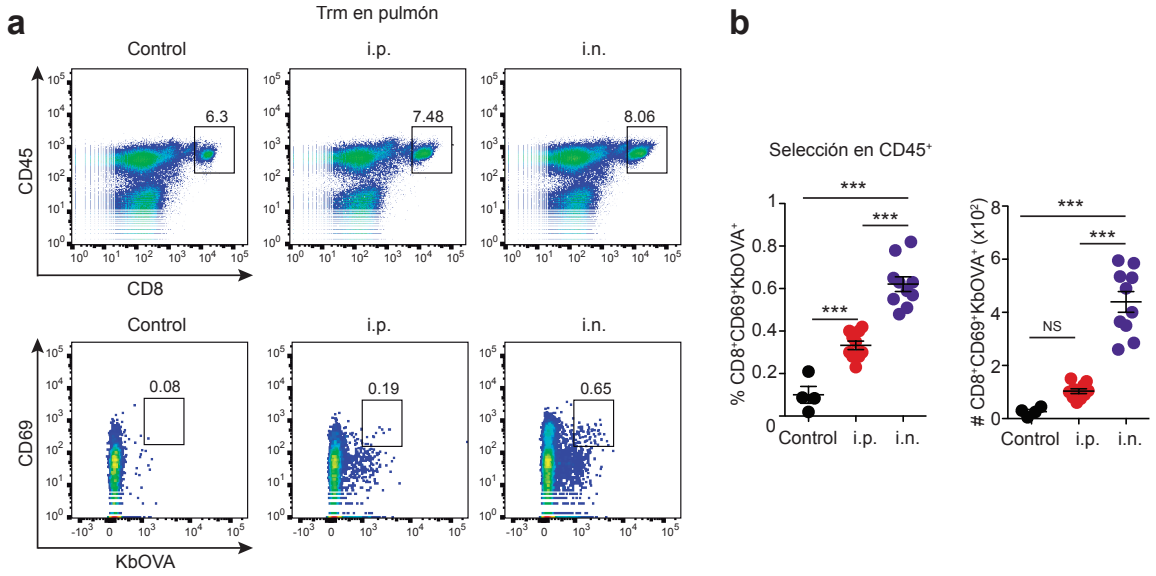

Figura R3. Generación de memoria T CD8$^+$ residente en pulmón mediante infección intranasal con rVACV-OVA

(**a**) Gráficos de puntos representativos del análisis por citometría de flujo, que muestran linfocitos de memoria residente (Trm) CD69$^+$, endógenos y específicos para OVA (paneles inferiores), seleccionados previamente en la población CD45$^+$CD8$^+$ (paneles superiores) en el pulmón, 30 días después de la infección intranasal. (**b**) Frecuencia (panel izquierdo) y número (panel derecho) de linfocitos Trm específicos para OVA en el pulmón, 30 días después de la infección i.p. e i.n. con rVACV-OVA. (**b**) Combinación de dos experimentos independientes, donde cada punto es un ratón. Se representa la media ± s.e.m (n=4-5/grupo). NS, no significativo; ***, p<0.001; mediante el test estadístico one-way ANOVA, aplicando un test de Bonferroni *a posteriori*.

A continuación, se estudió la contribución de linfocitos T CD8$^+$ de memoria circulante en el control del crecimiento tumoral. Los ratones se inmunizaron (i.p.) con rVACV-OVA, y 30 días después de la generación del repertorio de linfocitos de memoria circulante (Jiang *et al.* 2012) se inocularon con B16-OVA. Se utilizó un antagonista del receptor de la molécula S1P, conocido como FTY720, para inhibir la salida de linfocitos T desde los órganos linfoides secundarios a la sangre o a la linfa (Jiang *et al.* 2012) (**Figura R4a**). Así, se logró limitar la contribución de los linfocitos T de memoria circulante a la respuesta antitumoral.

La administración de FTY720 30 días después de la inmunización i.p. con rVACV-OVA redujo significativamente el número de linfocitos T de memoria circulantes en sangre, específicos para OVA, al mismo nivel que en ratones sin inmunizar (**Figura R4b-c**). Los linfocitos T de memoria circulante generados por la inmunización i.p. con rVACV-OVA fueron suficientes para retrasar el crecimiento del melanoma B16-OVA. El retraso del crecimiento tumoral se eliminó mediante la administración de FTY720 antes de la inoculación del tumor y durante su crecimiento (**Figura R4d**). Estos datos sugieren que la memoria T circulante protege contra el desarrollo de los tumores.

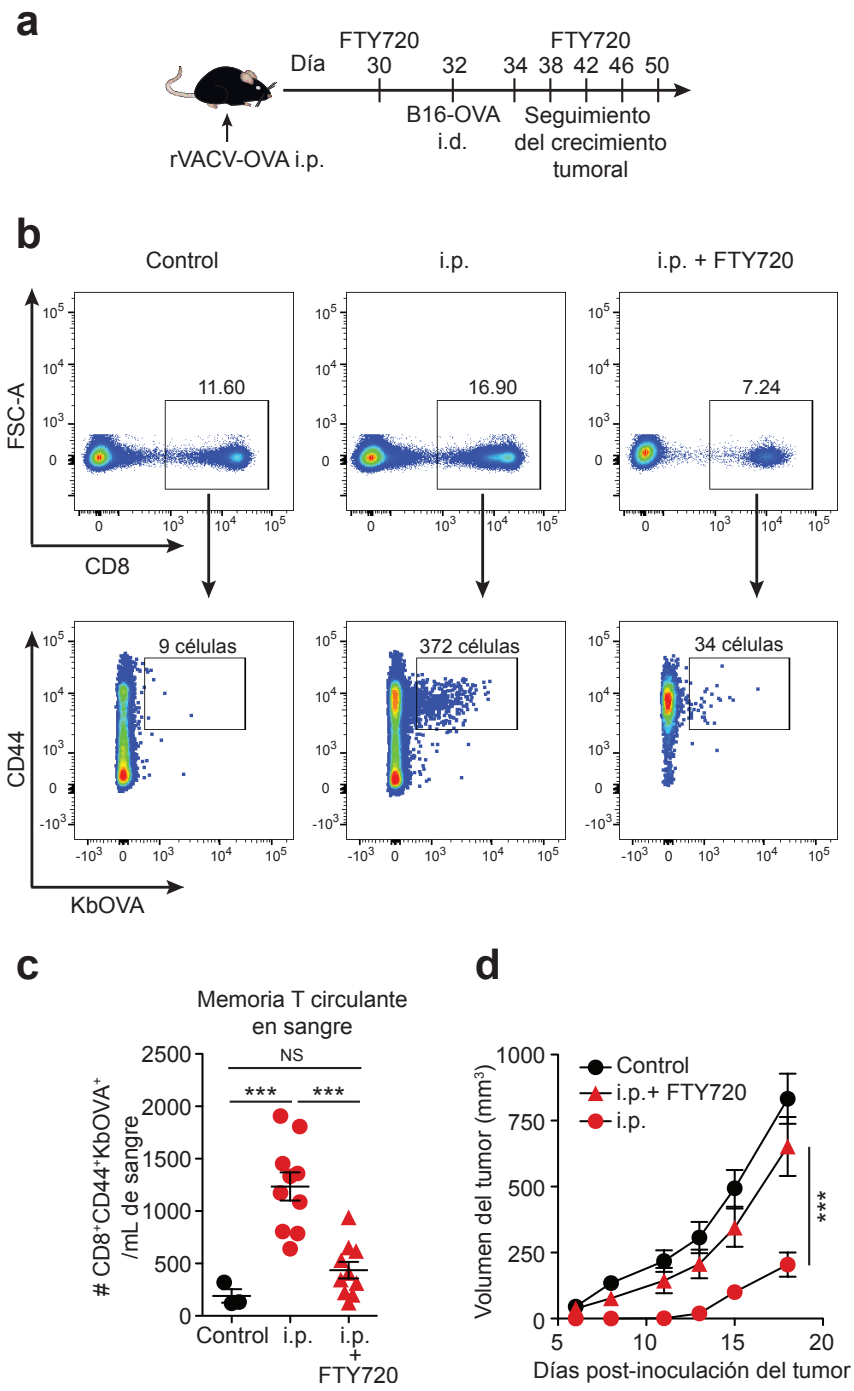

Figura R4. Los linfocitos T CD8$^+$ de memoria circulante son suficientes para retrasar el crecimiento tumoral

(**a**) Esquema de administración de FTY720. Los ratones se inmunizaron (i.p.) con rVACV-OVA. A día 30 y posteriormente cada 4 días, los ratones recibieron (i.p.) 50 µg de FTY720. A día 32, los ratones se inocularon (i.d.) con B16-OVA (10^6 células) en un flanco. (**b**) Gráficos de puntos representativos del análisis por citometría de flujo, que muestran linfocitos T CD8$^+$ de memoria, circulantes en sangre (panel superior), específicos para OVA (panel inferior), tras la primera dosis de FTY720 y previamente a la inoculación del tumor. (**c**) Número de linfocitos T CD8$^+$CD44$^+$KbOVA$^+$ de memoria circulante en sangre. (**d**) Curvas de crecimiento del tumor B16-OVA, representadas como el volumen del tumor (mm^3) en el tiempo (días). (**c-d**) Combinación de dos experimentos independientes, donde cada punto es un ratón y se representa la media ± s.e.m. (**c**) o la media aritmética del volumen de los tumores ± s.e.m. (**d**), (n=5-6/grupo sin inmunizar y 7-8/grupo inmunizado). NS, no significativo, ***, p<0.001; mediante el test estadístico one-way ANOVA (**c**), y el test estadístico two-way ANOVA (**d**) aplicando un test de Bonferroni *a posteriori*.

Simultáneamente, se evaluó la contribución de la Trm en el control inmunológico del crecimiento tumoral (**Figura R5a**).

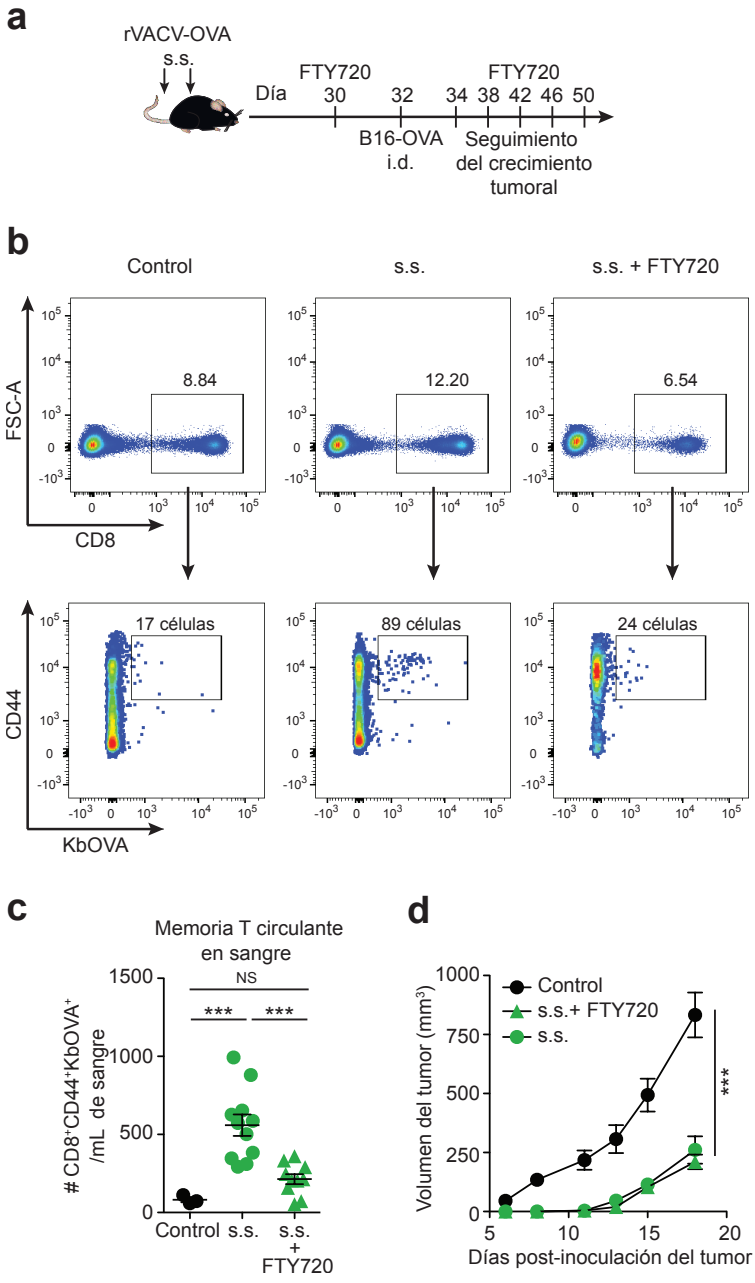

Figura R5. La memoria T CD8$^+$ residente es suficiente para retrasar el crecimiento tumoral
(**a**) Esquema de administración de FTY720. Los ratones se inmunizaron (s.s.) simultáneamente en la cola y en la espalda con rVACV-OVA. A día 30 y posteriormente cada 4 días, los ratones recibieron (i.p.) 50 µg de FTY720. A día 32, los ratones se inocularon (i.d.) con B16-OVA (10^6 células) en un flanco. (**b**) Gráficos de puntos representativos del análisis por citometría de flujo, que muestran linfocitos T CD8$^+$ circulantes en sangre (panel superior), específicos para OVA (panel inferior), tras la primera dosis de FTY720 y previamente a la inoculación del tumor. (**c**) Número de linfocitos T CD8$^+$CD44$^+$KbOVA$^+$ de memoria circulante en sangre. (**d**) Curvas de crecimiento del tumor B16-OVA, representadas como el volumen del tumor (mm^3) en el tiempo (días). (**c-d**) Combinación de dos experimentos independientes, donde cada punto es un ratón y se representa la media ± s.e.m. (**c**) o la media aritmética del volumen de los tumores ± s.e.m. (**d**) (n=5-6/grupo sin inmunizar y 7-8/grupo inmunizado). NS, no significativo, ***, p<0.001; mediante el test estadístico one-way ANOVA (**c**), y el test estadístico two-way ANOVA (**d**) aplicando un test de Bonferroni *a posteriori*.

La inmunización (s.s.) con rVACV-OVA generó tanto memoria circulante como Trm (**Figura R1 y R2**).

En ratones que recibieron FTY720 30 días después de la inmunización (s.s.) con rVACV-OVA disminuyó el número de linfocitos T de memoria circulantes en sangre, específicos para OVA, al mismo nivel que en ratones sin inmunizar (**Figura R5b-c**). En ratones inmunizados y tratados con FTY720 se limitó el efecto de la memoria circulante, pero no el de la memoria residente. En este grupo se retrasó el crecimiento tumoral al mismo nivel que en los ratones inmunizados y que no fueron tratados con el inhibidor (**Figura R5d**). Este resultado sugiere que los linfocitos Trm son suficientes para el rechazo del tumor.

En conjunto, los resultados indican que ambos tipos de memoria T $CD8^+$ (circulante y residente) son suficientes para retrasar el crecimiento del melanoma B16-OVA.

8.2 La memoria T $CD8^+$ residente en presencia de la memoria T $CD8^+$ circulante mejora la respuesta inmunitaria contra el tumor

Para estudiar la colaboración entre los linfocitos T $CD8^+$ de memoria residente y circulante durante el control del crecimiento tumoral, se utilizó una estrategia de parabiosis.

Los ratones en parabiosis compartieron la memoria T $CD8^+$ circulante, pero solamente los ratones inmunizados tenían Trm (**Figura R6a**). Brevemente, los ratones se inmunizaron con rVACV-OVA y 30 días después se unieron quirúrgicamente con ratones sin inmunizar. La memoria T $CD8^+$ circulante recirculó durante 30 días hasta lograr un equilibrio entre ambos parabiontes (**Figura R6b-c**). A continuación, los parabiontes se separaron y se mantuvieron en recuperación durante otros 30 días. Finalmente, los parabiontes individualizados se inocularon con B16-OVA.

Tanto los parabiontes inmunizados como los parabiontes sin inmunizar se protegieron significativamente del tumor, respecto a los ratones control (**Figura R6d-e**). Sin embargo, la incidencia de tumores en parabiontes no inmunizados que contenían linfocitos de memoria T $CD8^+$ circulante fue mayor que en parabiontes inmunizados (**Figura R6d**). El retraso en el inicio del tumor en parabiontes inmunizados que contenían

linfocitos Trm resultó en un retraso significativo del crecimiento y desarrollo del tumor (**Figura R6e**).

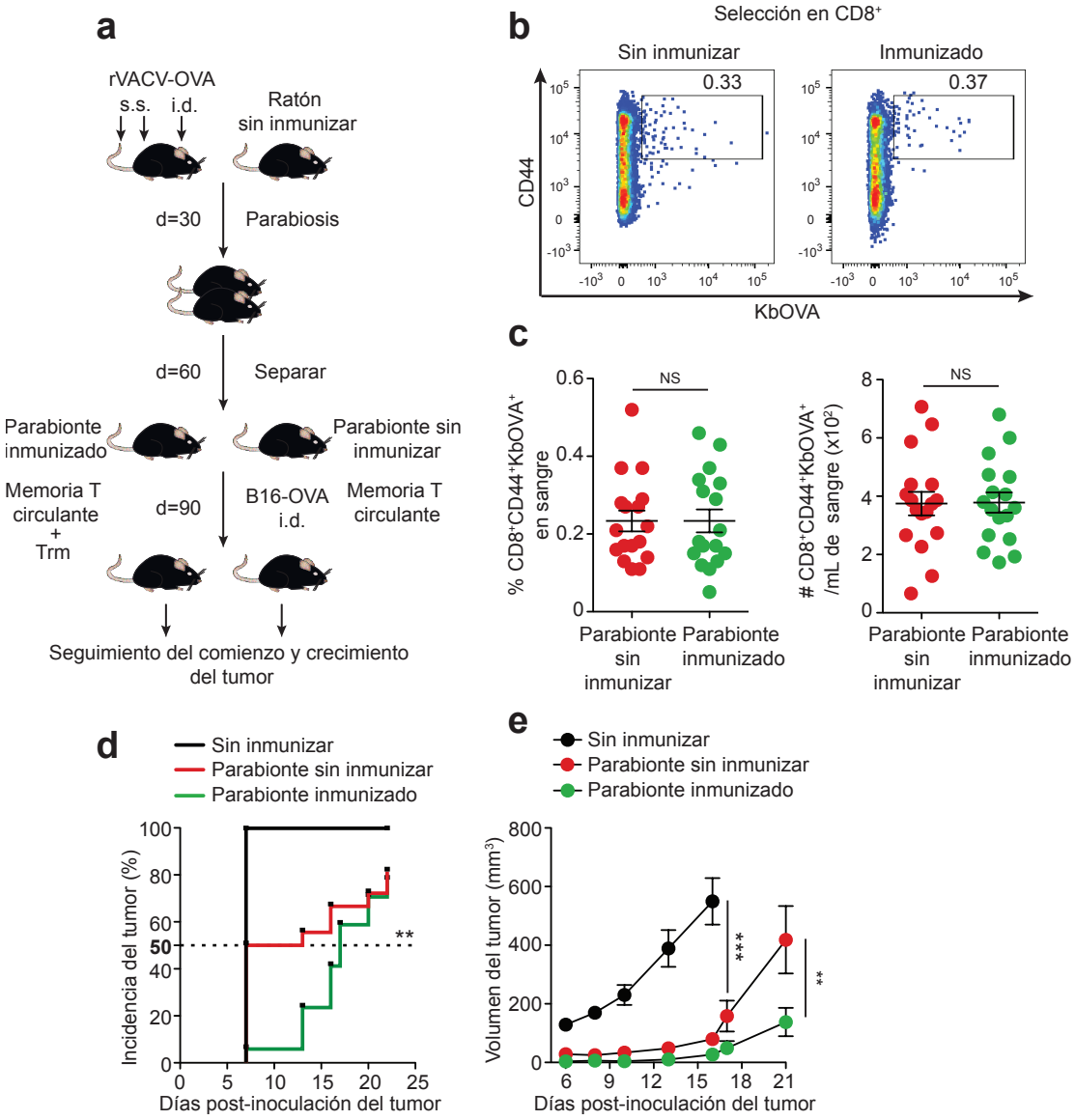

Figura R6. La inducción de memoria T residente aumenta la inmunidad antitumoral
(**a**) Esquema de la estrategia de parabiosis. Los ratones se inmunizaron simultáneamente en la cola (s.s.), la espalda (s.s.) y la oreja (i.d.) con rVACV-OVA. Posteriormente (30 días), los ratones inmunizados se unieron quirúrgicamente con ratones sin inmunizar. A continuación (30 días), los parabiontes se separaron y se mantuvieron en recuperación durante otros 30 días. Finalmente, los ratones individualizados se inocularon (i.d.) con B16-OVA (10^6 células) en un flanco. (**b**) Gráficos de puntos representativos del análisis por citometría de flujo, que muestran linfocitos T $CD8^+CD44^+KbOVA^+$ de memoria, circulantes en sangre, previamente a la inoculación del tumor. (**c**) Frecuencia (panel izquierdo) y número (panel derecho) de linfocitos T $CD8^+CD44^+KbOVA^+$ de memoria, circulantes en sangre, a tiempo anterior a la inoculación del tumor. (**d**) Incidencia del tumor, representada como la detección de tumores por primera vez (%) en el tiempo (días). La línea discontinua indica el 50% de ratones con tumores detectables. (**e**) Curvas de crecimiento del tumor B16-OVA, representada como el volumen del tumor (mm^3) en el tiempo (días). (**c-e**) Combinación de dos experimentos independientes, donde cada punto es un ratón y se representa como la media ± s.e.m. (**c**), como frecuencia (**d**) y como la media aritmética del volumen de los tumores ± s.e.m. (**e**), (n=5-6/grupo control y 8-9/grupo vacunado). NS, no significativo, ***, p<0.001; **, p<0.01; mediante el test estadístico de la t de Student con dos colas y sin parear (**c**), el test estadístico de regresión de Cox de efectos mixtos (**d**) y el test estadístico two-way ANOVA (**e**) aplicando un test de Bonferroni *a posteriori*.

Los resultados sugieren que los linfocitos Trm en presencia de linfocitos T CD8$^+$ de memoria circulante mejoran la respuesta antitumoral, si se compara con un escenario en el que solo participan linfocitos T CD8$^+$ de memoria circulante.

8.3 Los linfocitos T CD8$^+$ de memoria central generan memoria residente en un contexto viral

Tras la inmunización en piel con rVACV-OVA los linfocitos T OT-I naive (CD44^{lo}CD62L^{hi}) se convierten tanto en memoria circulante como en Trm de piel (Gaide *et al.* 2015). Se estudió la plasticidad de linfocitos T CD8$^+$ de memoria circulante para producir Trm en un contexto viral (**Figura R7**).

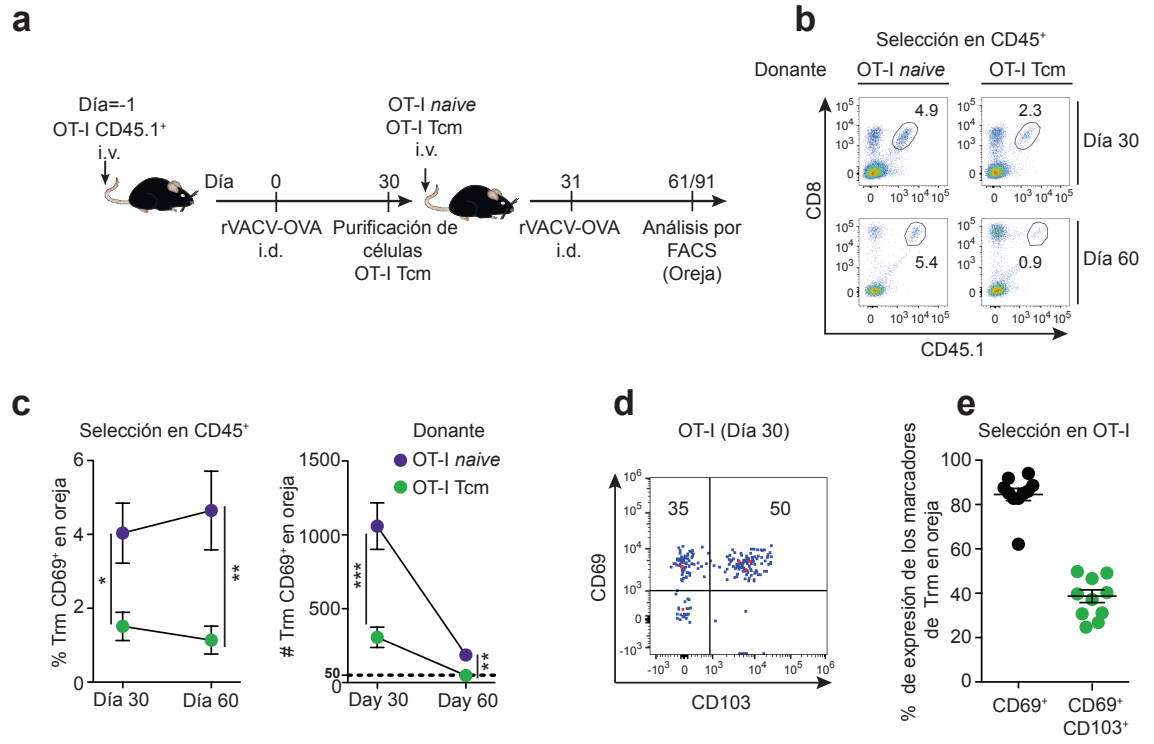

Figura R7. Los linfocitos T CD8$^+$ de memoria central se convierten en memoria residente después de una infección viral

(**a**) Esquema para la evaluación de la plasticidad de linfocitos T CD8$^+$ de memoria central (Tcm). Para la generación de linfocitos CD8$^+$ Tcm, los ratones se transfirieron con linfocitos T OT-I *naive* CD45.1$^+$ (1-3×10^5 células) y se inmunizaron (i.d.) con rVACV-OVA (5×10^4 p.f.u.) en la oreja. Después de 30 días, los linfocitos CD8$^+$ Tcm se purificaron. Nuevos ratones se transfirieron con linfocitos T OT-I CD45.1$^+$ *naive* o Tcm, un día antes de la inmunización (i.d) con rVACV-OVA en la oreja. (**b**) Gráficos de puntos representativos del análisis por citometría de flujo, que muestran linfocitos OT-I seleccionados previamente en la población CD45$^+$ de la oreja. (**c**) Frecuencia (panel izquierdo) y número (panel derecho) de linfocitos OT-I CD8$^+$CD69$^+$ (Trm, residentes) en la oreja. (**d**) Gráfico de puntos representativo del análisis por citometría de flujo, donde se muestra la expresión de los marcadores fenotípicos Trm, en linfocitos OT-I 30 d.p.i. (**e**) Frecuencia de expresión de los marcadores fenotípicos de Trm (CD69 y CD103), en linfocitos OT-I de la oreja 30 d.p.i. (**c, e**) Combinación de dos experimentos independientes, representados como la media aritmética ± s.e.m. (**c**) y como ratones individuales mostrando la media aritmética ± s.e.m. (**e**), (n=5-6/grupo). ***, p<0.001; **, p<0.01; *, p<0.05; mediante el test estadístico de la t de Student con dos colas y sin parear (**c**).

Para ello, los ratones se transfirieron con linfocitos T OT-I y se inmunizaron con rVACV-OVA. Después de 30 días se purificaron linfocitos T OT-I de memoria central (OT-I Tcm, $CD44^{hi}$ $CD62L^{hi}$). Se utilizaron linfocitos T OT-I *naive* como control positivo de plasticidad. Se evaluó la generación de linfocitos Trm, 30 o 60 días después de la transferencia de ambos tipos celulares (OT-I *naive* y OT-I Tcm) y la inmunización en la oreja con rVACV-OVA (**Figura R7a**).

Los linfocitos Tcm generaron Trm en piel, 30 o 60 días después de la infección viral, aunque con menor eficiencia que los linfocitos T OT-I *naive (***Figura R7b-c**). Más del 90% de los linfocitos T OT-I en la oreja derivados de linfocitos OT-I Tcm transferidos expresaron CD69 establemente, y el 50% de ellos expresó simultáneamente CD103 (**Figura R7d-e**), lo cual es consistente con resultados previos (Jiang *et al.* 2012; Gaide *et al.* 2015).

Para demostrar funcionalmente que los linfocitos T OT-I Trm derivados de linfocitos OT-I Tcm transferidos eran verdaderos linfocitos Trm, se evaluó su capacidad de migración por sangre o linfa una vez se establecieron en la piel de los ratones, mediante una estrategia de parabiosis (**Figura R8a**).

Los ratones se transfirieron con OT-I Tcm un día antes de la inmunización con rVACV-OVA. Después de 30 días, ratones transferidos e inmunizados se unieron quirúrgicamente con ratones sin inmunizar para crear parabiontes. A continuación, los ratones compartieron la memoria circulante durante 30 días (**Figura R8a**). Se analizaron los linfocitos T OT-I de memoria circulante en bazo y linfocitos T OT-I Trm en la oreja de ratones inmunizados y sin inmunizar.

Mientras en ambos parabiontes, inmunizados y sin inmunizar, los bazos presentaban la misma frecuencia y número de linfocitos T OT-I de memoria circulante (**Figura R8b**), solamente las orejas de parabiontes inmunizados tenían linfocitos Trm $CD69^{+}CD103^{+}$ (**Figura R8c-d**). Los resultados demuestran que las Trm derivadas de las Tcm son incapaces de migrar a través de la sangre o la linfa.

8.4 La memoria T $CD8^{+}$ central genera memoria residente después de la inoculación de un tumor

Para analizar si las Tcm se convierten en Trm después de la inoculación de un tumor, los ratones WT se transfirieron con linfocitos OT-I Tcm y se inocularon con B16-

OVA (**Figura R9a**). Se analizaron los linfocitos infiltrados en el tumor 20 días después. La mayoría de linfocitos OT-I que se encontraron dentro del tumor,

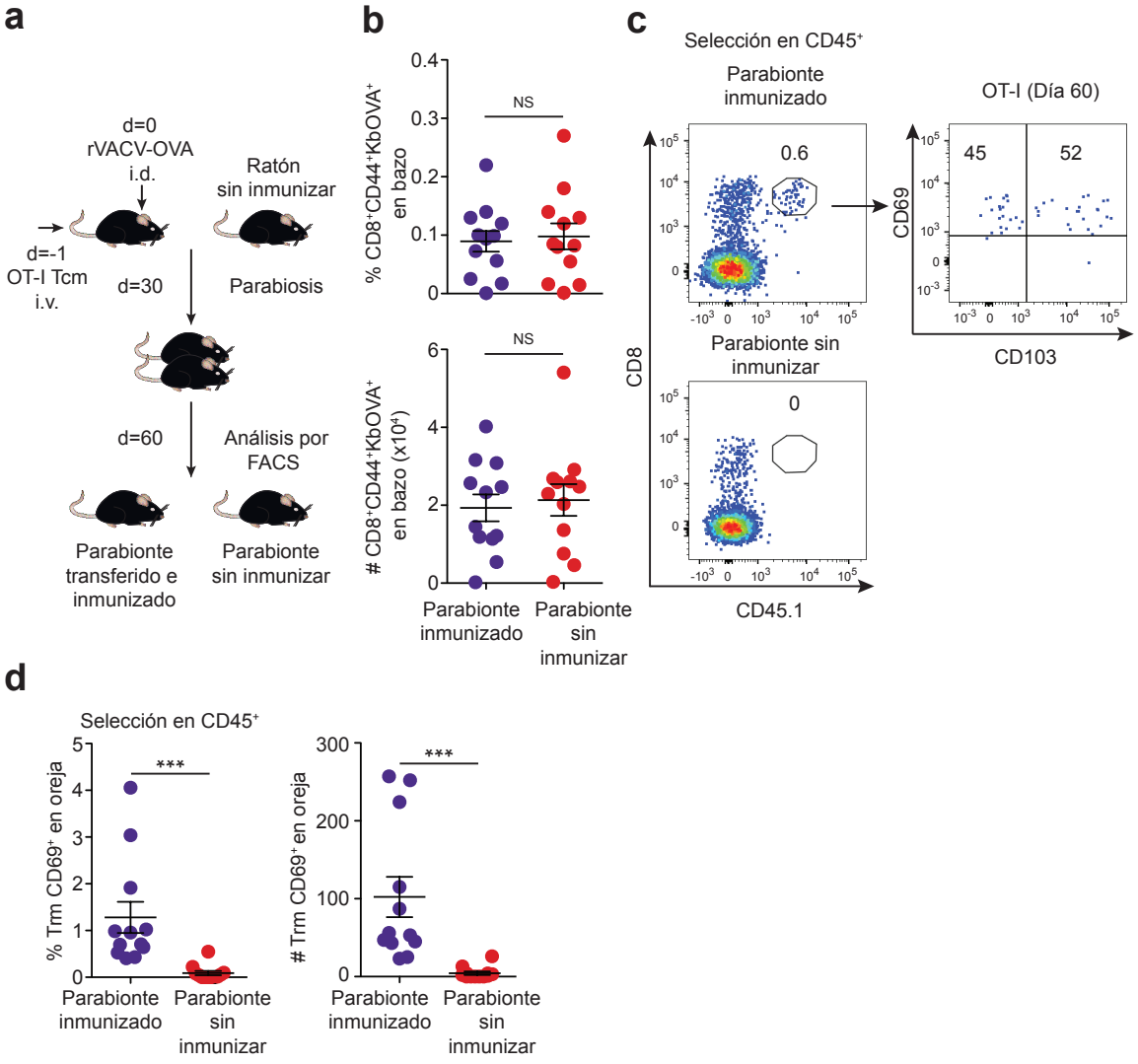

Figura R8. Los linfocitos T de memoria residente provenientes de memoria central no migran después de haberse establecido

(**a**) Esquema de evaluación de la residencia de linfocitos T mediante parabiosis. Para la generación de linfocitos T $CD8^+$ de memoria central (Tcm), los ratones se transfirieron con linfocitos T OT-I $CD45.1^+$ ($1\text{-}3\times10^5$ células) y se inmunizaron (i.d.) con rVACV-OVA (5×10^4 p.f.u.) en la oreja. Después de 30 días, los linfocitos $CD8^+$ Tcm se purificaron y se transfirieron. Nuevos ratones se transfirieron (i.v) con linfocitos OT-I $CD45.1^+$ Tcm y se inmunizaron (i.d.) con el virus rVACV-OVA en una oreja. Posteriormente (30 días), los ratones transferidos e inmunizados se unieron quirúrgicamente con ratones sin inmunizar. A continuación (30 días), se analizaron las orejas de los parabiontes mediante citometría de flujo para la detección de linfocitos Trm. (**b**) Frecuencia (panel superior) y número (panel inferior) de linfocitos T $CD8^+CD44^+KbOVA^+$ circulantes en el bazo de los parabiontes, 30 días después de la cirugía. (**c**) Gráficos de puntos representativos del análisis por citometría de flujo, que muestran linfocitos OT-I seleccionados dentro de la población $CD45^+$ en la oreja (panel izquierdo superior, parabionte inmunizado; panel izquierdo inferior, parabionte sin inmunizar), donde se evalúa la expresión de marcadores fenotípicos de linfocitos Trm (panel derecho, parabionte inmunizado). (**d**) Frecuencia (panel izquierdo) y número (panel derecho) de linfocitos T $CD8^+CD69^+$ en las orejas de los parabiontes indicados. (**b, d**) Combinación de dos experimentos independientes, donde cada punto es un ratón y se representa como la media aritmética ± s.e.m. (n=5-6/grupo). NS, no significativo, ***, $p<0.001$; mediante el test estadístico de la t de Student con dos colas y sin parear (**b**) y el test estadístico no paramétrico Mann-Whitney con dos colas (**d**).

expresaron marcadores fenotípicos de Trm. Más del 90% de los OT-I expresaron CD69 establemente, y el 50% de ellos expresó simultáneamente CD103 (**Figura R9b-d**).

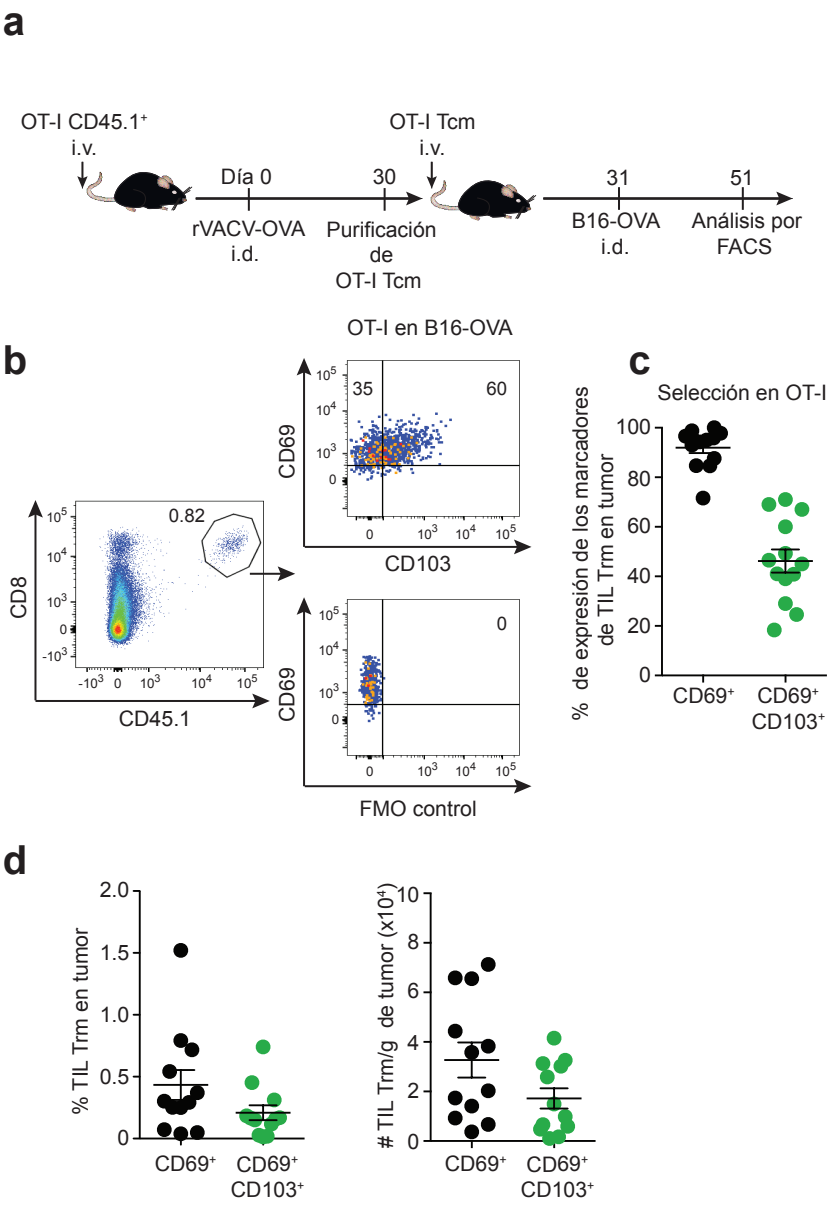

Figura R9. Los linfocitos T CD8$^+$ de memoria central expresan marcadores fenotípicos de linfocitos T CD8$^+$ de memoria residente cuando infiltran un melanoma B16

(**a**) Esquema para la evaluación de la plasticidad de la memoria T CD8$^+$ central (Tcm). Para generar Tcm los ratones se transfirieron con linfocitos T OT-I CD45.1$^+$ (1-3×10^5 células) y se inmunizaron (i.d.) con rVACV-OVA (5×10^4 p.f.u.) en la oreja. Después de 30 días la Tcm se purificó. Nuevos ratones se transfirieron con linfocitos OT-I CD45.1$^+$ Tcm, un día antes de la inoculación (i.d.) con B16-OVA en un flanco. (**b**) Gráficos de puntos representativos del análisis por citometría de flujo de linfocitos OT-I que infiltraron el tumor B16-OVA (panel izquierdo), donde se muestra la expresión de marcadores fenotípicos de Trm (panel superior derecho), en ratones que desarrollaron tumor durante 23 días. (**c**) Frecuencia de expresión de los marcadores fenotípicos de Trm, en linfocitos OT-I que infiltraron el tumor B16-OVA 23 días después de la inoculación. (**d**) Frecuencia (panel izquierdo) y número (panel derecho) de linfocitos OT-I, donde se indican los marcadores fenotípicos de Trm, en suspensiones celulares de melanoma B16-OVA de ratones que han desarrollado tumor durante 23 días. (**c**, **d**) Combinación de tres experimentos independientes, donde cada punto es un ratón y se representa como la media aritmética ± s.e.m. (n=3-5/grupo).

Para descartar que el proceso anterior fuera dependiente de una sola línea tumoral, se utilizó la línea de adenocarcinoma MC38-OVA como alternativa (**Figura R10a**).

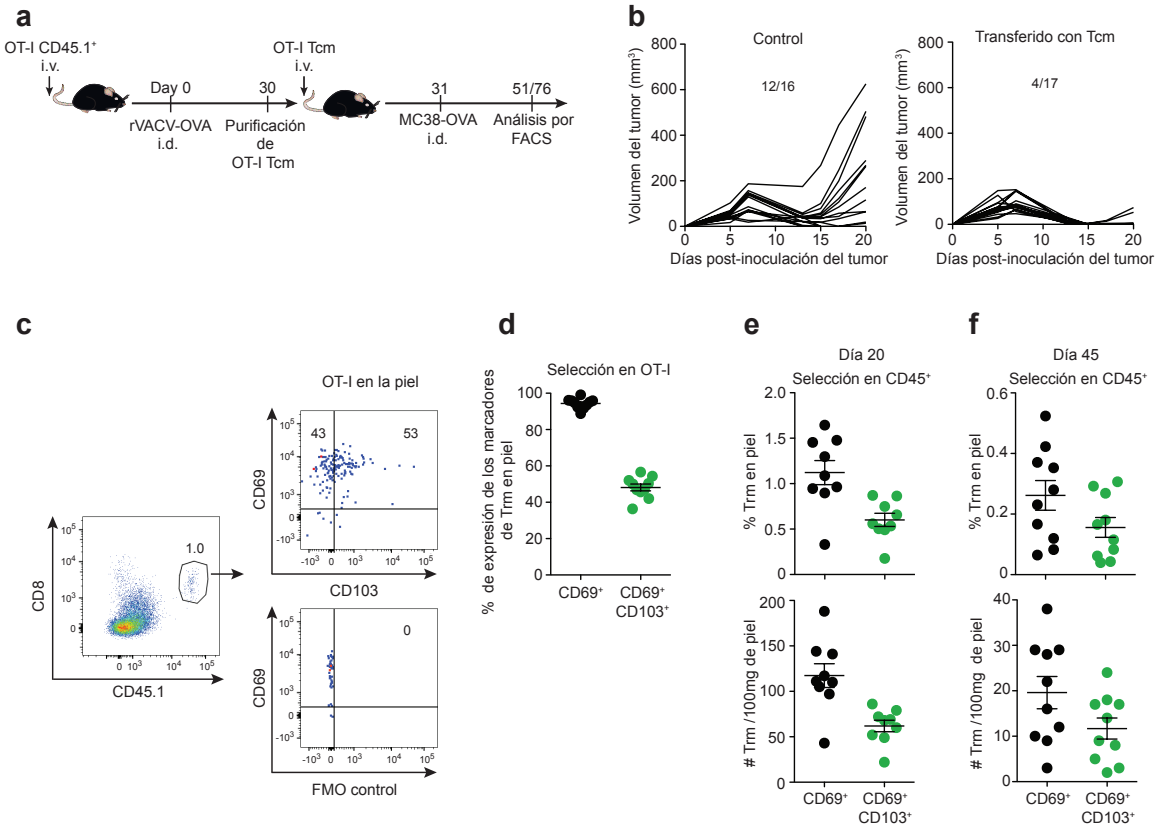

Figura R10. Los linfocitos T CD8$^+$ de memoria central permanecen en la piel como verdadera memoria residente, en ratones que rechazan el tumor MC38

(**a**) Esquema de evaluación de la plasticidad de linfocitos T CD8$^+$ de memoria central (Tcm). Para la generación de linfocitos CD8$^+$ Tcm los ratones se transfirieron con linfocitos T OT-I *naive* CD45.1$^+$ (1-3×10^5 células) y se inmunizaron (i.d.) con rVACV-OVA (5×10^4 p.f.u.) en la oreja. Después de 30 días, los linfocitos CD8$^+$ Tcm se purificaron. Nuevos ratones se transfirieron (i.v.) con linfocitos OT-I CD45.1$^+$ Tcm, un día antes de la inoculación (s.c.) del tumor MC38-OVA en un flanco. (**b**) Curvas individuales de crecimiento del tumor MC38-OVA, representadas como el volumen del tumor (mm^3) en el tiempo (días), en ratones control (panel izquierdo) y en ratones tratados con linfocitos OT-I Tcm un día antes de la inoculación del tumor (panel derecho). Los números en la parte superior del gráfico representan el número de animales que desarrollaron tumores relativo al total de animales utilizados en el ensayo. (**c**) Gráficos de puntos representativos del análisis por citometría de flujo en linfocitos OT-I que permanecieron en la piel de ratones que rechazaron completamente el tumor MC38-OVA (panel izquierdo), donde se muestra la expresión de los marcadores fenotípicos de linfocitos Trm (panel derecho). (**d**) Frecuencia de la expresión de los marcadores fenotípicos de linfocitos Trm (CD69 y CD103), en linfocitos OT-I residentes en la piel de ratones que rechazaron el tumor. (**e**, **f**) Frecuencia (panel superior) y número (panel inferior) de linfocitos OT-I expresando marcadores fenotípicos de linfocitos Trm que permanecieron en la piel de ratones que rechazaron el tumor, después de 20 (**e**) y 45 (**f**) días tras la inoculación del tumor. (**b, d-f**) Combinación de dos experimentos independientes, representados como las curvas de crecimiento de los tumores individuales (**b**), y cada ratón como un punto, representado como la media aritmética ± s.e.m. (**d, e, f**), (n=5 y 11/grupo control y n=10 y 7/grupo transferido con Tcm).

La transferencia adoptiva de linfocitos OT-I Tcm a los ratones eliminó totalmente el crecimiento y desarrollo del tumor MC38-OVA (**Figura R10b**). Esto permitió analizar la presencia de linfocitos Trm en las proximidades de la piel donde previamente se había

rechazado el tumor, después de 20 y 45 días de la inoculación del tumor. Más del 90% de los linfocitos OT-I que se encontraron en la piel expresaron CD69 establemente, y el 50% de ellos expresó simultáneamente CD103 (**Figura R10c-f**). Los resultados sugieren que los linfocitos Tcm retienen un potencial para generar linfocitos Trm en un contexto tumoral. Esta plasticidad de la memoria T contribuye a explicar por qué los linfocitos Tcm son suficientes para retrasar el crecimiento del tumor.

8.5 Anti-PD-1 aumenta la infiltración de linfocitos T CD8$^+$ con fenotipo Trm en el tumor

Se estudió el efecto del anticuerpo anti-PD-1 sobre la transferencia adoptiva de linfocitos OT-I Tcm y el control del crecimiento del tumor. Los linfocitos Tcm del ganglio linfático que drena el tumor (TdLN), y en especial los linfocitos parecidos a las Trm que infiltraron el tumor B16-OVA expresaron altos niveles de PD-1 (**Figura R11a-b**). Este dato sugería que se podía mejorar su función, si se bloqueaba PD-1. Los ratones con tumores se transfirieron con linfocitos Tcm y se trataron simultáneamente con el anticuerpo anti-PD-1 siguiendo un esquema terapéutico (**Figura R11c**). El tratamiento con anti-PD-1 y linfocitos Tcm disminuyó el desarrollo del tumor B16-OVA (**Figura R11d**), si se compara con la transferencia adoptiva de Tcm sola.

La frecuencia y el número de linfocitos OT-I con marcadores fenotípicos de Trm que infiltraron el tumor (**Figura R11e**), fue 10 veces mayor en los ratones que recibieron anti-PD-1 (**Figura R11f**). Sin embargo, el tratamiento con anti-PD-1 no afectó la frecuencia ni el número de OT-I en los dLNs (**Figura R11g**).

Para descartar que el efecto de anti-PD1 fuera dependiente de una sola línea tumoral se utilizó la línea de adenocarcinoma MC38-OVA como alternativa. Los linfocitos OT-I Tcm del TdLN y aquellos que infiltraron el tumor MC38-OVA expresaron altos niveles de PD-1 (**Figura R12a-b**). Los ratones con tumores se transfirieron con linfocitos Tcm y se trataron simultáneamente con anti-PD-1 (**Figura R12c**). El tratamiento con anti-PD-1 y linfocitos Tcm disminuyó el crecimiento del tumor MC38-OVA (**Figura R12d**).

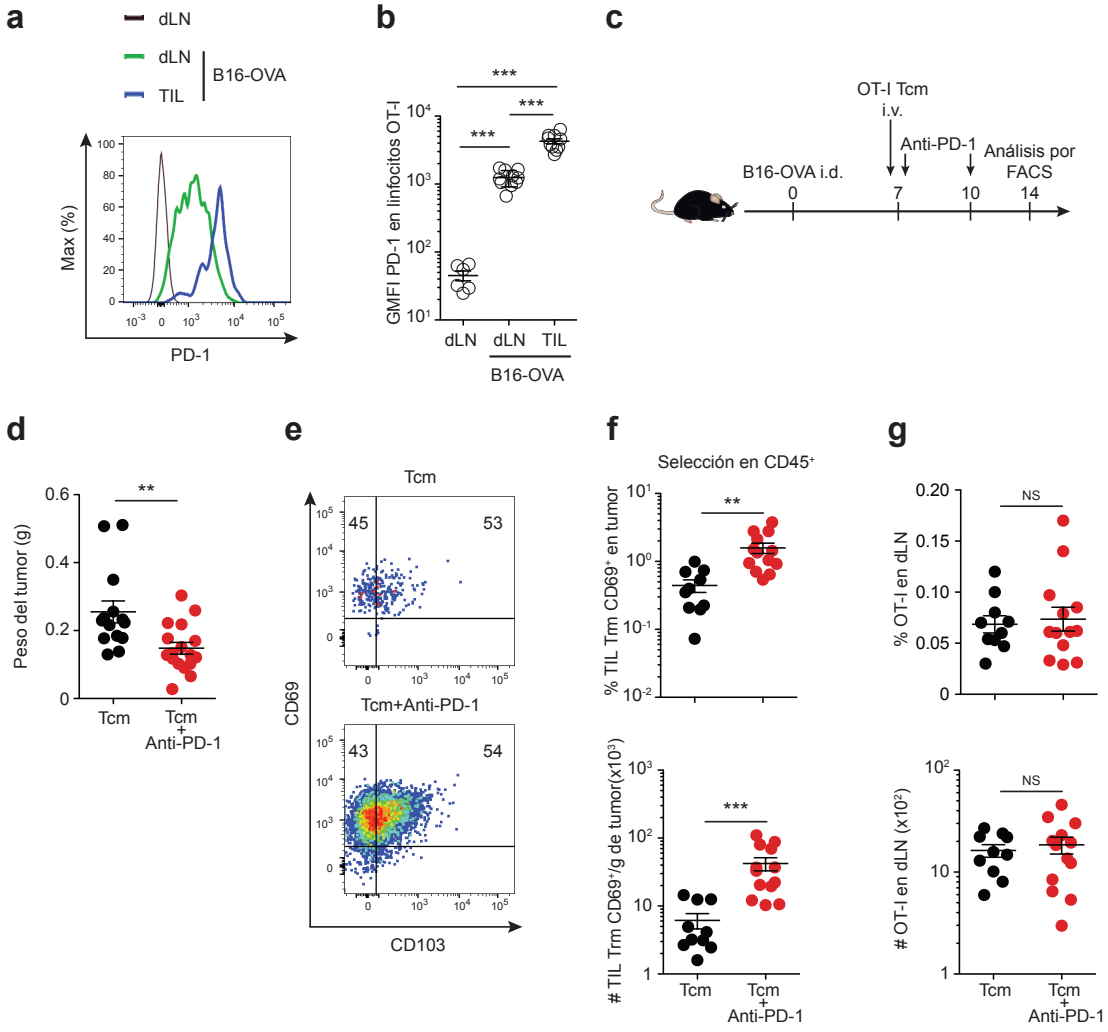

Figura R11. Anti-PD-1 aumenta la infiltración de linfocitos T con fenotipo Trm y retrasa el crecimiento del melanoma B16

Se inocularon (i.d.) ratones con B16-OVA y siete días después se transfirieron con linfocitos OT-I CD45.1$^+$ Tcm. (**a**) Histograma representativo del análisis por citometría de flujo de la expresión de PD-1 en linfocitos OT-I de memoria central (Tcm). El análisis por citometría de flujo se realizó 7 días después de la transferencia adoptiva, en los ganglios drenantes (dLN) y en los linfocitos que infiltraron el tumor (TIL). (**b**) Frecuencia de expresión de PD-1 en linfocitos transferidos, presentes en el dLN y dentro del tumor (TIL). (**c**) Esquema de inmunoterapia con Tcm y anti-PD-1. Los ratones se inocularon (i.d) con B16-OVA, se transfirieron con linfocitos OT-I CD45.1$^+$ Tcm y se trataron con anti-PD-1. (**d**) Peso del tumor en el momento del sacrificio. (**e**) Gráficos de puntos representativos del análisis por citometría de flujo de linfocitos OT-I que infiltraron el tumor, donde se muestra la expresión de marcadores fenotipos de Trm. (**f, g**) Frecuencia (panel superior) y número (panel inferior) de linfocitos T OT-I que infiltraron el tumor B16-OVA (**f**) o permanecieron en dLN (**g**). (**b, d, f, g**) Combinación de tres (**b**, **f**, **g**) o cuatro (**d**) experimentos independientes, donde cada punto es un ratón y se representa como la media aritmética ± s.e.m. (**b**) (n=2-3/grupo control, 3-4/grupo con tumores), (**d**, **f**, **g**) (n=3-5/grupo). NS, no significativo, ***, p<0.001; **, p<0.01; mediante el test estadístico one-way ANOVA (**b**) aplicando un test de Bonferroni *a posteriori*, el test estadístico de la t de Student con dos colas y sin parear (**f** panel superior, **g**) y el test estadístico no paramétrico Mann-Whitney con dos colas (**d**, **f** panel inferior).

Los linfocitos OT-I con marcadores fenotípicos de Trm que infiltraron el tumor fueron 10 veces mayor en la combinación (**Figura R12e**). Sin embargo, los linfocitos OT-I en los dLN no fueron diferentes en frecuencia, ni en número (**Figura R12f**).

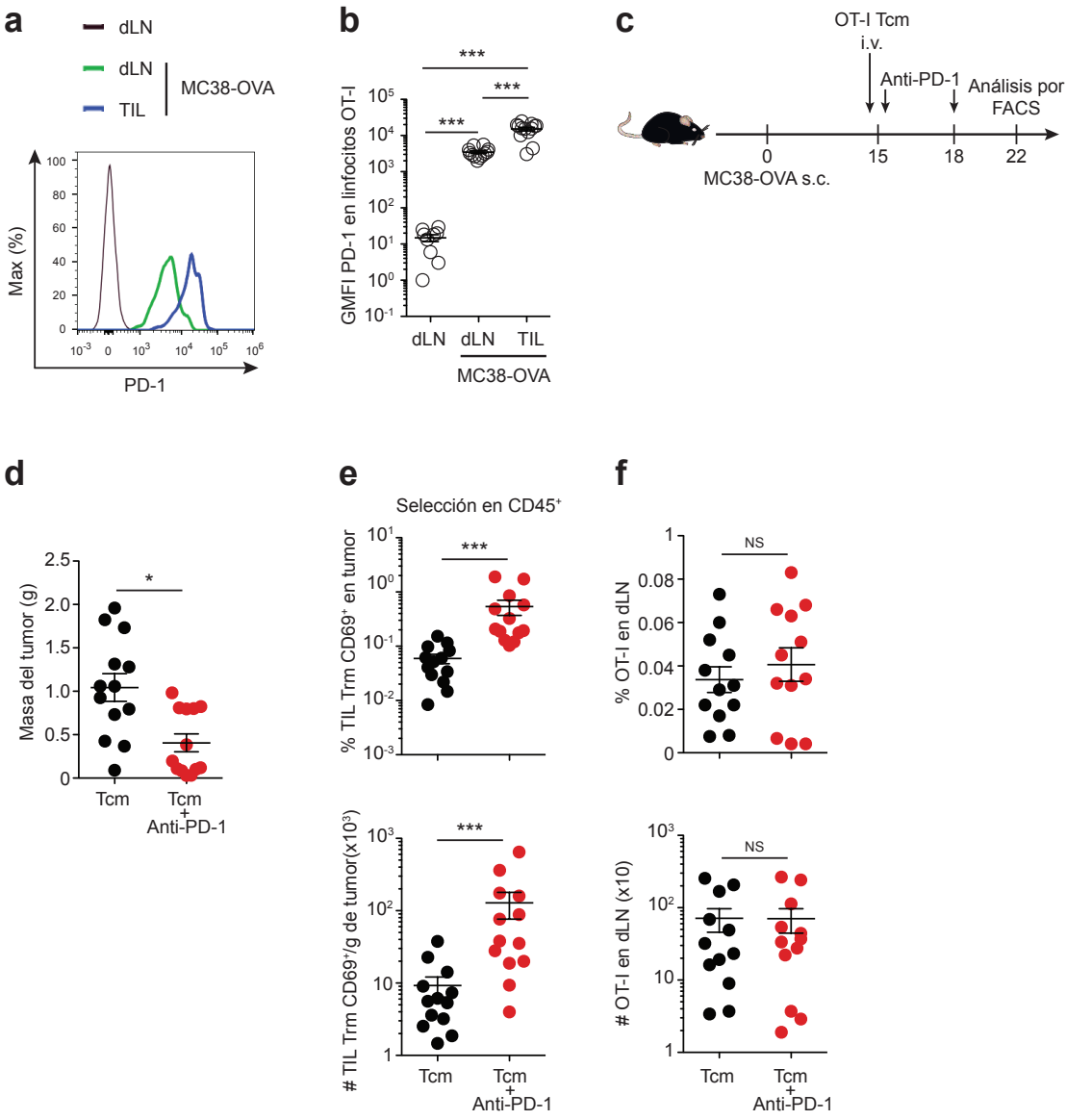

Figura R12. Anti-PD-1 aumenta la infiltración de linfocitos T con fenotipo Trm y retrasa el crecimiento del tumor MC38.

Se inocularon (s.c.) ratones con tumor MC38-OVA y 15 días después se transfirieron con linfocitos OT-I CD45.1$^+$ Tcm. (**a**) Histograma representativo del análisis por citometría de flujo de la expresión de PD-1 en linfocitos OT-I de memoria central (Tcm). El análisis por citometría de flujo se realizó 7 días después de la transferencia adoptiva, en linfocitos que infiltraron el ganglio drenante (dLN) y el tumor (TIL). (**b**) Frecuencia de la expresión de PD-1 en los linfocitos transferidos, presentes en el dLN y dentro del tumor (TIL). (**c**) Esquema de la inmunoterapia con Tcm y anti-PD-1. Los ratones se inocularon (s.c.) con tumor MC38-OVA, se transfirieron con linfocitos OT-I CD45.1$^+$ Tcm, y se trataron con anti-PD-1. (**d**) Peso del tumor en el momento del sacrificio. (**e, f**) Frecuencia (panel superior) y número (panel inferior) de linfocitos T OT-I CD69$^+$ que infiltraron el tumor MC38-OVA (**e**) o permanecieron en dLN (**f**). (**b**, **d**, **e**, **f**) Combinación de tres experimentos independientes, donde cada punto es un ratón y se representa como la media aritmética ± s.e.m. (**b**) (n=2-3/grupo control, 3-4/grupo con tumores), (**d**, **e**, **f**) (n=3-5/grupo). NS, no significativo, ***, p<0.001; *, p<0.05; mediante el test estadístico one-way ANOVA (**b**) aplicando un test de Bonferroni *a posteriori*, el test estadístico de la t de Student con dos colas y sin parear (**f** panel superior) y el test estadístico no paramétrico Mann-Whitney con dos colas (**d**, **e, f** panel inferior).

En conjunto, los resultados sugieren que el tratamiento con el anticuerpo anti-PD-1 aumenta la infiltración de linfocitos con marcadores fenotípicos de Trm y retrasa el crecimiento del tumor, después de una transferencia adoptiva con linfocitos Tcm.

8.6 La respuesta antitumoral de linfocitos T CD8$^+$ de memoria es deficiente en ratones *Batf3*$^{-/-}$

La generación de linfocitos Trm mediante la infección con rVACV-OVA depende de las DCs que realizan la presentación cruzada de antígenos y requieren la expresión de Batf3. Por el contrario, la generación de linfocitos Tcm es independiente (Iborra *et al.* 2016).

Consistentemente, se demostró que la generación de linfocitos Trm, endógenos y específicos para OVA (**Figura R13a-b**), pero no de linfocitos T CD8$^+$ de memoria circulante (**Figura R13c**), inducidos mediante la inmunización (s.s.) con rVACV-OVA fue deficiente en ratones *Batf3*$^{-/-}$.

Estos resultados sugerían que la deficiencia en la generación de Trm en ratones *Batf3*$^{-/-}$ disminuiría la eficiencia de la respuesta antitumoral. Para comprobar esta hipótesis, los ratones WT y *Batf3*$^{-/-}$ se dividieron en dos grupos experimentales. El primer grupo se inmunizó por vía s.s. e i.n., que producen Trm, mientras que el segundo grupo se inmunizó por vía i.p., que produce memoria circulante pero no produce Trm.

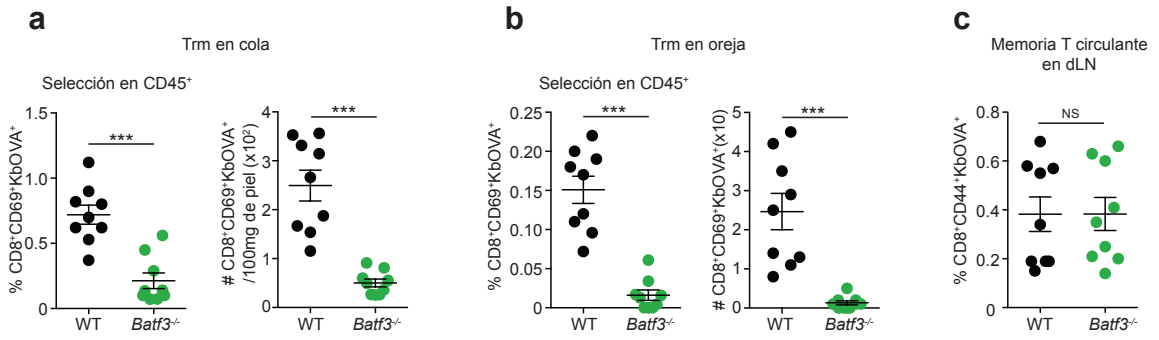

Figura R13. La generación de memoria T residente depende de células dendríticas que requieren la expresión de Batf3
Ratones WT y *Batf3*$^{-/-}$ se inmunizaron en la cola (s.s.) con rVACV-OVA. (**a**, **b**) Frecuencia (panel izquierdo) y número (panel derecho) de linfocitos T CD8$^+$ de memoria residente en la cola (**a**), en la oreja (**b**), frecuencia de linfocitos T CD8$^+$ de memoria circulante en el ganglio drenante (dLN) (**c**); endógenos, específicos para OVA, 30 días después de la inmunización. Combinación de dos experimentos independientes, donde cada punto es un ratón y se representa como la media aritmética ± s.e.m. (n=4-5/grupo). NS, no significativo, ***, p<0.001; mediante el test estadístico de la t de Student con dos colas y sin parear.

En el primer grupo experimental los ratones WT y *Batf3*$^{-/-}$ inmunizados por vía

s.s. se inocularon 30 días después con B16-OVA en un flanco (**Figura R14a**). El factor de transcripción Batf3 contribuyó significativamente a la respuesta antitumoral. Mientras que los ratones WT se protegieron, los ratones *Batf3*$^{-/-}$ no se protegieron del tumor después de la inmunización (**Figura R14b**). Los ratones inmunizados por la vía i.n. se inocularon 30 días después por vía i.v. con B16-OVA (**Figura R14c**). Consistentemente, los ratones WT se protegieron mientras que los ratones *Batf3*$^{-/-}$ no se protegieron del tumor después de la inmunización (i.n.). Estos resultados apoyan la hipótesis inicialmente planteada sobre las vías de s.s. e i.n., capaces de generar Trm.

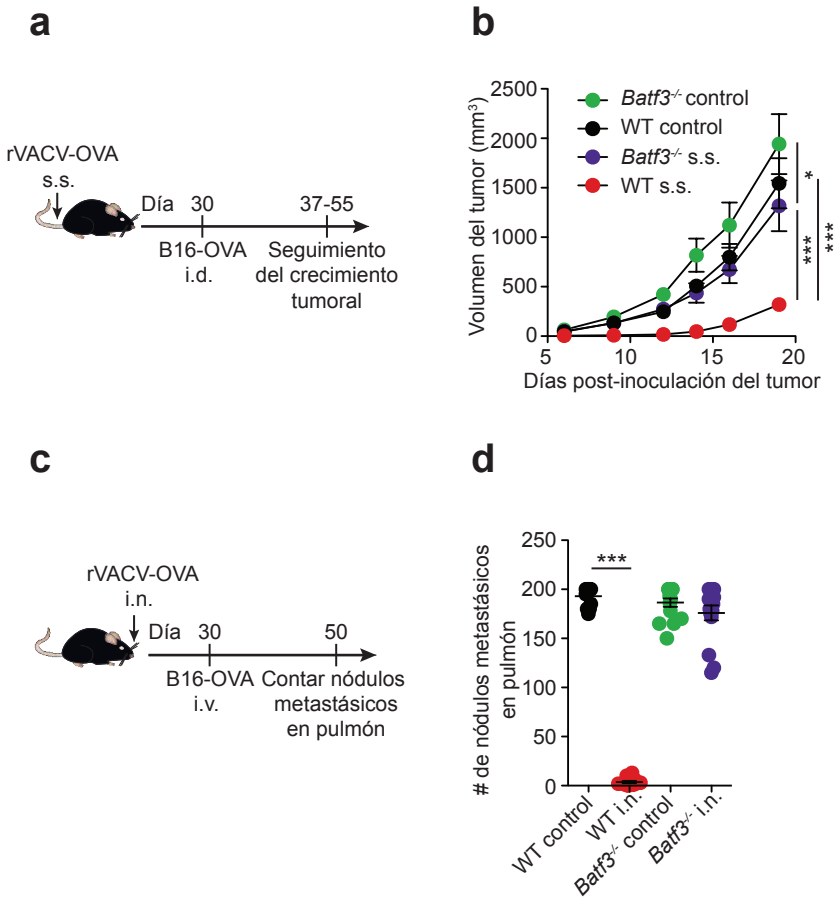

Figura R14. La inmunización con rVACV-OVA mediante escarificación de la piel o infección intranasal no protege ratones *Batf3*$^{-/-}$ contra el melanoma B16-OVA
(a) Esquema de inmunización (s.s.) contra el melanoma B16-OVA. Los ratones WT y *Batf3*$^{-/-}$ se inmunizaron (s.s.) con el virus rVACV-OVA en la cola, y se inocularon (i.d.) con B16-OVA (10^6 células) en un flanco 30 días después. (**b**) Curvas de crecimiento del tumor B16-OVA, representadas como el volumen del tumor (mm^3) en el tiempo (días). (**c**) Esquema de inmunización (i.n.) contra el melanoma B16-OVA. Alternativamente, los ratones WT y *Batf3*$^{-/-}$ se inmunizaron (i.n.) con rVACV-OVA, y se inocularon (i.v.) con B16-OVA (3×10^5 células), 30 días después. (**d**) Número de nódulos metastásicos B16-OVA, 20 días después de la inoculación i.v. (**b, d**) Combinación de dos experimentos independientes, representados como la media aritmética del volumen de los tumores ± s.e.m. (**b**) (n=6-8/grupo) y cada ratón como un punto mostrando la media aritmética ± s.e.m. (**d**) (n=5-7/grupo). ***, $p<0.001$; *, $p<0.05$; mediante el test estadístico two-way ANOVA (**b**) y el test estadístico one-way ANOVA (**d**), aplicando el test de Bonferroni *a posteriori*.

El segundo grupo experimental (WT y *Batf3*$^{-/-}$) se inmunizó mediante la vía i.p. y

se inoculó 30 días después con B16-OVA en un flanco (**Figura R15a**). En una vía de inmunización que no produce Trm, el factor de transcripción Batf3 también contribuyó al control del crecimiento del tumor, y los ratones *Batf3*$^{-/-}$ no se protegieron (**Figura R15b**). El modelo de metástasis en el pulmón confirmó los datos anteriores (**Figura R15c-d**). En ambos casos los ratones WT se protegieron.

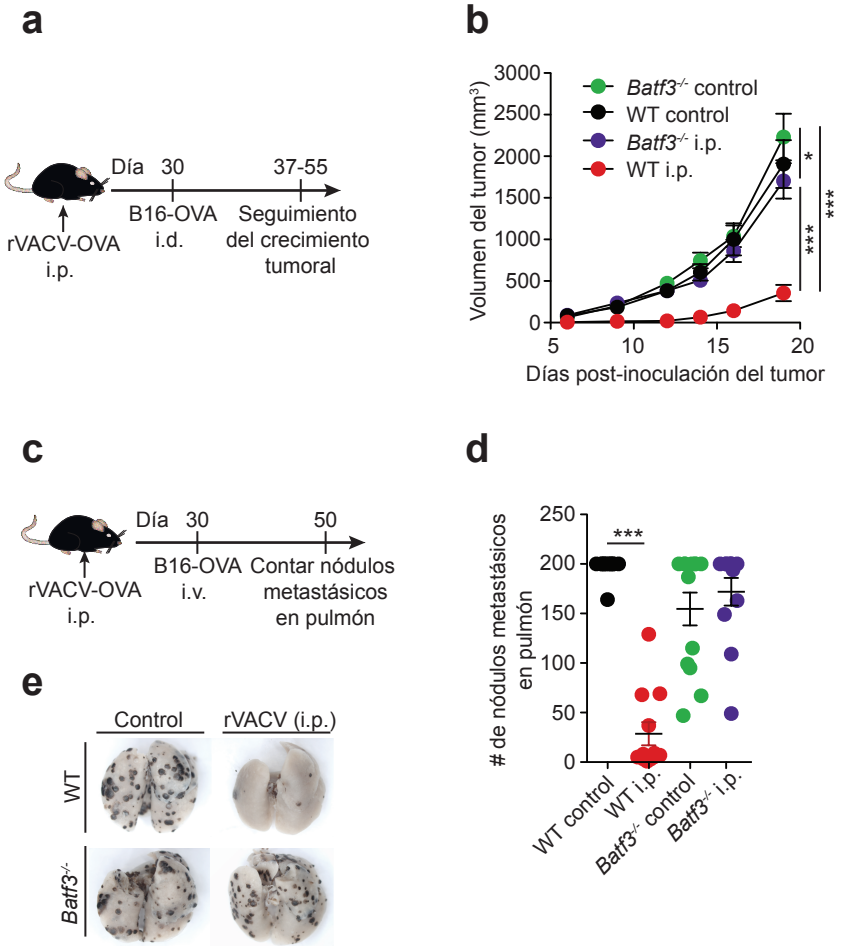

Figura R15. La inmunización con rVACV-OVA por vía intraperitoneal no protege a ratones *Batf3*$^{-/-}$ contra el melanoma B16-OVA

(**a**) Esquema de inmunización (i.p.) contra el melanoma B16-OVA. Los ratones WT y *Batf3*$^{-/-}$ se inmunizaron (i.p.) con rVACV-OVA, y se inocularon (i.d.) con B16-OVA (10^6 células) en un flanco 30 días después. (**b**) Curvas de crecimiento del tumor B16-OVA, representadas como el volumen del tumor (mm^3) en el tiempo (días). (**c**) Esquema de inmunización (i.p) contra el melanoma B16-OVA. Los ratones WT y *Batf3*$^{-/-}$ se inmunizaron (i.p.) con el virus rVACV-OVA, y se inocularon (i.v.) con el tumor B16-OVA (3×10^5 células) 30 días después. (**d**) Número de nódulos metastásicos B16-OVA, 20 días después de la inoculación i.v. (**e**) Imágenes representativas del crecimiento de nódulos metastásicos en los pulmones de los ratones, 20 días después de la inoculación i.v. (**b, d**) Combinación de dos experimentos independientes, representados como la media aritmética del volumen de los tumores ± s.e.m. (**b**) (n=6-8/grupo) y cada ratón como un punto mostrando la media aritmética ± s.e.m. (**d**) (n=5-7/grupo). ***, $p<0.001$; *, $p<0.05$; mediante el test estadístico two-way ANOVA (**b**) y el test estadístico one-way ANOVA (**d**), aplicando el test de Bonferroni *a posteriori*.

En conclusión, estos resultados demuestran que las DCs que requieren la expresión de Batf3 contribuyen a la respuesta antitumoral de memoria T CD8$^+$,

independientemente de su papel en la generación de Trm.

8.6.1 La reactivación de linfocitos T CD8$^+$ de memoria central contra el tumor depende de DCs que requieren la expresión de Batf3

A continuación, se estudió el posible mecanismo por el cual las DCs que requieren la expresión de Batf3 son importantes para la respuesta antitumoral de la memoria T CD8$^+$. En primer lugar, se descartó la posibilidad de que la memoria circulante T CD8$^+$ generada en los ratones *Batf3*$^{-/-}$ no funcionara correctamente. Los ratones WT y *Batf3*$^{-/-}$ se transfirieron con linfocitos T OT-I WT y se inmunizaron con rVACV-OVA para generar linfocitos Tcm en ambos genotipos. Los recipientes WT se transfirieron con linfocitos OT-I Tcm generados en ambos donantes y se inocularon con B16-OVA en un flanco (**Figura R16a**).

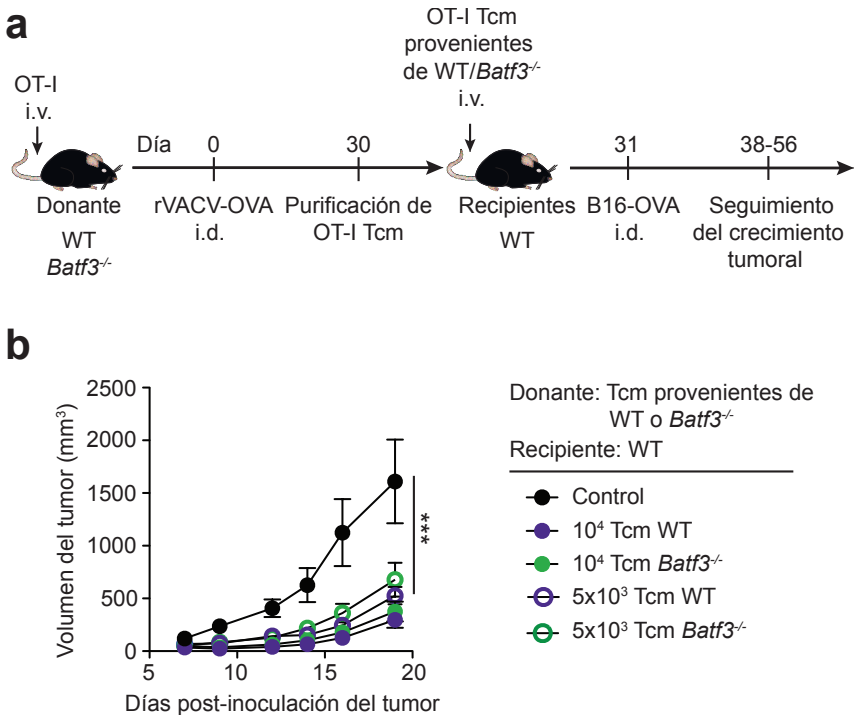

Figura R16. La memoria central generada en ratones *Batf3*$^{-/-}$ presenta una capacidad antitumoral tan eficiente como la generada en ratones WT

(a) Esquema de generación y transferencia de memoria central (Tcm). Para la generación de linfocitos Tcm, ratones WT y *Batf3*$^{-/-}$ se transfirieron con linfocitos T OT-I *naive* CD45.1$^+$ un día antes de la infección (i.d.) con rVACV-OVA en la oreja. Posteriormente (30 d), los linfocitos OT-I CD45.1$^+$ Tcm generados en ratones donantes WT y *Batf3*$^{-/-}$ se purificaron y se transfirieron a recipientes WT. Un día después de la transferencia los ratones se inocularon (i.d.) con B16-OVA (10^6 células) en un flanco. (**b**) Curvas de crecimiento del tumor B16-OVA, representadas como el volumen del tumor (mm^3) en el tiempo (días), que muestran los genotipos de los ratones donantes y recipientes. (**b**) Combinación de dos experimentos independientes, representados como la media aritmética del volumen del tumor ± s.e.m (n=6-8/grupo). ***, $p<0.001$; mediante el test estadístico two-way ANOVA, aplicando el test de Bonferroni *a posteriori.*

La transferencia de linfocitos Tcm retrasó el crecimiento del tumor, independientemente del ratón donante donde se generó la memoria (**Figura R16b**).

Además, se estudió la posibilidad de que las DCs que requieren la expresión de Batf3 en ratones recipientes fueran las encargadas de reactivar la memoria Tcm contra los tumores. Para esto, se generó memoria Tcm tanto en donantes WT como *Batf3*$^{-/-}$ y se transfirieron a recipientes WT y *Batf3*$^{-/-}$, que se inocularon posteriormente con B16-OVA (**Figura R17a**).

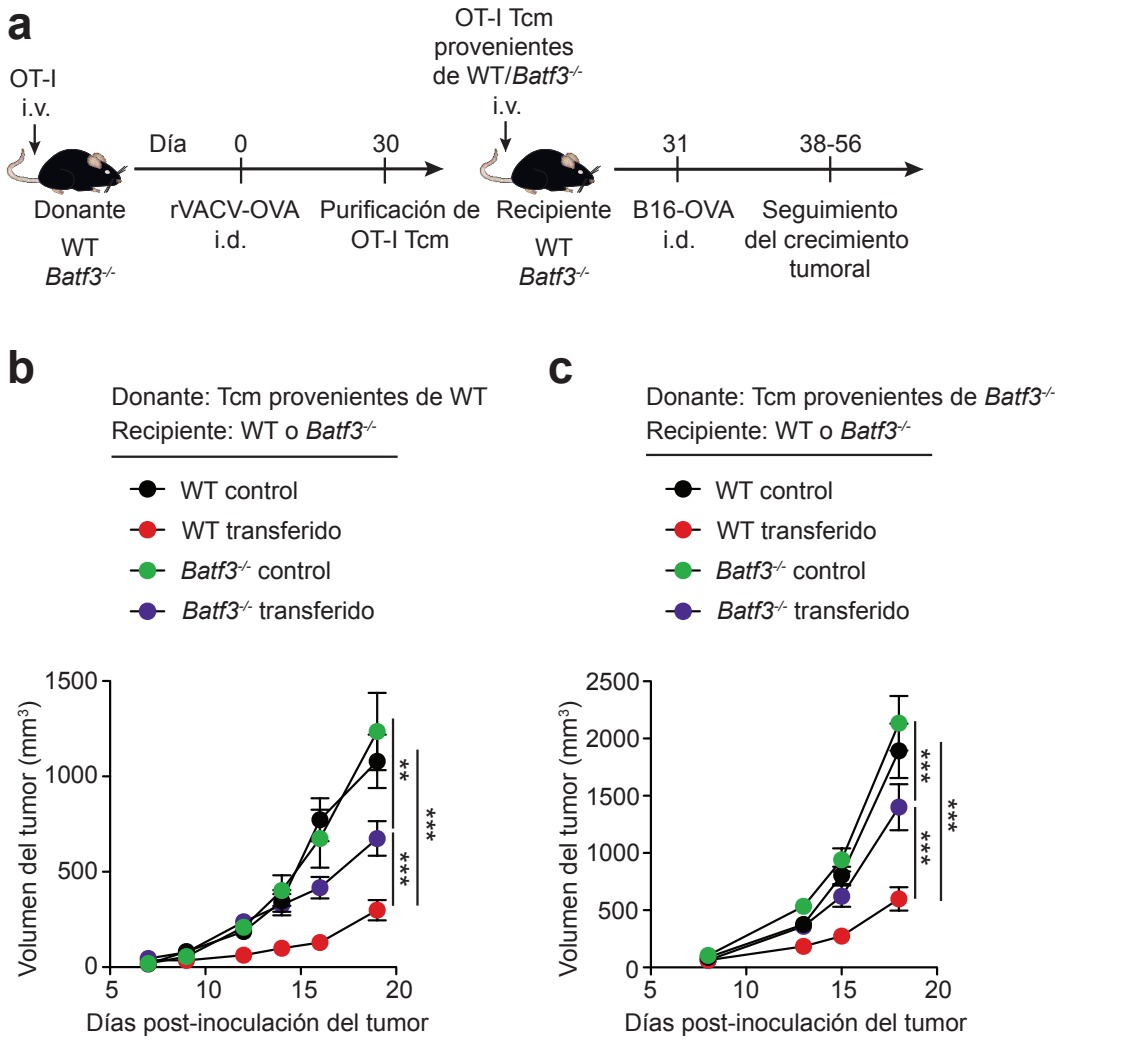

Figura R17. La reactivación de la memoria central en respuesta a tumores depende de células dendríticas que requieren la expresión de Batf3

(**a**) Esquema de generación y transferencia de memoria central (Tcm). Para la generación de linfocitos Tcm, ratones WT (**b**) y *Batf3*$^{-/-}$ (**c**) se transfirieron con linfocitos T OT-I CD45.1^{+} *naive* un día antes de la infección (i.d.) con el virus rVACV-OVA en la oreja. Posteriormente (30 d), los linfocitos OT-I CD45.1^{+} Tcm provenientes de ratones donantes WT y *Batf3*$^{-/-}$ se purificaron y se transfirieron a recipientes WT y *Batf3*$^{-/-}$. Un día después de la transferencia los ratones se inocularon (i.d.) con B16-OVA (10^6 células) en un flanco. (**b, c**) Curvas de crecimiento del tumor B16-OVA, representadas como el volumen del tumor (mm^3) en el tiempo (días), en ratones recipientes transferidos con Tcm provenientes de animales WT (**b**) o *Batf3*$^{-/-}$ (**c**). (**b, c**) Combinación de dos experimentos independientes, representados como la media aritmética del volumen del tumor ± s.e.m (n=6–8/grupo). ***, p<0.001; **, p<0.01; mediante el test estadístico two-way ANOVA, aplicando el test de Bonferroni *a posteriori*.

Independientemente del origen de los linfocitos Tcm, la transferencia adoptiva a ratones recipientes *Batf3*$^{-/-}$ fue ineficiente para controlar el crecimiento del tumor, si se compara con la transferencia a ratones WT (**Figura R17b-c**).

Estos datos demuestran que las DCs que requieren la expresión de Batf3 dirigen la reactivación de la memoria Tcm y su inmunidad antitumoral.

Discusión

9. Discusión

La generación de memoria T $CD8^+$ potente durante la inmunoterapia contra el cáncer podría suponer una ventaja, para prevenir la reaparición de nuevos tumores locales y metástasis. La memoria T puede recircular entre los órganos linfoides secundarios y los tejidos periféricos (memoria T circulante), o residir en los tejidos periféricos (Trm) una vez se ha establecido (Kaech *et al.* 2012). Cada tipo de memoria requiere diferentes estímulos durante el *priming* y la diferenciación (Iborra *et al.* 2016; Mueller *et al.* 2016). Tanto la memoria T circulante como Trm tienen diferentes propiedades efectoras (Mueller *et al.* 2016). Sin embargo, su interrelación en la inmunidad antitumoral no se ha estudiado con profundidad.

Con el objetivo de abordar esta interrogante se empleó un sistema de vacunación con VACV, para generar selectivamente los distintos tipos de memoria que se iban a estudiar (Iborra *et al.* 2016). Una vez que se estableció la memoria, los ratones se inocularon con varios modelos tumorales como el modelo de melanoma B16-OVA y de adenocarcinoma MC38-OVA. Se utilizaron tanto la inoculación del tumor en la piel para desarrollar tumores primarios, como la inoculación intravenosa para desarrollar nódulos metastásicos en los pulmones.

En el presente estudio se demostró que la memoria T circulante y la Trm colaboraban en la inmunidad contra tumores. Ambos tipos de memoria, circulante y residente, fueron suficientes para retrasar el crecimiento de los tumores. La inducción de Trm retrasó el comienzo de los tumores, disminuyó la cinética de crecimiento y consecuentemente aumentó la inmunidad antitumoral. La memoria circulante mantuvo suficiente grado de plasticidad para producir Trm dentro de los tumores, o en la piel de animales que habían rechazado el tumor. Asimismo, la Tcm generó Trm en un contexto de infección viral. Notablemente, la terapia con anti-PD-1 contribuyó con la transferencia adoptiva de Tcm y mejoró la respuesta antitumoral. Además, las DCs dependientes de Batf3 fueron críticas para la reactivación de la memoria T $CD8^+$ circulante durante la respuesta antitumoral.

9.1 Interrelación de la memoria circulante y residente durante la respuesta antitumoral

Las células Trm se generan después de la mayoría de infecciones virales que

afectan la piel o las mucosas (Mueller *et al.* 2016) y están ampliamente distribuidas en los tejidos (Steinert *et al.* 2015). La Trm responde con más rapidez que la memoria circulante después de una estimulación, y está equipada con una maquinaria efectora más potente que su contraparte circulante (Clark *et al.* 2015). Además, la Trm proporciona una protección superior tras una segunda infección viral en piel o en mucosas (Jiang *et al.* 2012; Gaide *et al.* 2015; Hondowicz *et al.* 2015). Estas células son suficientes para controlar la reinfección viral en presencia de FTY720, el cual limita la contribución de la memoria circulante (Jiang *et al.* 2012).

Para analizar la **suficiencia de las poblaciones de memoria circulante y residente** en la respuesta antitumoral, se generaron ambos tipos de memoria mediante distintos métodos de inmunización. Como no se contaba con un método para generar selectivamente memoria residente, se utilizó la escarificación de la piel. Este método generó ambos tipos de memoria, residente y circulante. La contribución de la memoria circulante a la inmunidad antitumoral se limitó mediante la inoculación del inhibidor FTY720, que reduce la salida de linfocitos T a circulación desde los órganos linfoides secundarios. Los experimentos con FTY720 demostraron que la Trm fue suficiente para disminuir el crecimiento tumoral.

Estos resultados han sido simultáneamente reproducidos por otro grupo de trabajo (Malik *et al.* 2017) en un modelo de vitíligo autoinmune. En este modelo se generan naturalmente Trm específica por melanoma. Estas células residen en los folículos pilosos que carecen de melanocitos. El mantenimiento de esta Trm es independiente a la reposición desde los órganos linfoides secundarios. Los linfocitos Trm expresan los marcadores fenotípicos CD103, CD69, y CLA, pero carecen de PD-1 o LAG-3. Además, son capaces de producir IFN-γ. Las células Trm $CD8^{+}CD103^{+}$ derivadas del vitíligo autoinmune son críticas para la protección contra el melanoma. El uso de FTY720 por estos investigadores corrobora que las células Trm naturalmente generadas, específicas por el melanoma, son suficientes para rechazar el tumor (Malik *et al.* 2017). Sin embargo, en nuestro modelo, la memoria T $CD8^{+}$ circulante también protegió eficazmente contra los tumores, en correspondencia con resultados previos (Klebanoff *et al.* 2005).

En relación a los efectos inespecíficos del inhibidor FTY720, para corroborar la suficiencia de Trm en el rechazo tumoral, el trasplante de piel que contiene solamente Trm podría ser una aproximación muy elegante. Sin olvidar que este es un proceso severo

donde se genera mucha inflamación y las porciones de piel que se trasplantan tienen un tamaño limitado.

Con el objetivo de estudiar la **interrelación entre la memoria circulante y residente** y comparar su eficiencia se utilizó un modelo de parabiosis. En este modelo se comparó como respondían a la inoculación de un tumor dos grupos de ratones parabiontes. El primer grupo de ratones contenía tanto memoria circulante como residente en piel, mientras que el segundo grupo de ratones contenía el mismo número de linfocitos de memoria circulante, pero no contenía memoria residente. En estos experimentos se demostró que el crecimiento de tumores fue menor en aquellos parabiontes que contenían ambos tipos de memoria, tanto circulante como Trm, en comparación con parabiontes que contenían solamente memoria T circulante.

Los datos anteriores sugieren que las poblaciones residentes y circulantes colaboran para aumentar la protección antitumoral (**Figura D1**). Algunas evidencias anteriores señalan la colaboración entre los linfocitos de memoria circulante y residente como un mecanismo efector de la Trm. Por ejemplo, la reinfección con VSV (del inglés, *vesicular stomatitis virus*) aumenta el reclutamiento de la memoria circulante desde la sangre (Borowitz *et al.* 1993; Sallusto *et al.* 2009).

Asimismo, la Trm en presencia de memoria circulante aumentó la respuesta contra el melanoma B16, lo cual sugiere cierta superioridad de la respuesta inmunitaria de Trm contra el tumor. Este resultado coincide con los datos obtenidos en un modelo de *prime-boost* con VACV. En este modelo, la Trm en presencia de FTY720 fue superior a la memoria circulante para proteger frente a la segunda infección con el mismo virus (Jiang *et al.* 2012). No se descarta que el reclutamiento de la memoria circulante podría contribuir a la superioridad de la Trm. Sin embargo, otra explicación podría radicar en la cinética de la respuesta de ambas memorias. Por ejemplo, en el modelo de hipersensibilidad por contacto con DNFB (del inglés, *dinitrofluorobenzene*), la Trm induce una respuesta rápida y potente, mientras la memoria circulante induce una respuesta de hipersensibilidad más lenta (Gaide *et al.* 2015).

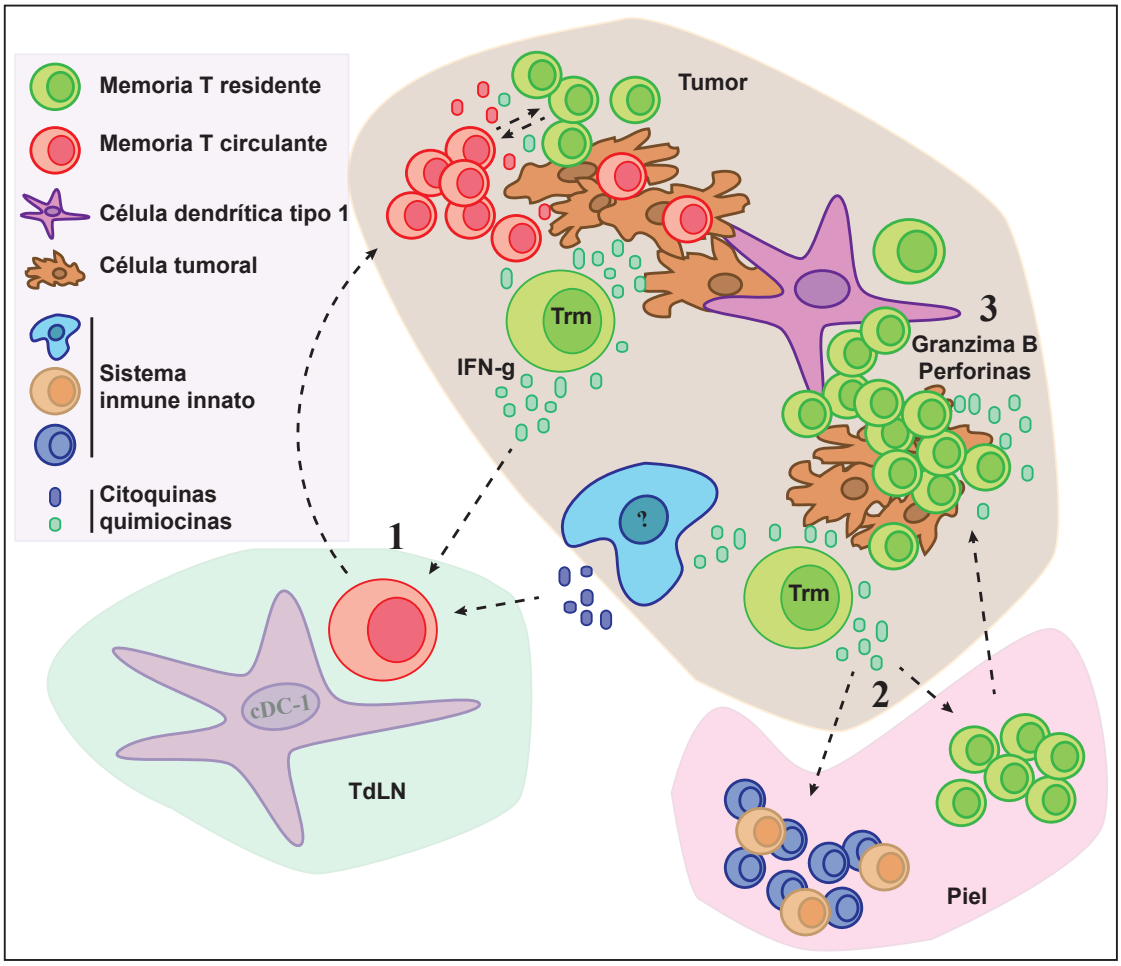

Figura D1. La inducción de memoria T residente aumenta la inmunidad antitumoral
La inmunización mediante escarificación de la piel genera tanto memoria circulante como memoria residente (Trm). La inducción de Trm aumenta la respuesta antitumoral y disminuye su crecimiento. Algunos mecanismos podrían explicar este fenómeno. Por ejemplo, (**1**) la Trm induce un reclutamiento de memoria circulante desde los órganos linfoides secundarios hacia el tumor. Este proceso podría estar mediado directamente por la producción de IFN-γ. No se descarta que la Trm induzca la producción de otras citoquinas/quimiocinas en células del sistema innato, que a su vez contribuyan al reclutamiento de la memoria circulante. (**2**) La Trm induce el reclutamiento de más linfocitos de memoria residente y de otros linfocitos de la inmunidad innata (**3**). La Trm utiliza como mecanismo efector la lisis directa de la célula tumoral diana, mediante la producción de granzima B y perforinas.

Aunque la presencia de Trm señaló una mayor actividad antitumoral, los mecanismos efectores de la Trm *in vivo* no se han estudiado profundamente (Cells ***et al.*** 2014). La Trm puede producir IFNγ y granzima B (Mackay ***et al.*** 2001; Jiang *et al.* 2012; Hu *et al.* 2015; Malik *et al.* 2017). Sin embargo, no está claro que la Trm utilice la lisis directa de células tumorales como mecanismo efector.

Para contrarrestar su baja tasa de proliferación, la Trm podría poblar densamente los tejidos (Steinert *et al.* 2015) o tener mecanismos efectores muy potentes que superen dichas limitaciones. Los experimentos recientes muestran que la Trm realiza su función efectora con mecanismos distintos a la lisis directa de una célula diana. Muchos de estos

mecanismos colocan a la Trm en la base de la interacción entre la inmunidad innata y adaptativa. Se cree que los linfocitos Trm son capaces de generar un estado de alerta inmunológica en el tejido, capaz de movilizar a las células y citoquinas no solo de la inmunidad innata, sino también de la inmunidad adaptativa. Por ejemplo, en un modelo de influenza las células Trm del pulmón protegen contra el virus en ausencia de proliferación o de función citotóxica, mediante una respuesta dependiente de IFN-γ y de otras citoquinas (von Andrian *et al.* 2003; Purwar *et al.* 2011). En mucosa, esta vez en el aparato reproductor femenino, la producción instantánea de citoquinas por células Trm induce la expresión en el endotelio de la molécula de residencia VCAM-1. Esto contribuye al reclutamiento de células NK, DC y células B al sitio de infección (Hu *et al.* 2015). Asimismo, la reestimulación de Trm induce la expresión de algunos genes de la inmunidad innata como IFITM-3 (Kupper *et al.* 2012). Este mecanismo de alerta en el modelo de *Staphylococcus epidermidis* y otros induce la activación local de la Trm. La consiguiente cascada inmunológica contribuye a la eliminación de muchos patógenos no relacionados antigénicamente (Kupper 2012; Hu *et al.* 2015; Naik *et al.* 2015).

En este trabajo se utilizó un modelo de vacunación con el antígeno exógeno OVA. Debido a la alta inmunogenicidad de este antígeno, para la generación de memoria se podría utilizar un modelo con antígenos endógenos y conseguir un escenario más fisiológico. Por ejemplo, la estrategia de *prime-boost* que utiliza para el *prime* el lentivirus que expresa gp100 (antígeno tumoral) y para el *boost* el VACV que expresa gp100 genera una respuesta antitumoral eficiente contra melanoma (Xiao *et al.* 2011). Esta protección se debe probablemente a la generación de una memoria circulante y residente muy potente, con capacidad para interaccionar.

La memoria circulante y la Trm colaboraron para asegurar una respuesta antitumoral más eficiente. Sin embargo, los mecanismos que explican esta interacción en el contexto tumoral requieren un estudio más profundo. No obstante, el retraso en el comienzo de los tumores y la consecuente disminución en su crecimiento en presencia de Trm, sugiere que estas células podrían ser particularmente beneficiosas en la prevención de metástasis.

9.2 Generación de Trm a partir de Tcm

Una de las principales características de la memoria circulante es su plasticidad. Los linfocitos T tienen programas de expresión génica flexibles, que les permiten

adaptarse a nuevas condiciones ambientales (Youngblood *et al.* 2015). Aunque la plasticidad entre los linfocitos T *naive*, de memoria central y efectora, ha sido ampliamente estudiada, **la plasticidad de la Tcm para generar Trm** es una asignatura pendiente para la comunidad científica.

La Tcm y la Trm se originan a partir de un mismo clon y comparten el repertorio de TCR (Gaide *et al.* 2015). Sin embargo, las células Trm requieren diferentes estímulos para el *priming* en los LN (Iborra *et al.* 2016). La generación óptima de la Trm después de una infección viral requiere señales proporcionadas únicamente por las DC dependientes de Batf3, que favorecen la expresión de T-bet y la retención en el LN (Iborra *et al.* 2016). A continuación, las células Trm migran hacia los tejidos, donde el microambiente local condiciona su diferenciación (Steinert *et al.* 2015; Mueller *et al.* 2016).

Con el objetivo de evaluar si la Tcm generaba Trm se utilizó un modelo de transferencia adoptiva de Tcm, seguido por la infección con un virus o la inoculación de un tumor (**Figura D2**).

La transferencia adoptiva de Tcm generó Trm en piel después de la infección con el VACV. Estas células Trm expresaron CD69 y CD103. Además, mediante experimentos de parabiosis se demostró que estas células Trm no migraban a través de la sangre o la linfa.

Asimismo, después de la inoculación con B16-OVA, las células Tcm transferidas expresaron marcadores fenotípicos asociados a la Trm dentro del tumor. Sin embargo, estas células recibían una estimulación antigénica persistente. En los ratones que rechazaron completamente el tumor MC38-OVA la Trm derivada de la Tcm permaneció en la piel. La eliminación del tumor MC38-OVA permitió la identificación de verdaderas células Trm en ausencia del antígeno, que expresaron CD69 y CD103,

Las células Tcm presentan un fenotipo más parecido a células madre y

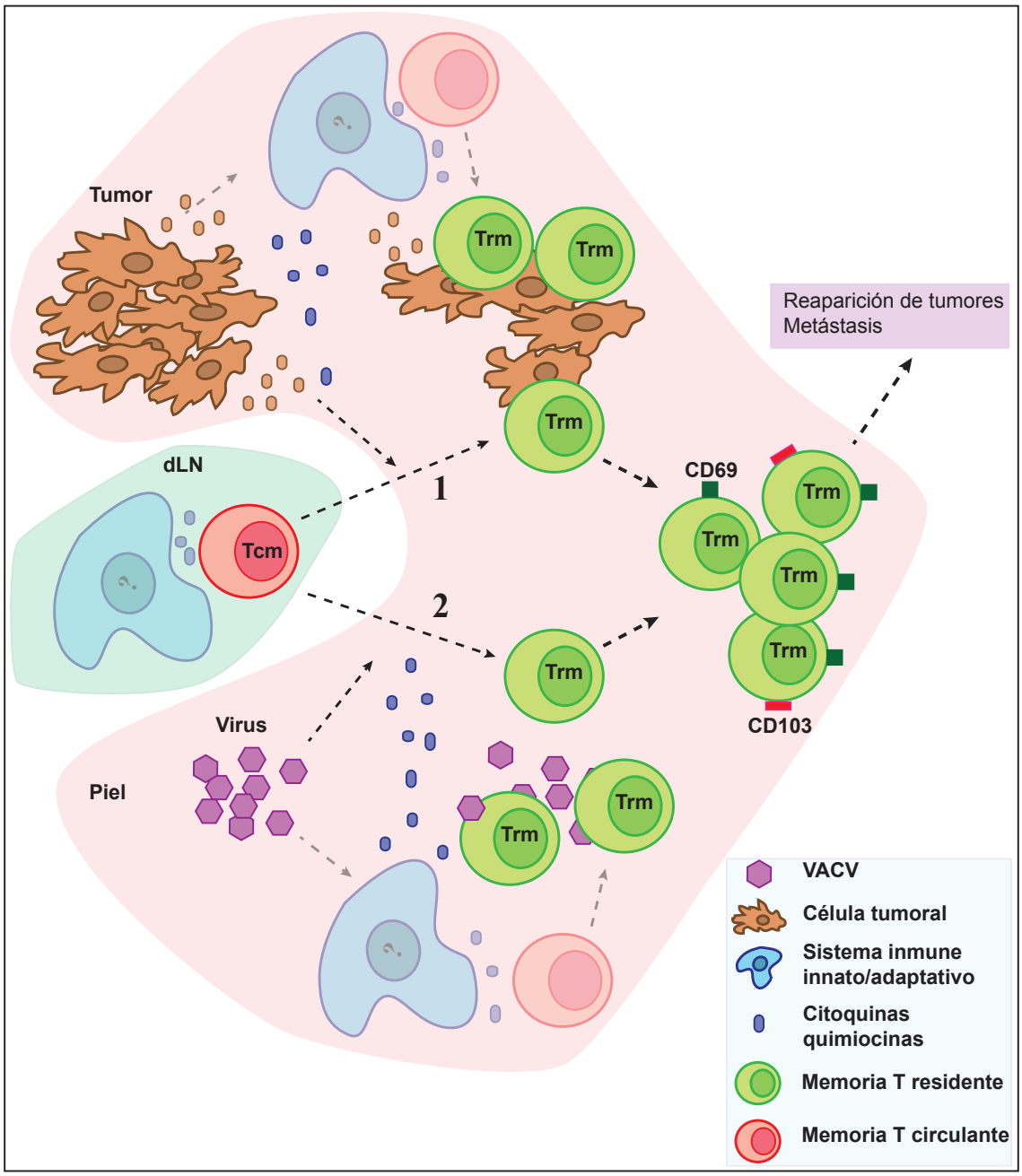

Figura D2. La memoria T CD8$^+$ central genera memoria residente en presencia de estímulos inflamatorios

(**1**) Después de la transferencia adoptiva de memoria central (Tcm) e inoculación con un tumor se genera memoria residente (Trm). La generación de Trm podría estar mediada por señales provenientes directamente del tumor. Aunque no se descarta que las células mieloides sean intermediarias entre las señales recibidas desde el tumor y las señales enviadas a la Tcm. (**2**) En el caso de la infección viral con VACV, se genera Trm a partir de Tcm tras la inmunización. Los virus podrían inducir la transformación directamente. Sin embargo, como VACV infecta directamente un gran número de células, las señales provenientes de estas también podrían inducir la transformación. En ambos casos la Trm expresa CD69 y CD103 y se podría inducir la señalización tanto en un órgano linfoide secundario como en el propio tumor o sitio de infección. Esta Trm es una alternativa potencial para la protección contra la reaparición de tumores y metástasis.

mayor capacidad proliferativa, mientras que las células Trm tienen mayor capacidad efectora e inducen un estado de alarma local (Wakim *et al.* 2010; Ariotti *et al.* 2014;

Schenkel *et al.* 2014; Naik *et al.* 2015). La capacidad de la Tcm para generar Trm después de una infección viral o la inoculación de un tumor apoya sus propiedades como células madre. Sin embargo, la Tcm no se convierte en Trm en ausencia de inflamación (Jiang *et al.* 2012).

Una de las teorías que explican la plasticidad de las células T de memoria es la existencia de células madre de memoria capaces de generar dos tipos celulares: uno con las mismas características para autorenovarse homeostáticamente, y otro con funciones más terminales (Fearon *et al.* 2001).

El modelo de células madre inmunológicas se apoya en la existencia de la Tscm. Son muchos los procedimientos para demostrar este hecho, por ejemplo, en un modelo de transferencia adoptiva de un único clon de células Tscm, estas células muestran capacidad de autorenovación y multipotencia (Graef *et al.* 2014).

Recientemente se han definido distintas subpoblaciones celulares con propiedades características de células madre. Por ejemplo, la subpoblación de linfocitos humanos Tcm y Tem caracterizada por una alta expresión de IL-18R y del receptor de NK CD161 muestran una mayor supervivencia durante la quimioterapia (Turtle *et al.* 2009). En modelos de cáncer e injerto contra huésped, otra población de células T $CD8^+$ que expresa $CD44^{lo}CD62L^{hi}$ y altos niveles de Sca-1, CD122 y Bcl-2 (Gattinoni *et al.* 2009), (Zhang *et al.* 2005) presenta una mayor capacidad proliferativa y una función superior al resto de Tcm.

Continuamente se debate si la plasticidad de células T de memoria es una propiedad intrínseca, es dependiente de las condiciones del microambiente, o es una combinación de ambas. En este sentido, los datos aquí descritos sugieren que ambos criterios son determinantes. Las células Tcm que se transfirieron por vía intravenosa, generaron tanto poblaciones de memoria circulante en los órganos linfoides secundarios como residente en los tejidos. Aunque la generación de Trm se limitó a la presencia de estímulos inflamatorios.

Algunos experimentos anteriores reflejan la relevancia del ambiente en la plasticidad T. Masopust y colaboradores (Masopust *et al.* 2006b) tomaron Trm de los intestinos y las transfirieron de nuevo al mismo organismo por vía intravenosa. Como resultado se generan células efectoras y varias subpoblaciones de memoria, después del reencuentro con el antígeno. Esta observación resalta la influencia de los estímulos del

microambiente para inducir la generación de cada tipo de memoria. Por el contrario, las células Trm tomadas del cerebro, transferidas al bazo por la vía intravenosa, y expuestas al antígeno, presentan una capacidad proliferativa muy limitada (Wakim *et al.* 2010). Estos datos sugieren que la diferenciación de Trm en cerebro está ligada a un programa genético intrínseco, que restringe su capacidad proliferativa fuera de él. En el experimento opuesto, tomando memoria T circulante de bazo y transfiriéndola al cerebro, esta mantiene un alto potencial proliferativo, si bien no se describe que sean capaces de generar Trm (Wakim *et al.* 2012).

Aunque se ha demostrado que la Tcm genera Trm en un contexto viral y tumoral, los procesos relacionados con esta transformación requieren estudios más profundos. Por ejemplo, una caracterización fenotípica exhaustiva junto al estudio de perfiles de expresión génica contribuirían a una definición más completa de estas células. Asimismo, la comparación de la función efectora entre la Trm generada a partir de Tcm o de linfocitos *naive*, guiaría la generación de Trm en las terapias contra la metástasis.

9.3 Terapias con anti-PD-1

El presente estudio sugiere que la inmunidad antitumoral mediada por células T $CD8^+$ surge a partir de una interrelación de la memoria T $CD8^+$ circulante y residente. Las células Tcm mostraron suficiente grado de plasticidad para producir Trm en un contexto tumoral. Ambos tipos celulares expresaron PD-1 en presencia del tumor, similar a los linfocitos T $CD103^+$ infiltrados en cáncer de ovario (Komdeur *et al.* 2016).

Para evaluar el **efecto de anti-PD-1 en la transferencia adoptiva de células T de memoria**, los ratones con tumores se inocularon con el anticuerpo y linfocitos T siguiendo un modelo terapéutico.

La terapia con anti-PD-1 en combinación con la transferencia adoptiva de Tcm aumentó la infiltración de linfocitos con características de Trm, y consecuentemente su actividad antitumoral. Este resultado se corresponde con resultados previos, donde se muestra que el tratamiento con anti-PD-1 expande la memoria T antitumoral en pacientes (Ribas *et al.* 2016). En los nódulos metastásicos de melanoma, los puntos de control inmunológico están particularmente enriquecidos en una población de células T con características fenotípicas y genotípicas de Trm. Esto sugiere que la población de Trm dentro de los TILs podría ser la mejor diana para el bloqueo de los puntos de control

inmunológico. La habilidad de la Trm de residir largos períodos de tiempo en los tejidos (Thome *et al.* 2015; Malik *et al.* 2017) podría ser la clave en la estabilidad de las respuestas clínicas observadas tras el bloqueo de los puntos de control inmunológico (Boddupalli *et al.* 2016). Además, otros anticuerpos inmunoestimuladores, como el anti-CD137 , también aumentan la respuesta de la memoria residente (Zhou *et al.* 2017).

Existe una fuerte correlación entre la expresión de PD-1 y la disfunción de los TIL $CD8^+$ específicos por antígenos tumorales. Sin embargo, en los modelos de MCMV y VACV, los linfocitos de memoria específicos para el virus que infiltran el tumor son altamente funcionales, independientemente de la expresión de PD-1. Los niveles de expresión de PD-1 y la funcionalidad de TILs correlaciona con una exposición reciente al antígeno (Erkes *et al.* 2017). La utilización de TILs como marcador de pronóstico de respuesta antitumoral debe tener en cuenta esos TILs, que reflejan una situación inmunológica inflamatoria independiente de los antígenos tumorales. Sin embargo, la actividad efectora de TILs de memoria específicos por el virus se debería estudiar con mayor profundidad, como alternativa para generar una respuesta citotóxica contra células tumorales.

La infiltración de linfocitos T con características de Trm aumentó después del tratamiento con anti- PD-1. El mecanismo que explica este resultado no se ha descrito completamente y requiere mayores esfuerzos. Se podría especular que anti-PD-1 simplemente aumenta el reclutamiento de linfocitos T de memoria al tumor. Sin embargo, teniendo en cuenta que este anticuerpo bloquea la señalización de muerte, la mayor infiltración podría deberse al aumento en la supervivencia de linfocitos dentro del tumor. Desde el punto de vista metabólico la señalización por PD-1 en linfocitos T limita la glicolisis y la utilización de glutamina como fuentes de energía. En consecuencia, los linfocitos T obtienen energía a partir de la oxidación de ácidos grasos (Patsoukis *et al.* 2015). La oxidación de ácidos grasos tiene una fuerte asociación con la longevidad de varios tipos celulares (Wang *et al.* 2008; Zaugg *et al.* 2011). Estos datos sugieren que la señalización por PD-1 permite a las células T sobrevivir largos períodos de tiempo utilizando el metabolismo de ácidos grasos. No se puede descartar que anti-PD-1 potencie la inducción de un fenotipo asociado a Trm y a su vez aumente la permanencia de estas células dentro del tumor. En cualquier caso, hay que destacar que los TILs mantienen su capacidad efectora, lo que se demostró con la disminución del crecimiento de los tumores. Además, el estudio de otros anticuerpos bloqueantes de los puntos de control

inmunológico en combinación con la transferencia adoptiva, contribuiría al desarrollo de terapias antitumorales más eficientes.

En conclusión, estos resultados sugieren que las estrategias de vacunación antitumoral deberían inducir ambos tipos de memoria circulante y residente (Sandoval *et al.* 2013), lo que en sinergia con los anticuerpos inmunoestimuladores mejoraría la inmunoterapia contra cáncer.

9.4 Las cDC-1 dependientes de Batf3 dirigen la reactivación de la respuesta de memoria antitumoral

Las DC son esenciales para la respuesta antitumoral después de la transferencia adoptiva de linfocitos T. La transferencia de linfocitos T OT-I activados previamente con anti-CD3 y anti-CD28 *in vitro* a animales que carecen de DC $CD103^+$, no protege contra tumores que expresan OVA. La abundancia de transcriptos primarios característicos de DC dependientes de Batf3 se correlaciona con un mejor resultado clínico en tumores de pacientes (Broz *et al.* 2014). Además, el éxito de terapias con anticuerpos inmunoestimuladores radica en la participación de estas células en la respuesta antitumoral, encargadas de realizar la presentación cruzada de antígenos tumorales (Salmon *et al.* 2016). En este caso, se establece una sinergia entre los anticuerpos inmunoestimuladores y la expansión y activación de las cDC-1, inducidas por FLT3L y poly (I:C) respectivamente (Salmon *et al.* 2016; Sanchez-Paulete *et al.* 2016). La población de DC dependientes de Batf3 es la mayor productora de IL-12, no solo en contextos de infección (Mashayekhi *et al.* 2011; Martínez-López *et al.* 2015; Everts *et al.* 2016), sino también en contextos tumorales (Ruffell *et al.* 2014). La IL-12 contribuye a la función efectora de células T $CD8^+$ y a la inhibición de células mieloides productoras de IL-10 (Ruffell *et al.* 2014).

Con el objetivo de evaluar la **relevancia de las cDC-1 en la respuesta antitumoral de la memoria T** se utilizó el modelo de ratón que carece de Batf3, en combinación con experimentos de transferencia adoptiva. Estos ensayos demostraron que las DC dependientes de Batf3 fueron necesarias para la reactivación eficiente de la Tcm y la promoción de la inmunidad antitumoral. La importancia de las cDC-1 en la respuesta de memoria se ha descrito anteriormente en distintos modelos de infección. Por ejemplo, las DC dependientes de Batf3 son críticas durante la reactivación de la memoria T $CD8^+$ en modelos de infección con *Listeria monocytogenes*, VSV o VACV (Alexandre *et al.*

2016).

La relevancia de las cDC-1 en la respuesta inmunitaria antitumoral ha llamado la atención sobre estas células como alternativa en la inmunoterapia contra cáncer. A esto se debe el creciente número de publicaciones enfocadas a relacionar las cDC-1 con los linfocitos T antitumorales. Algunos de los mecanismos que explican la función de cDC-1 se han descrito simultáneamente a nuestro trabajo (**Figura D3**). Por ejemplo, las DC $CD103^+$ son las únicas capaces de transportar antígenos tumorales al TdLN. En el TdLN son estas DC las que estimulan y activan la respuesta T $CD8^+$ específica por el tumor (Roberts *et al.* 2016; Salmon *et al.* 2016). Asimismo, las DC $CD103^+$ transfieren los antígenos a otras células mieloides residentes en LN con otras funciones. Todos los procesos anteriores son dependientes de CCR7 (Roberts *et al.* 2016).

En un modelo de melanoma espontáneo, las DC dependientes de Batf3 se requieren para el reclutamiento de linfocitos T $CD3^+$ *naive* al tumor (Spranger *et al.* 2015). La infiltración de linfocitos T en el tumor no ocurre siempre, y los mecanismos que explican este fenómeno no están completamente claros. Las DC $CD103^+$ intratumorales son las mayores productoras de las quimiocinas CXCL9 y CXCL10, las cuales promueven el reclutamiento de los linfocitos T $CXCR3^+$ efectores y reactivos contra el tumor (Spranger *et al.* 2017). La expresión de transcriptos primarios en las cDC-1 de los tumores humanos de melanoma correlaciona positivamente con la presencia de CXCL9 y CXCL10, así como con la infiltración de linfocitos T $CD8^+$ (Spranger *et al.* 2017).

Si se confirmara en pacientes que las DC intratumorales dependientes de Batf3 controlan el reclutamiento de linfocitos T, este descubrimiento podría tener muchas implicaciones para la inmunoterapia contra cáncer. Por ejemplo, la presencia o ausencia de cDC-1 en los tumores sería un criterio decisivo para predecir la respuesta clínica y definir el tratamiento más adecuado. Además, sería muy interesante investigar retrospectivamente si los pacientes que no han respondido a las inmunoterapias tenían bajos niveles en la infiltración de DC $CD141^+$, homólogas de las cDC-1 en humanos.

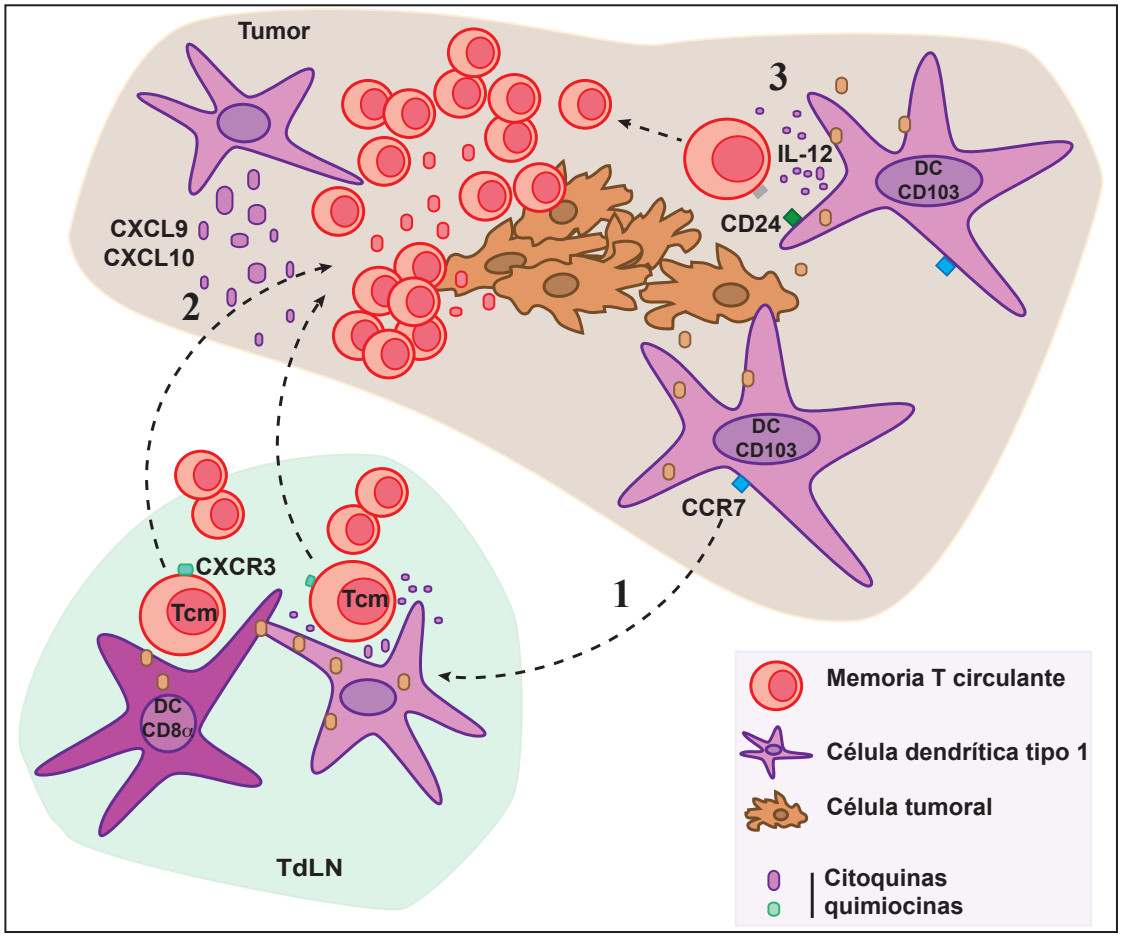

Figura D3. La reactivación de memoria T central depende de células dendríticas tipo 1
(**a**) Animales WT previamente transferidos con memoria central (Tcm) específica para OVA y posteriormente inoculados con B16-OVA se protegen contra el tumor. Las células dendríticas (DC) tipo 1 dependen del factor de transcripción Batf3 y están compuestas por las DC CD103$^+$ migratorias y las DC CD8α en los órganos linfoides secundarios. (**1**) Las DC CD103$^+$ transportan los antígenos del tumor hacia el ganglio linfático más cercano (TdLN), dependiente de CCR7. Estas células presentan los antígenos tumorales a la Tcm. Asimismo, transfieren los antígenos tumorales a otras células como las DC CD8α, que también realizan la presentación cruzada y el *priming* de los linfocitos T. (**2**) Las DC CD103$^+$ intratumorales secretan CXCL9 y CXCL10, lo cual induce el reclutamiento de linfocitos T de memoria que expresan CXCR3 desde el TdLN hacia el tumor. No se puede descartar que las DC CD103$^+$ presenten los antígenos y estimulen la Tcm dentro del tumor. (**3**) La activación de linfocitos T de memoria podría estar mediado por la secreción de IL-12 y la estimulación de CD24, ambos factores expresados en las DC CD103$^+$. En ausencia de Batf3, que por una parte reduce significativamente el número de DC CD103$^+$ en la piel y por otra parte las DC CD8α que permanecen en los TdLNs no son funcionales, no hay rechazo tumoral.

Si bien está claro el papel de las cDC-1 en la reactivación de la respuesta de memoria antitumoral. Algunos aspectos permanecen sin aclarar. Por ejemplo, aún no se ha demostrado donde ocurre la reactivación de linfocitos T de memoria. Aunque muchos resultados señalen el TdLN, no se debe descartar que en el caso de la memoria T con un umbral de activación menor, la señalización podría ocurrir directamente dentro del tumor. Además, se necesitan estudios adicionales para investigar el papel de las DC dependientes de Batf3 en la generación de Trm (Iborra *et al.* 2016) en el contexto tumoral, definir si la

Trm necesita una reactivación y que tipo de DC estaría implicada en este proceso (Shin *et al.* 2016).

Estos datos resaltan la relevancia de las cDC-1 en la inmunología tumoral y la inmunoterapia no solo para la integración de una respuesta primaria, sino también para la respuesta de memoria.

Conclusiones

10. Conclusiones

1. Tanto los linfocitos T $CD8^+$ de memoria residente como circulante son suficientes para la respuesta antitumoral.

2. La inducción de linfocitos T $CD8^+$ de memoria residente aumenta la eficiencia de la inmunidad antitumoral.

3. Los linfocitos T $CD8^+$ de memoria central muestran plasticidad para generar memoria residente tras la infección con un virus o la inoculación de un tumor.

4. La terapia combinada del anticuerpo anti-PD-1 con la transferencia adoptiva de linfocitos T $CD8^+$ de memoria central aumenta la respuesta antitumoral.

5. La reactivación de linfocitos T $CD8^+$ de memoria central contra los tumores es dependiente de las células dendríticas tipo 1.

Bibliografía

11. Bibliografía

Alexandre YO, Ghilas S, Sanchez C *et al.* XCR1$^+$ dendritic cells promote memory CD8$^+$ T cell recall upon secondary infections with Listeria monocytogenes or certain viruses. *J Exp Med* 2016;**213**:75-92.

von Andrian UH, Mempel TR. Homing and cellular traffic in lymph nodes. *Nat Rev Immunol* 2003;**3**:867-78.

Ansell SM, Lesokhin AM, Borrello I *et al.* PD-1 Blockade with Nivolumab in Relapsed or Refractory Hodgkin's Lymphoma. *N Engl J Med* 2015;**372**:311-9.

Ariotti S, Hogenbirk MA, Dijkgraaf FE *et al.* T cell memory. Skin-resident memory CD8$^+$ T cells trigger a state of tissue-wide pathogen alert. *Science* 2014;**346**:101-5.

Bedoui S, Heath WR. Krüppel-ling of IRF4-Dependent DCs into Two Functionally Distinct DC Subsets. *Immunity* 2015;**42**:785-7.

Berg EL, Yoshino T, Rott LS *et al*. The cutaneous lymphocyte antigen is a skin lymphocyte homing receptor for the vascular lectin endothelial cell-leukocyte adhesion molecule 1. *J Exp Med* 1991;**174**:1461-6.

Boddupalli CS, Bar N, Kadaveru K *et al.* Interlesional diversity of T cell receptors in melanoma with immune checkpoints enriched in tissue-resident memory T cells. *JCI Insight* 2016;**1**:1-13.

Bollard CM, Rooney CM, Heslop HE. T-cell therapy in the treatment of post-transplant lymphoproliferative disease. *Nat Rev Clin Oncol* 2012;**9**:510-9.

Borowitz MJ, Weidner A, Olsen EA *et al.* Abnormalities of circulating T-cell subpopulations in patients with cutaneous T-cell lymphoma: cutaneous lymphocyte-associated antigen expression on T cells correlates with extent of disease. *Leukemia* 1993;**7**:859-63.

Böttcher J, Knolle PA. Global transcriptional characterization of CD8$^+$ T cell memory. *Semin Immunol* 2015;**27**:4-9.

Brahmer JR, Tykodi SS, Chow LQM *et al.* Safety and Activity of Anti–PD-L1 Antibody in Patients with Advanced Cancer. *N Engl J Med* 2012;**366**:2455-65.

Briskin M, Winsor-Hines D, Shyjan A *et al.* Human mucosal addressin cell adhesion molecule-1 is preferentially expressed in intestinal tract and associated lymphoid tissue. *Am J Pathol* 1997;**151**:97-110.

Bromley SK, Thomas SY, Luster AD. Chemokine receptor CCR7 guides T cell exit from peripheral tissues and entry into afferent lymphatics. *Nat Immunol* 2005;**6**:895-901.

Bromley SK, Yan S, Tomura M *et al.* Recirculating Memory T cells are a Unique Subset of CD4$^+$ T Cells with a Distinct Phenotype and Migratory Pattern. *J Immunol* 2013;**190**:970-6.

Broz ML, Binnewies M, Boldajipour B *et al.* Dissecting the tumor myeloid compartment reveals rare activating antigen-presenting cells critical for T cell immunity. *Cancer Cell* 2014;**26**:638-52.

Butte MJ, Keir ME, Phamduy TB *et al.* PD-L1 interacts specifically with B7-1 to inhibit T cell proliferation. *Immunity* 2007;**27**:111-22.

Cahill RNP, Frost H, and Trnka Z.The effects of antigen on the migration of recirculating lymphocytes through single lymph nodes. *J Exp Med* 1976;**143**:870-88.

Campbell JJ, Haraldsen G, Pan J *et al.* The chemokine receptor CCR4 in vascular recognition by cutaneous but not intestinal memory T cells. *Nature* 1999;**400**:776-80.

Campbell JJ, Pan J, Butcher EC. Cutting Edge: Developmental Switches in Chemokine Responses During T Cell Maturation. *J Immunol* 1999;**163**:2353-2357.

Carbone FR. Tissue-Resident Memory T Cells and Fixed Immune Surveillance in Nonlymphoid Organs. *J Immunol* 2015;**195**:17-22.

Cella M, Jarrossay D, Facchetti F *et al.* Plasmacytoid monocytes migrate to inflamed lymph nodes and produce large amounts of type I interferon. *Nat Med* 1999;**5**:919-23.

Cells TMT, Schenkel JM, Masopust D. Review. *Immunity* 2014;**41**:886-97.

Chang JT, Wherry EJ, Goldrath AW. Molecular regulation of effector and memory T cell differentiation. 2014;**15**(12):1104-15

Chong BF, Murphy J-E, Kupper TS *et al.* E-Selectin, Thymus- and Activation-Regulated Chemokine/CCL17, and Intercellular Adhesion Molecule-1 Are Constitutively Coexpressed in Dermal Microvessels: A Foundation for a Cutaneous Immunosurveillance System. *J Immunol* 2004;**172**:1575-1581.

Cieri N, Camisa B, Cocchiarella F *et al.* IL-7 and IL-15 instruct the generation of human memory stem T cells from naive precursors. *Blood* 2013;**121**:573-584.

Clark RA. Resident memory T cells in human health and disease. *Sci Transl Med* 2015;**7**:269rv1.

Conejero L, Khouili SC, Martínez-Cano S *et al.* Lung CD103$^+$ dendritic cells restrain allergic airway

inflammation through IL-12 production. *JCI Insight* 2017;**2**(10).
Cyster JG, Schwab SR. Sphingosine-1-Phosphate and Lymphocyte Egress from Lymphoid Organs. *Annu Rev Immunol* 2012;**30**:69-94.
Diamond MS, Kinder M, Matsushita H *et al.* Type I interferon is selectively required by dendritic cells for immune rejection of tumors. *J Exp Med 2011*;208(10):1989–2003
Djenidi F, Adam J, Goubar A *et al.* $CD8^+CD103^+$ tumor-infiltrating lymphocytes are tumor-specific tissue-resident memory T cells and a prognostic factor for survival in lung cancer patients. *J Immunol* 2015;**194**:3475-86.
Dong H, Strome SE, Salomao DR *et al.* Tumor-associated B7-H1 promotes T-cell apoptosis: A potential mechanism of immune evasion. *Nat Med* 2002;**8**:793-800.
Dotti G, Gottschalk S, Savoldo B *et al.* Design and Development of Therapies using Chimeric Antigen Receptor-Expressing T cells. *Immunol Rev* 2014;**257**(1):107-26
Doulatov S, Notta F, Eppert K *et al.* Revised map of the human progenitor hierarchy shows the origin of macrophages and dendritic cells in early lymphoid development. *Nat Immunol* 2010;**11**:585-93.
Dustin ML, Bromley SK, Kan Z *et al.* Antigen receptor engagement delivers a stop signal to migrating T lymphocytes. *Proc Natl Acad Sci U S A* 1997;**94**:3909-13.
Edelson BT, KC W, Juang R *et al.* Peripheral $CD103^+$ dendritic cells form a unified subset developmentally related to $CD8\alpha^+$ conventional dendritic cells. *J Exp Med* 2010;**207**:823-36.
Erkes DA, Smith CJ, Wilski NA *et al.* Virus-Specific $CD8^+$ T Cells Infiltrate Melanoma Lesions and Retain Function Independently of PD-1 Expression. *J Immunol* 2017;198(7):2979-298.
Everts B, Tussiwand R, Dreesen L *et al.* Migratory $CD103^+$ dendritic cells suppress helminth-driven type 2 immunity through constitutive expression of IL-12. *J Exp Med* 2016;**213**:35-51.
Fearon DT, Manders P, Wagner SD. Arrested Differentiation, the Self-Renewing Memory Lymphocyte, and Vaccination. *Science* 2001;**293**:248-250.
Fife BT, Pauken KE, Eagar TN *et al.* Interactions between PD-1 and PD-L1 promote tolerance by blocking the TCR–induced stop signal. *Nat Immunol* 2009;**10**:1185-92.
Fox BA, Schendel DJ, Butterfield LH *et al.* Defining the critical hurdles in cancer immunotherapy. *J Transl Med* 2011;**9**:214.
Freeman GJ, Long AJ, Iwai Y *et al.* Engagement of the PD-1 immunoinhibitory receptor by a novel B7 family member leads to negative regulation of lymphocyte activation. *J Exp Med* 2000;**192**:1027-34.
Fuertes MB, Kacha AK, Kline J *et al.* Host type I IFN signals are required for antitumor $CD8^+$ T cell responses through $CD8\alpha^+$ dendritic cells. *J Exp Med* 2011, 208(10):2005–2016.
Gaide O, Emerson RO, Jiang X *et al.* Common clonal origin of central and resident memory T cells following skin immunization. *Nat Med* 2015;**21**:647-53.
Gattinoni L, Lugli E, Ji Y *et al.* A human memory T-cell subset with stem cell-like properties. *Nat Med* 2011;**17**:1290-7.
Gattinoni L, Zhong X-S, Palmer DC *et al.* Wnt signaling arrests effector T cell differentiation and generates $CD8^+$ memory stem cells. *Nat Med* 2009;**15**:808-13.
Gazzinelli RT, Hieny S, Wynn TA *et al.* Interleukin 12 is required for the T-lymphocyte-independent induction of interferon gamma by an intracellular parasite and induces resistance in T-cell-deficient hosts. *Proc Natl Acad Sci U S A* 1993;**90**:6115-9.
Gazzinelli RT, Wysocka M, Hayashi S *et al.* Parasite-induced IL-12 stimulates early IFN-gamma synthesis and resistance during acute infection with Toxoplasma gondii. *J Immunol* 1994;**153**:2533-2543.
Gebhardt T, Wakim LM, Eidsmo L *et al.* Memory T cells in nonlymphoid tissue that provide enhanced local immunity during infection with herpes simplex virus. *Nat Immunol* 2009;**10**:524-30.
Geissmann F, Jung S, Littman DR. Blood monocytes consist of two principal subsets with distinct migratory properties. *Immunity* 2003;**19**:71-82.
Graef P, Buchholz VR, Stemberger C *et al.* Serial transfer of single-cell-derived immunocompetence reveals stemness of $CD8^+$ central memory T cells. *Immunity* 2014;**41**:116-26.
Grigorova IL, Panteleev M, Cyster JG. Lymph node cortical sinus organization and relationship to lymphocyte egress dynamics and antigen exposure. *Proc Natl Acad Sci U S A* 2010;**107**:20447-52.
Hacker C, Kirsch RD, Ju X-S *et al.* Transcriptional profiling identifies Id2 function in dendritic cell development. *Nat Immunol* 2003;**4**:380-6.
Hadley GA, Higgins JMG. Integrin αEβ7: Molecular Features and Functional Significance in the Immune System. En: Gullberg D (ed.). *I Domain Integrins*. Dordrecht: Springer Netherlands, 2014, 97-110.
Hall JG, Morris B. The immediate effect of antigens on the cell output of a lymph node. *Br J Exp Pathol* 1965;**46**:450-4.
Hamann D, Baars PA, Rep MH *et al.* Phenotypic and functional separation of memory and effector human $CD8^+$ T cells. *J Exp Med* 1997;**186**:1407-18.
Hashimoto D, Chow A, Noizat C *et al.* Tissue-Resident Macrophages Self-Maintain Locally throughout

Adult Life with Minimal Contribution from Circulating Monocytes. *Immunity* 2013;**38**:792-804.
Hashimoto D, Miller J, Merad M. Dendritic cell and macrophage heterogeneity in vivo. *Immunity* 2011;**35**:323-35.
Headley MB, Bins A, Nip A *et al.* Visualization of immediate immune responses to pioneer metastatic cells in the lung. *Nature* 2016;**531**:513-7.
Heath WR, Carbone FR. Dendritic cell subsets in primary and secondary T cell responses at body surfaces. *Nat Immunol* 2009;**10**:1237-44.
Hettinger J, Richards DM, Hansson J *et al.* Origin of monocytes and macrophages in a committed progenitor. *Nat Immunol* 2013;**14**:821-30.
Hijnen D, Knol EF, Gent YY *et al.* $CD8^+$ T cells in the lesional skin of atopic dermatitis and psoriasis patients are an important source of IFN-γ, IL-13, IL-17 and IL-22. *J Invest Dermatol* 2013; **133**(4):973-9.
Hildner K, Edelson BT, Purtha WE *et al.* Batf3 deficiency reveals a critical role for $CD8\alpha^+$ dendritic cells in cytotoxic T cell immunity. *Science* 2008;**322**:1097-100.
Hogan RJ, Usherwood EJ, Zhong W *et al.* Activated Antigen-Specific $CD8^+$ T Cells Persist in the Lungs Following Recovery from Respiratory Virus Infections. *J Immunol* 2001;**166**:1813-1822.
Homey B, Alenius H, Muller A *et al.* CCL27-CCR10 interactions regulate T cell-mediated skin inflammation. *Nat Med* 2002;**8**:157-65.
Hondowicz BD, An D, Schenkel JM *et al.* Interleukin-2-Dependent Allergen-Specific Tissue-Resident Memory Cells Drive Asthma. *Immunity* 2015; **44**(1):155-66
Hou B, Benson A, Kuzmich L *et al.* Critical coordination of innate immune defense against Toxoplasma gondii by dendritic cells responding via their Toll-like receptors. *Proc Natl Acad Sci U S A* 2011;**108**:278-83.
Hu Y, Lee Y-T, Kaech SM *et al.* Smad4 Promotes Differentiation of Effector and Circulating Memory CD8 T Cells but Is Dispensable for Tissue-Resident Memory CD8 T Cells. *J Immunol* 2015;**194**(5):2407-14
Hume DA. The mononuclear phagocyte system. *Curr Opin Immunol* 2006;**18**:49-53.
Hume DA. Macrophages as APC and the dendritic cell myth. *J Immunol* 2008;**181**:5829-35.
Hume DA, Ross IL, Himes SR *et al.* The mononuclear phagocyte system revisited. *J Leukoc Biol* 2002;**72**:621-7.
Iborra S, Izquierdo HM, Martínez-López M *et al.* The DC receptor DNGR-1 mediates cross-priming of CTLs during vaccinia virus infection in mice. 2012;**122**(5):1628-43
Iborra S, Martinez-Lopez M, Khouili SC *et al.* Optimal Generation of Tissue-Resident but Not Circulating Memory T Cells during Viral Infection Requires Crosspriming by $DNGR\text{-}1^+$ Dendritic Cells. *Immunity* 2016;**45**:847-60.
Idoyaga J, Fiorese C, Zbytnuik L *et al.* Specialized role of migratory dendritic cells in peripheral tolerance induction. *J Clin Invest* 2013;**123**(2):844-54
Iijima N, Iwasaki A. A local macrophage chemokine network sustains protective tissue-resident memory CD4 T cells. *Science* 2014;346(6205):93-98
Ishida M, Iwai Y, Tanaka Y *et al.* Differential expression of PD-L1 and PD-L2, ligands for an inhibitory receptor PD-1, in the cells of lymphohematopoietic tissues. *Immunol Lett* 2002;**84**:57-62.
Iwata M, Hirakiyama A, Eshima Y *et al.* Retinoic acid imprints gut-homing specificity on T cells. *Immunity* 2004;**21**:527-38.
Jena B, Dotti G, Cooper LJN. Redirecting T-cell specificity by introducing a tumor-specific chimeric antigen receptor. *Blood* 2010;**116**:1035-44.
Jensen MC, Riddell SR. Design and implementation of adoptive therapy with chimeric antigen receptor-modified T cells. *Immunol Rev* 2014;**257**:127-44.
Jiang X, Clark R a, Liu L *et al.* Skin infection generates non-migratory memory $CD8^+$ TRM cells providing global skin immunity. *Nature* 2012;**483**:227-31.
Joshi NS, Cui W, Dominguez C *et al.* Increased numbers of pre-existing memory CD8 T cells and decreased T-bet expression can restrain terminal differentiation of secondary effector and memory CD8 T cells. *J Immunol* 2011;**187**:4068-76.
June CH, Blazar BR, Riley JL. Engineering lymphocyte subsets: tools, trials and tribulations. *Nat Rev Immunol* 2009;**9**:704-16.
Kaech SM, Cui W. Transcriptional control of effector and memory CD8+ T cell differentiation. *Nat Rev Immunol* 2012;**12**:749-61.
Kashiwada M, Pham N-LL, Pewe LL *et al.* NFIL3/E4BP4 is a key transcription factor for $CD8\alpha^+$ dendritic cell development. *Blood* 2011;**117**:6193-7.
Keir ME, Butte MJ, Freeman GJ *et al.* PD-1 and Its Ligands in Tolerance and Immunity. *Annu Rev Immunol* 2008;**26**:677-704.

Kershaw MH, Westwood JA, Darcy PK. Gene-engineered T cells for cancer therapy. *Nat Rev Cancer* 2013;**13**:525-41.

Klebanoff CA, Gattinoni L, Torabi-Parizi P *et al.* Central memory self/tumor-reactive $CD8^+$ T cells confer superior antitumor immunity compared with effector memory T cells. *Proc Natl Acad Sci U S A* 2005;**102**:9571-6.

Klebanoff CA, Scott CD, Leonardi AJ *et al.* Memory T cell-driven differentiation of naive cells impairs adoptive immunotherapy. *J Clin Invest* 2016;**126**:318-34.

Klonowski KD, Williams KJ, Marzo AL *et al.* Dynamics of Blood-Borne CD8 Memory T Cell Migration In Vivo. *Immunity* 2004;**20**:551-62.

Komdeur FL, Wouters MC, Workel HH *et al.* $CD103^+$ intraepithelial T cells in high-grade serous ovarian cancer are phenotypically diverse $TCR\alpha\beta^+$ $CD8\alpha\beta^+$ T cells that can be targeted for cancer immunotherapy. *Oncotarget* 2016;**7**:75130-44.

Kuklin NA, Rott L, Darling J *et al.* α4β7 independent pathway for $CD8^+$ T cell–mediated intestinal immunity to rotavirus. *J Clin Invest* 2000;**106**:1541-52.

Kupper TS. Old and New: Recent Innovations in Vaccine Biology and Skin T Cells. *J Invest Dermatol* 2012;**132**:829-34.

Kupper TS, Fuhlbrigge RC. Immune surveillance in the skin: mechanisms and clinical consequences. *Nat Rev Immunol* 2004;**4**:211-22.

Laidlaw BJ, Zhang N, Marshall HD *et al.* $CD4^+$ T cell help guides formation of $CD103^+$ lung-resident memory $CD8^+$ T cells during influenza viral infection. *Immunity* 2014;**41**:633-45.

Leen AM, Heslop HE, Brenner MK. Antiviral T-cell therapy. *Immunol Rev* 2014;**258**:12-29.

Liu L, Fuhlbrigge RC, Karibian K *et al.* Dynamic Programing of $CD8^+$ T Cell Trafficking after Live Viral Immunization. *Immunity* 2006;**25**:511-20.

Liu L, Zhong Q, Tian T *et al.* Epidermal injury and infection during poxvirus immunization is crucial for the generation of highly protective T cell-mediated immunity. *Nat Med* 2010;**16**:224-7.

Lugli E, Dominguez MH, Gattinoni L *et al.* Superior T memory stem cell persistence supports long-lived T cell memory. *J Clin Invest* 2013; **123**(2):594-9

Mackay CR, von Andrian UH. Memory T Cells-Local Heroes in the Struggle for Immunity. *Science* 2001;**291**:2323-2324.

Mackay LK, Braun A, Macleod BL *et al.* Cutting Edge: CD69 Interference with Sphingosine-1-Phosphate Receptor Function Regulates Peripheral T Cell Retention. *J Immunol* 2015;**194**(5):2059-63

Mackay LK, Rahimpour A, Ma JZ *et al.* The developmental pathway for $CD103^+CD8^+$ tissue-resident memory T cells of skin. *Nat Immunol* 2013;**14**:1294-301.

Mackay LK, Stock AT, Ma JZ *et al.* Long-lived epithelial immunity by tissue-resident memory T (TRM) cells in the absence of persisting local antigen presentation. *Proc Natl Acad Sci U S A* 2012;**109**:7037-42.

Maldonado-López R, De Smedt T, Michel P *et al.* $CD8\alpha^+$ and $CD8\alpha^-$ Subclasses of Dendritic Cells Direct the Development of Distinct T Helper Cells In Vivo . *J Exp Med* 1999;**189**:587-92.

Malik BT, Byrne KT, Vella JL *et al.* Resident memory T cells in the skin mediate durable immunity to melanoma. 2017:**2**(10)1-12.

Martínez-Lopez M, Iborra S, Conde-Garrosa R *et al.* Batf3-dependent $CD103^+$ dendritic cells are major producers of IL-12 that drive local Th1 immunity against Leishmania major infection in mice. *Eur J Immunol* 2015;**45**:119-29.

Mashayekhi M, Sandau MM, Dunay IR *et al.* $CD8\alpha^+$ dendritic cells are the critical source of interleukin-12 that controls acute infection by Toxoplasma gondii tachyzoites. *Immunity* 2011;**35**:249-59.

Masopust D, Ha S-J, Vezys V *et al.* Stimulation History Dictates Memory CD8 T Cell Phenotype: Implications for Prime-Boost Vaccination. *J Immunol* 2006a;**177**:831-839.

Masopust D, Vezys V, Marzo AL *et al.* Preferential Localization of Effector Memory Cells in Nonlymphoid Tissue. *Science* 2001;**291**:2413-2417.

Masopust D, Vezys V, Wherry EJ *et al.* Cutting edge: gut microenvironment promotes differentiation of a unique memory CD8 T cell population. *J Immunol* 2006b;**176**:2079-83.

Massoud AH, Yona M, Xue D *et al.* Dendritic cell immunoreceptor: a novel receptor for intravenous immunoglobulin mediates induction of regulatory T cells. *J Allergy Clin Immunol* 2014;**133**:853-63.

Maus M V, Fraietta JA, Levine BL *et al.* Adoptive Immunotherapy for Cancer or Viruses. *Annu Rev Immunol* 2014;**32**:189-225.

Mempel TR, Henrickson SE, von Andrian UH. T-cell priming by dendritic cells in lymph nodes occurs in three distinct phases. *Nature* 2004;**427**:154-9.

Miller JC, Brown BD, Shay T *et al.* Deciphering the transcriptional network of the dendritic cell lineage. *Nat Immunol* 2012;**13**:888-99.

Mueller SN, Gebhardt T, Carbone FR *et al.* Memory T cell subsets, migration patterns, and tissue residence.

Annu Rev Immunol 2013;**31**:137-61.
Mueller SN, Mackay LK. Tissue-resident memory T cells: local specialists in immune defence. *Nat Rev Immunol* 2016;**16**:79-89.
Murphy TL, Tussiwand R, Murphy KM. Specificity through cooperation: BATF-IRF interactions control immune-regulatory networks. *Nat Rev Immunol* 2013;**13**:499-509.
Naik S, Bouladoux N, Linehan JL *et al.* Commensal-dendritic-cell interaction specifies a unique protective skin immune signature. *Nature* 2015;**520**:104–108.
Naik SH, Perié L, Swart E *et al.* Diverse and heritable lineage imprinting of early haematopoietic progenitors. *Nature* 2013;**496**:229–232
Nakanishi Y, Lu B, Gerard C *et al.* $CD8^+$ T lymphocyte mobilization to virus-infected tissue requires $CD4^+$ T-cell help. *Nature* 2009;**462**:510-3.
Nestle F, Di Meglio P, Qin J *et al.* Skin immune sentinels in health and disease. *Nat Rev Immunol* 2009; **9**(10):679–691.
Nishimura H, Minato N, Nakano T *et al.* Immunological studies on PD-1 deficient mice: implication of PD-1 as a negative regulator for B cell responses. *Int Immunol* 1998;**10**:1563-72.
Nolz JC, Harty JT. Protective Capacity of Memory $CD8^+$ T Cells is Dictated by Antigen Exposure History and Nature of the Infection. *Immunity* 2011;**34**:781-93.
Nussenzweig MC, Steinman RM, Unkeless JC *et al.* Studies of the cell surface of mouse dendritic cells and other leukocytes. *J Exp Med* 1981;**154**:168-187.
Nussenzweig MC, Steinman RM, Witmer MD *et al.* A monoclonal antibody specific for mouse dendritic cells. *Proc Natl Acad Sci USA* 1982;**79**:161-5.
Onai N, Kurabayashi K, Hosoi-Amaike M *et al.* A Clonogenic Progenitor with Prominent Plasmacytoid Dendritic Cell Developmental Potential. *Immunity* 2013;**38**:943-57.
Park CO, Kupper TS. The emerging role of resident memory T cells in protective immunity and inflammatory disease. *Nat Med* 2015;**21**:688-97.
Patsoukis N, Bardhan K, Chatterjee P *et al.* PD-1 alters T-cell metabolic reprogramming by inhibiting glycolysis and promoting lipolysis and fatty acid oxidation. *Nat Commun* 2015;**6**:6692.
Persson EK, Uronen-Hansson H, Semmrich M *et al.* IRF4 Transcription-Factor-Dependent $CD103^+CD11b^+$ Dendritic Cells Drive Mucosal T Helper 17 Cell Differentiation. *Immunity* 2013;**38**:958-69.
Pfirschke C, Engblom C, Rickelt S *et al.* Immunogenic Chemotherapy Sensitizes Tumors to Checkpoint Blockade Therapy. *Immunity* 2016;**44**:343-54.
Pfirschke C, Siwicki M, Liao H-W *et al.* Tumor Microenvironment: No Effector T Cells without Dendritic Cells. *Cancer Cell* 2017;**31**:614-5.
Picker LJ, Treer JR, Ferguson-Darnell B *et al.* Control of lymphocyte recirculation in man. II. Differential regulation of the cutaneous lymphocyte-associated antigen, a tissue-selective homing receptor for skin-homing T cells. *J Immunol* 1993;**150**:1122-1136.
Piet B, de Bree GJ, Smids-Dierdorp BS *et al.* $CD8^+$ T cells with an intraepithelial phenotype upregulate cytotoxic function upon influenza infection in human lung . *J Clin Invest* 2011;**121**:2254-63.
Purwar R, Campbell J, Murphy G *et al.* Resident memory T cells (TRM) are abundant in human lung: diversity, function, and antigen specificity. *PLoS One* 2011;**6**(1)
Randolph GJ, Inaba K, Robbiani DF *et al.* Differentiation of Phagocytic Monocytes into Lymph Node Dendritic Cells In Vivo. *Immunity* 1999;**11**:753-61.
Rao UNM, Lee SJ, Luo W *et al.* Presence of Tumor-Infiltrating Lymphocytes and a Dominant Nodule Within Primary Melanoma Are Prognostic Factors for Relapse-Free Survival of Patients With Thick (T4) Primary Melanoma Pathologic Analysis of the E1690 and E1694 Intergroup Trials. *Am J Clin Pathol* 2010;**133**:646-53.
Reinhardt RL, Khoruts A, Merica R *et al.* Visualizing the generation of memory CD4 T cells in the whole body. *Nature* 2001;**410**:101-5.
Reis e Sousa C, Hieny S, Scharton-Kersten T *et al.* In vivo microbial stimulation induces rapid CD40 ligand-independent production of interleukin 12 by dendritic cells and their redistribution to T cell areas. *J Exp Med* 1997;**186**:1819-29.
Ribas A, Shin DS, Zaretsky J *et al.* PD-1 Blockade Expands Intratumoral Memory T Cells. *Cancer Immunol Res* 2016;**4**:194-203.
Robbins SH, Walzer T, Dembélé D *et al.* Novel insights into the relationships between dendritic cell subsets in human and mouse revealed by genome-wide expression profiling. *Genome Biol* 2008;**9**:R17.
Robert C, Long G V, Brady B *et al.* Nivolumab in Previously Untreated Melanoma without BRAF Mutation. *N Engl J Med* 2014;**372**:320-30.
Roberts EW, Broz ML, Binnewies M *et al.*Critical Role for $CD103^+$ / $CD141^+$ Dendritic Cells Bearing CCR7 for Tumor Antigen Trafficking and Priming of T Cell Immunity in Melanoma. *Cancer Cell*

2016; **30**(2):324-36
Rosenberg SA, Restifo NP. Adoptive cell transfer as personalized immunotherapy for human cancer. *Science* 2015;**348**:62-8.
Ruffell B, Chang-Strachan D, Chan V *et al.* Macrophage IL-10 Blocks $CD8^+$ T Cell-Dependent Responses to Chemotherapy by Suppressing IL-12 Expression in Intratumoral Dendritic Cells. *Cancer Cell* 2014;**26**:623-37.
Sadelain M. T-Cell Engineering for Cancer Immunotherapy. *Cancer J* 2009;**15**(6):451-5
Sallusto F, Lanzavecchia A. Heterogeneity of $CD4^+$ memory T cells: functional modules for tailored immunity. *Eur J Immunol* 2009;**39**:2076-82.
Sallusto F, Lenig D, Förster R *et al.* Two subsets of memory T lymphocytes with distinct homing potentials and effector functions. *Nature* 1999;**401**:708-12.
Salmon H, Idoyaga J, Rahman A *et al.* Expansion and Activation of $CD103^+$ Dendritic Cell Progenitors at the Tumor Site Enhances Tumor Responses to Therapeutic PD-L1 and BRAF Inhibition. *Immunity* 2016;**44**:924-38.
Sanchez-Paulete AR, Cueto FJ, Martínez-López M *et al.* Cancer Immunotherapy with Immunomodulatory Anti-CD137 and Anti-PD-1 Monoclonal Antibodies Requires BATF3-Dependent Dendritic Cells. *Cancer Discov* 2016;**6**:71-9.
Sancho D, Joffre OP, Keller AM *et al.* Identification of a dendritic cell receptor that couples sensing of necrosis to immunity. *Nature* 2009;**458**:899-903.
Sandoval F, Terme M, Nizard M *et al.* Mucosal imprinting of vaccine-induced $CD8^+$ T cells is crucial to inhibit the growth of mucosal tumors. *Sci Transl Med* 2013;**5**:172ra20.
Sathe P, Metcalf D, Vremec D *et al.* Lymphoid tissue and plasmacytoid dendritic cells and macrophages do not share a common macrophage-dendritic cell-restricted progenitor. *Immunity* 2014;**41**:104-15.
Satpathy AT, Wu X, Albring JC *et al.* Redefining the dendritic cell lineage. *Nat Immunol* 2012;**13**:1145-54.
Schenkel JM, Fraser KA, Beura LK *et al.* Resident memory CD8 T cells trigger protective innate and adaptive immune responses. 2014;**346**(6205):98–101.
Schiavoni G, Mattei F, Sestili P *et al.* ICSBP Is Essential for the Development of Mouse Type I Interferon-producing Cells and for the Generation and Activation of $CD8\alpha^+$ Dendritic Cells. *J Exp Med* 2002;**196**:1415-25.
Schuler G. and Steinman RM. Murine epidermal Langerhans cells mature into potent immunostimulatory dendritic cells in vitro. *J Exp Med* 1985;**161**:526-46.
Schlapbach C, Gehad A, Yang C *et al.* Human TH9 Cells Are Skin-Tropic and Have Autocrine and Paracrine Proinflammatory Capacity. *Sci Transl Med* 2014;**6**:219ra8.
Schlitzer A, McGovern N, Teo P *et al.* IRF4 transcription factor-dependent $CD11b^+$ dendritic cells in human and mouse control mucosal IL-17 cytokine responses. *Immunity* 2013;**38**:970-83.
Schraml BU, van Blijswijk J, Zelenay S *et al.* Genetic Tracing via DNGR-1 Expression History Defines Dendritic Cells as a Hematopoietic Lineage. *Cell* 2013;**154**:843-58.
Schraml BU, Reis e Sousa C. Defining dendritic cells. *Curr Opin Immunol* 2015;**32**:13-20.
Seneschal J, Clark RA, Gehad A *et al.* Human Epidermal Langerhans Cells Maintain Immune Homeostasis in Skin by Activating Skin Resident Regulatory T Cells. *Immunity* 2012;3**6**(5):873-84
Serbina N V, Salazar-Mather TP, Biron CA *et al.* TNF/iNOS-Producing Dendritic Cells Mediate Innate Immune Defense against Bacterial Infection. *Immunity* 2003;**19**:59-70.
Sharma P, Allison JP. The future of immune checkpoint therapy. *Science* 2015a;**348**:56-61.
Sharma P, Allison JP. Immune checkpoint targeting in cancer therapy: toward combination strategies with curative potential. *Cell* 2015b;**161**:205-14.
Sher A, Oswald IP, Hieny S *et al.* Toxoplasma gondii induces a T-independent IFN-γ response in natural killer cells that requires both adherent accessory cells and tumor necrosis factor-alpha. *J Immunol* 1993;**150**:3982-3989.
Sheridan BS, Pham Q-M, Lee Y-T *et al.* Oral Infection Drives a Distinct Population of Intestinal Resident Memory $CD8^+$ T Cells with Enhanced Protective Function. *Immunity* 2014;**40**(5):747-57.
Shimamura K, Takeichi M. Local and transient expression of E-cadherin involved in mouse embryonic brain morphogenesis. *Development* 1992;**116**:1011-1019.
Shin H, Iwasaki A. A vaccine strategy that protects against genital herpes by establishing local memory T cells. *Nature* 2012;**491**(7424):463-7
Shin H, Kumamoto Y, Gopinath S *et al.* $CD301b^+$ dendritic cells stimulate tissue-resident memory $CD8^+$ T cells to protect against genital HSV-2. *Nat Commun* 2016;**7**:13346.
Siegal FP, Kadowaki N, Shodell M *et al.* The Nature of the Principal Type 1 Interferon-Producing Cells in Human Blood. *Science* 1999;**284**:1835-1837.
Skon CN, Lee J-Y, Anderson KG *et al.* Transcriptional downregulation of S1pr1 is required for the establishment of resident memory $CD8^+$ T cells. *Nat Immunol* 2013;**14**(12):1285–1293.

Spranger S, Bao R, Gajewski TF. Melanoma-intrinsic β-catenin signalling prevents anti-tumour immunity. *Nature* 2015;**523**:231-5.
Spranger S, Dai D, Horton B *et al.* Tumor-Residing Batf3 Dendritic Cells Are Required for Effector T Cell Trafficking and Adoptive T Cell Therapy. *Cancer Cell* 2017;**31**:711-723.
Steinert EM, Schenkel JM, Fraser KA *et al.* Quantifying Memory CD8 T Cells Reveals Regionalization of Immunosurveillance. *Cell* 2015;**161**:737-49.
Steinman RM, Cohn ZA. Identification of a novel cell type in peripheral lymphoid organs of mice. *J Exp Med* 1973;**137**:1142-1162.
Steinman RM, Idoyaga J. Features of the dendritic cell lineage. *Immunol Rev* 2010;**234**:5-17.
Surh CD, Boyman O, Purton JF *et al.* Homeostasis of memory T cells. *Immunol Rev* 2006;**211**:154-63.
Tamura T, Tailor P, Yamaoka K *et al.* IFN Regulatory Factor-4 and -8 Govern Dendritic Cell Subset Development and Their Functional Diversity. *J Immunol* 2005;**174**:2573-2581.
Thome JJC, Farber DL. Emerging concepts in tissue-resident T cells : lessons from humans. *Trends Immunol* 2015;**36**:428-35.
Tomura M, Yoshida N, Tanaka J *et al.* Monitoring cellular movement in vivo with photoconvertible fluorescence protein «Kaede» transgenic mice. *Proc Natl Acad Sci U S A* 2008;**105**:10871-6.
Tumeh PC, Harview CL, Yearley JH *et al.* PD-1 blockade induces responses by inhibiting adaptive immune resistance. *Nature* 2014;**515**:568-71.
Turner DL, Farber DL. Mucosal resident memory CD4 T cells in protection and immunopathology. *Front Immunol* 2014;**5**:331.
Turtle CJ, Swanson HM, Fujii N *et al.* A distinct subset of self-renewing human memory $CD8^+$ T cells survives cytotoxic chemotherapy. *Immunity* 2009;**31**:834-44.
Tussiwand R, Lee W-L, Murphy TL *et al.* Compensatory dendritic cell development mediated by BATF-IRF interactions. *Nature* 2012;**490**:502-7.
Virgin HW, Wherry EJ, Ahmed R. Redefining Chronic Viral Infection. *Cell* 2009;**138**:30-50.
Wakim LM, Woodward-Davis A, Bevan MJ. Memory T cells persisting within the brain after local infection show functional adaptations to their tissue of residence. *Proc Natl Acad Sci U S A* 2010;**107**:17872-9.
Wakim LM, Woodward-Davis A, Liu R *et al.* The molecular signature of tissue resident memory CD8 T cells isolated from the brain. *J Immunol* 2012;**189**:3462-71.
Wang MC, O'Rourke EJ, Ruvkun G. Fat Metabolism Links Germline Stem Cells and Longevity in C. elegans. *Science* 2008;**322**:957-60.
Wang X, Li H, Matte-Martone C *et al.* Mechanisms of antigen presentation to T cells in murine graft-vs-host disease: cross-presentation and the appearance of cross-presentation. *Blood* 2011;**118**(24):6426-37
Watanabe R, Gehad A, Yang C *et al.* Human skin is protected by four functionally and phenotypically discrete populations of resident and recirculating memory T cells. 2015;**7**(279):279ra39
Watchmaker PB, Lahl K, Lee M *et al.* Transcriptional and functional profiling of human intestinal dendritic cells reveals conserved specialization and a role for Bcl-6 and Blimp-1 in terminal subset differentiation. *Nat Immunol* 2014;**15**:98-108.
Webb JR, Milne K, Nelson BH. Location, location, location: CD103 demarcates intraepithelial, prognostically favorable $CD8^+$ tumor-infiltrating lymphocytes in ovarian cancer. *Oncoimmunology* 2014;**3**:e27668.
Wei C-H, Trenney R, Sanchez-Alavez M *et al.* Tissue-Resident Memory $CD8^+$ T Cells Can Be Deleted by Soluble, but Not Cross-Presented Antigen. *J Immunol* 2005;**175**:6615-6623.
Wherry EJ. T cell exhaustion. *Nat Immunol* 2011;**131**:492-9.
Whitney PG, Bar E, Osorio F *et al.* Syk signaling in dendritic cells orchestrates innate resistance to systemic fungal infection. *PLoS Pathog* 2014;**10**:e1004276.
Wirth TC, Xue H-H, Rai D *et al.* Repetitive antigen stimulation induces stepwise transcriptome diversification but preserves a core signature of memory $CD8^+$ T cell differentiation. *Immunity* 2010;**33**:128-40.
Wu T, Hu Y, Lee YT *et al.* Lung-resident memory CD8 T cells (TRM) are indispensable for optimal cross-protection against pulmonary virus infection. *J Leukoc Biol* 2014;**95**:215-24.
Xiao H, Peng Y, Hong Y *et al.* Lentivector Prime and Vaccinia Virus Vector Boost Generate High-Quality CD8 Memory T Cells and Prevent Autochthonous Mouse Melanoma. *J Immunol* 2011;**187**:1788-96.
Yamazaki T, Akiba H, Iwai H *et al.* Expression of Programmed Death 1 Ligands by Murine T Cells and APC. *J Immunol* 2002;**169**:5538-5545.
Yokosuka T, Takamatsu M, Kobayashi-Imanishi W *et al.* Programmed cell death 1 forms negative costimulatory microclusters that directly inhibit T cell receptor signaling by recruiting phosphatase SHP2. *J Exp Med* 2012;**209**:1201-17.

Youngblood B, Hale JS, Ahmed R. Memory CD8 T cell transcriptional plasticity. *F1000Prime Rep*. 2015;**10**:1-10.

Youngblood B, Noto A, Porichis F *et al.* Prolonged Exposure to HIV Reinforces a Poised Epigenetic Program for PD-1 Expression in Virus-specific CD8 T Cells. *J Immunol* 2013;**191**:540-4.

Youngblood B, Oestreich KJ, Ha S-J *et al.* Chronic virus infection enforces demethylation of the locus that encodes PD-1 in antigen-specific $CD8^+$ T cells. *Immunity* 2011;**35**:400-12.

Zabel BA, Agace WW, Campbell JJ *et al.* Human G Protein–Coupled Receptor Gpr-9-6/Cc Chemokine Receptor 9 Is Selectively Expressed on Intestinal Homing T Lymphocytes, Mucosal Lymphocytes, and Thymocytes and Is Required for Thymus-Expressed Chemokine–Mediated Chemotaxis. *J Exp Med* 1999;**190**:1241-56.

Zaugg K, Yao Y, Reilly PT *et al.* Carnitine palmitoyltransferase 1C promotes cell survival and tumor growth under conditions of metabolic stress. *Genes Dev* 2011;**25**:1041-51.

Zhang Y, Joe G, Hexner E *et al.* Host-reactive $CD8^+$ memory stem cells in graft-versus-host disease. *Nat Med* 2005;**11**:1299-305.

Zhou AC, Wagar LE, Wortzman ME *et al.* Intrinsic 4-1BB signals are indispensable for the establishment of an influenza-specific tissue-resident memory CD8 T-cell population in the lung. *Mucosal Immunol* 2017, DOI: 10.1038/mi.2016.124.

Anexos

12. Anexo 1: Publicaciones

12.1 Publicaciones a las que ha dado lugar este trabajo

Enamorado, M. et al. Enhanced anti-tumor immunity requires the interplay between resident and circulating memory CD8 T cells. **Nat. Commun.** 8, 16073 doi: 10.1038/ncomms16073 (2017).

12.2 Otras publicaciones

Sancho D, **Enamorado M**, Garaude J. Innate immune function of mitochondrial metabolism. ***Front. in Immunol.*** 2017; **8**:257.

Iborra S, Martínez-López M, Khouili SC, **Enamorado M**, Cueto FJ, Conde-Garrosa R, Del Fresno C, Sancho D. DNGR-1-mediated cross-priming by Batf3-dependent DC selectively regulates the generation of $CD8^+$ resident memory T cells. ***Immunity***. 2016;45(4):847-860.

Garaude J, Acín-Pérez R, Martínez-Cano S, **Enamorado M**, Ugolini M, Nistal-Villán E, Hervás-Stubbs S, Pelegrín P, Sander LE, Enríquez JA, Sancho D. Host defence to bacteria involves adaptations of the mitochondrial respiratory chain in macrophages. ***Nat. Immunol***. 2016;**17**(9):1037-1045.

nature COMMUNICATIONS

ARTICLE

Received 11 Oct 2016 | Accepted 25 May 2017 | Published xx xxx 2017

DOI: 10.1038/ncomms16073 OPEN

Enhanced anti-tumor immunity requires the interplay between resident and circulating memory CD8$^+$ T cells

Michel Enamorado[1], Salvador Iborra[1], Elena Priego[1,2], Francisco J. Cueto[1,2], Juan A. Quintana[1], Sarai Martínez-Cano[1], Ernesto Mejías-Pérez[3], Mariano Esteban[3], Ignacio Melero[4,5], Andrés Hidalgo[1,6] & David Sancho[1]

The goal of successful anti-tumoural immunity is the development of long-term protective immunity to prevent relapse. Infiltration of tumours with CD8$^+$ T cells with a resident memory (Trm) phenotype correlates with improved survival. However, the interplay of circulating CD8$^+$ T cells and Trm cells remains poorly explored in tumour immunity. Using different vaccination strategies that fine-tune the generation of Trm cells or circulating memory T cells, here we show that, while both subsets are sufficient for anti-tumour immunity, the presence of Trm cells improves anti-tumour efficacy. Transferred central memory T cells generate Trm cells following viral infection or tumour challenge. Anti-PD-1 treatment promotes infiltration of transferred Tcm cells within tumours, improving anti-tumour immunity. Moreover, Batf3-dependent dendritic cells are essential for reactivation of circulating memory anti-tumour response. Our findings show the plasticity, collaboration and requirements for reactivation of memory CD8$^+$ T cells subsets needed for optimal tumour vaccination and immunotherapy.

[1] Centro Nacional de Investigaciones Cardiovasculares Carlos III (CNIC), Melchor Fernández Almagro, 3, Madrid 28029, Spain. [2] Universidad Autónoma de Madrid, Arzobispo Morcillo 4, Madrid 28029, Spain. [3] Department of Molecular and Cellular Biology, Centro Nacional de Biotecnología, Consejo Superior de Investigaciones Científicas (CNB-CSIC), Darwin 3, Madrid 28049, Spain. [4] Division of Immunology and Immunotherapy, Center for Applied Medical Research (CIMA), Centro de Investigación Biomédica en Red de Cáncer (CIBERONC), Spain. [5] University Clinic, University of Navarra and Instituto de Investigación Sanitaria de Navarra (IdISNA), Pío XII, 55, 31008 Pamplona, Spain. [6] Institute for Cardiovascular Prevention (IPEK), Ludwig-Maximilians-Universität, Pettenkoferstrasse 9, 80336 Munich, Germany. Correspondence and requests for materials should be addressed to D.S. (email: dsancho@cnic.es).

Generation of optimal cancer immunotherapy involves induction of effective memory against the primary tumour able to prevent relapse metastases and recurrence. Circulating memory cells patrol the blood and include central memory T (Tcm) cells that retain the capacity to enter lymph nodes (LNs). Conversely, tissue-resident memory T (Trm) cells are confined to parenchymal non-lymphoid tissues[1–7]. Trm are characterized by stable surface expression of CD69 and an enhanced effector ability that functionally provides a tissue-wide alert state against local reinfection[6–11].

In mice, cutaneous infection with recombinant vaccinia virus (rVACV) generates circulating memory CD8$^+$ T cells and skin Trm cells, whereas i.p. infection does not generate skin Trm cells[12]. Infected parabiotic mice with skin Trm cells are more resistant to a rechallenge dermal infection than their circulation-sharing partners lacking Trm cells[12]. Optimal generation of Trm cells requires Batf3-dependent dendritic cells (DCs) during priming following VACV infection[13]. *Batf3*$^{-/-}$ mice show impaired immunity against syngeneic fibrosarcomas with marked intrinsic immunogenicity[14]. Tumour infiltration by CD103$^+$ Batf3-dependent DCs correlates with tumour regression[15] and favours T-cell infiltration in mouse models of melanoma[16]. CD103$^+$ DCs mediate antigen capture within the tumour and cross-prime tumour-specific CD8$^+$ T cells, whose therapeutic effects can be amplified by immunostimulatory antibodies[17,18].

The interplay between circulating CD8$^+$ T cells and Trm cells in anti-tumour immunity is largely unexplored. Previous studies in human cancer show that the infiltration of tumours by T cells with a Trm cell-like phenotype correlates with improved overall survival in early stage non-small-cell lung carcinoma, pulmonary squamous cell carcinoma and high-grade serous epithelial ovarian cancer[19–21]. In addition, recent results suggest that vaccination routes that promote generation of Trm cells could be more effective for anti-tumour response[22,23]. These findings prompted us to analyse the relative contribution and plasticity of circulating memory CD8$^+$ T cells and Trm cells in a model of anti-tumour vaccination.

In the present study, we demonstrate that circulating CD8$^+$ T cells and Trm cells cooperate in anti-tumour immunity. The circulating memory compartment retains enough degree of plasticity to become cells with a Trm phenotype within the grafted tumour and reside in the skin after tumour elimination. Immunotherapy with anti-PD-1 synergizes with transfer of tumour-specific Tcm cells, increasing CD8$^+$ T-cell infiltration of tumours. In addition, Batf3-dependent DCs are crucial for reactivation of circulating CD8$^+$ T-cell memory, inducing anti-tumour immunity. Knowledge on the generation of optimal memory against tumour antigens is essential for improved cancer immunotherapy.

Results

Both Trm and circulating memory promote anti-tumour immunity. To investigate the potential interplay between circulating memory and Trm CD8$^+$ T cells in anti-tumour immunity we first infected mice with rVACV-OVA by different routes and measured circulating and resident memory at 30 d.p.i. Frequencies of endogenous OVA-specific circulating memory T cells were similar regardless the infection route (Fig. 1a and Supplementary Fig. 1a). Whereas intraperitoneal (i.p.) infection with rVACV-OVA was inefficient for the generation of Trm cells in the skin or the lung, skin scarification (s.s.) in the tail promoted Trm cells in the infection site and in a distant cutaneous site, and intranasal (i.n.) infection induced Trm cells in the lung (Fig. 1b–d and Supplementary Fig. 1b–d).

To address the contribution of circulating and Trm CD8$^+$ T cells to control tumour growth, mice were infected with rVACV-OVA by s.s. or i.p. and, after generation of resident and/or circulating memory from the endogenous repertoire 30 days later[12], were inoculated intradermally (i.d.) with B16-OVA cells (Fig. 2a). We used the S1P antagonist FTY720 to block egress of T cells from LN into blood[12] and, in this way, limit the contribution of circulating memory T cells to the recall response. FTY720 administration at 30 days following rVACV-OVA i.p. or s.s. infection significantly reduced the presence of blood OVA-specific T circulating memory to the numbers observed in naive mice (Fig. 2b,c). Circulating memory T cells generated by i.p. vaccination with rVACV-OVA were sufficient to delay B16-OVA melanoma growth and this effect was significantly impaired by administration of FTY720 just before tumour inoculation and during tumour growth (Fig. 2d), demonstrating that circulating memory T cells protect against tumour development. However, following s.s. with rVACV-OVA, FTY720 treatment failed to reverse the enhanced tumour rejection (Fig. 2e), suggesting that Trm cells generated by this route are also sufficient for effective anti-tumour immunity. Thus, both circulating memory and Trm CD8$^+$ T cells are sufficient for anti-tumour immunity, resulting in delayed growth of B16-OVA-derived melanoma.

Trm improve circulating memory-mediated immunity to melanoma. To study the potential contribution of Trm cells to control melanoma growth in the presence of circulating memory T cells, we employed a parabiosis strategy with mice sharing circulating memory, but with only one of the parabionts bearing Trm (Fig. 3a). Accordingly, mice were infected by s.s. with rVACV-OVA 30 days before surgical parabiosis with naive mice and, after allowing a further 30-day period to equilibrate circulating memory T cells (Fig. 3b), parabiont mice were separated, allowed to recover and injected i.d. with B16-OVA cells. When compared with tumour-challenged naive mice, both infected or uninfected parabionts were significantly protected (Fig. 3c,d). However, when compared with uninfected partners that shared circulating memory T cells, detectable tumour onset was delayed in infected parabionts containing Trm cells (Fig. 3c). The delayed tumour incidence in infected parabionts containing Trm cells also resulted in significantly reduced tumour growth (Fig. 3d). Thus, the presence of Trm cells together with circulating memory T cells improves anti-tumour immunity in contrast to an environment containing only circulating memory CD8$^+$ T cells.

Plasticity of Tcm to become Trm upon viral challenge. Next, we investigated the potential plasticity of circulating memory CD8$^+$ T cells to produce Trm cells. Naive OT-I (CD44^{lo}CD62L^{hi}) cells are plastic and can become both circulating and skin-resident memory T cells upon transfer to mice subsequently infected in the skin with rVACV-OVA to favour Trm cell differentiation[13,24]. Mice transferred with naive OT-I cells and challenged i.d. with rVACV-OVA were used as source for OT-I Tcm cells 30 d.p.i. (Fig. 4a). Using naive OT-I cells as a positive control, we tested whether transfer of OT-I Tcm cells (CD44^{hi} CD62L^{hi}) could generate Trm cells in the skin 30 days or 60 days after infection i.d. with rVACV-OVA along with Tcm or naive OT-I transfer (Fig. 4a). Notably, Tcm cells generated Trm cells, defined as OT-I T cells in the skin 30 days or 60 days after viral infection and OT-I Tcm cell transfer, albeit with a lower efficiency than naive T cells (Fig. 4b,c). The majority of skin OT-I Trm cells derived from transferred OT-I Tcm cells showed stable CD69 expression with 50% of them co-expressing CD103 (Fig. 4d), which is consistent with previous results[12,13].

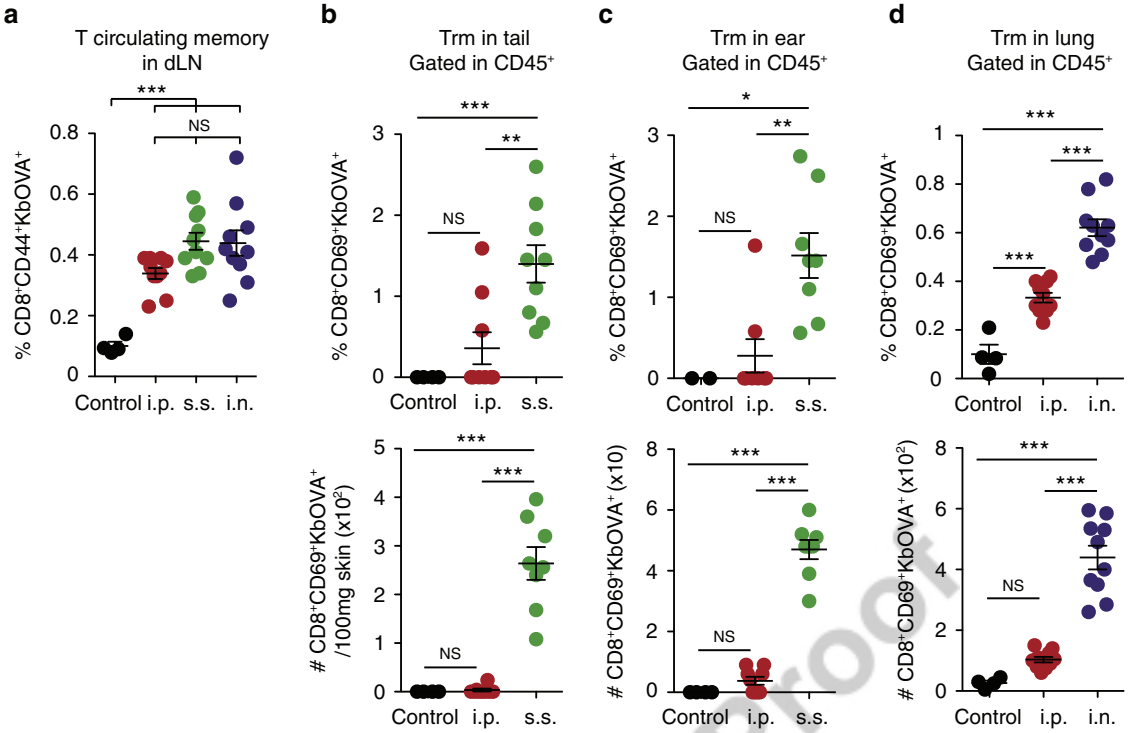

Figure 1 | Generation of Trm cells after different routes of rVACV-OVA infection. (**a**) Frequency of endogenous OVA-specific circulating memory CD8$^+$ T cells in the draining LN (dLN) 30 days after i.p. (5×10^4 p.f.u.), s.s. (2×10^6 p.f.u.) or i.n. (5×10^4 p.f.u.) infection with rVACV-OVA. (**b**–**d**) Frequency (top) and numbers (bottom) of endogenous OVA-specific Trm cells in the tail (**b**) and in the ear (**c**) 30 days after s.s. in the tail, and in the lung (**d**) 30 days after i.n. infection with rVACV-OVA. (**a**–**d**) Pool of two independent experiments represented as individual data and mean ± s.e.m. ($n=4$–5 per group). NS, not significant, ***$P<0.001$; **$P<0.01$; *$P<0.05$ by one-way ANOVA, with Bonferroni *post-hoc* test.

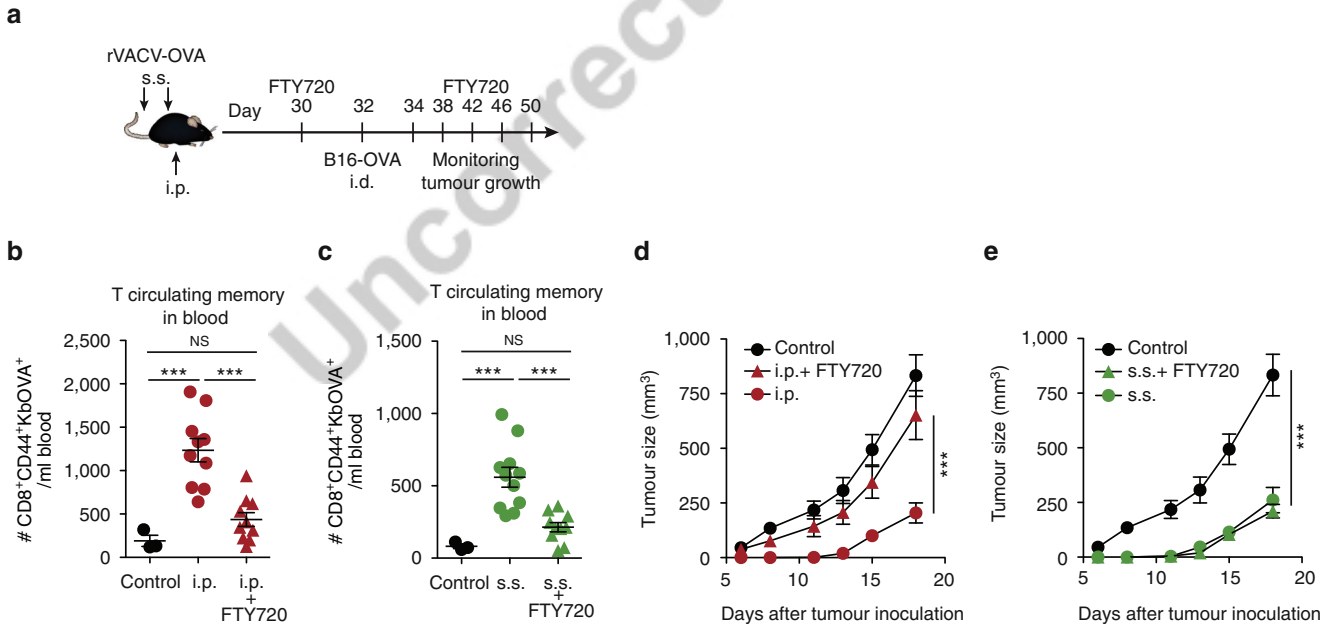

Figure 2 | Resident and circulating memory CD8$^+$ T cells are sufficient for anti-tumour immunity. (**a**) Scheme for FTY720 administration. Mice were s.s. or i.p. vaccinated with rVACV-OVA. Starting at day 30, mice were treated i.p. with 50 µg FTY720 every 4 days. At day 32, mice were inoculated (i.d.) with B16-OVA (10^6 cells) in the flank. (**b**,**c**) Absolute numbers of CD8$^+$CD44$^+$KbOVA$^+$ circulating memory T cells in the blood 32 d.p.i. and treated or not with FTY720 at day 30. (**d**,**e**) B16-OVA growth curve plotted as tumour size (mm^3) over time. Simultaneous experiments compared to the same control mice. Pool of two independent experiments represented as individual data and mean ± s.e.m. (**b**,**c**) and as tumour size mean ± s.e.m. (**d**,**e**) ($n=5$–6 per control group and 7–8 per vaccinated group). NS, not significant, ***$P<0.001$; **$P<0.01$; *$P<0.05$ by one-way ANOVA (**b**,**c**), and two-way ANOVA (**d**,**e**) with Bonferroni *post-hoc* test.

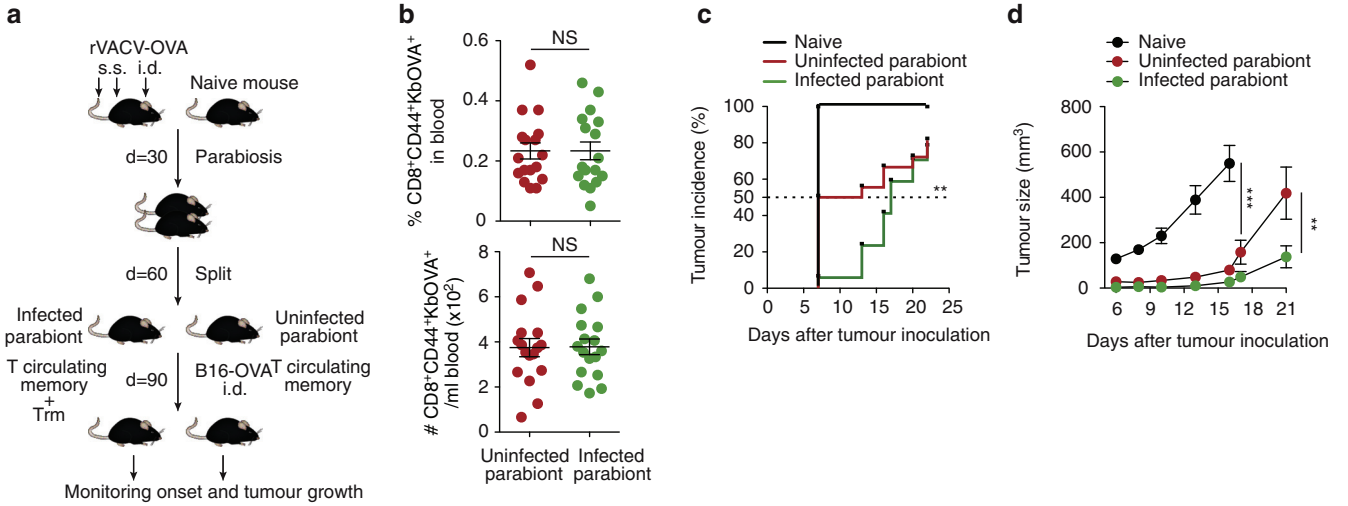

Figure 3 | Trm cells improve circulating memory-mediated immunity to melanoma. (**a**) Scheme for parabiosis strategy. Mice were s.s. and i.d. vaccinated with rVACV-OVA. After 30 days, vaccinated mice were each surgically joined with a naive mouse. Thirty days after surgery, parabiotic pairs were separated and allowed to recover for 30 days before i.d. inoculation of B16-OVA (10^6 cells) in the flank. (**b**) Frequency (top) and absolute numbers (bottom) of $CD8^+CD44^+KbOVA^+$ circulating memory T cells in the blood after parabiosis and before tumour inoculation. (**c**) Tumour incidence represented as the frequency of detectable tumours incidence over time. The dashed line indicates 50% of tumour incidence. (**d**) Tumour growth curve plotted as tumour size (mm^3) over time. Pool of two independent experiments represented as individual data and mean ± s.e.m. (**b**), as percentages (**c**) and as tumour size mean ± s.e.m. (**d**) ($n = 5$–6 per control group and 8–9 per vaccinated group). NS, not significant, $^{***}P<0.001$; $^{**}P<0.01$; $^{*}P<0.05$ by two-tailed unpaired Student's *t*-test (**b**), Cox mixed model (**c**) and two-way ANOVA (**d**) with Bonferroni *post-hoc* test.

To functionally demonstrate that OT-I Trm cells derived from Tcm cells following viral infection were truly resident, we tested their ability to migrate via blood or lymph once they were established (Fig. 4e). Mice were transferred with OT-I Tcm cells one day before infection with rVACV-OVA. After 30 d.p.i., surgical parabiosis of infected and naive mice was performed, leaving 30 days to equilibrate circulating memory compartments. Infected and non-infected parabionts were subsequently analysed for the presence of OT-I circulating memory cells in the spleen (Fig. 4f) and Trm cells in the ear (Fig. 4g,h). Only the infected parabionts exhibited OT-I Trm cells in the ear skin, functionally demonstrating that Trm derived from Tcm cells are unable to migrate via blood or lymph.

Tcm give rise to Trm cells upon tumour inoculation. To analyse whether Tcm cell plasticity to generate Trm cells is also found in the tumour setting, OT-I Tcm cells were transferred to recipient mice that were subsequently inoculated i.d. with B16-OVA cells or injected s.c. with MC38-OVA (Fig. 5a). Following 20 days of B16-OVA tumour development, OT-I cells with a Trm cell-like phenotype, with most OT-I T cells expressing CD69 and 50% of them co-expressing CD103, were found in the tumour mass (Fig. 5b–d). In addition, since Tcm transfer resulted in elimination of MC38-OVA (Fig. 5e), we analysed the presence of Trm cells in the skin that was in the proximity of the rejected tumour. Skin OT-I Trm cells expressing CD69 and CD103 were found 20 days and 45 days after tumour inoculation (Fig. 5f,g and Supplementary Fig. 2a,b). These data support the notion that Tcm retain potential to generate Trm cells upon tumour challenge. Such plasticity also contributes to explain that circulating memory T cells are sufficient for anti-tumour immunity.

Anti-PD-1 boosts Trm cells in the tumour after Tcm transfer. Next, we wondered whether anti-PD-1 would synergize with Tcm cell transfer for improved tumour immunotherapy. Indeed, Tcm cells in the tumour draining LN and, particularly, Trm-like cells infiltrating B16-OVA or MC38-OVA grafted tumours showed high PD-1 expression (Fig. 6a,b and Supplementary Fig. 3a,b), suggesting that their function could be enhanced by PD-1 blockade. We thus administered anti-PD-1 antibody concomitantly to Tcm transfer in a tumour therapy setting (Fig. 6c). The combination of Tcm and anti-PD-1 delayed the development of i.d. B16-OVA tumour (Fig. 6d) and s.c. MC38-OVA tumour (Fig. 6e) when compared to the treatment with Tcm cells alone. Notably, tumour-infiltrating lymphocytes with a Trm phenotype were increased in numbers and frequencies within $CD45^+$ cells more than tenfold in average upon anti-PD-1 treatment in both tumour settings (Fig. 6f,g and Supplementary Fig. 3c). In contrast, anti-PD-1 treatment did not affect the numbers or frequencies of OT-I Tcm cells in LNs draining B16-OVA (Supplementary Fig. 3d) or MC38-OVA (Supplementary Fig. 3e) tumours. These data show that anti-PD-1 treatment increases Trm-like tumour cell infiltrate and improves anti-tumour immunity following adoptive immunotherapy with Tcm cells.

Anti-tumour memory response is impaired in *Batf3*$^{-/-}$ mice. The generation of Trm cells but not circulating memory T cells by rVACV infection is dependent on Batf3-dependent cross-presenting DCs[13]. Consistent with this, we found that generation of endogenous repertoire OVA-specific Trm cells induced by s.s. with rVACV-OVA (Fig. 7a,b), but not circulating memory $CD8^+$ T cells (Fig. 7c), was impaired in *Batf3*$^{-/-}$ mice. We therefore hypothesized that impaired Trm cell generation in *Batf3*$^{-/-}$ mice could lead to a defective anti-tumour response. We found that Batf3 significantly contributed to anti-tumour immunity following s.s. of mice with rVACV-OVA (Fig. 7d). Batf3 was also required for effective anti-tumour response after i.n. infection with rVACV-OVA and subsequent intravenous (i.v.) challenge with B16-OVA cells (Fig. 7e). These results supported our initial hypothesis, as both s.s. and i.n. routes of infection generate Trm cells. However, Batf3 was also required to control tumour growth following routes that do not produce Trm, such as i.p. infection with rVACV-OVA and i.d. challenge with B16-OVA cells (Fig. 7f) or following i.p. infection with

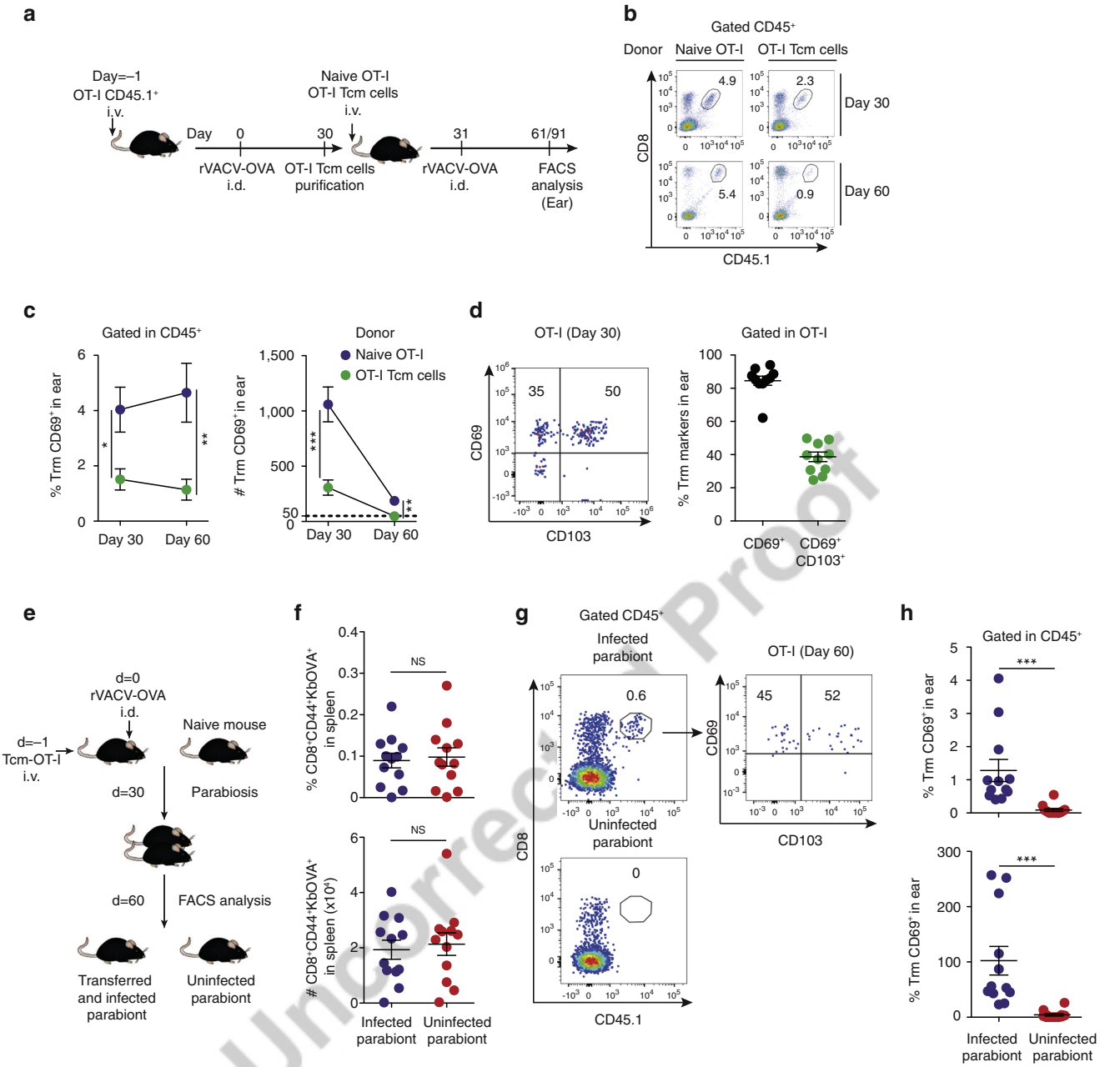

Figure 4 | Plasticity of central memory T cells to become Trm cells upon viral infection. (**a**) Scheme for testing Tcm cells plasticity. For generation of Tcm cells, mice were transferred with OT-I CD45.1$^+$ T cells (1–3 × 10^5 cells) and subsequently i.d. infected with rVACV-OVA (5 × 10^4 p.f.u.) in the ear. After 30 days, Tcm cells were sorted and transferred as indicated. (**b**–**d**) Mice were transferred with naive OT-I CD45.1$^+$ T cells or OT-I CD45.1$^+$ Tcm cells one day before i.d. challenge with rVACV-OVA in the ear. (**b**) Representative FACS dot-plots showing OT-I cells in the CD45$^+$ population in the ear at the indicated days p.i. (**c**) Frequency within CD45$^+$ cells (left) and absolute numbers (right) of CD69$^+$CD8$^+$ T cells in the ear at the indicated day p.i. (**d**) Representative FACS dot-plots (left) and frequency (right) of Trm expression markers in OT-I cells 30 d.p.i. (**e**) Scheme showing the parabiosis strategy. Mice were transferred with OT-I CD45.1$^+$ Tcm cells before i.d. ear infection with the rVACV-OVA. After 30 days, transferred and vaccinated mice were each surgically joined with a naive mouse. Thirty days after surgery, the ears of parabiont pairs were analysed for Trm detection by FACS. (**f**) Frequency (top) and absolute numbers (bottom) of CD8$^+$CD44$^+$KbOVA$^+$ circulating memory T cells in the spleen after 30 days of parabiosis. (**g**) Representative FACS dot-plots for OT-I cells identification in CD45$^+$ population in the ear (left top, infected parabiont; left bottom, uninfected parabiont) with a Trm phenotype (right, infected parabiont). (**h**) Frequency (top) and absolute number (bottom) of CD69$^+$CD8$^+$ T cells in the ear of the indicated parabiont. Pool of two independent experiments represented as mean ± s.e.m. (**c**) (n = 5–6 per group), as individual data and mean ± s.e.m. (**d**,**f**,**h**) (n = 5–6 per group). NS, not significant, ***P < 0.001; **P < 0.01; *P < 0.05 by two-tailed unpaired Student's t-test (**c**,**d**,**f**) and two-tailed nonparametric Mann–Whitney test (**h**).

rVACV-OVA and i.v. challenge with B16-OVA cells (Fig. 7g). Collectively these results demonstrate that Batf3-dependent DCs contribute to the anti-tumour CD8$^+$ T-cell memory response independently of their role in the generation of Trm cells.

Reactivation of Tcm cells is mediated by Batf3-dependent DCs. We next examined the possible mechanisms underlying the crucial need for Batf3-dependent DCs in anti-tumour memory response. To rule out the possibility that circulating memory

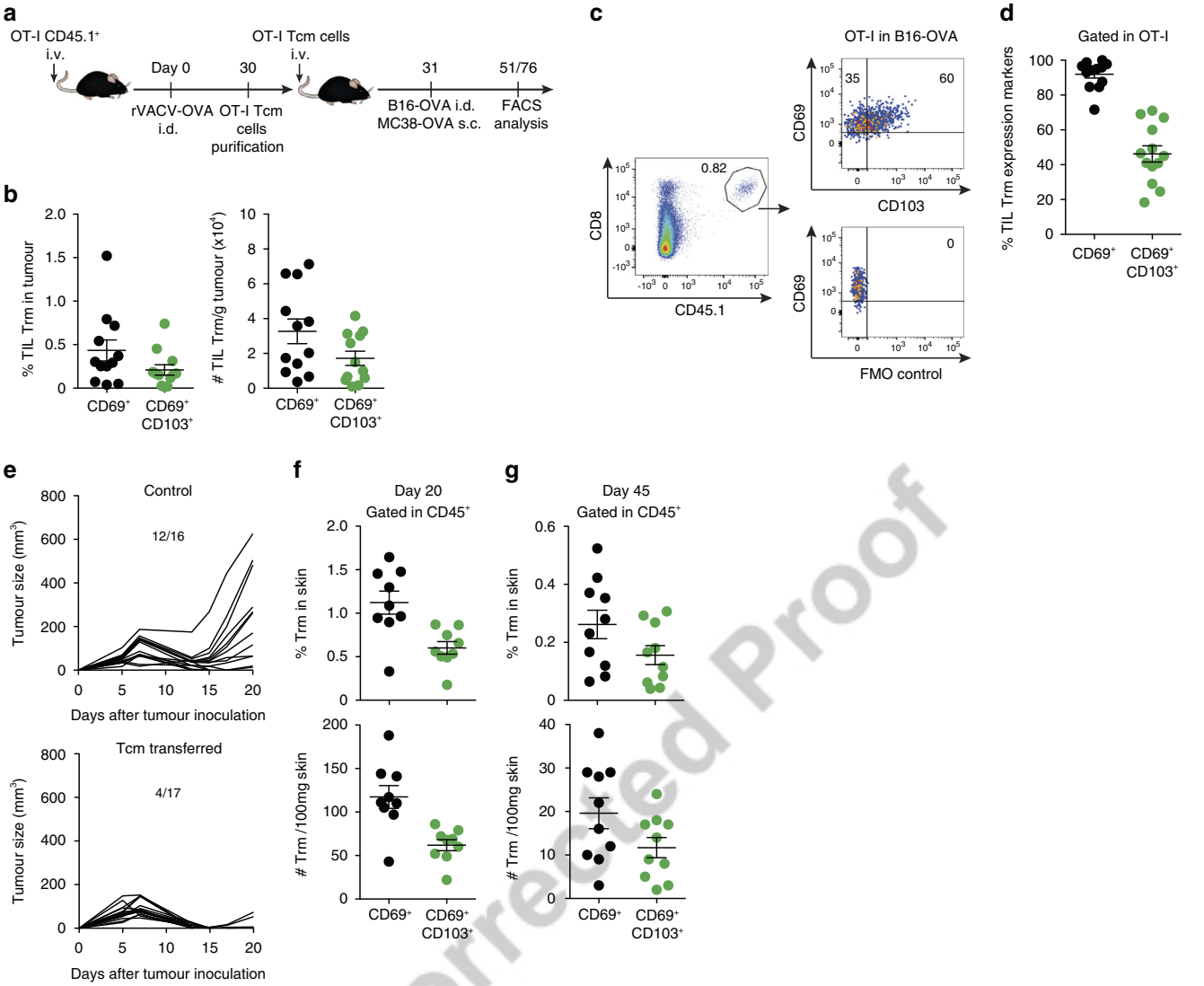

Figure 5 | Central memory T cells give rise to Trm cells after tumour inoculation. (**a**) Scheme for testing Tcm cells plasticity. For Tcm cells generation, mice were transferred with OT-I CD45.1$^+$ T cells ($1–3 \times 10^5$ cells) and subsequently i.d. infected with rVACV-OVA (5×10^4 p.f.u.) in the ear. After 30 days, Tcm cells were sorted and used for transfer. Mice were transferred with OT-I CD45.1$^+$ Tcm cells 1 day before i.d. injection with B16-OVA (**b**–**d**) or s.c. injection with MC38-OVA (**e**–**g**) in the flank. (**b**) Frequency (left) and absolute numbers (right) of OT-I cells in B16-OVA-derived cell suspensions with the indicated phenotype in tumour-bearing mice for 23 days. (**c**) Representative FACS dot-plots for OT-I identification (left) and Trm expression markers (right). (**d**) Frequency of Trm expression markers in OT-I cells in B16-OVA-bearing mice. (**e**) MC38-OVA growth curve plotted as individual tumour size (mm^3) over time in control mice (top) and in mice treated with Tcm the day before tumour inoculation (bottom). Frequency (top) and absolute numbers (bottom) of OT-I cells in skin-derived cell suspensions with the indicated phenotype, in MC38-OVA-free mice after 20 days (**f**) and 45 days (**g**) of tumour inoculation. Pool of three (**b**,**d**) and two (**e**–**g**) independent experiments represented as individual data and mean ± s.e.m. (**b**,**d**,**f**,**g**) ($n = 3–5$ per group) and as growth curve of individual tumours (**e**) ($n = 5$ and 11 per control group and $n = 10$ and 7 per Tcm transferred group).

CD8$^+$ T cells raised in *Batf3*$^{-/-}$ mice were not functional for anti-tumour immunity, we i.d. infected WT and *Batf3*$^{-/-}$ mice with rVACV-OVA following OT-I cells transfer, and then transferred purified OT-I Tcm cells to WT recipients (Fig. 8a). Following i.d. challenge with B16-OVA cells, Tcm cell transfer was equally effective in delaying tumour growth irrespective of whether they were generated in WT or in *Batf3*$^{-/-}$ mice (Fig. 8b). We thus hypothesized that recipient Batf3-deficient DCs would mediate inefficient reactivation of the transferred Tcm against the tumour. To test this, we generated OT-I Tcm cells in WT (Fig. 8c) or *Batf3*$^{-/-}$ (Fig. 8d) donor mice and transferred them to WT or *Batf3*$^{-/-}$ mice recipients that were i.d. challenged with B16-OVA cells. Independently of the origin of Tcm cells, transfer to *Batf3*$^{-/-}$ recipients resulted in impaired anti-tumour immunity with respect to transfer to WT recipients (Fig. 8c,d). These data demonstrate that Batf3-dependent DCs are requisite for reactivation of Tcm cells promoting anti-tumour immunity.

Discussion

Optimal tumour immunotherapy should generate a potent memory CD8$^+$ T cell to prevent local relapse and metastasis. Memory CD8$^+$ T cell can be either circulating or resident in the tissues (Trm) exhibiting different priming and differentiation requirements[3,5,6,13]. Circulating memory and Trm cells also show different effector behaviour[6], but their interplay in tumour immunity remains poorly characterized. In the present study, we demonstrate that circulating memory CD8$^+$ T cells and Trm cells cooperate in anti-tumour immunity, with the circulating

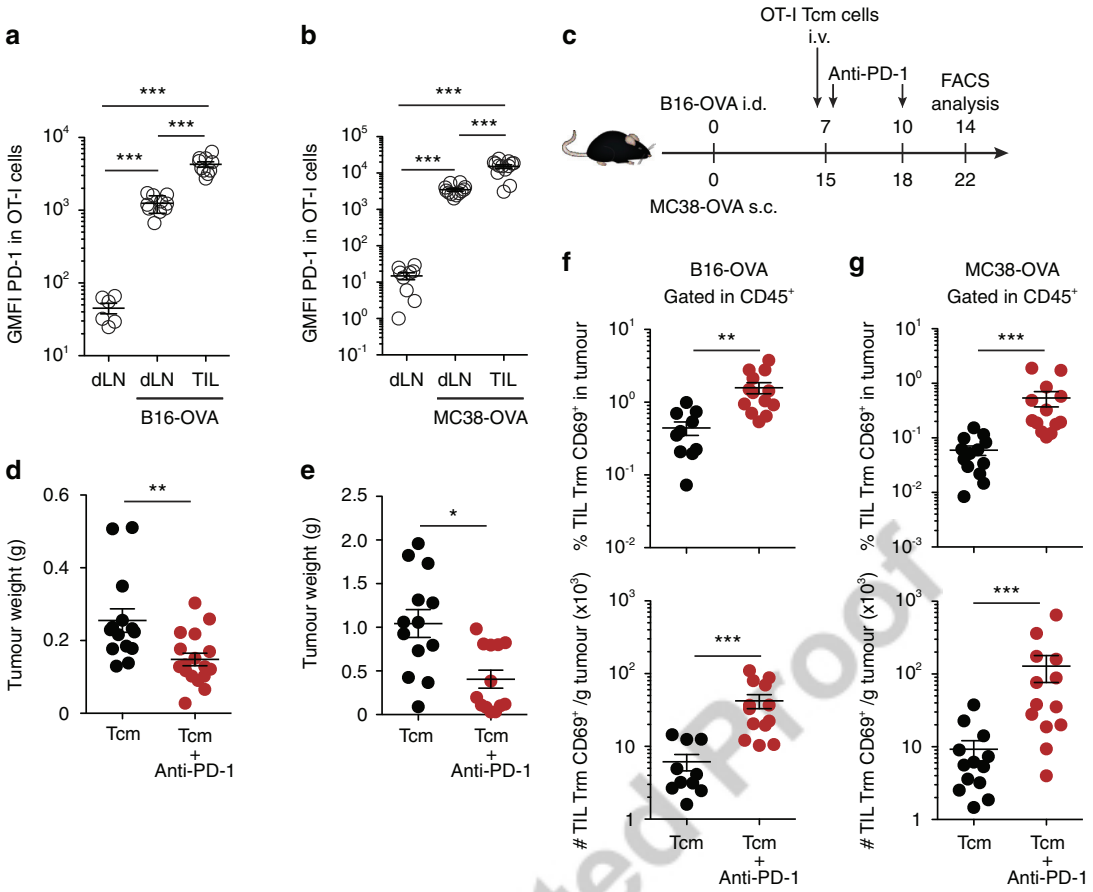

Figure 6 | Anti-PD1 boosts Trm-like cells in the tumour after Tcm transfer. (**a**,**b**) Untreated mice or mice injected i.d. with B16-OVA (**a**) or s.c. with MC38-OVA (**b**) were transferred with OT-I Tcm cells. Expression of PD-1 in OT-I cells was analysed 7 days later in draining LNs (dLN) or tumours. (**c**) Mice were injected with the indicated tumours, transferred i.v. with OT-I CD45.1$^+$ Tcm cells, and treated with anti-PD-1. (**d**,**e**) tumour weight at the time of killing following B16-OVA (**d**) or MC38-OVA (**e**) inoculation. (**f**,**g**) Frequency (top) and numbers (bottom) of OT-I CD69$^+$ infiltrating B16-OVA (**f**) or MC38-OVA (**g**) tumours in mice treated as indicated (**c**). Pool of four (**d**) and three (**a**,**b**,**e**–**g**) independent experiments represented as individual points and mean ± s.e.m. (**a**,**b**) ($n = 2$–3 per control group, 3–4 per tumour group), (**d**–**g**) ($n = 3$–5 per group). NS, not significant, $^{***}P < 0.001$; $^{**}P < 0.01$; $^{*}P < 0.05$ by one-way ANOVA (**a**,**b**) with Bonferroni *post-hoc* test, two-tailed unpaired Student's *t*-test (**f** top) and two-tailed nonparametric Mann–Whitney test (**d**-**f** bottom, **g**).

memory compartment retaining enough degree of plasticity to become resident memory cells within the grafted tumour or in the proximal skin following tumour elimination. Notably, anti-PD-1 therapy synergizes to improve anti-tumour immunity following Tcm transfer. Moreover, Batf3-dependent DCs are crucial for reactivation of circulating CD8$^+$ T-cell memory for anti-tumour immunity.

Trm cells are generated following most viral infections affecting the skin or mucosae[6] and are broadly distributed in tissues[7]. Trm cells respond faster to stimulation than circulating memory T cells, and they are equipped with a more potent effector response than their circulating counterparts[11]. Moreover, Trm cells provide superior protection upon viral reinfection in skin or mucosae and are sufficient to control viral reinfection in the presence of FTY720, which prevents the contribution of circulating memory T cells[12]. Our experiments using FTY720 showed that Trm were potentially sufficient for anti-tumour immunity. However, we also found that circulating memory CD8$^+$ T cells mediate effective anti-tumour immunity, in agreement with previous results[25]. Using a parabiosis strategy, we demonstrate that melanoma tumour growth is slower in mice containing both Trm and circulating memory T cells than in parabionts containing only circulating memory T cells, thus supporting the notion that resident and circulating memory subsets cooperate for enhanced anti-tumour immunity. The differential kinetics in the effector response of resident and circulating memory subsets has been shown in other experimental settings, such as cutaneous hypersensitivity, where Trm mediate rapid responses, whereas circulating memory T cells mediate delayed hypersensitivity[26]. Conceivably upon viral rechallenge, Trm cells trigger a local alarm state that promotes immunity[9,10,27]. Our data showing delayed tumour incidence and growth in the presence of Trm suggest that these cells could be particularly efficient in preventing metastasis.

The plasticity of Tcm cells to generate Trm cells had not been previously addressed. Tcm and Trm cells have a clonal origin, sharing TCR repertoires[26], but display distinct priming requirements in the LN[13]. Optimal generation of Trm cells following rVACV infection requires unique priming signals provided by Batf3-dependent DCs that favour T-bet expression and LN retention[13]. Subsequently, Trm cells migrate to the tissue, where the local microenvironment conditions Trm cells differentiation[6,7,28]. Tcm cells exhibit more stem-like and proliferative capacities after re-exposure to antigen, whereas Trm cells have a higher effector capacity and trigger a local alarm state[8–10]. We found that adoptive transfer of Tcm cells generates skin Trm cells upon rVACV infection. Moreover, following tumour challenge, transferred Tcm convert to cells with Trm

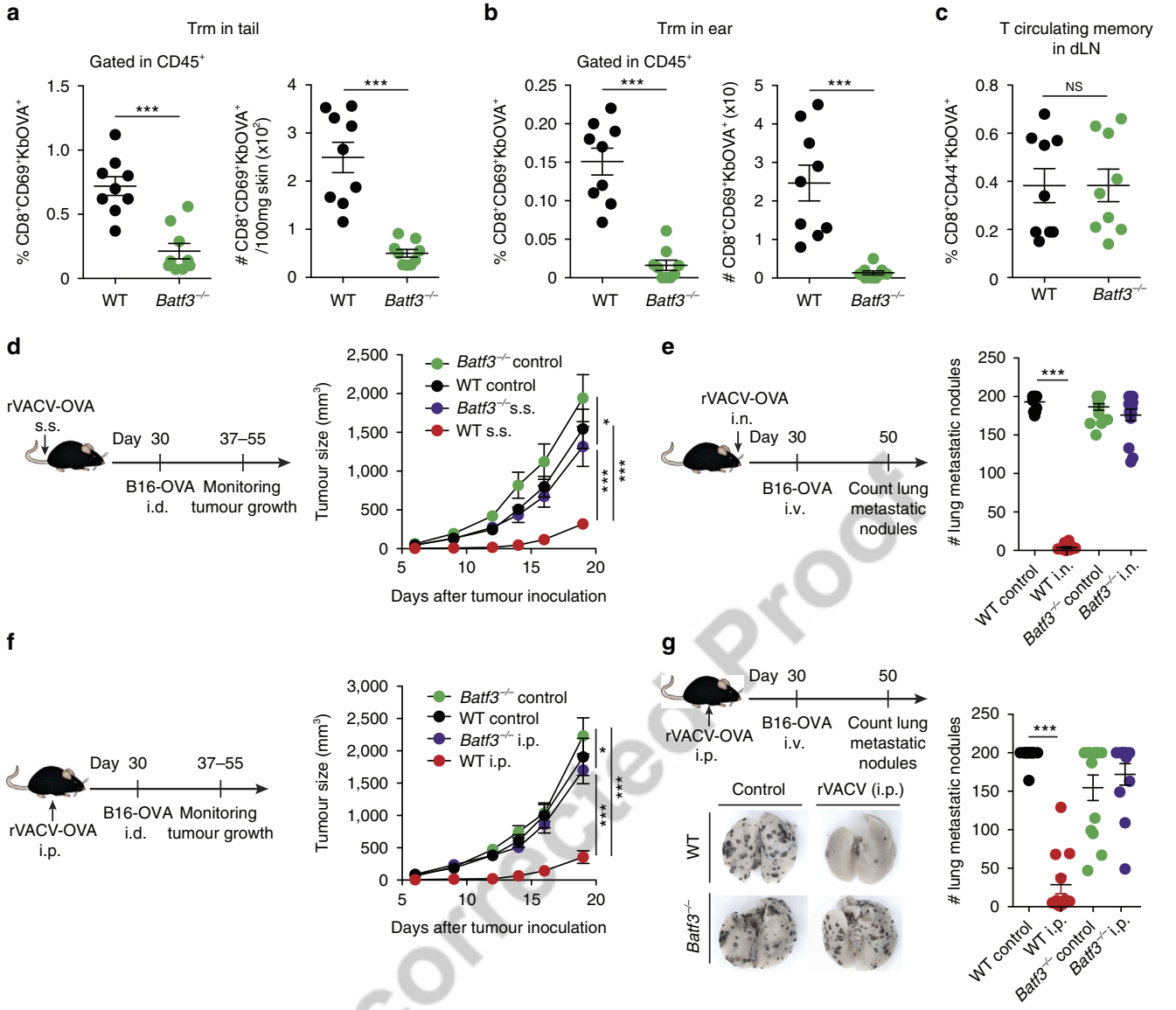

Figure 7 | Anti-tumour memory response is impaired in *Batf3*$^{-/-}$ mice. (**a**–**c**) Frequency (left) and absolute numbers (right) of endogenous OVA-specific Trm cells in the tail (**a**) and in the ear (**b**), and frequency of Kb-OVA^{+} circulating memory T cells in the draining LNs (dLN) (**c**) 30 days after s.s. infection with rVACV-OVA in the tail of WT and *Batf3*$^{-/-}$ mice. (**d**–**g**) WT and *Batf3*$^{-/-}$ mice were infected with rVACV-OVA by s.s. in the tail (**d**) i.n. (**e**) or i.p. (**f**,**g**). After 30 days, mice were i.d. inoculated with B16-OVA in the flank (**d**,**f**) and B16-OVA growth curve plotted as tumour size (mm^3) over time (right). Alternatively, B16-OVA was injected i.v. (3×10^5 cells) 30 days later (**e**,**g**) and number of lung B16-OVA nodules after 20 days since intravenous tumour challenge (right). (**g**) Representative images of lung B16-OVA metastatic nodules (bottom left). Pool of two independent experiments represented as individual data and mean ± s.e.m. (**a**–**c**,**e**,**g**) ($n=5$–7 per group) and as tumour size mean ± s.e.m. (**d**,**f**) ($n=6$–8 per group). NS, not significant, ***$P<0.001$; **$P<0.01$; *$P<0.05$ by two-tailed unpaired Student's *t*-test (**a**–**c**), two-way ANOVA (**d**,**f**) and one-way ANOVA (**e**,**g**) with Bonferroni *post-hoc* test.

phenotype within the tumour or in the proximal skin following tumour rejection. The capacity to generate Trm cells subsets upon reinfection or tumour challenge supports at least partial stemness properties of Tcm cells, which do not convert into Trm under steady-state conditions in the absence of viral infection or tumour implantation[12].

DCs are essential for anti-tumour immunity by adoptively transferred T cells, since transfer of preactivated OT-I cells to DC-depleted mice leads to impaired protection against tumour cells expressing OVA[15]. In the tumour context, recent studies show that Batf3-dependent CD103^{+} DCs play a crucial role in anti-tumour immunity[15–18,29]. Batf3-dependent DCs cross-present tumour antigens and generate a baseline anti-tumour response that can be potentiated by immunostimulating antibodies in synergy with expansion and activation of this DC subset using Flt3L and poly I:C (refs 17,18). Batf3-dependent DCs are also major producers of IL-12, not only in infectious settings[30–32], but also in the context of tumours, where IL-12 contributes to CD8 effector function[29]. In addition, Batf3-dependent DCs are required for the recruitment of naive CD3^{+} T cells to the tumour site[16] in a spontaneous melanoma model. Here we show that Batf3-dependent DCs are needed for effective reactivation of Tcm cells to promote anti-tumour immunity, which further supports the crucial role of this DC subset in tumour immunology and immunotherapy, not only for the primary response, but also for the memory response. Our data

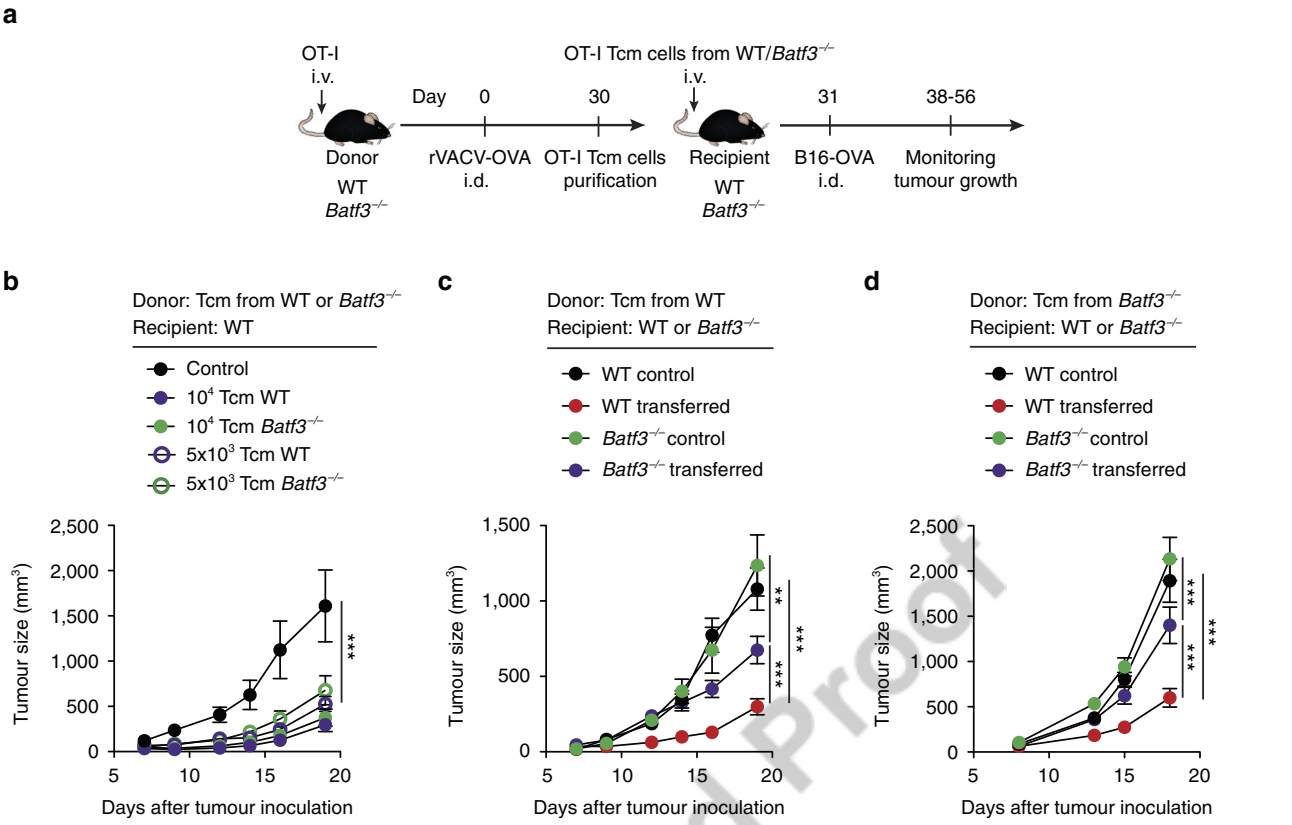

Figure 8 | Reactivation of anti-tumour Tcm cells is mediated by Batf3-dependent DCs. (**a**) For Tcm cell generation, WT and/or *Batf3*$^{-/-}$ mice were transferred with OT-I CD45.1^{+} T cells 1 day before i.d. infection with rVACV-OVA in the ear. After 30 days, OT-I CD45.1^{+} Tcm cells from donor mice were sorted and transferred to WT and/or *Batf3*$^{-/-}$ recipient mice. One day after transfer, mice were inoculated with B16-OVA cells (i.d.) in the flank. (**b**–**d**) B16-OVA growth curve plotted as tumour size (mm^3) over time in the indicated recipient mice transferred with Tcm cells from the indicated donor mice. Pool of two independent experiments represented as tumour size mean ± s.e.m. (**b**–**d**) ($n = 6$–8 per group). NS, not significant, ***$P < 0.001$; **$P < 0.01$; *$P < 0.05$ by two-way ANOVA (**b**–**d**) with Bonferroni *post-hoc* test.

in the tumour context concur with previous data on the role of Batf3-dependent DCs in reactivation of memory CD8^{+} T-cell recall response upon infection with Listeria monocytogenes, vesicular stomatitis virus or vaccinia virus[33]. We cannot rule out, however, that the role of Batf3-dependent DCs in generation of Trm[13] is also important in the context of tumours or that additional DC subsets may activate Trm[34].

Our results suggest that CD8-mediated anti-tumour immunity arises from the interplay between resident and circulating memory CD8^{+} T cells. Circulating memory cells show enough plasticity to generate Trm cells upon tumour challenge and they both express PD-1, similarly to CD103^{+} T cells infiltrating high-grade serous epithelial ovarian cancer[35]. Thus, anti-PD-1 therapy synergizes with transfer of Tcm cells for improved anti-tumour immunity, increasing the infiltration of Trm-like cells expressing PD-1 within the tumour. These results concur with previous results showing that anti-PD-1 expands intratumoural memory T cells in patients[36]. Within samples of melanoma, immune checkpoints are particularly enriched within T cells with phenotype and genomic features of Trm cells, suggesting that the Trm subset of TILs may be the major target of immune checkpoint blockade[37]. Moreover, other immunostimulatory antibodies, such as anti-CD137, could also enhance the resident memory response[38]. In conclusion, our results support the notion that anti-tumour vaccination strategies should aim at the generation of both circulating and resident memory CD8^{+} T-cell subsets[22,23,39], which could synergize with checkpoint antibody therapy for improved cancer immunotherapy.

Methods

Mice. Mice were bred and housed at the CNIC animal facility in specific pathogen-free conditions. *Batf3*$^{-/-}$ mice on the C57BL/6 background were kindly provided by Dr K.M. Murphy (Washington University, St Louis, MO, USA)[14]. OT-I transgenic mice (C57BL/6-Tg (TcraTcrb)1100Mjb/J) were mated with B6-SJL (Ptprca Pepcb/BoyJ) mice expressing the CD45.1 allele, both from The Jackson Laboratory (Bar Harbor, ME, USA). We used 7- to 10-week-old animals (males or females) for all experiments. Experiments were repeated 2–3 times to reach statistical significance. No blinding or randomization strategy was used and no animal was excluded from analysis. The local ethics committee approved all animal studies. All animal procedures conformed to EU Directive 2010/63EU and Recommendation 2007/526/EC regarding the protection of animals used for experimental and other scientific purposes, enforced in Spanish law under Real Decreto 1201/2005. Mice were allocated randomly in the different experimental procedures.

Viral infection and tumour challenge. Recombinant vaccinia virus expressing full-length ovalbumin (OVA) protein (rVACV-OVA) was a gift from J.W. Yewdell and J.R. Bennink (NIH, Bethesda, MD, USA) and was kindly provided by M. del Val (CBMSO, Madrid, Spain). Growth of viral stocks and titration was performed as described in CV1 cells[40]. Mice were infected with rVACV-OVA by the following routes: s.s. at the base of the tail ($1–2 \times 10^6$ p.f.u.) or in the back (10^6 p.f.u.), i.d. in the ear pinnae (5×10^4 or 10^6 p.f.u.), i.n. (5×10^4 p.f.u.) or i.p. (5×10^4 or $1–2 \times 10^6$ p.f.u.). T cells were considered memory cells 30 d.p.i (ref. 12). Mice were inoculated with the OVA-expressing B16 melanoma cell line (B16-OVA)[17] i.d. in the flank (10^6 cells) or OVA-expressing MC38 tumour cell line (MC38-OVA)[17] s.c. in the flank (2×10^6 cells), and tumour growth was monitored for 20–30 days. Tumour volumes were calculated using the following formula: $V = D \times d^2/2$, where V is volume (mm^3), D is larger diameter (mm) and d is smaller diameter (mm). Alternatively, mice were injected i.v. with B16-OVA (3×10^5 cells) and killed 20 days later. Lungs were fixed in Fekete's solution and tumours were counted. FTY720 (Cayman Chemical) was administered i.p. at a dose of 2.5 mg kg^{-1} in aqueous solution every 4 days. All cell lines used were tested for mycoplasma routinely.

Generation and analysis of OT-I Tcm and Trm cells. To generate OT-I Tcm cells, mice were transferred i.v. with 1–3 × 10^5 naive OT-I cells 1 day before i.d. ear infection with rVACV-OVA (5 × 10^4 p.f.u.). Tcm cells were FACS-sorted (Sy3200, Sony) from spleens and draining LNs 30 d.p.i. Mice were transferred with 10^4 naive OT-I or 1–2 × 10^4 OT-I Tcm cells 1 day before virus challenge, with 2 × 10^4 OT-I Tcm cells 1 day before B16-OVA inoculation and 3 × 10^3 or 2 × 10^4 OT-I Tcm cells 1 day before MC38-OVA inoculation. For virus challenge, mice were infected with rVACV-OVA (5 × 10^4 p.f.u.) i.d. in the ear, and the memory response was analysed at 30 days or 60 d.p.i. Tumour inoculation (B16-OVA cells, i.d.; MC38-OVA cells, s.c.) was performed as indicated above. For analysis of tumour-infiltrating lymphocytes, mice were killed 20–23 days after tumour inoculation. For analysis of skin-infiltrating lymphocytes, mice were killed 20 or 45 days after tumour inoculation. For anti-PD-1 antibody treatment, mice were transferred with 1–2 × 10^4 OT-I Tcm cells when the tumour reached 100–150 mm^2 (day 7, for B16-OVA; day 15–18, for MC38-OVA), and inoculated i.p. the same day of the Tcm transfer and 3 days later, with 100 µg of anti-PD-1 antibody (RMP1-14, BioXcell). For FACS analysis mice were killed at day 7 after Tcm transference.

Parabiosis. Parabiosis was performed as described[12]. For tumour inoculation, wild-type (WT) mice were infected with rVACV-OVA (10^6 p.f.u.) by s.s. in the tail and in the back and i.d. in the ear 30 days before surgical joining with naive mouse to create parabionts. After 30 days, mice were separated and kept for recovery after surgery for 30 days. Finally, both parabiont mice were i.d. challenged with B16-OVA cells as indicated. To analyse the migratory capacity of Trm cells that derive from Tcm cells, WT mice were transferred with 2 × 10^4 OT-I Tcm cells i.v. one day before i.d. infection with rVACV-OVA (5 × 10^4 p.f.u.) in the ear. After 30 days, infected mice were joined with naive mice and kept in parabiosis for 30 days. Finally, ears and spleens of both parabionts were analysed by FACS.

Flow cytometry. Allophycocyanin-labelled dextramers specific for OVA H-2Kb (257-SIINFEKL-264) were purchased from Immudex (Copenhagen, Denmark). Samples for flow cytometry were stained with the appropriate antibody cocktails in ice-cold PBS supplemented with 2 mM EDTA and 1% FBS. Anti-mouse CD45 (clone 30F11), CD8α (clone 53-6.7), CD103 (clone 2E7), CD44 (clone IM7), CD45.1 (clone A20) and CD45.2 (clone 104) antibodies were obtained from eBioscience. Anti-mouse CD62L (clone MEL-14) and CD69 (clone H1.2F3) antibodies were obtained from BD Biosciences. Anti-mouse CD279 (PD-1, clone 29F.1A12) was obtained from Biolegend. Events were acquired using an LSRFortessa SORP (Becton Dickinson) flow cytometer or Spectral Cell Analyzer SP6800 (Sony) and data were analysed using FlowJo V10 software (Tree Star).

Statistical analysis. Statistical analysis was performed using Prism v6 (GraphPad Software Inc., La Jolla, CA, USA). We estimated *a priori* that minimal informative differences are 1 SD, and estimated sample sizes using software 'Gpower 1.3', taking into account the following considerations. (a) The differences to be detected, 1 SD comparing each group of mice. Ratio (effect size) differs to detect/SD = 1. (b) Taking into account the above data, the number of animals in total for a contrast *t*-test of mean differences between two independent groups with two tails is 17. Power = 0.8 and significance level = 0.05. Variance equality among groups was determined using F-test. Statistical significance for comparison between two groups of samples showing a normal distribution (Shapiro–Wilk test for normality) was determined using the unpaired two-tailed Student's *t*-test. For comparison between two groups with a no normal distribution, two-tailed Mann–Whitney nonparametric test was used. For comparison of more than two groups, one-way or two-way ANOVA with Bonferroni *post-hoc* test was used. For Fig. 3c, Cox mixed model was applied when comparing tumour incidence of two groups, keeping the information about the experimental groups. We used the coxme function of the R package with the same name, to the cohort between day 0 and day 17, where two parabiont groups reach 50% of incidence. A P value <0.05 was considered significant.

Data availability. The authors declare that the data supporting the findings of this study are available within the article and its Supplementary Information files, or available from the authors on request.

Q2

References

1. Gebhardt, T. *et al.* Memory T cells in nonlymphoid tissue that provide enhanced local immunity during infection with herpes simplex virus. *Nat. Immunol.* **10,** 524–530 (2009).
2. Gebhardt, T. *et al.* Different patterns of peripheral migration by memory $CD4^+$ and $CD8^+$ T cells. *Nature* **477,** 216–219 (2011).
3. Mueller, S. N., Gebhardt, T., Carbone, F. R. & Heath, W. R. Memory T cell subsets, migration patterns, and tissue residence. *Annu. Rev. Immunol.* **31,** 137–161 (2013).
4. Farber, D. L., Yudanin, N. A. & Restifo, N. P. Human memory T cells: generation, compartmentalization and homeostasis. *Nat. Rev. Immunol.* **14,** 24–35 (2014).
5. Park, C. O. & Kupper, T. S. The emerging role of resident memory T cells in protective immunity and inflammatory disease. *Nat. Med.* **21,** 688–697 (2015).
6. Mueller, S. N. & Mackay, L. K. Tissue-resident memory T cells: local specialists in immune defence. *Nat. Rev. Immunol.* **16,** 79–89 (2016).
7. Steinert, E. M. *et al.* Quantifying memory CD8 T cells reveals regionalization of immunosurveillance. *Cell* **161,** 737–749 (2015).
8. Wakim, L. M., Woodward-Davis, A. & Bevan, M. J. Memory T cells persisting within the brain after local infection show functional adaptations to their tissue of residence. *Proc. Natl Acad. Sci. USA* **107,** 17872–17879 (2010).
9. Ariotti, S. *et al.* T cell memory. Skin-resident memory CD8(+) T cells trigger a state of tissue-wide pathogen alert. *Science* **346,** 101–105 (2014).
10. Schenkel, J. M. *et al.* T cell memory. Resident memory CD8 T cells trigger protective innate and adaptive immune responses. *Science* **346,** 98–101 (2014).
11. Clark, R. A. Resident memory T cells in human health and disease. *Sci. Transl. Med.* **7,** 269rv261 (2015).
12. Jiang, X. *et al.* Skin infection generates non-migratory memory $CD8^+$ T(RM) cells providing global skin immunity. *Nature* **483,** 227–231 (2012).
13. Iborra, S. *et al.* Optimal generation of tissue-resident but not circulating memory T cells during viral infection requires crosspriming by DNGR-1^+ dendritic cells. *Immunity* **45,** 847–860 (2016).
14. Hildner, K. *et al.* Batf3 deficiency reveals a critical role for CD8alpha$^+$ dendritic cells in cytotoxic T cell immunity. *Science* **322,** 1097–1100 (2008).
15. Broz, M. L. *et al.* Dissecting the tumor myeloid compartment reveals rare activating antigen-presenting cells critical for T cell immunity. *Cancer Cell* **26,** 638–652 (2014).
16. Spranger, S., Bao, R. & Gajewski, T. F. Melanoma-intrinsic beta-catenin signalling prevents anti-tumour immunity. *Nature* **523,** 231–235 (2015).
17. Sanchez-Paulete, A. R. *et al.* Cancer immunotherapy with immunomodulatory anti-CD137 and anti-PD-1 monoclonal antibodies requires BATF3-dependent dendritic cells. *Cancer Discov.* **6,** 71–79 (2016).
18. Salmon, H. *et al.* Expansion and activation of CD103(+) dendritic cell progenitors at the tumor site enhances tumor responses to therapeutic PD-L1 and BRAF inhibition. *Immunity* **44,** 924–938 (2016).
19. Djenidi, F. *et al.* $CD8^+CD103^+$ tumor-infiltrating lymphocytes are tumor-specific tissue-resident memory T cells and a prognostic factor for survival in lung cancer patients. *J. Immunol.* **194,** 3475–3486 (2015).
20. Koh, J. *et al.* Prognostic implications of intratumoral $CD103^+$ tumor-infiltrating lymphocytes in pulmonary squamous cell carcinoma. *Oncotarget* **8,** 13762–13769 (2017).
21. Webb, J. R., Milne, K., Watson, P., Deleeuw, R. J. & Nelson, B. H. Tumor-infiltrating lymphocytes expressing the tissue resident memory marker CD103 are associated with increased survival in high-grade serous ovarian cancer. *Clin. Cancer Res.* **20,** 434–444 (2014).
22. Sun, Y. Y. *et al.* Local HPV recombinant vaccinia boost following priming with an HPV DNA vaccine enhances local HPV-specific $CD8^+$ T-cell-mediated tumor control in the genital tract. *Clin. Cancer Res.* **22,** 657–669 (2016).
23. Nizard, M., Roussel, H. & Tartour, E. Resident memory T cells as surrogate markers of the efficacy of cancer vaccines. *Clin. Cancer Res.* **22,** 530–532 (2016).
24. Khan, T. N., Mooster, J. L., Kilgore, A. M., Osborn, J. F. & Nolz, J. C. Local antigen in nonlymphoid tissue promotes resident memory $CD8^+$ T cell formation during viral infection. *J. Exp. Med.* **213,** 951–966 (2016).
25. Klebanoff, C. A. *et al.* Central memory self/tumor-reactive $CD8^+$ T cells confer superior antitumor immunity compared with effector memory T cells. *Proc. Natl Acad. Sci. USA* **102,** 9571–9576 (2005).
26. Gaide, O. *et al.* Common clonal origin of central and resident memory T cells following skin immunization. *Nat. Med.* **21,** 647–653 (2015).
27. Schenkel, J. M., Fraser, K. A., Vezys, V. & Masopust, D. Sensing and alarm function of resident memory CD8(+) T cells. *Nat. Immunol.* **14,** 509–513 (2013).
28. Mackay, L. K. *et al.* T-box transcription factors combine with the cytokines TGF-beta and IL-15 to control tissue-resident memory T cell fate. *Immunity* **43,** 1101–1111 (2015).
29. Ruffell, B. *et al.* Macrophage IL-10 blocks $CD8^+$ T cell-dependent responses to chemotherapy by suppressing IL-12 expression in intratumoral dendritic cells. *Cancer Cell* **26,** 623–637 (2014).
30. Mashayekhi, M. *et al.* CD8α(+) dendritic cells are the critical source of interleukin-12 that controls acute infection by toxoplasma gondii tachyzoites. *Immunity* **35,** 249–259 (2011).
31. Martinez-Lopez, M., Iborra, S., Conde-Garrosa, R. & Sancho, D. Batf3-dependent $CD103^+$ dendritic cells are major producers of IL-12 that drive local Th1 immunity against Leishmania major infection in mice. *Eur. J. Immunol.* **45,** 119–129 (2015).
32. Everts, B. *et al.* Migratory $CD103^+$ dendritic cells suppress helminth-driven type 2 immunity through constitutive expression of IL-12. *J. Exp. Med.* **213,** 35–51 (2016).
33. Alexandre, Y. O. *et al.* $XCR1^+$ dendritic cells promote memory $CD8^+$ T cell recall upon secondary infections with Listeria monocytogenes or certain viruses. *J. Exp. Med.* **213,** 75–92 (2016).

34. Shin, H., Kumamoto, Y., Gopinath, S. & Iwasaki, A. CD301b$^+$ dendritic cells stimulate tissue-resident memory CD8$^+$ T cells to protect against genital HSV-2. *Nat. Commun.* **7,** 13346 (2016).
35. Komdeur, F. L. *et al.* CD103$^+$ intraepithelial T cells in high-grade serous ovarian cancer are phenotypically diverse TCRalphabeta$^+$ CD8alphabeta$^+$ T cells that can be targeted for cancer immunotherapy. *Oncotarget* **7,** 75130–75144 (2016).
36. Ribas, A. *et al.* PD-1 blockade expands intratumoral memory T cells. *Cancer Immunol. Res.* **4,** 194–203 (2016).
37. Boddupalli, C. S. *et al.* Interlesional diversity of T cell receptors in melanoma with immune checkpoints enriched in tissue-resident memory T cells. *JCI Insight* **1,** e88955 (2016).
38. Zhou, A. C., Wagar, L. E., Wortzman, M. E. & Watts, T. H. Intrinsic 4-1BB signals are indispensable for the establishment of an influenza-specific tissue-resident memory CD8 T-cell population in the lung. *Mucosal Immunol.* (2017).
39. Sandoval, F. *et al.* Mucosal imprinting of vaccine-induced CD8(+) T cells is crucial to inhibit the growth of mucosal tumors. *Sci. Transl. Med.* **5,** 172ra120 (2013).
40. Iborra, S. *et al.* The DC receptor DNGR-1 mediates cross-priming of CTLs during vaccinia virus infection in mice. *J. Clin. Invest.* **122,** 1628–1643 (2012).

Acknowledgements

We are grateful to N. Anandasabapathy, J. Pardo and members of the D.S. lab for discussions and critical reading of the manuscript. We also thank R.A. Mota for the contribution to the development of animal models. We thank the CNIC facilities, personnel and to K. McCreath for editorial assistance. We are indebted to all the scientists who have shared reagents with us, as indicated in Methods. M.E. is the recipient of a CNIC International PhD Programme fellowship 'La Caixa'-Severo Ochoa, 2013 Call (OSLC-CNIC-2013-04). S.I. is funded by grant SAF2015-74561-JIN. I.M. is supported by Asociación Española contra el Cáncer and Fundación BBVA. A.H. is funded by the Spanish Ministry of Economy, Industry and Competitiveness (MEIC) and European Fund for Regional Development (FEDER) (SAF2015-65607-R). D.S. lab is funded by the MEIC and FEDER (SAF-2013-42920-R and SAF-2016-79040-R), and the Fondation ACTERIA. D.S. and I.M. lab are funded by the European Commission (635122-PROCROP H2020). D.S. and A.H. lab are funded by the CNIC. The CNIC is supported by the MEIC and the Pro CNIC Foundation, and is a Severo Ochoa Center of Excellence (SEV-2015-0505).

Author Contributions

M.E. and D.S. conceived and designed the project. M.E., S.I., J.A.Q. and A.H. developed methodology. M.E., E.P. and S.I. acquired the data. M.E., S.I. and D.S. analysed and interpreted the data. M.E. and D.S. wrote and reviewed the manuscript. F.J.C., S.M.-C., E.M.-P., I.M. and M.Est. contributed with administrative, technical and material support. All the authors discussed the results and the manuscript.

Additional information

Supplementary Information accompanies this paper at http://www.nature.com/naturecommunications

Competing interests: I.M. is a consultant for BMS, Merck-Serono, Roche-Genentech, AstraZeneca, Heliox, Boehringer-Ingelheim, Alligator and Bioncotech. The other authors declare have no competing interests.

Reprints and permission information is available online at http://npg.nature.com/reprintsandpermissions/

How to cite this article: Enamorado, M. *et al.* Enhanced anti-tumor immunity requires the interplay between resident and circulating memory CD8$^+$ T cells. *Nat. Commun.* **8,** 16073 doi: 10.1038/ncomms16073 (2017).

Publisher's note: Springer Nature remains neutral with regard to jurisdictional claims in published maps and institutional affiliations.

frontiers in Immunology

MINI REVIEW
published: 08 May 2017
doi: 10.3389/fimmu.2017.00527

Innate Immune Function of Mitochondrial Metabolism

David Sancho[1], Michel Enamorado[1] and Johan Garaude[2]**

[1] Centro Nacional de Investigaciones Cardiovasculares Carlos III (CNIC), Madrid, Spain, [2] Institute for Regenerative Medicine and Biotherapy, INSERM U1183, Montpellier, France

Sensing of microbe-associated molecular patterns or danger signals by innate immune receptors drives a complex exchange of information. Innate receptor signaling not only triggers transcriptional events but also induces profound changes in metabolic fluxes, redox balance, and metabolite abundance thereby influencing immune cell function. Mitochondria are at the core of metabolic adaptation to the changing environment. The close interaction between mitochondrial metabolism and immune signaling has emerged as a central regulator of innate sensing. Metabolic processes generate a constant flow of electrons that eventually end up in the mitochondrial electron transport chain (ETC). Two electron carriers and four respiratory complexes that can assemble as larger molecular supercomplexes compose the ETC in the mitochondrial inner membrane. While the meaning and biological relevance of such structural organization is a matter of passionate debates, recent data support that innate stimuli remodel the ETC. We will review the function of mitochondrial metabolism and ETC dynamics as innate rheostats that regulate signaling, transcription, and epigenetics to orchestrate innate immune responses.

Keywords: innate immune response, immunometabolism, electron transport chain, mitochondria, macrophages, dendritic cells, cytokines, inflammation

OPEN ACCESS

Edited by:
Ping-Chih Ho, University of Lausanne, Switzerland

Reviewed by:
Tiffany Horng, Harvard University, USA
Pu-Ste Liu, Kaohsiung Medical University, Taiwan

****Correspondence:***
David Sancho
dsancho@cnic.es;
Johan Garaude
johan.garaude@inserm.fr

Specialty section:
This article was submitted to Molecular Innate Immunity, a section of the journal Frontiers in Immunology

Received: *22 December 2016*
Accepted: *19 April 2017*
Published: *08 May 2017*

Citation:
Sancho D, Enamorado M and Garaude J (2017) Innate Immune Function of Mitochondrial Metabolism. Front. Immunol. 8:527. doi: 10.3389/fimmu.2017.00527

INTRODUCTION: MYELOID CELLS REPROGRAM THEIR METABOLISM IN RESPONSE TO ENVIRONMENTAL CUES

Ligation of pattern recognition receptors, cytokine receptors, and phagocytosis of dying or dead cells provoke key changes in myeloid cell metabolism that are only beginning to be explored (1). As an example, tissue damage-derived signals can modulate myeloid cell metabolic reprogramming since uptake of apoptotic cells increases the mitochondrial membrane potential to downregulate phagocytosis (2). Another relevant example of metabolic consequences induced by innate immune signal is the stimulation of mouse macrophages and bone marrow-derived dendritic cells differentiated with GM-CSF (GM-DCs) with agonists for toll-like receptors (TLRs) or for the β-glucan receptor Dectin-1, which result in aerobic glycolysis (the Warburg effect) (1, 3–8). Many recent reviews have already remarkably described the recent advances in our understanding of metabolic reprogramming from a "metabolic flux" point of view (1, 9–13). However, recent works have provided new elements on the mechanisms bridging innate immune recognition and mitochondrial metabolic functions, suggesting that mitochondria regulate their electron flow as adaptation to innate immune signals. Here, we will summarize some of these findings that point toward a key function of the mitochondrial respiratory chain in governing innate immune cell fate.

MITOCHONDRIA, A METABOLIC RHEOSTAT FOR INNATE IMMUNE RECEPTORS

Metabolism As a Flow of Electrons

Metabolism is often seen as a complex arrangement of metabolic fluxes, redox signaling, and translational or posttranslational events that are mutually dependent. However, metabolism can also be seen as a flow of electrons through multiple parallel and alternative pathways where metabolites act as potential carriers of electrons. From this point of view, the main and ultimate acceptor of electrons is the mitochondrial electron transport chain (ETC). Many catabolic processes indeed supply electrons to the ETC in the form of reducing equivalents of nicotinamide adenine dinucleotide (NADH) or flavin adenine dinucleotide ($FADH_2$), whose relative proportion depends on the nature of the fuel used (14). The capacity of the cell to use different fuels efficiently is thus critical for its ability to adapt to changing environmental cues (15). Mitochondria must therefore regulate their location, biogenesis, fusion or fission, structure, and internal metabolite fluxes in response to changes in fuel source or signals received by cell membrane receptors or intracellular sensors. In turn, mitochondria control cell metabolism by governing the balance of anabolism (lipogenesis and antioxidant defenses from citrate, gluconeogenesis, serine, and glycine biosynthesis from pyruvate, nucleotide biosynthesis) and catabolism (Krebs cycle, β-oxidation, oxidative phosphorylation) (16). Mitochondria are central for ATP synthesis, redox balance, reactive oxygen species (ROS) production, thermogenesis, and generation of metabolites, all of which impact cell function. Since the release of cytochrome *c* to the cytosol is a major trigger for apoptosis, mitochondria also regulate cell survival.

The ETC comprises two electron carriers [coenzyme Q (CoQ)/ubiquinone and cytochrome *c*] and four respiratory complexes [complexes I–IV (CI–CIV)], which, excluding CII, can assemble as larger molecular supercomplexes (SCs) in the mitochondrial inner membrane (16) (**Figure 1**). The assembly of SCs is dynamic and may adapt the electron flux to the available substrates (17, 18). The nature of the fuel conditions the proportion of electrons feeding into the ETC from NADH and $FADH_2$, with a NADH/$FADH_2$ electron ratio of 5 following full oxidation of glucose and a ratio of 2 following oxidation of the fatty acid palmitate (14, 17, 18). The H^+ gradient generated by the ETC is then used by the H^+-ATP synthase (CV) to generate ATP. Recent results support the notion that innate sensing of microbial features leads to adaptations in SC assembly and electron flow through the ETC in mouse macrophages (5, 19) suggesting that ETC exerts key functions in macrophage activation processes (**Figure 1**).

Mitochondria As Platforms for Innate Signaling

Mitochondria can both generate ligands and serve as signaling platform for innate sensing receptors (12). First, some mitochondrial-derived molecules trigger immune receptors. This is the case for mitochondrial *N*-formyl peptides, which are damage-associated molecular patterns that activate receptors such as formyl peptide receptor-1 to promote cytokine production (20). Furthermore, mitochondrial DNA (mtDNA) has hypomethylated CpG that can trigger TLR9 activation (20). mtDNA can access the cytosol through an altered permeability of the mitochondrial membrane to activate the NLRP3 inflammasome (21, 22). Later, it was discovered that glycolytic enzymes can directly contribute to innate sensing of microbes. Hexokinase is a glycolysis enzyme associated with the voltage-dependent anion channel (VDAC) in the outer mitochondrial membrane (23). Following degradation of microbe-associated peptidoglycans in the phagosomes of mouse macrophages and DCs, peptidoglycan-derived *N*-acetylglucosamine binds to hexokinase causing its dissociation from the mitochondria outer membranes and VDAC (24). The NLRP3 inflammasome is subsequently activated, possibly relying on variations of the mitochondrial membrane permeability and the access of mtDNA to the cytosol. Thus, hexokinase moonlights as a regulator of NLRP3 activation and subsequent maturation of pro-IL-1β to promote an antibacterial pro-inflammatory response (24, 25). In addition, cytosolic location of mtDNA can also induce antiviral immunity by triggering the DNA sensor cGAS and the STING-IRF3-dependent pathway to promote IFN-I production (26).

Another example of how the outer mitochondrial membrane acts as a scaffold structure involved in innate sensing is the mitochondrial antiviral-signaling protein (MAVS) that binds to mitochondrial-associated membranes connecting the endoplasmic reticulum to the outer mitochondrial membrane (27). RIG-I binds to and promotes MAVS aggregates in the outer mitochondrial membrane to trigger downstream signaling (28). Thus, signaling and adaptor proteins downstream of pattern recognition receptor (PRR) sensing pathways can localize to mitochondria raising the possibility that PRRs could modulate mitochondrial functions. Such a regulatory role has been already suggested for tumor necrosis factor receptor-associated factor 6 (TRAF6), which can interact with evolutionarily conserved signaling intermediate in toll pathways (ECSIT), a protein involved in CI assembly (29, 30).

Metabolic Reprogramming in Macrophages upon Innate Immune Receptor Engagement

The specificities of macrophage metabolism compared to other immune cells have been a subject of interest for a long time as exemplified by pioneer works from the 80s (31–33). Our current appreciation of metabolic reprogramming led us to postulate that most inflammatory agonists for PRRs engage similar metabolic adaptations, although some specificities on the outcomes for host defense may exist. The main characteristic of metabolic adaptations upon innate immune receptor engagement is a strong induction of glycolysis even in presence of substantial oxygen (1, 3–8). Indeed, mouse macrophage stimulation with the TLR4 agonist lipopolysaccharide (LPS), the main component of Gram-negative bacterial cell wall, induces the activation of transcription factor hypoxia-inducible factor-1α (HIF-1α) (8) that controls the expression of several enzymes implicated in glycolysis (34, 35). LPS-activated mouse macrophages express a highly active

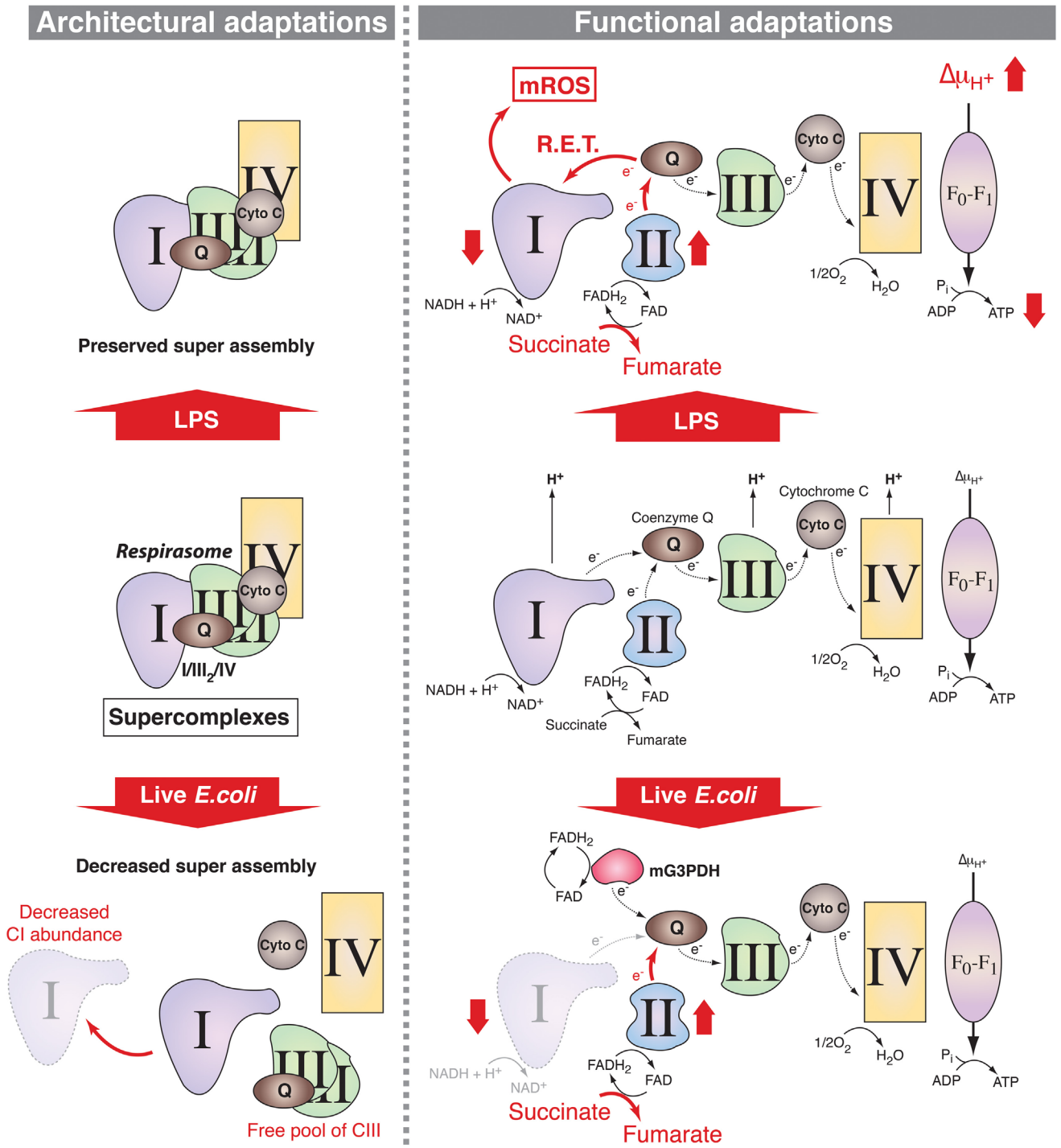

FIGURE 1 | **Mitochondrial respiratory chain adaptations following innate immune sensing**. Mitochondrial respiratory complexes, except for CII, can associate into supercomplexes (SCs) including the respirasome, composed of CI + $CIII_2$ + CIV (left panel). In lipopolysaccharide (LPS)-stimulated mouse macrophages, SC assembly is preserved (upper left) but there are functional adaptations such as increase in CII (succinate dehydrogenase) activity, which enhances succinate oxidation along with increased mitochondrial membrane potential and decreased mitochondrial ATP synthase-mediated production of ATP (upper right). This is accompanied by a decrease in the NAD^+/NADH ratio, supporting a possible reverse electron transport (RET) from coenzyme Q to CI thereby inducing the production of mitochondrial reactive oxygen species (mROS). Upon detection of live *Escherichia coli*, increase in phagosomal reactive oxygen species mediates Fgr-dependent activation of CII and decrease in CI-containing SCs probably due to CI disassembly. This provokes a change in electron flow in the electron transport chain, with a drop in the entry of electron derived from NADH that is compensated by the induction of the activities of $FADH_2$-consuming enzymes CII and mitochondrial glycerol-3-phosphate dehydrogenase (mG3PDH). The increase in CII activity generates fumarate that modulates macrophage function.

isoform of phosphofructokinase-2 that promotes glycolysis (36) and LPS induces pyruvate kinase M2, which associates with and stabilizes HIF-1α to further induce glycolysis and enhance proinflammatory cytokines (37, 38). Such induction of glycolytic flux was also found in phagocytic cells activated through TLR2 (4, 39), TLR3 (4, 5), TLR7/8 (4, 5), TLR9 (4, 40), or Dectin-1 (3, 41), indicating that enhanced glycolysis might be a common feature to PRR-activated cells. The detection of a number of microbes including *Salmonella typhimurium* (5, 37), *Escherichia coli* (5), or *Mycobacterium tuberculosis* (37, 42, 43) strongly induce glycolysis in mouse macrophages. However, inflammasome activation of caspase-1 mediates the cleavage of glycolytic enzymes, e.g., during NLRC4 sensing of *S. typhimurium* (44) highlighting the complex interplay between PRRs and myeloid cell metabolism. In fact, induction of glycolysis does not seem to solely contribute to metabolic reprogramming but might also directly sustain pathogen sensing and host defense.

Although glycolysis is thought to largely contribute to ATP production in activated myeloid cells (40, 45), it also provides metabolic intermediates that could feed other metabolic pathways to serve macromolecule synthesis (45). Along with glycolysis, the pentose phosphate pathway (PPP) is induced in LPS-activated mouse macrophages (7). The mechanisms engaged are not fully understood, but they likely involve the inhibition of the PPP inhibitor carbohydrate kinase-like protein (46).

Because the glucose catabolic product pyruvate is diverted from entry to mitochondria in activated macrophages and is rather metabolized to lactate, it was tempting to speculate that engagement of innate immune receptors could globally dampen mitochondrial respiration. However, innate stimulation also activates pathways such as glutaminolysis to replenish the tricarboxylic acid (TCA) cycle and maintain global metabolic flux (7, 8, 47) likely avoiding cell death. Thus, a significant activity of the mitochondrial respiratory chain and the mitochondrial membrane potential must be maintained. This is partially achieved by an increase in anaplerosis including glutaminolysis (7, 8), which feeds the TCA cycle at α-ketoglutarate, and the aspartate–argininosuccinate shunt, which feeds the TCA cycle at malate and fumarate (7). Glutaminolysis is also enhanced in human monocytes trained with β-glucan, which triggers the C-type lectin receptor Dectin-1 (41, 48), suggesting that induction of such metabolic feature is not limited to TLRs. Therefore, an important issue to address is whether different PRRs induce specific metabolic reprogramming signatures, which would allow specific manipulation of myeloid cell metabolism for therapy.

How innate immune receptors regulate lipid metabolism in macrophages is a field of active research. On the one hand, engagement of TLRs upon recognition of various bacteria enhances fatty acid uptake and incorporation to triglycerides for storage and simultaneously decrease fatty acid oxidation and lipolysis suggesting that lipids may serve other needs than energy production in activated mouse macrophages (6, 49, 50). In line with this, fatty acid catabolism is not induced in LPS-activated macrophages compared to alternatively activated macrophages (7). Consistently, mouse macrophage fatty acid synthase is induced during sepsis in a mechanism depending on the mitochondrial uncoupling protein 2 (UCP2) (51). On the other hand, fatty acid oxidation is increased in mouse and human macrophages primed in conditions that activate the NLRP3 inflammasome, a process that requires mitochondrial NADPH oxidase 4 (NOX4)-dependent ROS production (52). Therefore, it is clear that needs for lipid metabolism in activated macrophages is significantly increased but whether this fulfills mitochondrial energy production requirements or rather constitutes the primal building blocks for anabolism needs to be further investigated.

Mitochondrial Respiratory Chain Adaptations in Macrophages upon Innate Immune Receptor Engagement

As stated above, most catabolic processes converge on the mitochondrial ETC by supplying electrons in the form of the reductive equivalents NADH and $FADH_2$. The intramitochondrial NADH/$FADH_2$ ratio depends on the nature of the fuels that feed the mitochondrial metabolism and the respiratory chain adapts to these fuel source fluctuations (16), particularly during PRR-mediated macrophage activation. Indeed, two recent studies provide evidence that changes in the ETC occur in activated mouse macrophages (5, 19). The phagocytosis of live Gram-negative bacteria by mouse macrophages trigger a profound change in ETC structural organization (5) (**Figure 1**). This is characterized by a decreased abundance of ETC SCs that contain CI and a relative increase in the free form of CIII and is accompanied by a substantial decrease in the activity of CI. By contrast, the activity of the glycerol 3-phosphate dehydrogenase and CII, two enzymes that use $FADH_2$, are increased in response to live bacteria or to TLR-mediated sensing of bacterial RNA. CII activity is driven by the production of phagosomal ROS. This activates the ROS-dependent tyrosine kinase Fgr, which was previously found to phosphorylate CII (53). Consistently, CII was essential to mitochondrial respiration in bacteria-activated macrophages. This work thus suggests that adjustments of the organization of the ETC and of the activity of its components are required for metabolic reprogramming in macrophages. A study by O'Neill and colleagues has further precised the mechanism by which ETC integrates signals emerging from TLRs (19) (**Figure 1**). The combination of enhanced succinate dehydrogenase (SDH) activity and increased mitochondrial potential in LPS-activated mouse macrophages allows for the induction of mitochondrial ROS production at the level of CI thereby reprogramming mitochondria from ATP production to ROS production in order to establish an inflammatory state. This is consistent with a previous study showing that metformin-mediated inhibition of CI-dependent ROS production suppresses the inflammatory capacity of activated mouse macrophages (54). These data point out CI as a major regulator of inflammatory macrophages. This is backed up by genetical evidences demonstrating that mouse macrophages deficient for the CI subunit NDUFS4 exhibit an inflammatory phenotype (55). Interestingly, the deletion of TLR2/4 in NDUFS4-deficient mice attenuated the inflammatory phenotype (55), highlighting the close relationship between TLRs and the ETC. However, the contributions of mitochondrial respiratory chain to innate immune functions seems not limited to TLRs since the engagement of Dectin-1 in human monocytes induces

accumulation of CII-product fumarate, which can induce an epigenetic program accounting for trained immunity by inhibiting KDM5 histone demethylases (41). Whether adaptations of the ETC reflect solely the metabolic fluctuations within activated macrophages or can be directly regulated by signals emerging from innate immune receptors remains to be clarified.

FUNCTIONAL CONSEQUENCES OF MITOCHONDRIAL ADAPTATIONS IN MACROPHAGES

Regulation of Macrophage Polarization and Cytokine Response

The finding that IL-4, a well-known inducer of alternatively activated mouse macrophages (M2), promotes a distinct metabolic reprogramming compared to pro-inflammatory (M1) mouse macrophage stimulating LPS/IFN-γ indicates that mitochondrial metabolism adjusts to the type of immune responses required to eliminate the threats encountered (1). M1 mouse macrophages produce high amount of pro-inflammatory cytokines and antimicrobial peptides and excel in phagocytosing and destroying microbes. Those macrophages exhibit a high glycolytic rate and present two breaks in the TCA cycle, one at isocitrate dehydrogenase, the enzyme that converts isocitrate to α-ketoglutarate, and another one at SDH that catalyzes the oxidation of succinate to fumarate (7). M2 mouse macrophages are essential at fighting against helminth infection, exert tissue repair functions, and conserve an intact TCA cycle (7). The specificities of metabolic fluxes in differentiated macrophages is a subject of intense research and has been reviewed elsewhere (1). However, whether mitochondrial ETC organization and its functional adjustments reflect the metabolic specificities of M1 and M2 macrophages is still poorly understood. A recent report nevertheless showed that LPS + IFN-γ treatment promotes NO that inhibits mitochondrial respiration thereby preventing the repolarization of M1 into M2 macrophages in mice and humans upon IL-4 treatment (56). In line with this, various reports suggest that manipulating the ETC modulates the balance between pro- and anti-inflammatory cytokine production. The use of the CI inhibitors metformin and rotenone decreased mitochondrial ROS production in LPS-activated mouse macrophages thereby reducing IL-1β production and boosting IL-10 production (54). In addition to their function as TLR7 agonists, imiquimod and CL097 also inhibited the quinone oxidoreductases NQO2 and CI, inducing ROS that contributed to NLRP3 activation (57). Conversely, the CII inhibitor dimethyl malonate enhanced the production of IL-1RA and IL-10 and promote an anti-inflammatory response by preventing mitochondrial ROS generation and succinate oxidation (19).

Mitochondrial metabolites, e.g., those related to α-ketoglutarate, such as succinate and fumarate, regulate transcription and influence the pattern of cytokine production that characterizes differentiated macrophages. Succinate is accumulated in M1 mouse macrophages and was originally thought to stabilize HIF-1α through inhibition of prolyl hydroxylases (58). However, new evidence shows that succinate rather drives CII activity, which in turn promotes mitochondrial reactive oxygen species (mROS) production to stabilize HIF-1α (19), thereby promoting pro-inflammatory cytokine IL-1β expression (8) (**Figure 2**). Succinate may also contribute to increased reverse electron transport and ROS production from CI (59), a process that is potentially important for macrophage function (60). Likewise, SDH (part of the CII) metabolizes succinate to fumarate in the TCA cycle, and fumarate inhibits histone demethylases thus regulating epigenetics (41). In this process, CII accepts the electrons from $FADH_2$, and this function as electron carrier drives modulation of ROS signaling (60). These results establish how ROS drives expression of pro-inflammatory cytokines that characterize M1 macrophages but the mechanism by which succinate inhibits anti-inflammatory gene expression is still an open question. Taken together, those studies show the great potential of mitochondrial metabolism for regulation of transcription, cytokine production, and macrophage polarization that can be exploited for therapy.

Regulation of Macrophage Bactericidal Functions

Although phagosomal ROS are considered to be a main component of bacteria killing machinery within macrophages, mitochondria seem to significantly contribute to antibacterial functions by generating a substantial amount of ROS (**Figure 2**). Engagement of a cell membrane-associated TLRs (TLR1, TLR2, and TLR4) results in the recruitment of mitochondria to macrophage phagosomes and increases mROS production. This response involves translocation of the TLR signaling adaptor TRAF6 to mitochondria where it engages the mitochondrial respiratory complex I assembly adaptor ECSIT (30). Consistently, mouse macrophages that lack ECSIT or TRAF6 show decreased levels of TLR-induced ROS and impaired ability to kill intracellular bacteria. In addition, reducing mouse macrophage mROS levels by expressing catalase in mitochondria results in defective bacterial killing, confirming the role of mROS in bactericidal activity (30). Additional studies support the notion that suppressing mROS production regulates antibacterial innate immune responses. Mice deficient for UCP2 and infected with a lethal load of *Toxoplasma gondii* were significantly more resistant compared with wild-type (WT) animals. Consistently, UCP2-deficient macrophages generated more ROS in response to *T. gondii* underlying this enhanced parasite-killing capacity (61). A subsequent study detailed a similar phenotype, demonstrating that $Ucp2^{-/-}$ mice were more resistant to *Listeria monocytogenes* and display higher splenic ROS levels than WT mice (62). LPS stimulation also reduces macrophage UCP2 expression, indicating that the abundance of UCP2 in the cell regulates mROS generation following TLR4 engagement (63). Additionally, it was demonstrated that IFNγ induces an estrogen-related receptor-α (ERRα)- and a proliferator-activated receptor-γ co-activator (PGC1β)-dependent transcriptional program in mouse macrophages that induces mitochondrial function and mROS production upon bacterial infection (64). Consequently, ERRα- or PGC1β-deficient macrophages produce less ROS upon *L. monocytogenes* challenge and display a reduced bacteria killing capacity (64). In this context, ETC re-arrangement may also regulate mROS production by controlling electron leak within

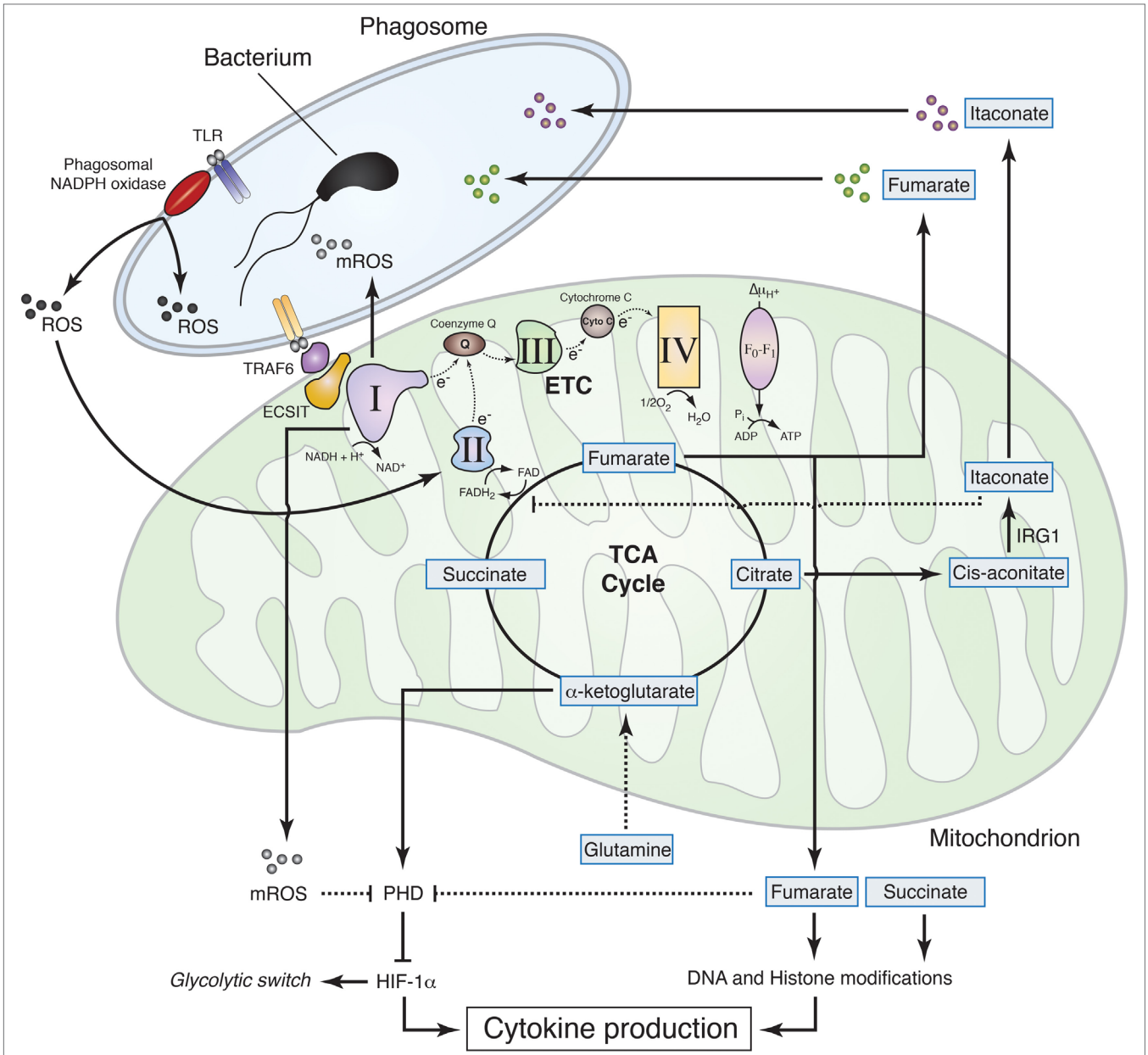

FIGURE 2 | Mitochondrial metabolism contributions to macrophage effector functions. Sensing of live Gram-negative bacteria by toll-like receptors (TLR) induces the production of phagosomal reactive oxygen species (ROS) by phagosomal NADPH oxidase. Phagosomal ROS directly contribute to the killing of the bacteria inside the phagosome and induce CII activity thereby promoting fumarate accumulation, which exerts bactericidal properties and modulates histone posttranslational modifications to control cytokine production. The increase in CII activity is associated with a reduction in CI activity and a subsequent increase in mitochondrial ROS (mROS). TLR mediates recruitment of the mitochondria to the phagosome through tumor necrosis factor receptor-associated factor 6 (TRAF6)–evolutionarily conserved signaling intermediate in toll pathways (ECSIT) interaction and concomitantly increases mROS, which contribute to bacteria killing in the phagosome and inhibit prolyl hydroxylase (PHD), thus promoting hypoxia-inducible factor-1α (HIF-1α) stabilization. TLR signaling also induces accumulation of succinate, which, together with fumarate, inhibits α-ketoglutarate-dependent DNA hydroxylases and histone demethylases, regulating cytokine expression and glycolytic switch. Succinate oxidation, in turn, is required to induce mROS production at the level of CI, thereby inhibiting PHD, stabilizing HIF-1α, and further controlling cytokine production. In addition to fumarate, other tricarboxylic acid cycle-related metabolites exhibit antibactericidal properties. Citrate is used to produce itaconate through the decarboxylation of *cis*-aconitate by IRG1. Itaconate was found to have antimicrobial properties and to regulate succinate dehydrogenase (CII) activity in lipopolysaccharide-activated macrophages.

the respiratory complexes (16). Future studies will likely provide additional details on the role of ETC architecture and electron flow for antimicrobial function of mitochondria.

The notion that mitochondria are important players for the microbicidal properties of macrophage has recently gained further interest with the finding that mitochondrial metabolites

directly contribute to macrophage bactericidal functions. The mitochondrial protein immune responsive gene 1 (IRG1) is highly expressed in mouse and human macrophages during inflammation. It metabolizes *cis*-aconitate into itaconate, which can drive the production of β-oxidation-dependent mitochondrial ROS (65). Importantly, itaconate inhibits citrate-lyase in different bacterial strains and thus shows direct antimicrobial activity (66) (**Figure 2**). IFNs induce IRG1, which in turn accumulates in mitochondria that closely associate with *Legionella*-containing vacuoles, as step that may be required for bacteria killing (67). In addition, itaconate has been postulated to modulate mouse macrophage metabolism and effector functions by inhibiting SDH. Indeed, *Irg1*$^{-/-}$ mice, which cannot produce itaconate, have decreased level of succinate and increased mitochondrial respiration and inflammatory cytokine production upon LPS stimulation (68). Reorganization of the ETC may also participate to such processes, since the SDH product fumarate can directly inhibit bacteria proliferation in response to ETC adjustments upon sensing of viable bacteria (5) (**Figure 2**). Notably, the substrate of SDH succinate did not show antimicrobial properties as compared to fumarate, revealing specific immune properties of closely related mitochondria-derived metabolites (5).

CONCLUDING REMARKS

Since mitochondria have emerged as key conductors of the metabolic adaptations to the innate sensing by modulating the electron flow in the ETC (5, 19), a key open question is whether targeting of mitochondrial metabolism can be used to modulate immune cell function with substantial improvement for therapeutic strategies. This would be particularly interesting for enhanced vaccination and modulation of immunity and tolerance when targeting DCs, or for the treatment of inflammatory diseases in the case of targeting macrophages. In the later, mitochondrial manipulation would constitute an approach of choice to facilitate macrophage repolarization (56). Because some mitochondrial metabolites and the use of ETC CI or CII inhibitors can modulate cytokine production (8, 19, 41, 54, 57), such approach seems very promising. Moreover, mitochondrial ROS and metabolites, such as fumarate or itaconate, show a direct microbicidal effect (5, 30, 66). The exciting findings in this rapidly moving field thus emphasize the great potential of targeting mitochondrial metabolism for modulation of transcription, polarization, cytokine production, and microbicidal capacity of macrophages with potential to offer new therapeutic approaches.

AUTHOR CONTRIBUTIONS

DS, ME, and JG conceived and wrote the manuscript. JG did the figures.

FUNDING

DS's laboratory is funded by the CNIC and grants from the Spanish Ministry of Economy, Industry and Competitiveness (MINECO) and European Fund for Regional Development (FEDER) (SAF-2016-79040-R), the European Commission (635122-PROCROP H2020), the Fondation ACTERIA, and the European Research Council. The CNIC is supported by the MINECO and the Pro-CNIC Foundation, and is a Severo Ochoa Center of Excellence (MINECO award SEV-2015-0505). ME is the recipient of a CNIC International PhD Programme fellowship "la Caixa"—Severo Ochoa, 2013 Call (OSLC-CNIC-2013-04). JG's laboratory is funded by INSERM and a European FP7-Marie Curie Career Integration Grant (332881).

REFERENCES

1. O'Neill LA, Pearce EJ. Immunometabolism governs dendritic cell and macrophage function. *J Exp Med* (2016) 213(1):15–23. doi:10.1084/jem.20151570
2. Park D, Han CZ, Elliott MR, Kinchen JM, Trampont PC, Das S, et al. Continued clearance of apoptotic cells critically depends on the phagocyte Ucp2 protein. *Nature* (2011) 477(7363):220–4. doi:10.1038/nature10340
3. Cheng S-C, Quintin J, Cramer RA, Shepardson KM, Saeed S, Kumar V, et al. mTOR- and HIF-1α-mediated aerobic glycolysis as metabolic basis for trained immunity. *Science* (2014) 345(6204):1250684. doi:10.1126/science.1250684
4. Everts B, Amiel E, Huang SC, Smith AM, Chang CH, Lam WY, et al. TLR-driven early glycolytic reprogramming via the kinases TBK1-IKK? supports the anabolic demands of dendritic cell activation. *Nat Immunol* (2014) 15(4):323–32. doi:10.1038/ni.2833
5. Garaude J, Acin-Perez R, Martinez-Cano S, Enamorado M, Ugolini M, Nistal-Villan E, et al. Mitochondrial respiratory-chain adaptations in macrophages contribute to antibacterial host defense. *Nat Immunol* (2016) 17(9):1037–45. doi:10.1038/ni.3509
6. Huang SC, Everts B, Ivanova Y, O'Sullivan D, Nascimento M, Smith AM, et al. Cell-intrinsic lysosomal lipolysis is essential for alternative activation of macrophages. *Nat Immunol* (2014) 15(9):846–55. doi:10.1038/ni.2956
7. Jha AK, Huang SC, Sergushichev A, Lampropoulou V, Ivanova Y, Loginicheva E, et al. Network integration of parallel metabolic and transcriptional data reveals metabolic modules that regulate macrophage polarization. *Immunity* (2015) 42(3):419–30. doi:10.1016/j.immuni.2015.02.005
8. Tannahill GM, Curtis AM, Adamik J, Palsson-McDermott EM, McGettrick AF, Goel G, et al. Succinate is an inflammatory signal that induces IL-1beta through HIF-1alpha. *Nature* (2013) 496(7444):238–42. doi:10.1038/nature11986
9. Mills EL, O'Neill LA. Reprogramming mitochondrial metabolism in macrophages as an anti-inflammatory signal. *Eur J Immunol* (2016) 46(1):13–21. doi:10.1002/eji.201445427
10. Gleeson LE, Sheedy FJ. Metabolic reprogramming and inflammation: fuelling the host response to pathogens. *Semin Immunol* (2016) 28(5):450–68. doi:10.1016/j.smim.2016.10.007
11. Pearce EJ, Everts B. Dendritic cell metabolism. *Nat Rev Immunol* (2015) 15(1):18–29. doi:10.1038/nri3771
12. Weinberg SE, Sena LA, Chandel NS. Mitochondria in the regulation of innate and adaptive immunity. *Immunity* (2015) 42(3):406–17. doi:10.1016/j.immuni.2015.02.002
13. Arts RJ, Joosten LA, Netea MG. Immunometabolic circuits in trained immunity. *Semin Immunol* (2016) 28(5):425–30. doi:10.1016/j.smim.2016.09.002
14. Speijer D. Oxygen radicals shaping evolution: why fatty acid catabolism leads to peroxisomes while neurons do without it: FADH(2)/NADH flux ratios determining mitochondrial radical formation were crucial for the eukaryotic invention of peroxisomes and catabolic tissue differentiation. *Bioessays* (2011) 33(2):88–94. doi:10.1002/bies.201000097
15. Stanley IA, Ribeiro SM, Gimenez-Cassina A, Norberg E, Danial NN. Changing appetites: the adaptive advantages of fuel choice. *Trends Cell Biol* (2014) 24(2):118–27. doi:10.1016/j.tcb.2013.07.010
16. Enriquez JA. Supramolecular organization of respiratory complexes. *Annu Rev Physiol* (2016) 78:533–61. doi:10.1146/annurev-physiol-021115-105031

17. Lapuente-Brun E, Moreno-Loshuertos R, Acin-Perez R, Latorre-Pellicer A, Colas C, Balsa E, et al. Supercomplex assembly determines electron flux in the mitochondrial electron transport chain. *Science* (2013) 340(6140):1567–70. doi:10.1126/science.1230381
18. Guaras A, Perales-Clemente E, Calvo E, Acin-Perez R, Loureiro-Lopez M, Pujol C, et al. The CoQH2/CoQ ratio serves as a sensor of respiratory chain efficiency. *Cell Rep* (2016) 15(1):197–209. doi:10.1016/j.celrep.2016.03.009
19. Mills EL, Kelly B, Logan A, Costa AS, Varma M, Bryant CE, et al. Succinate dehydrogenase supports metabolic repurposing of mitochondria to drive inflammatory macrophages. *Cell* (2016) 167(2):457–70 e413. doi:10.1016/j.cell.2016.08.064
20. Zhang Q, Raoof M, Chen Y, Sumi Y, Sursal T, Junger W, et al. Circulating mitochondrial DAMPs cause inflammatory responses to injury. *Nature* (2010) 464(7285):104–7. doi:10.1038/nature08780
21. Nakahira K, Haspel JA, Rathinam VA, Lee SJ, Dolinay T, Lam HC, et al. Autophagy proteins regulate innate immune responses by inhibiting the release of mitochondrial DNA mediated by the NALP3 inflammasome. *Nat Immunol* (2011) 12(3):222–30. doi:10.1038/ni.1980
22. Shimada K, Crother TR, Karlin J, Dagvadorj J, Chiba N, Chen S, et al. Oxidized mitochondrial DNA activates the NLRP3 inflammasome during apoptosis. *Immunity* (2012) 36(3):401–14. doi:10.1016/j.immuni.2012.01.009
23. Pastorino JG, Hoek JB. Regulation of hexokinase binding to VDAC. *J Bioenerg Biomembr* (2008) 40(3):171–82. doi:10.1007/s10863-008-9148-8
24. Wolf AJ, Reyes CN, Liang W, Becker C, Shimada K, Wheeler ML, et al. Hexokinase is an innate immune receptor for the detection of bacterial peptidoglycan. *Cell* (2016) 166(3):624–36. doi:10.1016/j.cell.2016.05.076
25. Moon J-S, Hisata S, Park M-A, DeNicola GM, Ryter SW, Nakahira K, et al. mTORC1-induced HK1-dependent glycolysis regulates NLRP3 inflammasome activation. *Cell Rep* (2015) 12(1):102–15. doi:10.1016/j.celrep.2015.05.046
26. West AP, Khoury-Hanold W, Staron M, Tal MC, Pineda CM, Lang SM, et al. Mitochondrial DNA stress primes the antiviral innate immune response. *Nature* (2015) 520(7548):553–7. doi:10.1038/nature14156
27. Horner SM, Liu HM, Park HS, Briley J, Gale M Jr. Mitochondrial-associated endoplasmic reticulum membranes (MAM) form innate immune synapses and are targeted by hepatitis C virus. *Proc Natl Acad Sci U S A* (2011) 108(35):14590–5. doi:10.1073/pnas.1110133108
28. Hou F, Sun L, Zheng H, Skaug B, Jiang QX, Chen ZJ. MAVS forms functional prion-like aggregates to activate and propagate antiviral innate immune response. *Cell* (2011) 146(3):448–61. doi:10.1016/j.cell.2011.06.041
29. Vogel RO, Janssen RJ, van den Brand MA, Dieteren CE, Verkaart S, Koopman WJ, et al. Cytosolic signaling protein ECSIT also localizes to mitochondria where it interacts with chaperone NDUFAF1 and functions in complex I assembly. *Genes Dev* (2007) 21(5):615–24. doi:10.1101/gad.408407
30. West AP, Brodsky IE, Rahner C, Woo DK, Erdjument-Bromage H, Tempst P, et al. TLR signalling augments macrophage bactericidal activity through mitochondrial ROS. *Nature* (2011) 472(7344):476–80. doi:10.1038/nature09973
31. Fukuzumi M, Shinomiya H, Shimizu Y, Ohishi K, Utsumi S. Endotoxin-induced enhancement of glucose influx into murine peritoneal macrophages via GLUT1. *Infect Immun* (1996) 64(1):108–12.
32. Hard GC. Some biochemical aspects of the immune macrophage. *Br J Exp Pathol* (1970) 51(1):97–105.
33. Newsholme P, Curi R, Gordon S, Newsholme EA. Metabolism of glucose, glutamine, long-chain fatty acids and ketone bodies by murine macrophages. *Biochem J* (1986) 239(1):121–5. doi:10.1042/bj2390121
34. Kim JW, Tchernyshyov I, Semenza GL, Dang CV. HIF-1-mediated expression of pyruvate dehydrogenase kinase: a metabolic switch required for cellular adaptation to hypoxia. *Cell Metab* (2006) 3(3):177–85. doi:10.1016/j.cmet.2006.02.002
35. Semenza GL, Jiang BH, Leung SW, Passantino R, Concordet JP, Maire P, et al. Hypoxia response elements in the aldolase A, enolase 1, and lactate dehydrogenase A gene promoters contain essential binding sites for hypoxia-inducible factor 1. *J Biol Chem* (1996) 271(51):32529–37. doi:10.1074/jbc.271.51.32529
36. Rodríguez-Prados J-C, Través PG, Cuenca J, Rico D, Aragonés J, Martín-Sanz P, et al. Substrate fate in activated macrophages: a comparison between innate, classic, and alternative activation. *J Immunol* (2010) 185(1):605–14. doi:10.4049/jimmunol.0901698
37. Palsson-McDermott EM, Curtis AM, Goel G, Lauterbach MA, Sheedy FJ, Gleeson LE, et al. Pyruvate kinase M2 regulates Hif-1alpha activity and IL-1beta induction and is a critical determinant of the Warburg effect in LPS-activated macrophages. *Cell Metab* (2015) 21(1):65–80. doi:10.1016/j.cmet.2014.12.005
38. Yang L, Xie M, Yang M, Yu Y, Zhu S, Hou W, et al. PKM2 regulates the Warburg effect and promotes HMGB1 release in sepsis. *Nat Commun* (2014) 5:4436. doi:10.1038/ncomms5436
39. Lachmandas E, Beigier-Bompadre M, Cheng SC, Kumar V, van Laarhoven A, Wang X, et al. Rewiring cellular metabolism via the AKT/mTOR pathway contributes to host defence against *Mycobacterium tuberculosis* in human and murine cells. *Eur J Immunol* (2016) 46(11):2574–86. doi:10.1002/eji.201546259
40. Krawczyk CM, Holowka T, Sun J, Blagih J, Amiel E, DeBerardinis RJ, et al. Toll-like receptor-induced changes in glycolytic metabolism regulate dendritic cell activation. *Blood* (2010) 115(23):4742–9. doi:10.1182/blood-2009-10-249540
41. Arts RJ, Novakovic B, Ter Horst R, Carvalho A, Bekkering S, Lachmandas E, et al. Glutaminolysis and fumarate accumulation integrate immunometabolic and epigenetic programs in trained immunity. *Cell Metab* (2016) 24(6):807–19. doi:10.1016/j.cmet.2016.10.008
42. Gleeson LE, Sheedy FJ, Palsson-McDermott EM, Triglia D, O'Leary SM, O'Sullivan MP, et al. Cutting edge: *Mycobacterium tuberculosis* induces aerobic glycolysis in human alveolar macrophages that is required for control of intracellular bacillary replication. *J Immunol* (2016) 196(6):2444–9. doi:10.4049/jimmunol.1501612
43. Mehrotra P, Jamwal SV, Saquib N, Sinha N, Siddiqui Z, Manivel V, et al. Pathogenicity of *Mycobacterium tuberculosis* is expressed by regulating metabolic thresholds of the host macrophage. *PLoS Pathog* (2014) 10(7):e1004265. doi:10.1371/journal.ppat.1004265
44. Shao W, Yeretssian G, Doiron K, Hussain SN, Saleh M. The caspase-1 digestome identifies the glycolysis pathway as a target during infection and septic shock. *J Biol Chem* (2007) 282(50):36321–9. doi:10.1074/jbc.M708182200
45. Everts B, Amiel E, van der Windt GJ, Freitas TC, Chott R, Yarasheski KE, et al. Commitment to glycolysis sustains survival of NO-producing inflammatory dendritic cells. *Blood* (2012) 120(7):1422–31. doi:10.1182/blood-2012-03-419747
46. Haschemi A, Kosma P, Gille L, Evans CR, Burant CF, Starkl P, et al. The sedoheptulose kinase CARKL directs macrophage polarization through control of glucose metabolism. *Cell Metab* (2012) 15(6):813–26. doi:10.1016/j.cmet.2012.04.023
47. Meiser J, Kramer L, Sapcariu SC, Battello N, Ghelfi J, D'Herouel AF, et al. Pro-inflammatory macrophages sustain pyruvate oxidation through pyruvate dehydrogenase for the synthesis of itaconate and to enable cytokine expression. *J Biol Chem* (2016) 291(8):3932–46. doi:10.1074/jbc.M115.676817
48. Quintin J, Saeed S, Martens JH, Giamarellos-Bourboulis EJ, Ifrim DC, Logie C, et al. *Candida albicans* infection affords protection against reinfection via functional reprogramming of monocytes. *Cell Host Microbe* (2012) 12(2):223–32. doi:10.1016/j.chom.2012.06.006
49. Feingold KR, Shigenaga JK, Kazemi MR, McDonald CM, Patzek SM, Cross AS, et al. Mechanisms of triglyceride accumulation in activated macrophages. *J Leukoc Biol* (2012) 92(4):829–39. doi:10.1189/jlb.1111537
50. Nicolaou G, Goodall AH, Erridge C. Diverse bacteria promote macrophage foam cell formation via toll-like receptor-dependent lipid body biosynthesis. *J Atheroscler Thromb* (2012) 19(2):137–48. doi:10.5551/jat.10249
51. Hondowicz BD, An D, Schenkel JM, Kim KS, Steach HR, Krishnamurty AT, et al. Interleukin-2-dependent allergen-specific tissue-resident memory cells drive asthma. *Immunity* (2015) 44(1):155–66. doi:10.1016/j.immuni.2015.11.004
52. Moon J-S, Nakahira K, Chung K-P, DeNicola GM, Koo MJ, Pabón MA, et al. NOX4-dependent fatty acid oxidation promotes NLRP3 inflammasome activation in macrophages. *Nat Med* (2016) 22(9):1002–12. doi:10.1038/nm.4153
53. Acin-Perez R, Carrascoso I, Baixauli F, Roche-Molina M, Latorre-Pellicer A, Fernandez-Silva P, et al. ROS-triggered phosphorylation of complex II by Fgr kinase regulates cellular adaptation to fuel use. *Cell Metab* (2014) 19(6):1020–33. doi:10.1016/j.cmet.2014.04.015
54. Kelly B, Tannahill GM, Murphy MP, O'Neill LA. Metformin inhibits the production of reactive oxygen species from NADH: ubiquinone oxidoreductase to limit induction of interleukin-1beta (IL-1beta) and boosts interleukin-10

(IL-10) in lipopolysaccharide (LPS)-activated macrophages. *J Biol Chem* (2015) 290(33):20348–59. doi:10.1074/jbc.M115.662114
55. Jin Z, Wei W, Yang M, Du Y, Wan Y. Mitochondrial complex I activity suppresses inflammation and enhances bone resorption by shifting macrophage-osteoclast polarization. *Cell Metab* (2014) 20(3):483–98. doi:10.1016/j.cmet.2014.07.011
56. Van den Bossche J, Baardman J, Otto NA, van der Velden S, Neele AE, van den Berg SM, et al. Mitochondrial dysfunction prevents repolarization of inflammatory macrophages. *Cell Rep* (2016) 17(3):684–96. doi:10.1016/j.celrep.2016.09.008
57. Groß CJ, Mishra R, Schneider KS, Médard G, Wettmarshausen J, Dittlein DC, et al. K+ Efflux-independent NLRP3 inflammasome activation by small molecules targeting mitochondria. *Immunity* (2016) 45(4):1–14. doi:10.1016/j.immuni.2016.08.010
58. Selak MA, Armour SM, MacKenzie ED, Boulahbel H, Watson DG, Mansfield KD, et al. Succinate links TCA cycle dysfunction to oncogenesis by inhibiting HIF-alpha prolyl hydroxylase. *Cancer Cell* (2005) 7(1):77–85. doi:10.1016/j.ccr.2004.11.022
59. Chouchani ET, Pell VR, Gaude E, Aksentijević D, Sundier SY, Robb EL, et al. Ischaemic accumulation of succinate controls reperfusion injury through mitochondrial ROS. *Nature* (2014) 515(7527):431–5. doi:10.1038/nature13909
60. Mills E, O'Neill LA. Succinate: a metabolic signal in inflammation. *Trends Cell Biol* (2014) 24(5):313–20. doi:10.1016/j.tcb.2013.11.008
61. Arsenijevic D, Onuma H, Pecqueur C, Raimbault S, Manning BS, Miroux B, et al. Disruption of the uncoupling protein-2 gene in mice reveals a role in immunity and reactive oxygen species production. *Nat Genet* (2000) 26(4):435–9. doi:10.1038/82565
62. Rousset S, Emre Y, Join-Lambert O, Hurtaud C, Ricquier D, Cassard-Doulcier AM. The uncoupling protein 2 modulates the cytokine balance in innate immunity. *Cytokine* (2006) 35(3–4):135–42. doi:10.1016/j.cyto.2006.07.012
63. Emre Y, Hurtaud C, Nubel T, Criscuolo F, Ricquier D, Cassard-Doulcier AM. Mitochondria contribute to LPS-induced MAPK activation via uncoupling protein UCP2 in macrophages. *Biochem J* (2007) 402(2):271–8. doi:10.1042/BJ20061430
64. Sonoda J, Laganiere J, Mehl IR, Barish GD, Chong LW, Li X, et al. Nuclear receptor ERR alpha and coactivator PGC-1 beta are effectors of IFN-gamma-induced host defense. *Genes Dev* (2007) 21(15):1909–20. doi:10.1101/gad.1553007
65. Hall CJ, Boyle RH, Astin JW, Flores MV, Oehlers SH, Sanderson LE, et al. Immunoresponsive gene 1 augments bactericidal activity of macrophage-lineage cells by regulating β-oxidation-dependent mitochondrial ROS production. *Cell Metab* (2013) 18(2):265–78. doi:10.1016/j.cmet.2013.06.018
66. Michelucci A, Cordes T, Ghelfi J, Pailot A, Reiling N, Goldmann O, et al. Immune-responsive gene 1 protein links metabolism to immunity by catalyzing itaconic acid production. *Proc Natl Acad Sci U S A* (2013) 110(19):7820–5. doi:10.1073/pnas.1218599110
67. Naujoks J, Tabeling C, Dill BD, Hoffmann C, Brown AS, Kunze M, et al. IFNs modify the proteome of *Legionella*-containing vacuoles and restrict infection via IRG1-derived itaconic acid. *PLoS Pathog* (2016) 12(2):e1005408. doi:10.1371/journal.ppat.1005408
68. Lampropoulou V, Sergushichev A, Bambouskova M, Nair S, Vincent EE, Loginicheva E, et al. Itaconate links inhibition of succinate dehydrogenase with macrophage metabolic remodeling and regulation of inflammation. *Cell Metab* (2016) 24(1):158–66. doi:10.1016/j.cmet.2016.06.004

Conflict of Interest Statement: The authors declare that the research was conducted in the absence of any commercial or financial relationships that could be construed as a potential conflict of interest.

Article

Immunity

Optimal Generation of Tissue-Resident but Not Circulating Memory T Cells during Viral Infection Requires Crosspriming by DNGR-1$^+$ Dendritic Cells

Graphical Abstract

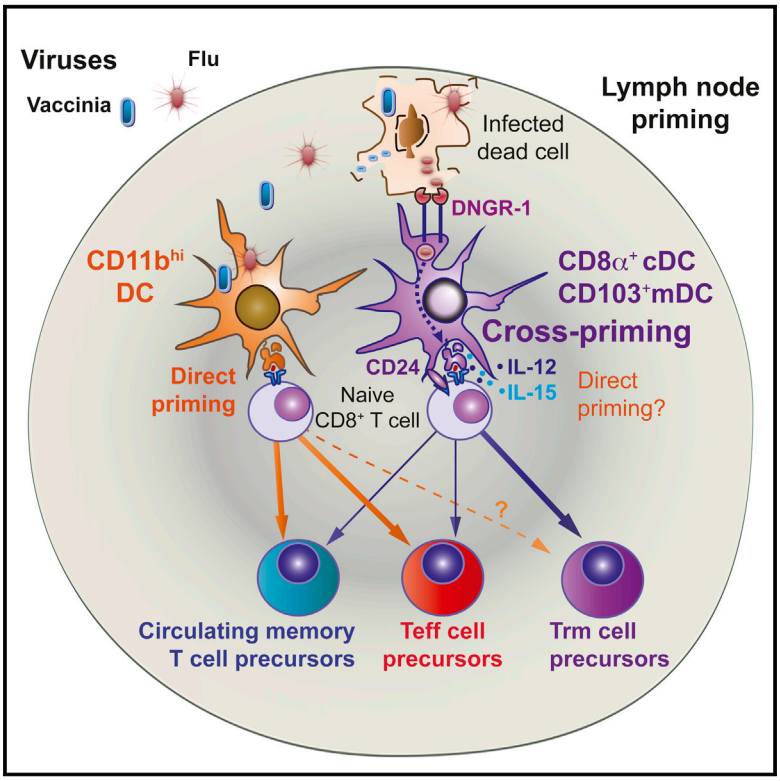

Authors

Salvador Iborra, María Martínez-López, Sofía C. Khouili, ..., Ruth Conde-Garrosa, Carlos del Fresno, David Sancho

Correspondence

siborra@cnic.es (S.I.), dsancho@cnic.es (D.S.)

In Brief

Priming of tissue-resident memory T cells (Trm) is not well characterized. Iborra et al. find that prolonged antigen crosspresentation in combination with specific signals from DNGR-1$^+$ dendritic cells are required for optimal Trm priming but not for their differentiation, and are dispensable for the generation of circulating memory T cells.

Highlights

- Distinct priming requirements of Trm versus circulating memory in viral infection
- Genetic or antibody blockade of crosspriming selectively impairs Trm generation
- Unique signals from DNGR-1$^+$ DC induce T-bet and retain naive T cells for LN priming
- Protective mucosal immunity depends on optimal Trm induction by DNGR-1$^+$ DC

Iborra et al., 2016, Immunity *45*, 847–860
October 18, 2016
http://dx.doi.org/10.1016/j.immuni.2016.08.019

CellPress

Immunity
Article

Optimal Generation of Tissue-Resident but Not Circulating Memory T Cells during Viral Infection Requires Crosspriming by DNGR-1$^+$ Dendritic Cells

Salvador Iborra,[1,*] María Martínez-López,[1] Sofía C. Khouili,[1] Michel Enamorado,[1] Francisco J. Cueto,[1,2] Ruth Conde-Garrosa,[1] Carlos del Fresno,[1] and David Sancho[1,3,*]
[1]Centro Nacional de Investigaciones Cardiovasculares Carlos III (CNIC), Melchor Fernández Almagro 3, Madrid, 28029, Spain
[2]Department of Biochemistry, Faculty of Medicine, Universidad Autónoma de Madrid, Calle Arzobispo Morcillo 4, Madrid, 28029, Spain
[3]Lead contact
*Correspondence: siborra@cnic.es (S.I.), dsancho@cnic.es (D.S.)
http://dx.doi.org/10.1016/j.immuni.2016.08.019

SUMMARY

Despite the crucial role of tissue-resident memory T (Trm) cells in protective immunity, their priming remains poorly understood. Here, we have shown differential priming requirements for Trm versus circulating memory CD8$^+$ T cells. In vaccinia cutaneous-infected mice, DNGR-1-mediated cross-presentation was required for optimal Trm cell priming but not for their skin differentiation or for circulating memory T cell generation. DNGR-1$^+$ dendritic cells (DCs) promoted T-bet transcription-factor induction and retention of CD8$^+$ T cells in the lymph nodes (LNs). Inhibition of LN egress enhanced Trm cell generation, whereas genetic or antibody blockade of DNGR-1 or specific signals provided during priming by DNGR-1$^+$ DCs, such as interleukin-12 (IL-12), IL-15, or CD24, impaired Trm cell priming. DNGR-1 also regulated Trm cell generation during influenza infection. Moreover, protective immunity depended on optimal Trm cell induction by DNGR-1$^+$ DCs. Our results reveal specific priming requirements for CD8$^+$ Trm cells during viral infection and vaccination.

INTRODUCTION

During infection, naive T cells in secondary lymphoid organs are primed by dendritic cells (DCs) to become either long-lived memory T cells or short-lived effectors. Based on their trafficking properties, memory T cells are subdivided among circulating memory cells and tissue-resident memory T (Trm) cells (Mueller and Mackay, 2016). Trm cells are found in all tissues and, depending on location, are characterized by stable expression of CD69, variable CD103 expression, and enhanced effector ability (Ariotti et al., 2014; Bergsbaken and Bevan, 2015; Mackay et al., 2013; Masopust et al., 2006; Schenkel et al., 2014; Skon et al., 2013; Steinert et al., 2015). Trm cells are crucial for surveying and mounting an effective and rapid immune response upon reinfection in skin and mucosae (Gebhardt et al., 2009; Jiang et al., 2012; Mackay et al., 2015; Steinert et al., 2015). Moreover, upon antigen contact, activated Trm cells orchestrate circulating memory T cell response, drive maturation of DCs, and boost local immunity, thus establishing a tissue-wide pathogen alert state (Ariotti et al., 2014; Schenkel et al., 2014; Schenkel et al., 2013).

Trm cells derive from precursors characterized by low expression of KLRG1 transcription factor that migrate into the tissue where they are retained following downregulation of Krüppel-like factor 2 (KLF2) and its target gene sphingosine 1-phosphate receptor $S1P_1$ (S1P) (Gebhardt et al., 2009; Mackay et al., 2013; Masopust et al., 2010; Skon et al., 2013), along with downregulation of T-box transcription factors (Eomes and T-bet) (Mackay et al., 2015). Trm and circulating memory T cells have the same clonal origin (Gaide et al., 2015), but Trm cells retain high-affinity T cell receptors (TCRs) (Frost et al., 2015). Whether these Trm cell precursors have specific priming requirements different from those of circulating memory cells is not known.

Cutaneous infection with vaccinia virus (VACV) in mice generates circulating memory and Trm CD8$^+$ T cells, the latter accumulating in the skin (Jiang et al., 2012). Similarly to many viruses, VACV infects DCs and thereby provides antigens for direct presentation via MHC class I molecules (Xu et al., 2010). However, DCs can also acquire VACV antigens from infected cells, leading to CTL "crosspriming," which contributes to prolonged antigen availability (Heipertz et al., 2014). Crosspriming to VACV largely depends on DNGR-1 (CLEC9A) (Iborra et al., 2012), a C-type lectin receptor that favors DC cross-presentation of dead-cell-associated antigens (Sancho et al., 2009). DNGR-1 is highly expressed by mouse CD8α^+ DCs in lymphoid organs and CD103$^+$ DCs in non-lymphoid tissues, as well as their human equivalents (Huysamen et al., 2008; Poulin et al., 2010; Sancho et al., 2008). The development and function of CD8α^+ family DCs require the action of the transcription factor Batf3 (Hildner et al., 2008; Seillet et al., 2013). Here, we report that upon VACV skin infection, Batf3-dependent DCs, operationally acting through DNGR-1-mediated cross-presentation and specific signals including IL-12, IL-15, and costimulation through CD24, are required for optimal generation of skin Trm but not effector T cells or circulating memory T cells. Moreover, DNGR-1-mediated crosspriming also controls lung Trm cell generation following influenza A virus infection and supports effective mucosal vaccination. These data reveal priming requirements that selectively impact on the Trm cell compartment.

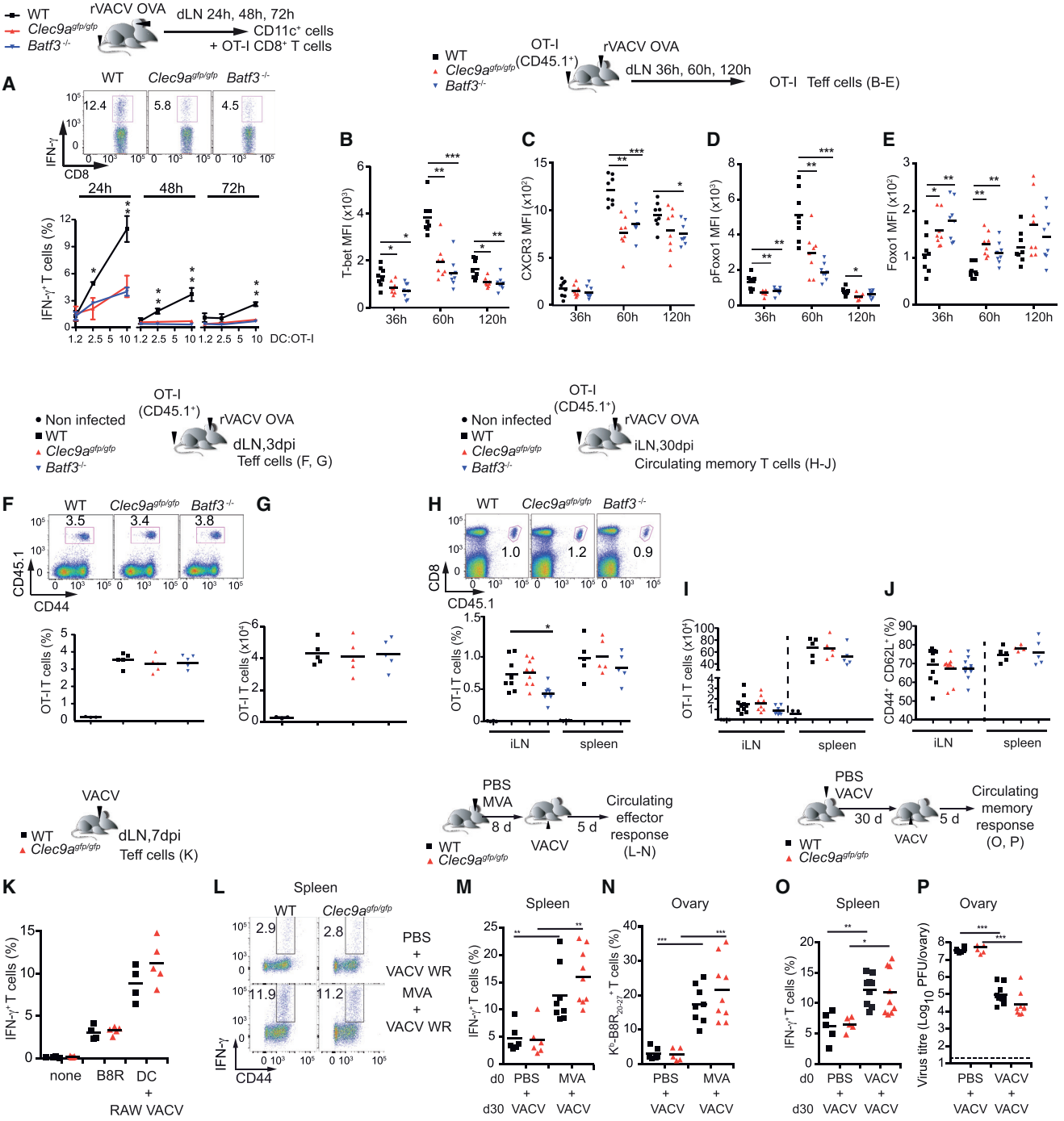

Figure 1. Crosspresentation Modulates CD8$^+$ T Cell-Priming without Affecting Effector and Circulating Memory Responses

(A) CD11c$^+$ DCs were purified from dLN at the indicated time points after skin infection with rVACV-OVA (1×10^6 pfu) in the indicated mice. DCs were co-cultured for 6 hr with in vitro expanded OT-I T cells and cells were stained for CD8 and intracellular IFN-γ. Upper panel shows representative plots at 24 hr of co-culture in the DC:OT-I 10:1 ratio. Lower panel shows frequencies of IFN-γ$^+$ OT-I T cells in the CD8$^+$ compartment found at the indicated ratios DC: OT-I co-culture and time points p.i. of extraction of CD11c$^+$ cells from dLN. Arithmetic mean ± SEM is shown, n = 3 pooled experiments.

(B–E) Mice of the genotype in the legend were infected with rVACV-OVA (5×10^4 pfu) and transferred with 10^5 CD45.1$^+$ OT-I T cells. At the indicated time points T-bet (B), CXCR3 (C), phosphorylated Foxo1 (D), and Foxo1 (E) MFI was measured in OT-I T cells from the dLN by flow cytometry.

(F–J) The indicated mice were infected with rVACV-OVA and transferred with OT-I T cells as in (B). Frequencies (F and H) and numbers (G and I) of CD45.1$^+$ OT-I T cells were determined 3 days p.i. in the dLN in the CD8$^+$ compartment (F and G) or in the spleen and inguinal LN (iLN) 30 days p.i. (H and I). Representative plots are shown in (F) and (H). (J) Frequencies of CD44$^+$ CD62L$^+$ in OTI cells in the iLN and spleen 30 days p.i.

(legend continued on next page)

RESULTS

Crosspresentation Modulates CD8$^+$ T Cell-Priming without Affecting Effector and Circulating Memory CD8$^+$ T Cell Response

To test whether crosspresentation can affect immunity to viruses whose antigens can be both directly presented and cross-presented, we analyzed CD8$^+$ T cell immunity to VACV intradermal (i.d.) infection comparing WT mice with two independent genetic mouse models with deficient crosspresentation of VACV antigens: DNGR-1-deficient mice (*Clec9a*$^{gfp/gfp}$) (Iborra et al., 2012) and *Batf3*$^{-/-}$ mice (Hildner et al., 2008; Seillet et al., 2013). Antigen presentation by CD11c$^+$ DCs purified from dLN of rVACV-OVA skin-infected mice at day 1, 2, and 3 post infection (p.i.) resulted in interferon-γ (IFN-γ) production by OVA-specific OT-I CD8$^+$ T cells (Figure 1A) or VACV-B8R-specific CTLs (Figure S1A). VACV antigen presentation was transient in WT mice (Norbury et al., 2002) and both the intensity and the persistence of antigen presentation were lower in the absence of DNGR-1 or Batf3 (Figures 1A and S1A). Next, we analyzed whether defective crosspriming affects the expression of transcription factors involved in memory or effector differentiation. We found impaired induction of T-bet and its target CXCR3 during priming of OT-I T cells adoptively transferred in Batf3- or DNGR-1-deficient mice infected in the skin with rVACV-OVA (Figures 1B and 1C and S1B). Upon T cell priming, forkhead box transcription factor Foxo1 is rapidly phosphorylated and degraded (Rao et al., 2012), and we found that crosspriming deficiency resulted in weaker phosphorylation and degradation of Foxo1 (Figures 1D and 1E and S1B). In contrast, the expression of the transcription factor Eomes (Figures S1B and S1C), which promotes central memory T cell generation, was not affected.

Despite impaired crosspriming, OT-I T cells transferred to mice infected in the skin with rVACV-OVA expanded normally (Figures 1F and 1G). Similarly, the frequency of endogenous circulating effector CD8$^+$ T cells against the immunodominant VACV epitope, tracked with H-2K^b-B8R tetramers 7 days p.i. with VACV WR i.d. was comparable (Figures S1D and S1E). Next, we explored whether impaired crosspriming affects memory CD8$^+$ T cell generation. Upon rVACV-OVA skin infection, frequency, and numbers of transferred OT-I T cells, including both central and effector memory phenotype, were similar in the absence of crosspresentation (Figures 1H–1J). Similarly, infection with VACV WR (i.d.) elicited comparable circulating B8R-specific CD8$^+$ T cell memory responses (Figures S1F–S1H).

To assess the function of circulating effector and memory CTLs, we focused on DNGR-1-deficient and WT mice, because Batf3-dependent DCs play a role in CTL recall responses (Alexandre et al., 2016). Draining LN effector T cells showed similar IFN-γ production upon restimulation with VACV antigens or B8R peptide in WT and DNGR-1-deficient mice primed i.d. with VACV WR at day 7 p.i. (Figure 1K). To test whether the equivalent effector response resulted in similar viral clearance, we primed WT and DNGR-1-deficient mice with non-replicative MVA (i.d.) and subsequently infected i.p. with VACV WR 5 days later. Effector responses at day 8 p.i. with VACV WR were equal in the spleen (Figures 1L and 1M) and the ovary (Figure 1N) of both mouse genotypes, which led to complete clearance of virus in the ovaries (data not shown). In addition, DNGR-1 deficiency did not affect secondary responses by circulating memory CD8$^+$ T cells analyzed in mice inoculated with VACV in the ear and i.p. challenged 30 days later with the same virus. The frequency of IFN-γ$^+$ B8R-specific CD8$^+$ T cells in the spleen of vaccinated DNGR-1 deficient mice 5 days after secondary infection (Figure 1O), as well as their viral load in the ovary (Figure 1P), was comparable to WT mice. We conclude that crosspriming increases T-bet during priming, but it is not essential for the generation of functional effector and circulating memory CD8$^+$ T cells.

Defective Crosspresentation Impairs Skin Trm Cell Responses to i.d. VACV Infection

Whereas crosspresentation is dispensable for the generation of a circulating memory CD8$^+$ T cell pool, the frequency of skin-resident (CD8$^+$CD69$^+$) Trm cells in the CD45$^+$ compartment was markedly reduced in the infection site or in a distant site in the absence of DNGR-1 or Batf3 upon skin infection with VACV WR (Figure 2A). A vast percentage of these skin CD8$^+$ Trm cells were specific for the virus and produced IFN-γ upon VACV-specific restimulation (Figure S2A). Consequently, numbers and frequencies of B8R-specific Trm cells were reduced in the skin CD45$^+$ compartment of mice with defective crosspresentation (Figures 2B and S2B). Similarly, crosspriming-deficient mice transferred with OT-I T cells showed impaired frequency (Figure 2C and S2C) and numbers (Figure S2D) of skin Trm cells, further confirmed by immunofluorescence of skin samples 30 days p.i. (Figure 2D). We analyzed the kinetics of Trm cell differentiation in the skin using CD103 as specific marker. The formation of CD103$^+$ OT-I T cells was slower between 7 and 14 days in the absence of crosspriming, suggesting a lower number of Trm cell precursors seeded in the skin (Figure 2E).

To ask whether the net reduction in Trm cell generation in *Clec9a*$^{gfp/gfp}$ or *Batf3*$^{-/-}$ mice relies on reduced priming, we mimicked it in WT mice by delaying the transfer of OT-I T cells following rVACV-OVA skin infection and infecting i.d. with

(K) Mice were infected i.d. in the ear with VACV WR and draining LN cells restimulated with VACV B8R peptide or with DCs pretreated with RAW 264.7 cells infected with VACV. Frequencies of IFN-γ producing cells in the CD8$^+$ compartment shown as individual data and arithmetic mean from a representative experiment of two performed.

(L–N) The indicated mice were inoculated with MVA or not (PBS) in both ears and i.p challenged with VACV WR 8 days later. Representative plots (L) and frequencies in the CD8$^+$ compartment (M) of IFN-γ production by spleen cells stimulated ex vivo with B8R VACV peptide 5 days after challenge infection. (N) Frequencies of K^b-B8R$_{20-27}$ VACV-specific T cells in the CD8$^+$ compartment in the ovary of infected mice.

(O and P) The indicated mice were infected with VACV WR or not (PBS) in both ears and challenged i.p. with VACV WR 30 days later. (O) Frequencies of IFN-γ production in the CD8$^+$ compartment of spleen cells stimulated ex vivo with B8R VACV peptide. (P) Viral load in the ovary of infected mice. (F–J, M–P). Average and individual data pooled from at least two representative independent experiments and arithmetic mean are shown. *$p < 0.05$; **$p < 0.01$; ***$p < 0.001$ (one-way ANOVA with Bonferroni post hoc test). See also Figure S1.

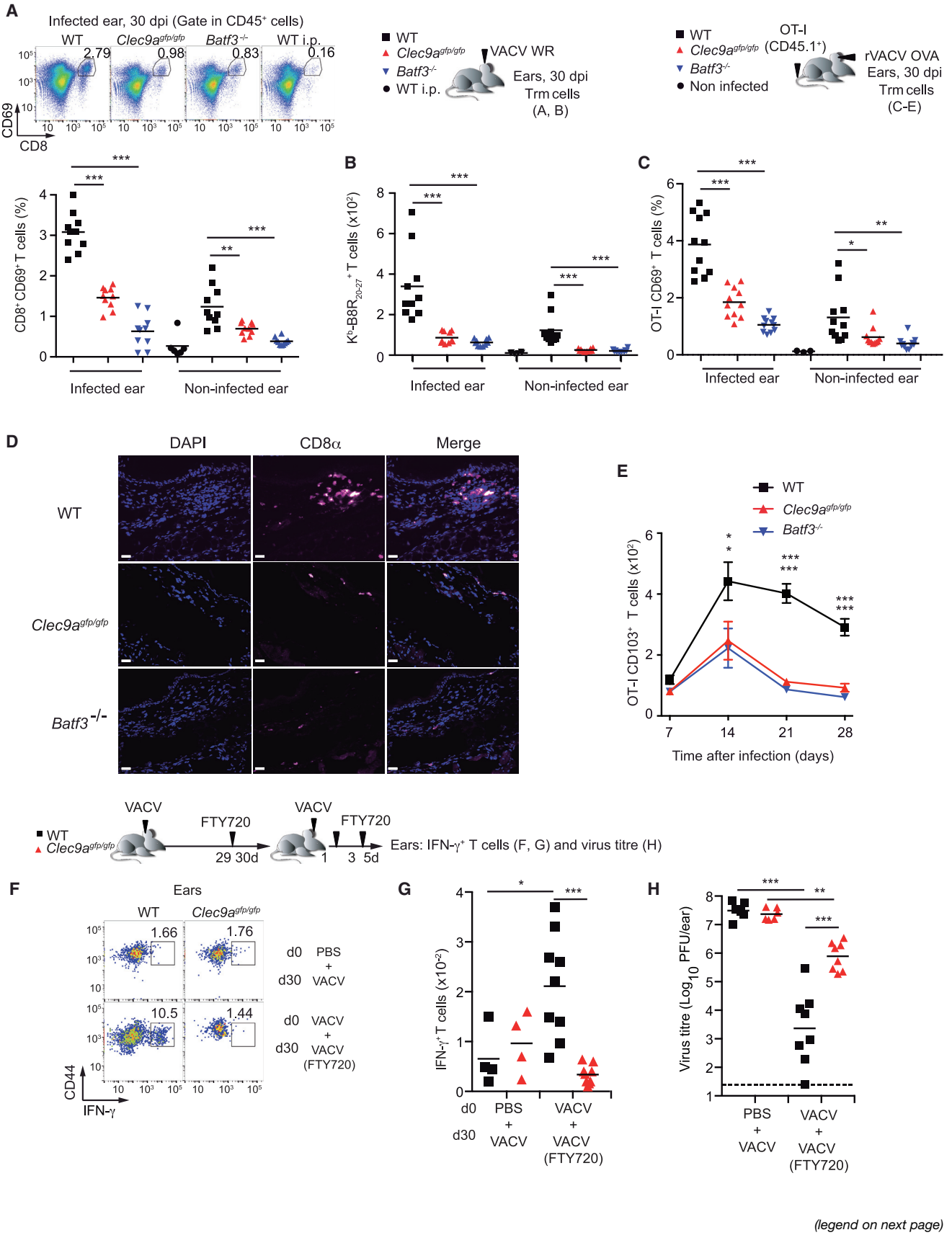

(legend on next page)

VACV-WR just before OT-I T cell transfer to equalize the inflammatory environment. Delayed transfer of OT-I T cells did not affect circulating memory T cell generation (Figures S2E and S2G), while deeply impaired Trm cell generation (Figures S2F and S2H). Thus, reducing priming signals preferentially impairs Trm over circulating memory T cell generation, supporting distinct priming thresholds for generation of both compartments.

To determine whether the reduced skin Trm cell numbers found in cross-priming-deficient mice impacts their resistance to skin reinfection, we challenged WT and DNGR-1-deficient mice previously infected in one ear with a second VACV skin infection in the opposite ear 30 days after the initial infection. FTY720, a S1P inhibitor that blocks egress of circulating memory T cells from lymph nodes into blood, was administered at days −1, 1, and 3 post challenge to limit the contribution of circulating memory cells to the recall response (Jiang et al., 2012). The number of skin $CD8^+$ T cells producing IFN-γ in response to VACV peptide (B8R-specific) was severely impaired in vaccinated DNGR-1-deficient mice compared with vaccinated WT mice, reducing Trm cell numbers to those found in non-immunized controls (Figures 2F and 2G). Impaired Trm cell generation in vaccinated DNGR-1-deficient mice resulted in defective viral clearance (Figure 2H).

DNGR-1-Mediated Crosspresentation Is Required for Optimal Trm Cell Priming but Direct Presentation Allows Further Differentiation in the Skin

We explored whether the contribution of DNGR-1 and Batf3-dependent DCs to Trm cell generation was restricted to the priming step in the dLN or they could also affect Trm cell differentiation in the skin. Transferred OT-I $CD8^+$ cells primed by skin rVACV-OVA infection in a donor mouse developed efficiently into both circulating memory $CD8^+$ T cells and skin Trm cells only when recipient mice were also dermally infected with rVACV-OVA (Figures S3A–S3C), consistent with a recent study (Khan et al., 2016). Next, we purified primed OT-I T cells from the dLN of WT, *Clec9a*$^{gfp/gfp}$, or *Batf3*$^{-/-}$ mice 3 days p.i. with rVACV-OVA i.d. and transferred them to WT, *Clec9a*$^{gfp/gfp}$, or *Batf3*$^{-/-}$ recipients previously infected i.d. (Figure 3A). Frequencies and numbers of circulating memory T cells generated 30 days post-transfer were comparable in all cases (Figures 3A and 3B and S3D). Notably, T cells primed in WT mice gave rise to similar frequencies and numbers of Trm cells regardless of the recipient genotype, whereas T cells primed in *Clec9a*$^{gfp/gfp}$ or *Batf3*$^{-/-}$ mice generated both lower frequencies and numbers of skin Trm cells in WT recipients (Figures 3A and 3C and S3E).

The data above suggested that crosspriming in the LN is required for the generation of committed Trm cell precursors, but not to their differentiation in the skin. To further confirm this, we used anti-DNGR-1 blocking antibodies that block cross-priming to dead-cell-associated antigen in vivo (Sancho et al., 2009). As VACV antigen presentation by $CD11c^+$ cells in the dLN takes place during the first 3 days p.i. (Figures 1A and S1A and Norbury et al., 2002), we tested the effects of DNGR-1 blockade during or after the priming in response to skin VACV-WR infection. Blockade of DNGR-1 at any stage did not affect circulating memory T cell generation (Figure 3D). Blockade of DNGR-1 during priming, but not at later stages, impaired generation of endogenous Trm cells (Figures 3E and S3F). These results further support the important contribution of DNGR-1 for priming of Trm cell precursors using a genetic-independent approach.

Defective Crosspriming Leads to Early T Cell Egress from LN

Reduced crosspriming did not influence the systemic $CD8^+$ T cell effector response but could potentially reduce skin-homing CTLs. However, the number of effector OT-I T cells in the skin early upon rVACV-OVA skin infection was increased in *Clec9a*$^{gfp/gfp}$ and *Batf3*$^{-/-}$ mice (Figures 4A and S4A). This early increase was accompanied by augmented expression of KLRG1 (Figures 4B and S4B), a marker of short-lived effector cells (Joshi et al., 2007) and increased T-bet expression in OT-I T cells in the skin of mice with defective crosspriming (Figures 4C and S4C), consistent with a negative role of high expression of T-bet during Trm cell differentiation (Laidlaw et al., 2014; Mackay et al., 2015). The predominance of short-lived effectors would explain their reduced ability to fully differentiate into $CD103^+$ Trm cells (Figure 2E).

Increased OT-I Teff cells in the skin might indicate premature egress from the LN of newly-primed effector CTL in the absence of signals from crosspriming DCs. Indeed, we found higher frequencies of primed proliferating OT-I T cells (Figures 4D and S4D) and B8R-specific endogenous $CD8^+$ T cells (Figure S4E) in the blood of VACV-infected *Clec9a*$^{gfp/gfp}$ and *Batf3*$^{-/-}$ mice. To investigate the cause of early egress, we measured *S1pr1*

Figure 2. Defective Crosspresentation Impairs Skin Trm Cell Responses to i.d. VACV Infection

(A) The indicated mice were infected with VACV WR (5×10^4 pfu, i.d.). Representative plots (upper panels) and individual data showing frequencies of Trm cells in the skin 30 days p.i. ($CD8^+$ $CD69^+$ in $CD45^+$ cells).

(B) Number of K^b-$B8R_{20-27}$ VACV-specific T cells in the ear 30 days p.i.

(C) Frequencies of OT-I Trm cells in the infected or non-infected ear 30 days following transfer of 10^5 OT-I T cells and i.d. infection with rVACV-OVA (OT-I $CD69^+$ in $CD45^+$ cells).

(D) Immunofluorescence staining of $CD8^+$ T cells 30 days p.i. in the infected skin of mice treated as in (C). One representative image of 10 independent images acquired in two independent experiments.

(E) Kinetics of $CD103^+$ Trm cell accumulation in the skin in the indicated mice after treatment as in (C). Graph shows arithmetic mean ± SEM of n = 10 pooled samples from two independent experiments.

(F–H) The indicated mice were infected with VACV (5×10^4 pfu, i.d.) or not (PBS) in the left ear, and challenged in the right ear with VACV 30 days later. Mice were treated with FTY720 at day −1, 1, and 3 after challenge infection. Representative plots (F) showing IFN-γ production by $CD8^+$ T cells from the right ear stimulated ex vivo with B8R VACV peptide 5 days after challenge.

(G) Numbers of IFN-γ^+ $CD8^+$ T cells in the ear upon restimulation with B8R peptide.

(H) Viral load in the infected ear. (A–C, G, H) Arithmetic mean and individual data pooled from at least two representative independent experiments are shown. *p < 0.05; **p < 0.01; ***p < 0.001 (one-way ANOVA with Bonferroni post hoc test). See also Figure S2.

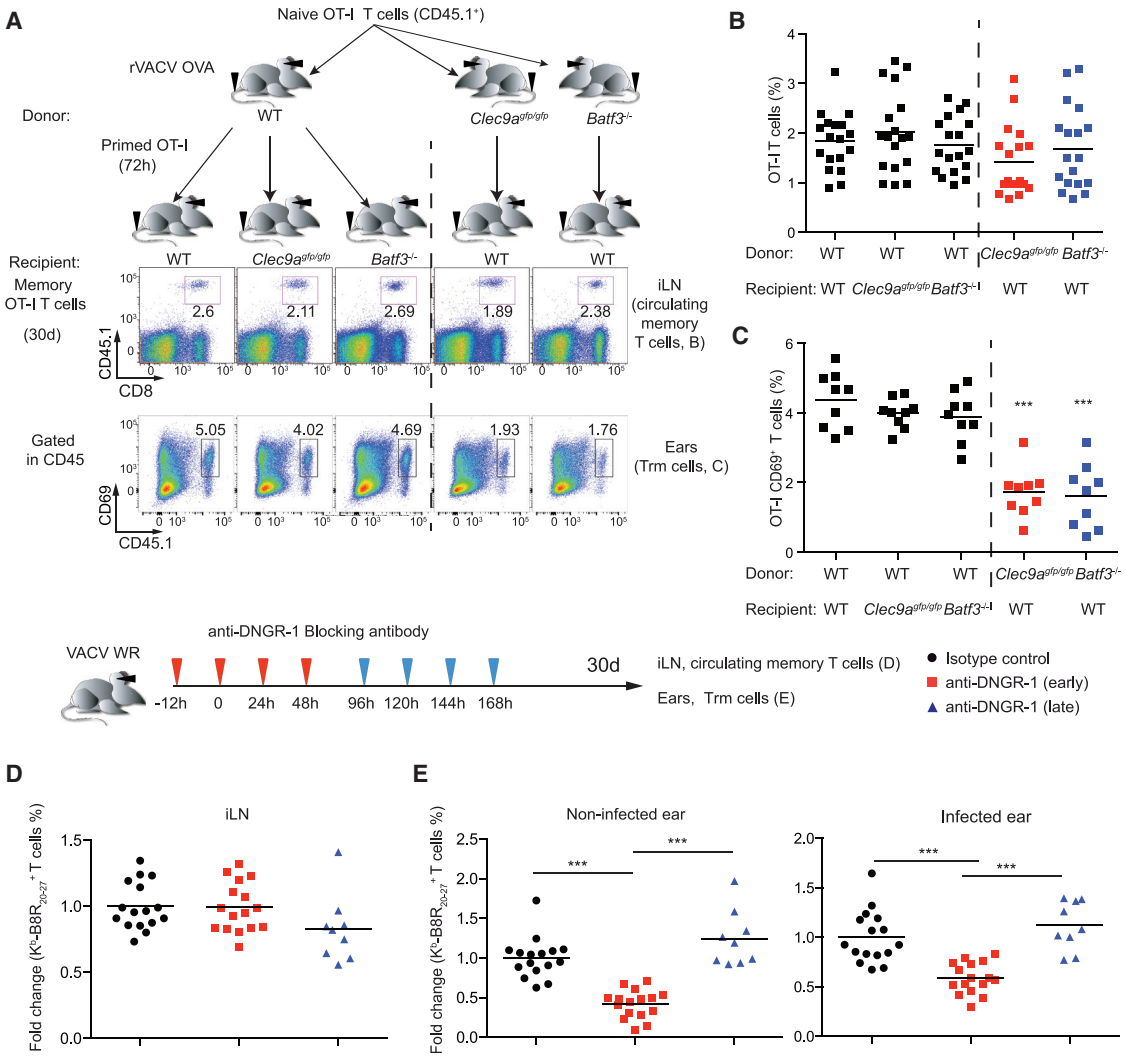

Figure 3. DNGR-1-Mediated Crosspresentation Is Required for Optimal Trm Cell Priming but Direct Presentation Allows Further Differentiation in the Skin

(A) Experimental setup. CD45.1$^+$ OT-I T cells were injected in WT, DNGR-1-deficient (*Clec9a*$^{gfp/gfp}$) and *Batf3*$^{-/-}$ and subsequently infected (i.d. 5 × 10^4 pfu and s.s. 1 × 10^6 pfu) with rVACV-OVA. After 72 hr, OT-I T cells from the dLN of WT donor mice were transferred to rVACV-OVA skin-infected WT, *Clec9a*$^{gfp/gfp}$ and *Batf3*$^{-/-}$ recipients, whereas OT-I T cells from the dLN of *Clec9a*$^{gfp/gfp}$ and *Batf3*$^{-/-}$ donor mice were transferred to WT mice. Representative plots showing CD45.1 and CD8 staining of inguinal LN (iLN, upper panels) and CD45.1 and CD69 in the ears (lower panels) in the recipient mice 30 days after the transfer. Frequencies of (B) circulating OT-I T cells in iLN or (C) OT-I Trm cells in the CD45$^+$ compartment in the ear.

(D and E) WT mice were treated with a blocking antibody against DNGR-1 during priming (red arrows) or after priming (blue arrows). A third group of mice received a control antibody. Frequencies of K^b-8R$_{20\text{-}27}$ VACV-specific T cells in the CD8$^+$ compartment in the inguinal LN (iLN) and Trm cells in the non-infected or infected ear were assessed 30 days p.i. with VACV-WR (5 × 10^4 pfu, i.d.). Graphs depict fold change of the frequencies of (D) VACV-specific circulating memory CD8$^+$ T cells or (E) Trm cells with respect to the mean in WT mice treated with isotype control. (B–E) Arithmetic mean and individual data pooled from at least two representative independent experiments are shown. *p < 0.05; **p < 0.01; ***p < 0.001 (one way ANOVA with Bonferroni post hoc test). See also Figure S3.

mRNA expression in OT-I T cells present in the dLN at different times after rVACV-OVA i.d. infection. As expected, *S1pr1* expression was downregulated between 36–60 hr p.i. in WT mice (Figure 4E), facilitating retention of newly-primed OT-I T cells in the LN. However, *S1pr1* downregulation was less persistent in the absence of crosspresentation (Figure 4E). *S1pr1* expression and T cell trafficking is positively regulated by KLF2 (Skon et al., 2013). Consistent with the findings on *S1pr1*, the downregulation of *Klf2* mRNA in OT-I T cells was more transient in crosspriming-deficient mice (Figure 4F). These data suggest that absence of crosspriming leads to early egress of CD8$^+$ T cells.

To determine whether early egress contributes to defective Trm cell generation, we infected OT-I-transferred mice with rVACV-OVA i.d. and provided a single treatment with FTY720 36 hr later, thus inhibiting T cell egress to the blood (Figure S4F). The acute FTY720 treatment early p.i. increased generation of both circulating memory and Trm cells in WT mice (Figures 4G–4I and S4G–S4H). Notably, FTY720 treatment could partially rescue the defect in Trm cell generation in DNGR-1 and Batf3-deficient

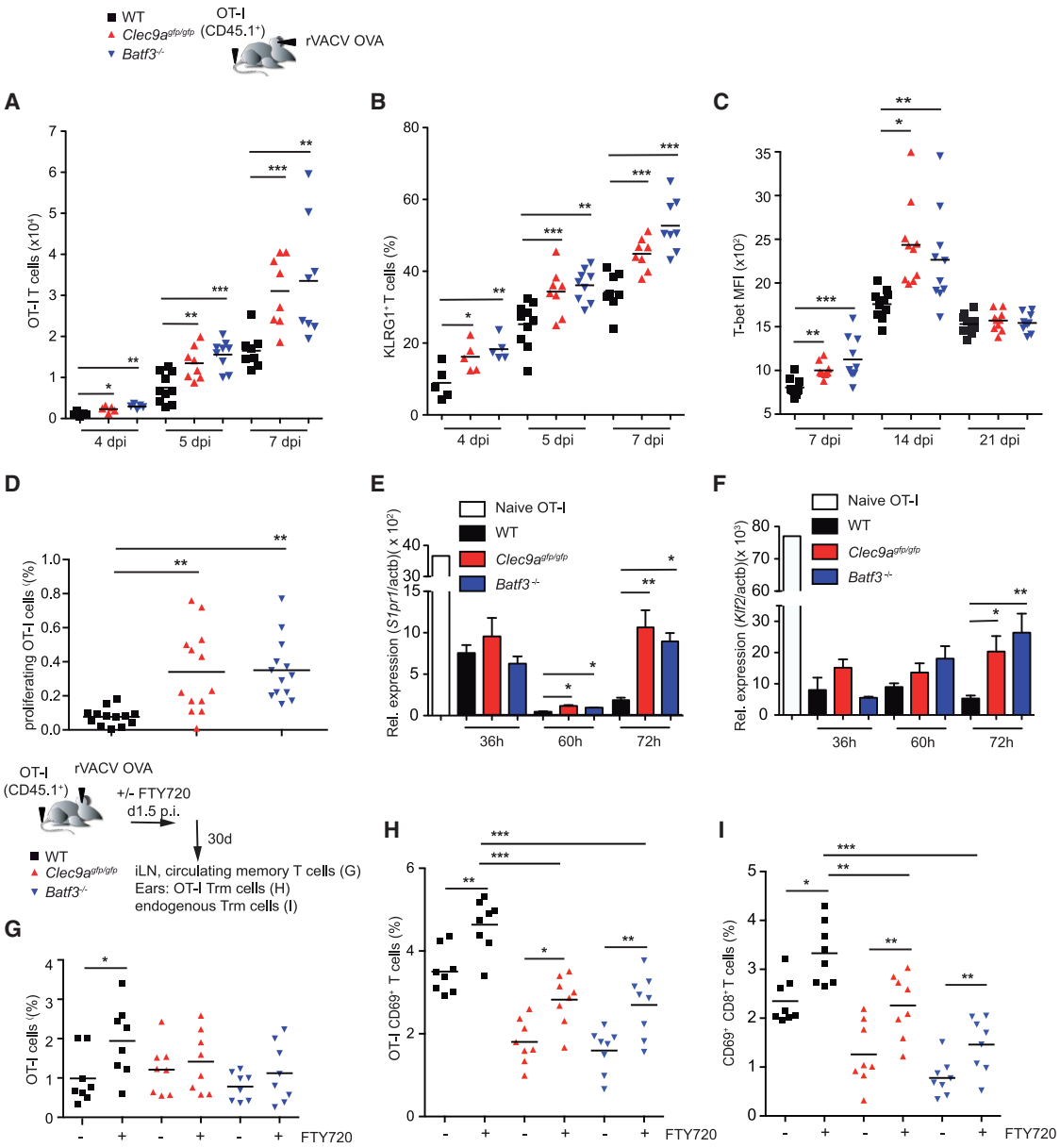

Figure 4. Defective Crosspriming Leads to Early T Cell Egress from the LN

(A) Number of OT-I T cells in the ears of the indicated mice 4, 5, and 7 days following i.d. infection with rVACV-OVA (5×10^4 pfu) in the ear and i.v. transfer of OT-I T cells.

(B) Frequency of KLRG1$^+$ in OT-I T cells in the ear of mice treated as in (A).

(C) T-bet expression (MFI) in OT-I T cells in the ear of mice treated as in (A).

(D) Frequency of proliferating OT-I in CD8$^+$ T cells from peripheral blood was determined 3 days p.i. in mice infected as in (A) and transferred with CellTrace-Violet-labeled OT-I T cells.

(E and F) OT-I T cells were purified from dLN at the marked time points following i.d. infection with rVACV-OVA in the indicated mice and (E) relative expression of *S1pr1* mRNA or (F) *Klf2* mRNA is shown.

(G and H) Mice were infected with rVACV-OVA, transferred with OT-I T cells and treated (or not) with FTY720 at day 1.5 p.i.

(G) Frequencies of circulating memory OT-I T cells in the iLN 30 days after i.d. infection.

(H) Frequencies of OT-I CD69$^+$ cells or (I) endogenous CD8$^+$ CD69$^+$ T cells in the CD45$^+$ compartment in the ear of mice 30 days after i.d. infection. Statistics is shown only for the effect of FTY720 treatment in each group. (A–D, G–I) Arithmetic mean and individual data pooled from at least two representative experiments are shown. (E and F) Graph shows arithmetic mean + SEM, n = 4 pooled samples of dLN OT-I T cells from four mice each obtained in three independent experiments. (A–H) *$p < 0.05$; **$p < 0.01$; ***$p < 0.001$ (one-way ANOVA with Bonferroni post hoc test). See also Figure S4.

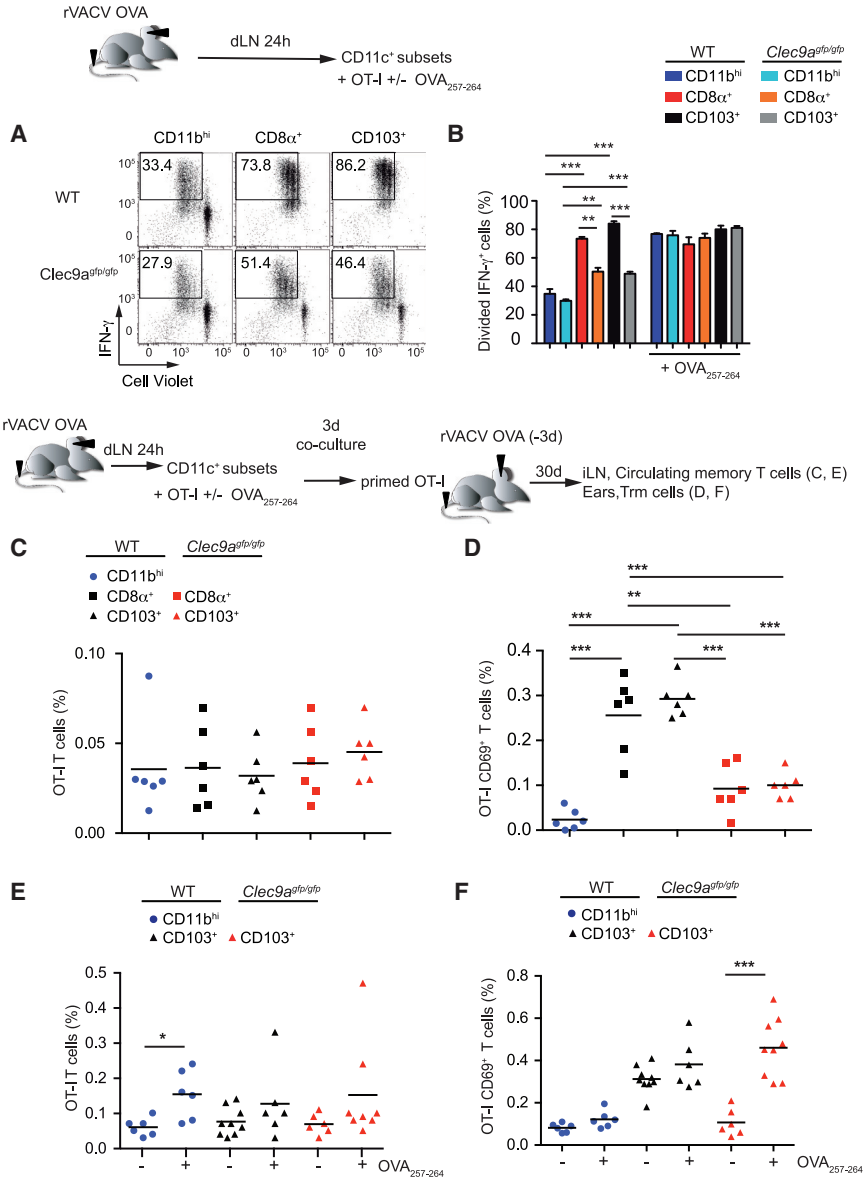

Figure 5. CD8α⁺ and CD103⁺ DCs Provide Unique Priming Signals for Trm Generation

(A) Representative plots showing IFN-γ staining and CellTrace-Violet dilution of naive OT-I T cells co-cultured at a ratio 10:1 DC: naive OT-I T cells for 3 days with the indicated DC subsets sorted from dLN of WT mice 24 hr following i.d. and s.s infection with rVACV-OVA, and re-stimulated with RMA cells loaded with 1 μM $OVA_{257-264}$ peptide for IFN-γ production.

(B) Frequencies of divided IFN-γ⁺ OT-I T cells in the experimental setting explained in (B) in which the co-culture with DCs was performed in the presence or absence of $OVA_{257-264}$ peptide (5 nM) (Graph shows arithmetic mean + SEM, n = 3 pooled independent experiments).

(C and D) Naive purified OT-I T cells were co-cultured with the indicated DC subsets from WT and DNGR-1-deficient (*Clec9a*$^{gfp/gfp}$) mice as in (A). After 3 days co-culture, 10^4 OT-I T cells were transferred to WT mice infected i.d. in the ear with rVACV-OVA 3 days before. Frequencies of OT-I T cells in iLN (C) or OT-I CD69⁺ cells in the CD45⁺ compartment in the ear (D) 30 days after OT-I T cell transfer are shown.

(E and F) Frequencies of OT-I T cells in iLN (E) or OT-I CD69⁺ cells in the CD45⁺ compartment in the ear (F) of mice treated as in (D), in which OT-I:DC subset co-cultures were performed in the presence or absence of $OVA_{257-264}$ (5 nM). (C–F) Arithmetic mean and individual data pooled from at least two representative independent experiments are shown. (B–F) *$p < 0.05$; **$p < 0.01$; ***$p < 0.001$ (B–D) one-way ANOVA with Bonferroni post hoc test (E and F) Student t test comparing $OVA_{257-264}$ peptide presence or absence for each group. See also Figure S5.

mice, but not to the FTY720-treated WT control (Figures 4H and 4I and S4H). These data indicate that retention of CD8⁺ T cells in the LN favors Trm cell generation but it is not sufficient to compensate for specific signals provided by Batf3-dependent DNGR1⁺ DCs.

CD8α⁺ and CD103⁺ DCs Provide Unique Priming Signals for Trm Cell Generation

To determine which DC subsets prime Trm cell precursors, we skin infected WT mice with rVACV-OVA and 24 hr later CD11c⁺ cells from dLN were sorted into the CD11b^{hi} CD8α⁻ and CD11b^{lo} CD8α⁺ conventional DCs (cDCs) and CD103⁺ migratory DCs (mDCs) subsets. CD103⁺ mDCs and CD8α⁺ cDCs induced increased proliferation and IFN-γ production by naive OTI cells compared to CD11b^{hi} cDCs (Figures 5A and 5B). This advantage was lost in the absence of DNGR-1, while adding exogenous pre-processed OVA peptide compensated any deficiency (Figures 5A and 5B).

To test whether in vitro priming by DNGR-1⁺ DC subsets was superior at generation of Trm cell precursors we transferred OT-I T cells co-cultured with DC subsets purified from rVACV-OVA infected mice as above to WT mice infected 3d before with i.d. rVACV-OVA. After 30 days, transferred OT-I T cells generated comparable frequencies and numbers of circulating memory T cells regardless of the DC subset used for in vitro priming or the presence or absence of DNGR-1 (Figures 5C, S5A and S5B). Notably, CD103⁺ and CD8α⁺ DCs were superior at generating Trm cells, and this occurred in a DNGR-1-dependent fashion (Figures 5D, S5C, and S5D). The deficiency in the generation of Trm cell precursors by *Clec9a*$^{gfp/gfp}$ CD103⁺ DCs was compensated by excess OVA peptide at the in vitro co-culture stage, showing that DNGR-1-mediated crosspresentation is a key step and specifically pinpointing signal 1 provision by this DC subset as a pivotal determinant in Trm cell priming (Figures 5E and 5F and S5E). In contrast, the inability of the CD11b^{hi} cDC subset to generate Trm cell precursors could not be rescued by excess OVA peptide (Figures 5F and S5E), supporting that DNGR-1⁺ DCs provide specific signals that directly prime naive CD8⁺ T cells to become Trm cell precursors.

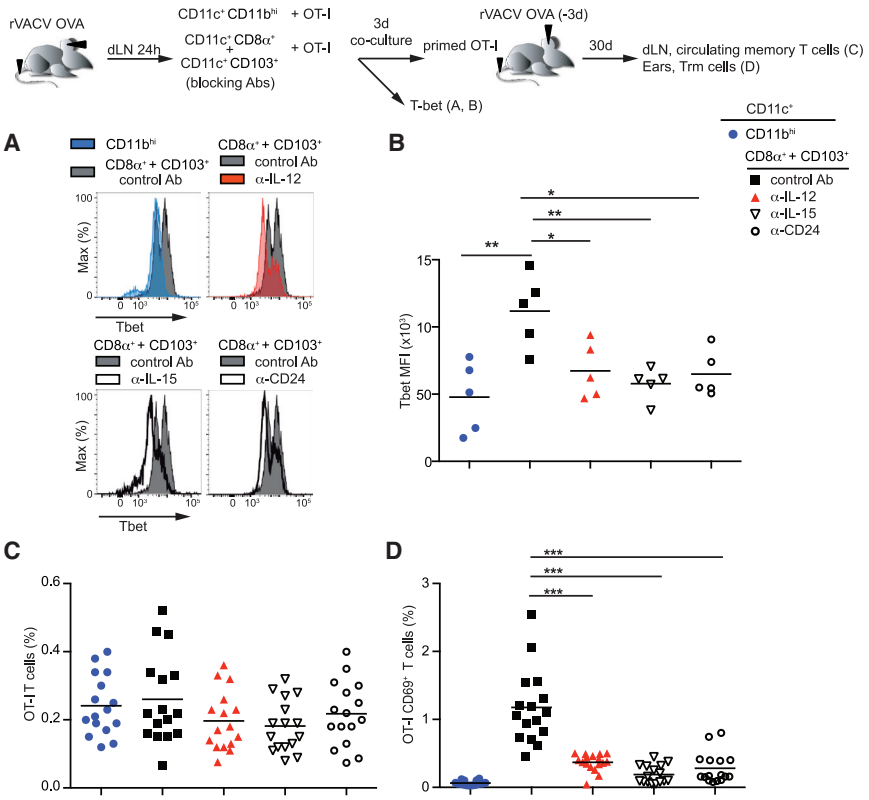

Figure 6. IL-12, IL-15, and CD24 from DNGR-1$^+$ DCs Are Required for Optimal Trm but Not Circulating Memory Cell Generation

(A) Representative plots showing T-bet expression of OT-I T cells co-cultured at a ratio 10:1 DC: naive OT-I T cells for 3 days with the indicated DC subsets from WT mice obtained as in Figure 5A and in the presence of control antibody or blocking antibodies against IL-12, IL-15, or CD24.

(B) MFI measured by flow cytometry are shown. Each dot represents one independent experiment.

(C and D) Naive purified OT-I T cells were co-cultured with the indicated DC subsets, and treated with blocking antibodies as in A. After 3 days co-culture, 10^4 OT-I T cells were transferred to WT mice infected i.d. in the ear with rVACV-OVA 3 days before. Frequencies of OT-I T cells in iLN (C) or or OT-I CD69$^+$ cells in the CD45$^+$ compartment in the ear (D) 30 days after OT-I transfer are shown.

(C and D) Arithmetic mean and individual data pooled from four independent experiments are shown. *$p < 0.05$; **$p < 0.01$; ***$p < 0.001$ (one-way ANOVA with Bonferroni post hoc test).

IL-12, IL-15, and CD24 from DNGR-1$^+$ DCs Are Required for Optimal Trm but Not Circulating Memory T Cell Generation

CD103$^+$ DC and CD8α^+ DCs are superior at supplying some type 2 and 3 signals that increase T-bet expression, including CD24, IL-12, and IL-15 (Kim et al., 2014; Martínez-López et al., 2015; Mashayekhi et al., 2011; Muzaki et al., 2016; Sosinowski et al., 2013). In order to test their effect on Trm cell priming, we purified CD11b^{hi} DCs and CD103$^+$ and CD8α^+ DCs from dLN of skin-infected rVACV-OVA and co-cultured them with naive OT-I T cells as above and blocking antibodies as indicated. T-bet induction in OT-I T cells was higher after co-culture with CD103$^+$ and CD8α^+ DCs compared with CD11b^{hi} DCs, and was reduced by the blockade of IL-12, IL-15, or CD24 during the co-culture (Figures 6A and 6B).

The blockade of IL-12, IL-15, or CD24 did not affect the generation of circulating memory T cells 30 days after the transfer of OT-I T cells primed in the co-culture with DCs (Figure 6C). In contrast, IL-12, IL-15, or CD24 blockade impaired the priming of Trm cell precursors by DNGR-1$^+$ DCs (Figure 6D). These results support that, together with increased and prolonged signal 1 via DNGR-1, additional signals from CD103$^+$ and CD8α^+ DCs that promote T-bet expression during priming (including CD24, IL-12, or IL-15) selectively favor Trm over circulating memory T cell generation.

Deficient Crosspriming Selectively Impairs Lung Trm Cell Generation and Vaccination

To extend our results, we tested generation of circulating memory T cells and lung Trm cells following intranasal (i.n.) infection with influenza A virus. We tracked lung CD8$^+$ Trm cells 40 days after influenza PR8 virus infection (Laidlaw et al., 2014) (Figure S6A). DNGR-1 deficiency resulted in impaired endogenous generation of Trm cells specific for two influenza epitopes analyzed (NP and PA) (Figure 7A and S6B–S6D). In the case of NP, CD103$^+$ and CD103$^-$ Trm cells were generated, whereas for PA, most Trm cells generated were CD103$^+$. In contrast, DNGR-1 deficiency did not affect generation of NP-specific circulating memory T cells in the inguinal LN, while PA-specific circulating memory T cells were even increased (Figure 7B and S6E–S6G). These results further support the notion that priming of Trm cells and circulating memory T cells is differentially regulated by DNGR1$^+$ DCs in several viral infection models.

Next, we investigated whether a recombinant VACV expressing the influenza nucleoprotein (rVACV-NP) could generate NP-specific Trm cells in a DNGR-1 and Batf3-dependent fashion. Following rVACV-NP intranasal (i.n.) administration, crosspresentation deficiency did not affect the early CD8$^+$ T cell effector responses (Figure S6H) or circulating memory CD8$^+$ T cell compartment in the LN (Figure 7C). In contrast, the lung-resident CD8$^+$ T cell memory compartment was severely depleted in the absence of DNGR-1 or Batf3 (Figure 7D and S6I).

To test the effect of deficient Trm cell generation on vaccination, we used rVACV-NP administered i.n. as a vaccine vector against influenza A virus. In this model, protection from influenza virus infection is dependent on memory CD8$^+$ T cells specific for NP (Slütter et al., 2013). We found that, in contrast to WT mice, *Clec9a*$^{gfp/gfp}$ and *Batf3*$^{-/-}$ mice were not protected against pulmonary influenza virus challenge 60d after i.n. infection with rVACV-NP (Figures 7E and 7F). In conclusion, protective mucosal immunity depends on optimal Trm cell induction by DNGR-1$^+$ DCs.

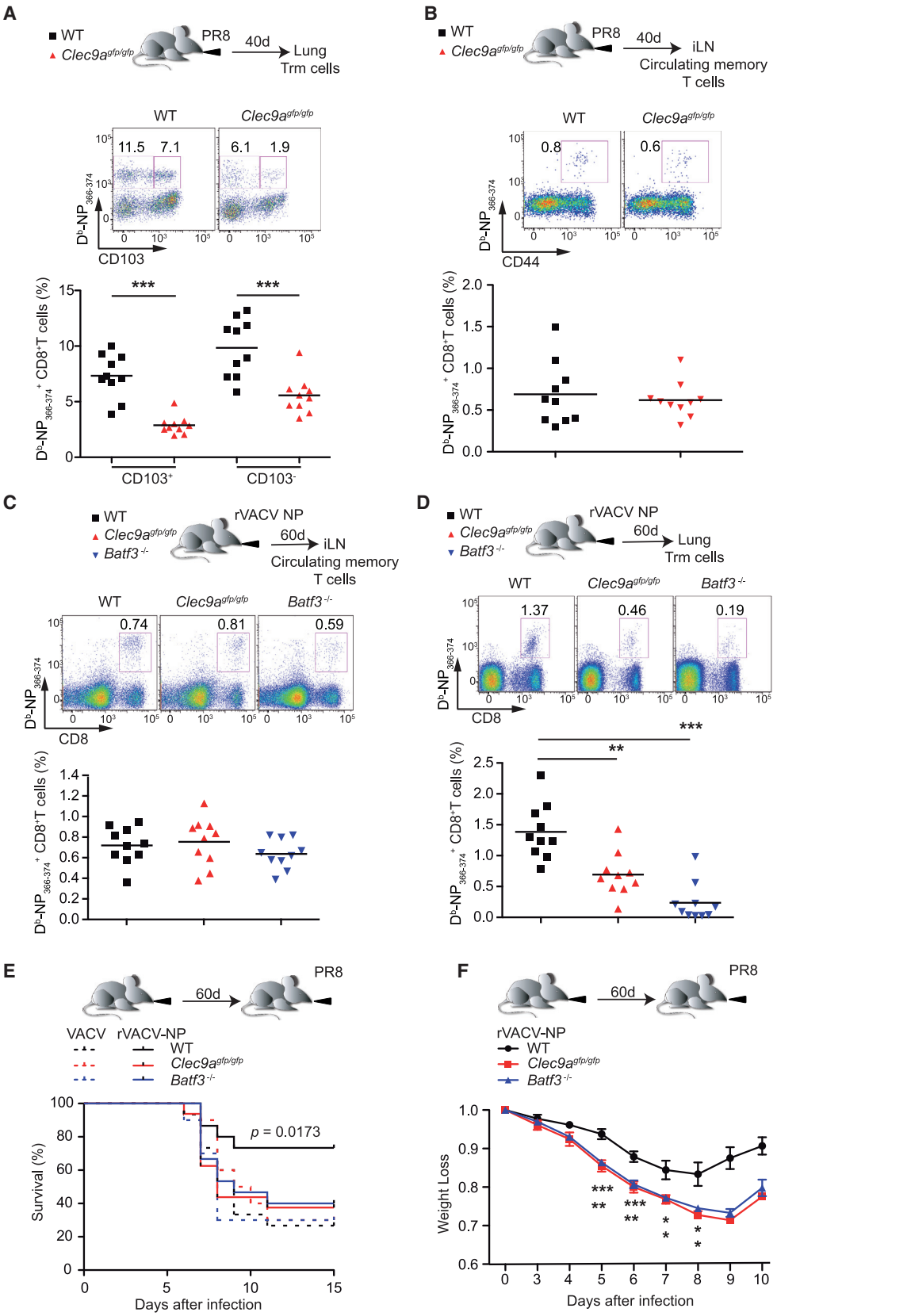

(legend on next page)

DISCUSSION

The induction of long-lived cell-mediated immunity in non-lymphoid tissues is a major challenge for rational vaccine design. Recent contributions focus on how Trm cells are differentiated in non-lymphoid tissues (Bergsbaken and Bevan, 2015; Mackay et al., 2013; Mackay et al., 2015; Skon et al., 2013; Wakim et al., 2010; Wakim et al., 2012), but specific priming requirements for Trm cell generation are unknown. Fate decision between effector and memory $CD8^+$ T cell differentiation occurs early upon T cell priming (Iborra et al., 2013; Kim et al., 2014; Rao et al., 2010). The reconstitution of mature Trm cells upon adoptive transfer with a $KLRG1^{lo}$ subset from day 7 spleen supports the existence of an imprinted Trm precursor generated in secondary lymphoid organs (Mackay et al., 2013). Our data support that Trm and circulating memory cell precursors are generated together in the LN, consistent with a common naive T cell precursor for both subsets (Gaide et al., 2015). Our results indicate that strength and duration of specific priming signals from DCs differentially affect these TCR-identical cells to generate circulating versus tissue-resident memory $CD8^+$ T cells.

Crosspriming results in transient inactivation of Foxo1 in CD8 T cells favoring their retention in the LN. Foxo1 inactivation depends on the kinase mTORC1 (Rao et al., 2012), and rapamycin, a well-known mTORC1 kinase inhibitor, enhances circulating memory T cell precursor differentiation in vivo when administered at low doses (Araki et al., 2009; Pearce et al., 2009) but selectively impairs Trm cell generation (Sowell et al., 2014). Crosspriming also transiently induced T-bet correlating with generation of Trm cell precursors in the LN. While low-affinity T cells, which exhibit low expression of T-bet during priming, preferentially differentiate into central memory cell precursors (Knudson et al., 2013), Trm cells are enriched in high-affinity TCRs compared with their circulating counterparts (Frost et al., 2015). T-bet induction at priming might also favor longer retention in the LN (Mackay et al., 2015) of T cells that finally egress with lower T-bet and KLRG1 expression. Indeed, we found higher expression of T-bet and KLRG1 in skin T cells of crosspriming-deficient mice, consistent with a negative role of high expression of T-bet during Trm cell differentiation in the skin (Laidlaw et al., 2014; Mackay et al., 2015). Notably, impaired crosspriming does not impact Eomes expression, which would explain the lack of an effect on circulating memory T cell generation (Iborra et al., 2013; Joshi et al., 2007; Rao et al., 2010).

Consistent with previous reports (Xu et al., 2010), our current data support that direct presentation is sufficient for generation of a fully functional circulating effector and memory response against most VACV-derived peptides. DNGR-1-mediated crosspriming is required for optimal generation of effector CTLs against peptides that are highly or strictly dependent on cross-presentation, as we previously described (Iborra et al., 2012), and to induce Trm cell precursors that generate functional Trm cells that promote resistance upon reinfection in barrier tissues. Crosspresentation might prolong antigen availability for $CD8^+$ T cells (Heipertz et al., 2014), which has been shown to determine fate decisions during priming (Henrickson et al., 2013). Our data show that the strength and persistence of antigen presentation was impaired in the absence of DNGR-1 crosspriming, preferentially decreasing the generation of Trm over circulating memory T cells. These results suggest that the priming threshold for the generation of Trm cell precursors differs from that for circulating memory T cell precursors. Reduced availability of antigen and/or activating signals over time has been linked to memory differentiation, whereas increased stimulation over time promotes effector and/or effector-memory differentiation (Badovinac et al., 2007; D'Souza and Hedrick, 2006). Our results suggest that Trm cell precursors are more related to an effector differentiation pathway as they require strong priming by Batf3-dependent DCs.

The KLF2-dependent receptor S1P is downregulated after T cell activation, leading to retention in the dLN during priming (Carlson et al., 2006). When priming signals are decreased, KLF2 and S1P are upregulated, allowing primed T cells to egress from the LN and access the skin, where inflammatory signals again result in KLF2 and S1P downregulation (Skon et al., 2013). We found that downregulation of KLF2 and S1P during priming in the LN was more transient in the absence of crosspresentation. As a probable consequence, T cells exit to the blood in greater numbers and are recruited to the skin earlier, but because they are $KLRG1^+$ they might not generate Trm cells in the skin (Mackay et al., 2013), but rather behave as terminal effectors (Joshi et al., 2007; Sarkar et al., 2008). Supporting this, we found increased skin effector T cell contraction rate and reduced rate of generation of Trm in crosspriming-deficient mice. Inhibition of S1P-mediated egress with FTY720 resulted in significantly more Trm cells in WT mice. However, inhibition of egress was not sufficient to fully rescue the impaired Trm cell generation in the absence of crosspresentation.

Our data show that priming of naive $CD8^+$ T cells to induce Trm cell precursors was mediated by Batf3-dependent DCs in the LN and required DNGR-1. However, Batf3 and DNGR-1 were not required for local differentiation of Trm cell precursors in the skin, which also required antigen presentation. It is conceivable that different DC subsets work cooperatively to promote priming in the LN and differentiation in the skin, as human lung tissue-resident $CD1c^+$ DCs, but not Batf3-dependent $CD141^+$ DCs,

Figure 7. Deficient Crosspriming Selectively Impairs Lung Trm Cell Generation and Vaccination

(A and B) Memory $CD8^+$ T cells were assessed 40 days after i.n. challenge with influenza A virus PR8 (0.2 × LD50) in WT and DNGR-1-deficient (*Clec9a*$^{gfp/gfp}$) mice. (A) Representative plots and frequencies in the $CD8^+$ compartment of $CD103^+$ and $CD103^-$ D^b-$NP_{366-374}$ tetramer positive in lung-localized (unlabelled CD8β cells) $CD45^+CD8^+$ T cells (see Figure S6A). (B) Frequencies of D^b-$NP_{366-374}$ tetramer-positive in the circulating memory $CD8^+$ T cells in iLN.

(C and D) Mice were infected i.n. with rVACV-NP and analyzed 60 days p.i. (C) Representative plots and frequencies of D^b-$NP_{366-374}$ tetramer-positive circulating memory $CD8^+$ T cells in the inguinal LN (iLN). (D) Representative plots and frequencies of D^b-$NP_{366-374}$ tetramer positive $CD8^+$ T cells in lung-localized $CD45^+$cells.

(E and F) Mice were immunized with 5×10^3 pfu of rVACV-NP or VACV-WR and 60 days later challenged with influenza A virus PR8 (2 × LD50). (E) Survival curves (p = log rank test) (F) weight loss, mean ± SEM. (A–D) Arithmetic mean and individual data pooled from at least two representative independent experiments are shown. (E and F) n = 10, one experiment representative of two performed. (A–D, F). *$p < 0.05$; **$p < 0.01$; ***$p < 0.001$ (A, B, F) Student's t test; (C and D) one-way ANOVA with Bonferroni post hoc test). See also Figure S6.

drive differentiation of CD8$^+$ T cells with a Trm cell phenotype (Yu et al., 2013). This need of antigen for Trm cell lodgment and differentiation in tissues has been described (Wakim et al., 2010), but is not found in other systems (Casey et al., 2012; Mackay et al., 2013; Mackay et al., 2012), suggesting that priming or differentiation requirements depend on the pathogen or inflammatory insult (Gaide et al., 2015). In fact, a remaining Trm cell fraction in our system can be still generated in the absence of crosspriming. Notably, supplementation with pre-processed antigen in vitro did not rescue the inability of CD11b^{hi} DCs to generate cell Trm precursors, indicating that only CD103$^+$ or CD8α^+ crosspresenting DCs can provide the appropriate signals for priming Trm cells during VACV infection. There are specific signals that qualitatively distinguish priming via Batf3-dependent DCs versus CD11b^{hi} DCs, including CD24, IL-12, and IL-15 (Kim et al., 2014; Martínez-López et al., 2015; Mashayekhi et al., 2011; Muzaki et al., 2016; Sosinowski et al., 2013). We found that blockade on the priming capacity of DNGR-1$^+$ DCs mediated by any of these signals impaired T-bet expression during priming and Trm but not circulating memory T cell generation. Our data indicate that priming *in cis* by DNGR-1$^+$ DCs is needed for Trm cell generation, which occurs operationally via DNGR-1-mediated crosspriming and might depend on the nature of the infection (Desch et al., 2014).

Our results contribute to open research avenues investigating the differential factors needed for improving priming of Trm cell responses and thus more effective skin or mucosal CD8$^+$ T cell vaccination. Optimal immunization would require adequate access of antigen and adjuvants to promote priming via Batf3-dependent DCs, conditions that enhance Trm cell generation without negatively affecting circulating memory T cell generation.

EXPERIMENTAL PROCEDURES

Mice

Mouse colonies were bred at the CNIC in specific pathogen-free conditions. *Clec9a$^{gfp/gfp}$* mice (DNGR-1-deficient, B6(Cg)-Clec9atm1.1Crs/J) (Sancho et al., 2009) and *Batf3$^{-/-}$* mice (B6.129S(C)-Batf3tm1Kmm/J, kindly provided by Dr. K. M. Murphy, Washington University, St. Louis, MO) (Hildner et al., 2008) were backcrossed to the C57BL/6 background. OT-I transgenic mice (*C57BL/6-Tg(TcraTcrb)1100Mjb/J*) were mated with B6-SJL (*Ptprc^a Pepc^b/BoyJ*) expressing CD45.1 allele, both from The Jackson Laboratory. Animal studies were approved by the local ethics committee. All animal procedures conformed to EU Directive 2010/63EU and Recommendation 2007/526/EC regarding the protection of animals used for experimental and other scientific purposes, enforced in Spanish law under Real Decreto 1201/2005.

Viral Infections, Adoptive Transfer, and FTY720 Treatment

VACV WR strain, rVACV expressing full-length OVA and the rVACV containing the *influenza* A/*Puerto Rico*/8/34 virus *nucleoprotein* were a gift from J. W. Yewdell and J. R. Bennink (NIH, Bethesda, MD) and were kindly provided by M. del Val (CBMSO, Madrid). Stocks were grown and virus titration was performed as described (Iborra et al., 2012). Mice were infected i.n. (5×10^3 pfu), or i.d. into the ear pinnae (5×10^4 or 1×10^6 pfu) or by skin scarification (s.s.) in the base of tail (1×10^6 pfu) or i.p. (1×10^6 pfu) with the stated VACV strain or i.d. (1×10^5) with MVA (B. Moss, NIH, Bethesda, MD), where indicated. Influenza A/Puerto Rico/8/34 PR8 virus was kindly provided by E. Nistal-Villán (University CEU San Pablo, Madrid). Naive OT-I T cells (10^5), in vivo primed OT-I T cells (10^5), in vitro activated OT-I T cells (10^4) purified by negative selection or B8R-specific CD8 T cells (5×10^3) sorted by flow cytometry were adoptively transferred to mice where indicated. FTY720 (Cayman Chemical) was inoculated i.p. (7 mg/kg) in aqueous solution.

Processing of Ears, Lungs, and dLN

Ears, lungs, or LNs were harvested from naive mice or mice infected at the indicated times and single-cell suspensions were prepared by liberase/DNase digestion. DCs from LN were enriched using anti-CD11c-microbeads (Miltenyi Biotec). CD8$^+$ T cells were enriched by negative selection using a cocktail of biotin-conjugated antibodies (anti-CD11c, CD11b, B220, MHC-II, CD4, NK1.1) followed by separation with Streptavidin-microbeads (Miltenyi Biotec). T cells were restimulated to induce cytokine production by co-culture with DCs for 6 hr, and brefeldin A (Sigma, 5 μg/ml) added for the last 4 hr of culture. When needed, enriched CD11c$^+$ cells were further sorted into CD11b^{lo}CD8α^+CD103$^-$, migratory CD11b^{lo}CD8α^- CD103$^+$and CD11b^{hi} CD8α^- CD103$^-$ DCs in a BD FACSAria Sorter or a Sony Synergy 4L Cell Sorter. Where indicated, DC subsets were co-cultured with naive OT-I T cells in the presence or not of blocking antibodies to IL-12 (C17.8; In Vivo Ready Tonbo Biosciences), IL-15 (AIO.3, eBioscience), CD24 (clone M1/69, gifted by C. Ardavín), or control antibody (rat IgG).

Peptides, Tetramers, Antibodies, and Flow Cytometry

The ^{20}TSYKFESV^{27} (B8R) peptide was a kind gift from Hisse M. Van Santen (CBMSO, Madrid). The peptide ^{257}SIINFEKL^{264} from ovalbumin was purchased from GenScript. APC-labeled tetramers specific for VACV, H-2K^b (^{20}TSYKFESV^{27}, *B8R*), and for Influenza A virus, H2-D^b (^{366}ASNENMETM^{374}, NP) and H2-D^b (^{224}SSLENFRAYV^{233}, PA) were provided by the NIH Tetramer Facility at Emory University. APC-labeled dextramers specific for OVA H-2K^b (^{257}SIINFEKL^{264}) were purchased from Immudex.

Samples for flow cytometry were stained in ice-cold PBS supplemented with 2mM EDTA, 1% FCS, and 0.2% sodium azide, with the appropriate antibody cocktails. Anti-mouse CD45, CD4, CD8α, CD8β, CD11b, CD11c, CD103, CD62L, CD44, CXCR3, KLRG1, Eomes, T-bet, IFN-γ, and I-A^b (MHC-II) antibodies conjugated to biotin, FITC, PE, PerCP-Cy5.5, V450, or APC were obtained from eBioscience, BD PharMingen, and BioLegend. APC-Cy7 CD8 was from Tonbo Biosciences. For proliferation assays, OT-I T cells were fluorescently labeled (5 μM, CellTraceTM Violet). Antibodies to Foxo1 phosphorylated at Ser256 and total Foxo1 antibody (L27) were from Cell Signaling. Intracellular staining of transcription factors was performed using the Foxp3-fixation-permeabilization buffer from eBioscience. Events were acquired using a FACSCanto flow cytometer or FACSDiva (Becton Dickinson) and data were analyzed using FlowJo software (Tree Star). Intravascular staining was performed as described (Laidlaw et al., 2014). Briefly, a total of 3 μg anti–CD8β was injected i.v. At 3 min after injection, the animals were sacrificed, bled, and perfused with 10 ml cold PBS. The LNs and lung were harvested and lymphocytes were isolated as described.

Statistical Analysis

The statistical analysis was performed using Prism software (GraphPad Software). Variance equality among groups was determined using F-test. Statistical significance for comparison between two groups of samples coming from a normal distribution (Shapiro-Wilk test for normality) was determined using the unpaired two-tailed Student's t test. For comparison of more than two groups, one-way ANOVA and Bonferroni post hoc test was used. A p value < 0.05 was considered significant. Mice were used randomly in the different experimental procedures.

SUPPLEMENTAL INFORMATION

Supplemental Information includes six figures and Supplemental Experimental Procedures and can be found with this article online at http://dx.doi.org/10.1016/j.immuni.2016.08.019.

AUTHOR CONTRIBUTIONS

S.I., M. M.-L., S.C.K, M.E., F.J.C., R.C.-G. and C.d.F. did the experiments. S.I. and D.S. conceived and designed experiments, analyzed data, and wrote the manuscript. All the authors discussed the results and the manuscript.

ACKNOWLEDGMENTS

We are grateful to C. Reis e Sousa, E. Fernández-Malavé, M. del Val, J. Boettcher, M. Robinson, and members of the D.S. laboratory for discussions

and critical reading of the manuscript. We thank the CNIC facilities, personnel, and S. Bartlett for editorial assistance. We acknowledge the NIH Tetramer Core Facility (contract HHSN272201300006C) for MHC-I tetramers. S.I. is funded by grant SAF2015-74561-JIN. Work in the D.S. laboratory is funded by the CNIC and grants from the Spanish Ministry of Economy and Competitiveness (MINECO, SAF-2013-42920R), the European Commission (635122-PROCROP H2020), and the European Research Council (ERC-2010-StG 260414). The CNIC is supported by the MINECO and the Pro-CNIC Foundation and is a Severo Ochoa Center of Excellence (MINECO award SEV-2015-0505).

Received: October 29, 2015
Revised: February 15, 2016
Accepted: August 10, 2016
Published: September 27, 2016

REFERENCES

Alexandre, Y.O., Ghilas, S., Sanchez, C., Le Bon, A., Crozat, K., and Dalod, M. (2016). XCR1+ dendritic cells promote memory CD8+ T cell recall upon secondary infections with Listeria monocytogenes or certain viruses. J. Exp. Med. *213*, 75–92.

Araki, K., Turner, A.P., Shaffer, V.O., Gangappa, S., Keller, S.A., Bachmann, M.F., Larsen, C.P., and Ahmed, R. (2009). mTOR regulates memory CD8 T-cell differentiation. Nature *460*, 108–112.

Ariotti, S., Hogenbirk, M.A., Dijkgraaf, F.E., Visser, L.L., Hoekstra, M.E., Song, J.Y., Jacobs, H., Haanen, J.B., and Schumacher, T.N. (2014). T cell memory. Skin-resident memory $CD8^+$ T cells trigger a state of tissue-wide pathogen alert. Science *346*, 101–105.

Badovinac, V.P., Haring, J.S., and Harty, J.T. (2007). Initial T cell receptor transgenic cell precursor frequency dictates critical aspects of the CD8(+) T cell response to infection. Immunity *26*, 827–841.

Bergsbaken, T., and Bevan, M.J. (2015). Proinflammatory microenvironments within the intestine regulate the differentiation of tissue-resident $CD8^+$ T cells responding to infection. Nat. Immunol. *16*, 406–414.

Carlson, C.M., Endrizzi, B.T., Wu, J., Ding, X., Weinreich, M.A., Walsh, E.R., Wani, M.A., Lingrel, J.B., Hogquist, K.A., and Jameson, S.C. (2006). Kruppel-like factor 2 regulates thymocyte and T-cell migration. Nature *442*, 299–302.

Casey, K.A., Fraser, K.A., Schenkel, J.M., Moran, A., Abt, M.C., Beura, L.K., Lucas, P.J., Artis, D., Wherry, E.J., Hogquist, K., et al. (2012). Antigen-independent differentiation and maintenance of effector-like resident memory T cells in tissues. J. Immunol. *188*, 4866–4875.

D'Souza, W.N., and Hedrick, S.M. (2006). Cutting edge: latecomer CD8 T cells are imprinted with a unique differentiation program. J. Immunol. *177*, 777–781.

Desch, A.N., Gibbings, S.L., Clambey, E.T., Janssen, W.J., Slansky, J.E., Kedl, R.M., Henson, P.M., and Jakubzick, C. (2014). Dendritic cell subsets require cis-activation for cytotoxic CD8 T-cell induction. Nat. Commun. *5*, 4674.

Frost, E.L., Kersh, A.E., Evavold, B.D., and Lukacher, A.E. (2015). Cutting Edge: Resident Memory CD8 T Cells Express High-Affinity TCRs. J. Immunol. *195*, 3520–3524.

Gaide, O., Emerson, R.O., Jiang, X., Gulati, N., Nizza, S., Desmarais, C., Robins, H., Krueger, J.G., Clark, R.A., and Kupper, T.S. (2015). Common clonal origin of central and resident memory T cells following skin immunization. Nat. Med. *21*, 647–653.

Gebhardt, T., Wakim, L.M., Eidsmo, L., Reading, P.C., Heath, W.R., and Carbone, F.R. (2009). Memory T cells in nonlymphoid tissue that provide enhanced local immunity during infection with herpes simplex virus. Nat. Immunol. *10*, 524–530.

Heipertz, E.L., Davies, M.L., Lin, E., and Norbury, C.C. (2014). Prolonged antigen presentation following an acute virus infection requires direct and then cross-presentation. J. Immunol. *193*, 4169–4177.

Henrickson, S.E., Perro, M., Loughhead, S.M., Senman, B., Stutte, S., Quigley, M., Alexe, G., Iannacone, M., Flynn, M.P., Omid, S., et al. (2013). Antigen availability determines $CD8^+$ T cell-dendritic cell interaction kinetics and memory fate decisions. Immunity *39*, 496–507.

Hildner, K., Edelson, B.T., Purtha, W.E., Diamond, M., Matsushita, H., Kohyama, M., Calderon, B., Schraml, B.U., Unanue, E.R., Diamond, M.S., et al. (2008). Batf3 deficiency reveals a critical role for CD8alpha+ dendritic cells in cytotoxic T cell immunity. Science *322*, 1097–1100.

Huysamen, C., Willment, J.A., Dennehy, K.M., and Brown, G.D. (2008). CLEC9A is a novel activation C-type lectin-like receptor expressed on BDCA3+ dendritic cells and a subset of monocytes. J. Biol. Chem. *283*, 16693–16701.

Iborra, S., Izquierdo, H.M., Martínez-López, M., Blanco-Menéndez, N., Reis e Sousa, C., and Sancho, D. (2012). The DC receptor DNGR-1 mediates cross-priming of CTLs during vaccinia virus infection in mice. J. Clin. Invest. *122*, 1628–1643.

Iborra, S., Ramos, M., Arana, D.M., Lázaro, S., Aguilar, F., Santos, E., López, D., Fernández-Malavé, E., and Del Val, M. (2013). N-ras couples antigen receptor signaling to Eomesodermin and to functional CD8+ T cell memory but not to effector differentiation. J. Exp. Med. *210*, 1463–1479.

Jiang, X., Clark, R.A., Liu, L., Wagers, A.J., Fuhlbrigge, R.C., and Kupper, T.S. (2012). Skin infection generates non-migratory memory CD8+ T(RM) cells providing global skin immunity. Nature *483*, 227–231.

Joshi, N.S., Cui, W., Chandele, A., Lee, H.K., Urso, D.R., Hagman, J., Gapin, L., and Kaech, S.M. (2007). Inflammation directs memory precursor and short-lived effector CD8(+) T cell fates via the graded expression of T-bet transcription factor. Immunity *27*, 281–295.

Khan, T.N., Mooster, J.L., Kilgore, A.M., Osborn, J.F., and Nolz, J.C. (2016). Local antigen in nonlymphoid tissue promotes resident memory CD8+ T cell formation during viral infection. J. Exp. Med. *213*, 951–966.

Kim, T.S., Gorski, S.A., Hahn, S., Murphy, K.M., and Braciale, T.J. (2014). Distinct dendritic cell subsets dictate the fate decision between effector and memory CD8(+) T cell differentiation by a CD24-dependent mechanism. Immunity *40*, 400–413.

Knudson, K.M., Goplen, N.P., Cunningham, C.A., Daniels, M.A., and Teixeiro, E. (2013). Low-affinity T cells are programmed to maintain normal primary responses but are impaired in their recall to low-affinity ligands. Cell Rep. *4*, 554–565.

Laidlaw, B.J., Zhang, N., Marshall, H.D., Staron, M.M., Guan, T., Hu, Y., Cauley, L.S., Craft, J., and Kaech, S.M. (2014). CD4+ T cell help guides formation of CD103+ lung-resident memory CD8+ T cells during influenza viral infection. Immunity *41*, 633–645.

Mackay, L.K., Stock, A.T., Ma, J.Z., Jones, C.M., Kent, S.J., Mueller, S.N., Heath, W.R., Carbone, F.R., and Gebhardt, T. (2012). Long-lived epithelial immunity by tissue-resident memory T (T_{RM}) cells in the absence of persisting local antigen presentation. Proc. Natl. Acad. Sci. USA *109*, 7037–7042.

Mackay, L.K., Rahimpour, A., Ma, J.Z., Collins, N., Stock, A.T., Hafon, M.L., Vega-Ramos, J., Lauzurica, P., Mueller, S.N., Stefanovic, T., et al. (2013). The developmental pathway for CD103(+)CD8+ tissue-resident memory T cells of skin. Nat. Immunol. *14*, 1294–1301.

Mackay, L.K., Wynne-Jones, E., Freestone, D., Pellicci, D.G., Mielke, L.A., Newman, D.M., Braun, A., Masson, F., Kallies, A., Belz, G.T., and Carbone, F.R. (2015). T-box Transcription Factors Combine with the Cytokines TGF-β and IL-15 to Control Tissue-Resident Memory T Cell Fate. Immunity *43*, 1101–1111.

Martínez-López, M., Iborra, S., Conde-Garrosa, R., and Sancho, D. (2015). Batf3-dependent CD103+ dendritic cells are major producers of IL-12 that drive local Th1 immunity against Leishmania major infection in mice. Eur. J. Immunol. *45*, 119–129.

Mashayekhi, M., Sandau, M.M., Dunay, I.R., Frickel, E.M., Khan, A., Goldszmid, R.S., Sher, A., Ploegh, H.L., Murphy, T.L., Sibley, L.D., and Murphy, K.M. (2011). CD8α(+) dendritic cells are the critical source of interleukin-12 that controls acute infection by Toxoplasma gondii tachyzoites. Immunity *35*, 249–259.

Masopust, D., Vezys, V., Wherry, E.J., Barber, D.L., and Ahmed, R. (2006). Cutting edge: gut microenvironment promotes differentiation of a unique memory CD8 T cell population. J. Immunol. *176*, 2079–2083.

Masopust, D., Choo, D., Vezys, V., Wherry, E.J., Duraiswamy, J., Akondy, R., Wang, J., Casey, K.A., Barber, D.L., Kawamura, K.S., et al. (2010). Dynamic T cell migration program provides resident memory within intestinal epithelium. J. Exp. Med. *207*, 553–564.

Mueller, S.N., and Mackay, L.K. (2016). Tissue-resident memory T cells: local specialists in immune defence. Nat. Rev. Immunol. *16*, 79–89.

Muzaki, A.R., Tetlak, P., Sheng, J., Loh, S.C., Setiagani, Y.A., Poidinger, M., Zolezzi, F., Karjalainen, K., and Ruedl, C. (2016). Intestinal CD103(+)CD11b(-) dendritic cells restrain colitis via IFN-γ-induced anti-inflammatory response in epithelial cells. Mucosal Immunol. *9*, 336–351.

Norbury, C.C., Malide, D., Gibbs, J.S., Bennink, J.R., and Yewdell, J.W. (2002). Visualizing priming of virus-specific CD8+ T cells by infected dendritic cells in vivo. Nat. Immunol. *3*, 265–271.

Pearce, E.L., Walsh, M.C., Cejas, P.J., Harms, G.M., Shen, H., Wang, L.S., Jones, R.G., and Choi, Y. (2009). Enhancing CD8 T-cell memory by modulating fatty acid metabolism. Nature *460*, 103–107.

Poulin, L.F., Salio, M., Griessinger, E., Anjos-Afonso, F., Craciun, L., Chen, J.-L., Keller, A.M., Joffre, O., Zelenay, S., Nye, E., et al. (2010). Characterization of human DNGR-1+ BDCA3+ leukocytes as putative equivalents of mouse CD8alpha+ dendritic cells. J. Exp. Med. *207*, 1261–1271.

Rao, R.R., Li, Q., Odunsi, K., and Shrikant, P.A. (2010). The mTOR kinase determines effector versus memory CD8+ T cell fate by regulating the expression of transcription factors T-bet and Eomesodermin. Immunity *32*, 67–78.

Rao, R.R., Li, Q., Gubbels Bupp, M.R., and Shrikant, P.A. (2012). Transcription factor Foxo1 represses T-bet-mediated effector functions and promotes memory CD8(+) T cell differentiation. Immunity *36*, 374–387.

Sancho, D., Mourão-Sá, D., Joffre, O.P., Schulz, O., Rogers, N.C., Pennington, D.J., Carlyle, J.R., and Reis e Sousa, C. (2008). Tumor therapy in mice via antigen targeting to a novel, DC-restricted C-type lectin. J. Clin. Invest. *118*, 2098–2110.

Sancho, D., Joffre, O.P., Keller, A.M., Rogers, N.C., Martínez, D., Hernanz-Falcón, P., Rosewell, I., and Reis e Sousa, C. (2009). Identification of a dendritic cell receptor that couples sensing of necrosis to immunity. Nature *458*, 899–903.

Sarkar, S., Kalia, V., Haining, W.N., Konieczny, B.T., Subramaniam, S., and Ahmed, R. (2008). Functional and genomic profiling of effector CD8 T cell subsets with distinct memory fates. J. Exp. Med. *205*, 625–640.

Schenkel, J.M., Fraser, K.A., Vezys, V., and Masopust, D. (2013). Sensing and alarm function of resident memory CD8$^+$ T cells. Nat. Immunol. *14*, 509–513.

Schenkel, J.M., Fraser, K.A., Beura, L.K., Pauken, K.E., Vezys, V., and Masopust, D. (2014). T cell memory. Resident memory CD8 T cells trigger protective innate and adaptive immune responses. Science *346*, 98–101.

Seillet, C., Jackson, J.T., Markey, K.A., Brady, H.J.M., Hill, G.R., Macdonald, K.P.A., Nutt, S.L., and Belz, G.T. (2013). CD8α+ DCs can be induced in the absence of transcription factors Id2, Nfil3, and Batf3. Blood *121*, 1574–1583.

Skon, C.N., Lee, J.Y., Anderson, K.G., Masopust, D., Hogquist, K.A., and Jameson, S.C. (2013). Transcriptional downregulation of S1pr1 is required for the establishment of resident memory CD8+ T cells. Nat. Immunol. *14*, 1285–1293.

Slütter, B., Pewe, L.L., Kaech, S.M., and Harty, J.T. (2013). Lung airway-surveilling CXCR3(hi) memory CD8(+) T cells are critical for protection against influenza A virus. Immunity *39*, 939–948.

Sosinowski, T., White, J.T., Cross, E.W., Haluszczak, C., Marrack, P., Gapin, L., and Kedl, R.M. (2013). CD8α+ dendritic cell trans presentation of IL-15 to naive CD8+ T cells produces antigen-inexperienced T cells in the periphery with memory phenotype and function. J. Immunol. *190*, 1936–1947.

Sowell, R.T., Rogozinska, M., Nelson, C.E., Vezys, V., and Marzo, A.L. (2014). Cutting edge: generation of effector cells that localize to mucosal tissues and form resident memory CD8 T cells is controlled by mTOR. J. Immunol. *193*, 2067–2071.

Steinert, E.M., Schenkel, J.M., Fraser, K.A., Beura, L.K., Manlove, L.S., Igyártó, B.Z., Southern, P.J., and Masopust, D. (2015). Quantifying Memory CD8 T Cells Reveals Regionalization of Immunosurveillance. Cell *161*, 737–749.

Wakim, L.M., Woodward-Davis, A., and Bevan, M.J. (2010). Memory T cells persisting within the brain after local infection show functional adaptations to their tissue of residence. Proc. Natl. Acad. Sci. USA *107*, 17872–17879.

Wakim, L.M., Woodward-Davis, A., Liu, R., Hu, Y., Villadangos, J., Smyth, G., and Bevan, M.J. (2012). The molecular signature of tissue resident memory CD8 T cells isolated from the brain. J. Immunol. *189*, 3462–3471.

Xu, R.-H., Remakus, S., Ma, X., Roscoe, F., and Sigal, L.J. (2010). Direct presentation is sufficient for an efficient anti-viral CD8+ T cell response. PLoS Pathog. *6*, e1000768.

Yu, C.I., Becker, C., Wang, Y., Marches, F., Helft, J., Leboeuf, M., Anguiano, E., Pourpe, S., Goller, K., Pascual, V., et al. (2013). Human CD1c+ dendritic cells drive the differentiation of CD103+ CD8+ mucosal effector T cells via the cytokine TGF-β. Immunity *38*, 818–830.

nature immunology

Mitochondrial respiratory-chain adaptations in macrophages contribute to antibacterial host defense

Johan Garaude[1,2,9,10], Rebeca Acín-Pérez[1,9], Sarai Martínez-Cano[1], Michel Enamorado[1], Matteo Ugolini[3], Estanislao Nistal-Villán[4,8], Sandra Hervás-Stubbs[4,5], Pablo Pelegrín[6], Leif E Sander[3], José A Enríquez[1,7,10] & David Sancho[1,10]

Macrophages tightly scale their core metabolism after being activated, but the precise regulation of the mitochondrial electron-transport chain (ETC) and its functional implications are currently unknown. Here we found that recognition of live bacteria by macrophages transiently decreased assembly of the ETC complex I (CI) and CI-containing super-complexes and switched the relative contributions of CI and CII to mitochondrial respiration. This was mediated by phagosomal NADPH oxidase and the reactive oxygen species (ROS)-dependent tyrosine kinase Fgr. It required Toll-like receptor signaling and the NLRP3 inflammasome, which were both connected to bacterial viability–specific immune responses. Inhibition of CII during infection with *Escherichia coli* normalized serum concentrations of interleukin 1β (IL-1β) and IL-10 to those in mice treated with dead bacteria and impaired control of bacteria. We have thus identified ETC adaptations as an early immunological-metabolic checkpoint that adjusts innate immune responses to bacterial infection.

Macrophages are phagocytic immune cells that reside in most tissues and thus constitute the first line of host defense against invading microorganisms[1]. They express a wide variety of innate immunological receptors, which allows them to precisely determine microbial features such as pathogenicity, invasiveness or viability to 'fine tune' their differentiation program[2,3]. To meet their immunological functions, macrophages metabolize a variety of carbon substrates, including glucose, fatty acids, ketone bodies and amino acids. Adaptations of cellular metabolism thus seem to be critically associated with macrophage activation[4–7] and might contribute to macrophage functional requirements[8–10]. The activation of macrophages by the Gram-negative bacterial cell-wall component lipopolysaccharide (LPS) via Toll-like receptor 4 (TLR4) induces profound metabolic reprogramming that culminates in enhanced glycolysis, while glutamine replenishes the tricarboxylic acid (TCA) cycle through glutaminolysis[5,7]. In turn, both accumulation of the TCA intermediate succinate and induction of the glycolytic enzyme hexokinase-1 contribute to production of the pro-inflammatory cytokine interleukin 1β (IL-1β) by regulating transcription of the gene encoding pro-IL-1β[7] and activating the NLRP3 inflammasome[11], respectively. Accumulation of TCA-cycle intermediates might also directly contribute to macrophage antimicrobial functions. For example, LPS-activated macrophages accumulate citrate[5] that can be metabolized to itaconic acid, which exerts direct antibacterial effects on various pathogens, including *Salmonella enterica* Typhimurium, *Mycobacterium tuberculosis* or *Legionella pneumophila*[12,13].

At the core of the metabolic pathways is the mitochondrion, a bioenergetic organelle that not only contributes to energy supply, biosynthesis or cellular redox maintenance but also serves as a signaling platform for various innate immunological signaling pathways[9,10,14]. Mitochondria balance their contribution to anabolism and catabolism in response to the availability of fuel and oxygen, as well as in response to extracellular signals, including danger signals and cytokines[8,9]. All catabolic processes converge on the mitochondrial electron-transport chain (ETC) by supplying electrons in the form of the reductive equivalents NADH and $FADH_2$. The ETC comprises two electron carriers (coenzyme Q and cytochrome *c*) and four respiratory complexes (CI–CIV); these complexes, except for CII, can dynamically assemble as larger molecular super-complexes (SCs) in the mitochondrial inner membrane[15,16]. The dynamic assembly of respiratory complexes into SCs has been proposed to confer functional advantages to the cells by potentiating electron flux within the ETC, preventing the generation of ROS by sequestering reactive intermediates or stabilizing individual respiratory complexes[15]. Whether super-assembly

[1]Centro Nacional de Investigaciones Cardiovasculares Carlos III (CNIC), Madrid, Spain. [2]Institute for Regenerative Medicine and Biotherapies, Institut National pour la Santé et la Recherche Médicale, U1183, Montpellier, France. [3]Department of Infectious Diseases and Pulmonary Medicine, Charité Hospital Berlin, Berlin, Germany. [4]Centro de Investigación Médica Aplicada, Universidad de Navarra, Pamplona, Spain. [5]Instituto de Investigación Sanitaria de Navarra (IDISNA), Recinto de Complejo Hospitalario de Navarra, Pamplona, Spain. [6]Unidad de Inflamación y Cirugía Experimental, Centro de Investigación Biomédica en Red en el Área Temática de Enfermedades Hepáticas y Digestivas, Hospital Clínico Universitario Virgen de la Arrixaca, Instituto Murciano de Investigación Biosanitaria-Arrixaca (IMIB-Arrixaca), Murcia, Spain. [7]Departamento de Bioquímica y Biología Molecular y Celular, Universidad de Zaragoza, Zaragoza, Spain. [8]Present address: Microbiology Section, Department of Pharmaceutical and Health Science, Faculty of Pharmacy, University CEU San Pablo, Madrid, Spain. [9]These authors contributed equally to this work. [10]These authors jointly supervised this work. Correspondence should be addressed to J.G. (johan.garaude@inserm.fr), J.A.E. (jaenriquez@cnic.es) or D.S. (dsancho@cnic.es).

Received 27 April; accepted 3 June; published online 27 June 2016; doi:10.1038/ni.3509

of ETC respiratory complexes can contribute to immunological function remains to be determined. Nevertheless, several studies have highlighted the potential importance of ETC respiratory complexes in macrophage activation. Chemical inhibition of CI impairs production of the pro-inflammatory cytokine IL-1β while inducing secretion of the anti-inflammatory cytokine IL-10 in activated macrophages[17]. In contrast, genetic ablation of the CI subunit NDUFS4 promotes an inflammatory macrophage phenotype[18], which suggests that CI activity dampens macrophage activation.

Here, we investigated whether ETC adaptations contributed to the metabolic switch that occurs in myeloid cells after they were activated via innate immune receptors[5,7] and would therefore affect antimicrobial responses. We report that the recognition of viable Gram-negative bacteria through TLR- and NLRP3-dependent pathways transiently decreased the abundance of SCs within the macrophage mitochondria due to destabilization of CI. The resultant dampening of CI activity was accompanied by an increase in the activity of CII. The induction of CII activity was not observed after phagocytosis of dead bacteria but was restored via bacterial RNA, a viability-associated pathogen-associated molecular pattern that signals microbial life to the immune system[19]. Conversely, inhibition of CII during challenge with viable bacteria normalized the amount of IL-1β and IL-10 to that found after an encounter with dead bacteria. Our findings identify a critical role for the mitochondrial ETC in innate immune responses to bacterial infection and highlight potential therapeutic interest in manipulating the ETC.

RESULTS

Sensing of bacteria affects mitochondrial ETC architecture

To determine whether the activation of innate immune cells affects the mitochondrial respiratory chain, we first analyzed the ETC organization of CD1 mouse bone-marrow-derived macrophages (BMDMs) left unchallenged ('resting') or challenged for 1.5 h with viable *Escherichia coli* K12, strain DH5α (called simply '*E. coli*' here). Unlike C57BL/6 mice, CD1 mice express the long isoform of SC-assembly factor I and consequently assemble CIV-containing SCs, which reflects the situation in human cells[20]. Two-dimensional gel analysis of mitochondria isolated from CD1 BMDMs revealed respiratory SCs containing CI plus dimerized CIII plus CIV (CI + $CIII_2$ + CIV), CI plus dimerized CIII (CI + $CIII_2$) or dimerized CIII plus CIV ($CIII_2$ + CIV)[20,21] in both resting macrophages and stimulated macrophages (**Fig. 1a** and **Supplementary Fig. 1a**). We then analyzed whole-BMDM lysates by Coomassie-blue-stained native PAGE (blue native (BN)-PAGE). We observed a lower abundance of CI and CI-containing SCs (CI + $CIII_2$ + CIV and CI + $CIII_2$) in CD1 BMDMs that had phagocytosed live *E. coli* than in untreated BMDMs (**Fig. 1b**). The amount of various ETC subunits (at the level of protein) was unaffected by *E. coli* challenge, despite mild transcriptional variation of some ETC-subunit-encoding nuclear genes (**Supplementary Fig. 1b–f**); this suggested that the changes in SC abundance were due to alterations in SC assembly rather than to changes in protein expression. BMDMs from C57BL/6 mice (called 'wild-type' mice here) also exhibited a transient reduction in the amount of CI- and CIII-containing SCs when incubated with *E. coli* (**Fig. 1b–e** and **Supplementary Fig. 2a,b**). Therefore, the disassembly of SCs after detection of viable bacteria affected all CI-containing SCs. ETC alterations were also observed in mouse peritoneal macrophages incubated with *E. coli* (**Supplementary Fig. 2c**) and were also evident after recognition of *Salmonella enterica* serovar Typhimurium SL1344 (*S. enterica* Typhimurium) by BMDMs (**Supplementary Fig. 2d–f**). Thus, our data indicated that the recognition of Gram-negative bacteria by macrophages induced modifications of the ETC architecture that were characterized by a decrease in the abundance of CI-associated structures.

Detection of bacteria modulates ETC-complex activity

Macrophages activated through innate immune receptors use glutamine rather than glucose or fatty acids as the carbon source for oxidative phosphorylation[4–7]. This adaptation results in a shift in the proportion of NADH-$FADH_2$ electrons that feed the ETC[22], which requires modulation of the proportions of the various SCs[20,23]. Stimulation of BMDMs with *E. coli* or *S. enterica* Typhimurium transiently impaired the in-gel NADH dehydrogenase activity of CI within CI + $CIII_2$ + CIV and CI + $CIII_2$ SCs (**Fig. 1b,d** and **Supplementary Fig. 2f**), which indicated a lower abundance of CI within SCs. Assessment of the activity of CI and that of CI + CIII in mitochondria isolated from BMDMs, by quantitative spectrophotometry, also indicated diminished CI-mediated respiration in response to *E. coli* relative to that in the resting condition (**Fig. 2a**). However, we found that the activity of CII and that of CII + CIII was increased and that the total activity of CIII and CIV remained unaltered in this context (**Fig. 2a**). To determine whether the decreased CI activity 'translated' into a drop in energy production, we measured the mitochondrial ATP-production rate in permeabilized BMDMs in the presence of glutamate plus malate, which generates intramitochondrial NADH that feeds electrons to CI[20]. CI-dependent ATP production was lower in BMDMs incubated with *E. coli* than in resting cells (**Fig. 2b**). Thus, macrophage responses to bacteria were characterized by diminished assembly of CI into SCs and decreased overall CI activity, consistent with an anti-inflammatory role for CI in macrophages[18]. In line with the effect of LPS on macrophages[4,5,7], *E. coli*–stimulated BMDMs had much lower oxygen consumption on a glucose substrate than that of resting BMDMs, while they exerted a high glycolytic activity that increased their extracellular acidification rate (ECAR) and lactate production at 18 h after infection relative to that of resting BMDMs (**Supplementary Fig. 3a–c**). However, we found that the maximal respiration rate (MRR) was greater in *E. coli*-treated BMDMs at 2 h after challenge than in untreated cells (**Fig. 2c** and **Supplementary Fig. 3d**). This created a situation in which the spare respiratory capacity (SRC) (**Fig. 2d**), ECAR (**Fig. 2e**) and lactate production (**Fig. 2f**) were increased simultaneously in BMDMs after recognition of *E. coli*. Together these data indicated that the detection of *E. coli* by macrophages decreased the activity of ETC CI and thereby modulated mitochondrial respiratory parameters.

Recognition of bacteria stimulates mitochondrial CII

The concomitant decrease in the activity of CI + CIII and the increased MRR of *E. coli*–stimulated macrophages on a glucose substrate seemed to be contradictory and suggested that an alternative electron source would compensate for the expected decrease in NADH (CI)-dependent electron flux. We investigated whether bacterial infection–driven alterations in the macrophage ETC and the resulting diminished CI activity would favor the use of electrons from $FADH_2$-oxidizing enzymes, as shown before[15,20,24]. We found much more CII enzymatic activity in peritoneal macrophages (**Fig. 3a**) or human $CD14^+CD16^-$ primary monocytes (**Fig. 3b**) challenged with *E. coli* and in BMDMs challenged with *S. enterica* Typhimurium (**Fig. 3c**) than in their untreated counterparts. In addition, BMDMs incubated with *E. coli* increased their CII-mediated ATP production rate compared with that of resting cells (**Fig. 3d**). The enhanced activity of CII (**Fig. 3e**) and of CII + CIII (**Fig. 3f**) was transient. The use of glucose catabolism to increase the maximum respiration rate despite a decrease in CI function would necessitate the delivery of NADH

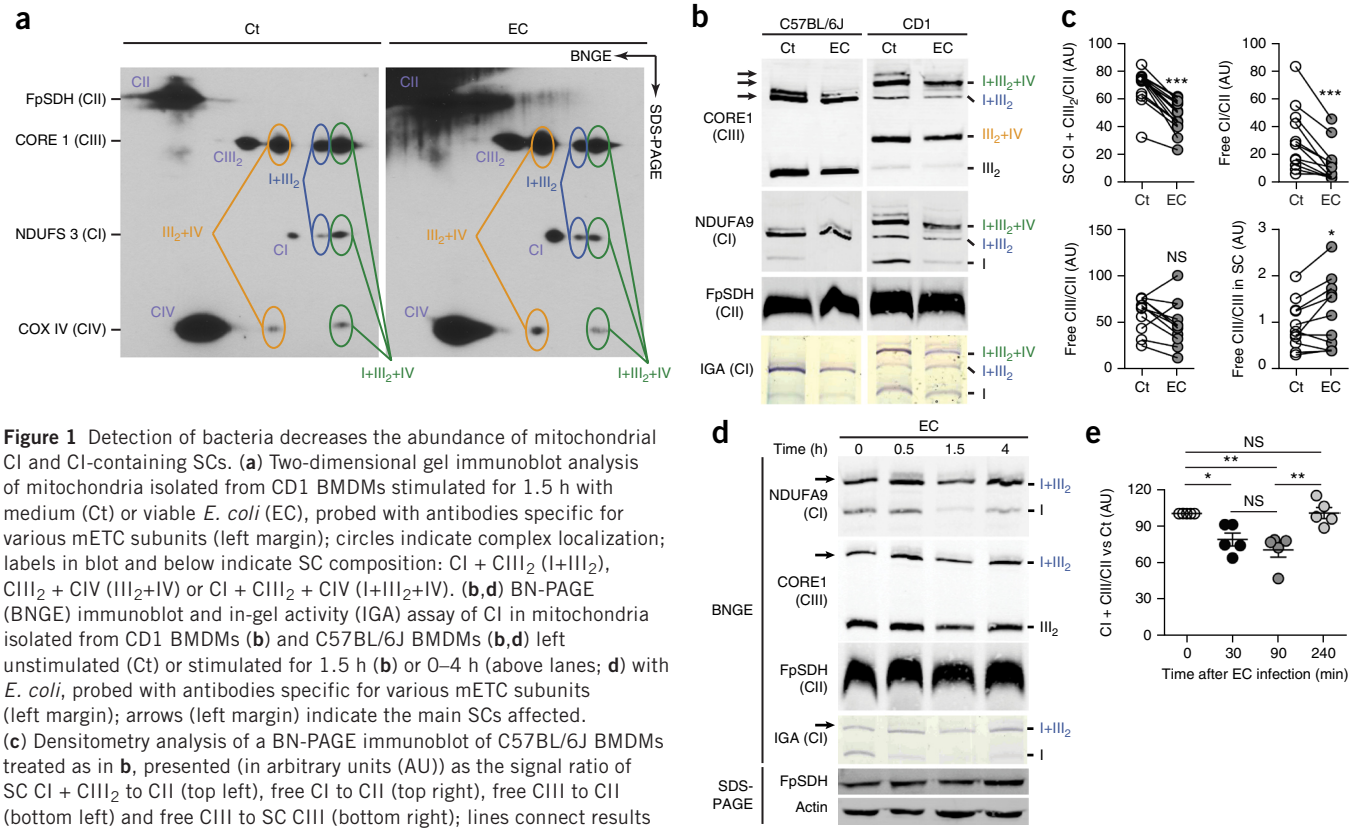

Figure 1 Detection of bacteria decreases the abundance of mitochondrial CI and CI-containing SCs. (**a**) Two-dimensional gel immunoblot analysis of mitochondria isolated from CD1 BMDMs stimulated for 1.5 h with medium (Ct) or viable *E. coli* (EC), probed with antibodies specific for various mETC subunits (left margin); circles indicate complex localization; labels in blot and below indicate SC composition: CI + $CIII_2$ ($I+III_2$), $CIII_2$ + CIV (III_2+IV) or CI + $CIII_2$ + CIV ($I+III_2$+IV). (**b**,**d**) BN-PAGE (BNGE) immunoblot and in-gel activity (IGA) assay of CI in mitochondria isolated from CD1 BMDMs (**b**) and C57BL/6J BMDMs (**b**,**d**) left unstimulated (Ct) or stimulated for 1.5 h (**b**) or 0–4 h (above lanes; **d**) with *E. coli*, probed with antibodies specific for various mETC subunits (left margin); arrows (left margin) indicate the main SCs affected. (**c**) Densitometry analysis of a BN-PAGE immunoblot of C57BL/6J BMDMs treated as in **b**, presented (in arbitrary units (AU)) as the signal ratio of SC CI + $CIII_2$ to CII (top left), free CI to CII (top right), free CIII to CII (bottom left) and free CIII to SC CIII (bottom right); lines connect results for the same experiment. (**e**) Densitometry analysis of BN-PAGE immunoblot of C57BL/6J BMDMs treated as in **d**, presented (as in **d**) as the ratio of SC CI + $CIII_2$ to CII, versus that of untreated cells (Ct). Each symbol represents an individual experiment; small horizontal lines indicate the mean (± s.e.m.). NS, not significant ($P > 0.05$); *$P < 0.05$, **$P < 0.01$ and ***$P < 0.001$ (paired *t*-test analysis (**c**) or one-way analysis of variance (ANOVA) followed by Tukey's post-test analysis (**e**)). Data are from one experiment representative of three (**a**,**b**,**d**) or ten (**b**) experiments with similar results, or are from three (**e**) or ten (**c**) independent experiments.

electrons generated by glycolysis to the mitochondrial ETC without the utilization of CI. This can be achieved by shuttling of cytoplasmic NADH electrons to coenzyme Q by mitochondria-bound glycerol-3-phosphate dehydrogenase (mG3PDH)[25]. Similar to the activity of CII, the activity of mG3PDH (**Fig. 3g**,**h**) and of mG3PDH + CIII (**Fig. 3i**) was greater in BMDMs challenged with *E. coli* than in cells in the resting condition. Nevertheless, the increased CII activity reached a maximum at 0.5–1.5 h after *E. coli* challenge (**Fig. 3e**), whereas the induction of mG3PDH was maintained for a longer time (**Fig. 3h**). Together these data indicated that the recognition of *E. coli* by macrophages induced a transient increase in the activity of mitochondrial $FADH_2$-dependent enzymes that feed electrons to CIII.

Phagosomal NADPH oxidase triggers ETC adaptations

Mitochondrial ROS (mROS), which increase within a few hours after *E. coli* is sensed[26], are inherent to ETC function, which makes them potential regulators of CII activity in *E. coli*–stimulated macrophages. We were unable to detect substantial enhancement of mROS production in BMDMs at 1. 5 h after *E. coli* challenge compared with mROS production in BMDMs left untreated or treated with the mROS-inducer rotenone (**Supplementary Fig. 4a**,**b**). However, we found that both the mROS-specific inhibitor mitoQ[27] and the broad antioxidant N-acetyl cysteine decreased CII enzymatic activity in untreated or *E. coli*-stimulated BMDMs (**Fig. 4a**), which suggested that mROS were required for proper CII function in macrophages. We next investigated if an alternative source of ROS, phagosomal NADPH oxidase[28], was a regulator of CII activity. In BMDMs, 15 min of challenge with *E. coli* strongly induced ROS production compared with such production in untreated cells (**Supplementary Fig. 4c**). BMDMs deficient in the NADPH oxidase subunit $gp91^{phox}$ (*Cybb*$^{-/-}$; called '*Gp91phox*$^{-/-}$' here) did not produce ROS in response to *E. coli*, in contrast to the production of ROS by wild-type BMDMs (**Supplementary Fig. 4d-e**); this demonstrated that the NADPH oxidase mediated ROS production in this context. In contrast to wild-type cells, *Gp91phox*$^{-/-}$ BMDMs did not increase the enzymatic activity of CII in response to *E. coli* (**Fig. 4b**). Consequently, the *E. coli*–mediated increase in SRC observed in wild-type BMDMs was absent in *Gp91phox*$^{-/-}$ BMDMs (**Fig. 4c** and **Supplementary Fig. 4f**,**g**), while the induction of ECAR was similar in wild-type and *Gp91phox*$^{-/-}$ cells (**Fig. 4d**). The absence of $gp91^{phox}$ also prevented the decrease in the abundance of SCs in mitochondria isolated from *E. coli*–stimulated BMDMs that was observed in wild-type cells (**Fig. 4e**,**f**). Together these results indicated that phagosomal ROS were an early inducer of ETC adaptations in macrophages during the sensing of bacteria and acted together with mROS to complete those adaptations.

E. coli–mediated induction of CII activity requires Fgr

CII activity adapts to fuel use through H_2O_2-mediated activation via phosphorylation of the CII subunit SDHA by the Src-family tyrosine kinase Fgr[29], the partner kinase of the phosphatase PTPMT1 (ref. 30). Fgr deficiency prevented the decrease in abundance of SCs induced by *E. coli* challenge in permeabilized wild-type BMDMs (**Supplementary Fig. 5a–e**) and in mitochondria isolated from wild-type BMDMs (**Supplementary Fig. 5f–i**). *E. coli*–treated BMDMs from *Fgr*$^{-/-}$

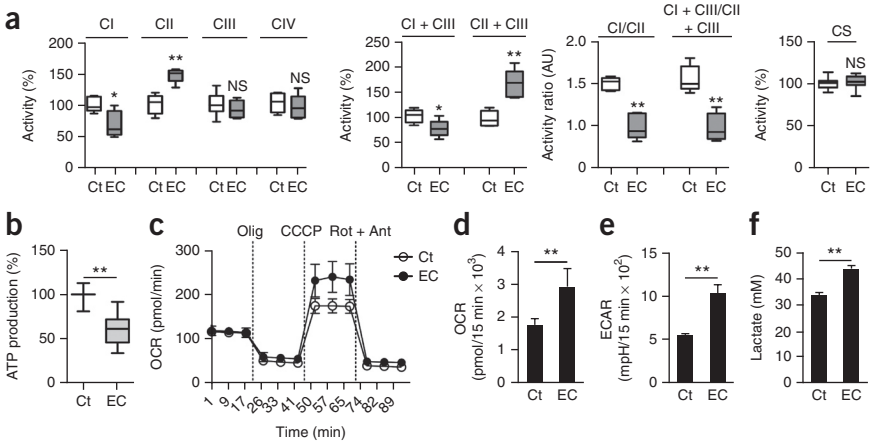

Figure 2 Detection of bacteria induces changes in the activity of mitochondrial ETC complexes and influences mitochondrial respiration and glycolysis. (**a**) Spectrophotometry analyzing the activity of various mitochondrial respiratory complexes (above plots) in mitochondria isolated from BMDMs left untreated or treated for 1.5 h with *E. coli*, normalized to the activity of citrate synthase (CS) in those mitochondria (presented relative to that in mitochondria from untreated cells; far right) relative to that in mitochondria isolated from untreated cells, set as 100% (far left and middle left), or presented as the ratio of the activity of various complexes (above plots; middle right). Specific activity (in IU per mg protein; mean ± s.e.m.) corresponding to 100% activity: 0.105 ± 0.013 (CI), 0.040 ± 0.008 (CII), 0.055 ± 0.01 (CIII), 0.1 ± 0.03 (CIV), 0.23 ± 0.01 (CI + CIII), 0.02 ± 0.003 (CII + CIII) and 0.3 ± 0.01 (CS). (**b**) ATP synthesis in wild-type BMDMs left untreated or treated with *E. coli*, in the presence of glutamate plus malate, presented relative to that in untreated cells, set as 100% (corresponding to a rate of 153 ± 24.9 nmol ATP per min per mg protein (mean ± s.e.m.)). (**c**) Oxygen-consumption rate (OCR) of wild-type BMDMs left untreated or treated for 2 h with *E. coli*, then sequentially treated (vertical dotted lines) with oligomycin (Olig), the oxidative-phosphorylation inhibitor CCCP, and the ETC inhibitors rotenone and antimycin (Rot + Ant). (**d**–**f**) SRC (assessed as OCR) (**d**), basal ECAR (**e**) and extracellular lactate concentration (**f**) of wild-type BMDMs left untreated or treated for 2 h with *E. coli*. $*P < 0.01$ and $**P < 0.001$ (two-tailed unpaired Student's *t*-test). Data are from three (**a**,**d**–**f**) or eight (**b**) independent experiments (mean and s.e.m.) or one experiment representative of three independent experiments with similar results (**c**; mean ± s.d.).

mice did not show the decrease in CI activity or the increase in CII activity observed in wild-type BMDMs in response to *E. coli* (**Fig. 5a** and **Supplementary Fig. 5j**). Similarly, *Fgr*$^{-/-}$ BMDMs preserved their CI-dependent ATP production and did not enhance their CII-mediated ATP production after detecting *E. coli*, in contrast to wild-type BMDMs (**Fig. 5b**). As a consequence, *Fgr*$^{-/-}$ BMDMs challenged with *E. coli* did not show a higher MRR (**Supplementary Fig. 5k**) or greater SRC (**Fig. 5c**) than that of resting *Fgr*$^{-/-}$ BMDMs but did show an increase in ECAR (**Fig. 5d**) and lactate production (**Fig. 5e**) similar to that of wild-type BMDMs stimulated with *E. coli*. These results indicated that Fgr was an important regulator of macrophage ETC adaptations during bacterial infection.

Metabolic reprogramming toward glycolysis and the accumulation of succinate[7], together with an increase in mROS production[26], contributes to the antimicrobial functions of macrophages. In line with that, *Fgr*$^{-/-}$ BMDMs had more intracellular *E. coli* upon infection *in vitro* than that of wild-type BMDMs (**Fig. 5f**), indicative of enhanced survival of the bacteria within *Fgr*$^{-/-}$ BMDMs. However, Fgr-deficient and wild-type mice had an equal number of colony-forming units (CFU) of *E. coli* in the spleen after intraperitoneal infection with this bacteria (**Supplementary Fig. 5l**,**m**). In line with that, induction of the inflammatory-cytokine-encoding genes *Il1b*, *Ifnb* and *Tnf* in response to challenge with *E. coli* was similar in wild-type and *Fgr*$^{-/-}$ BMDMs (**Supplementary Fig. 5n**), despite slightly

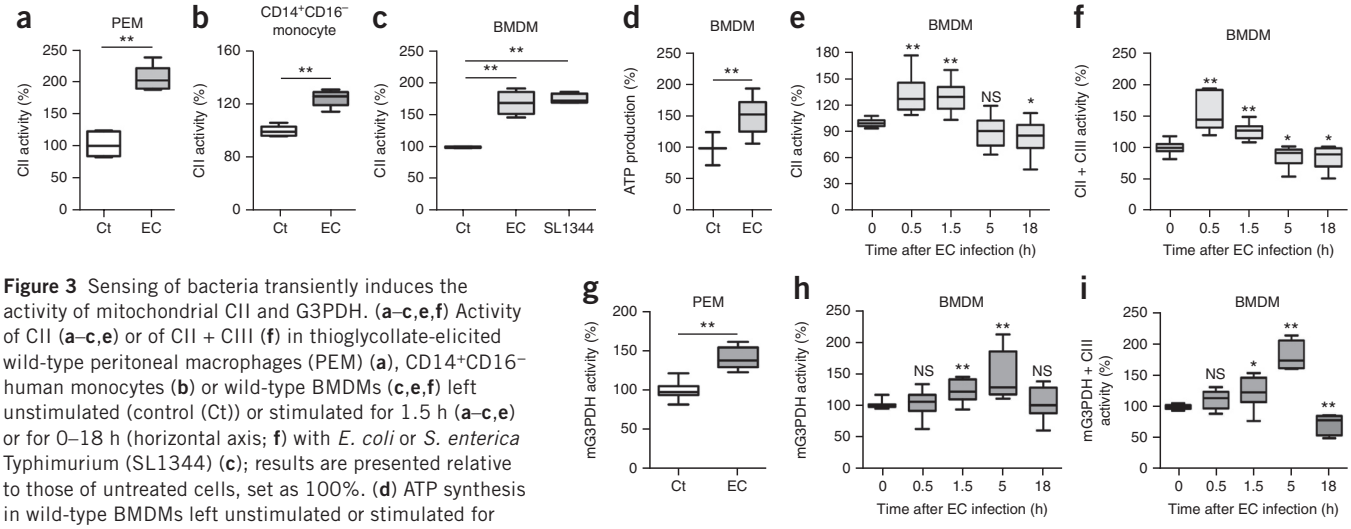

Figure 3 Sensing of bacteria transiently induces the activity of mitochondrial CII and G3PDH. (**a**–**c**,**e**,**f**) Activity of CII (**a**–**c**,**e**) or of CII + CIII (**f**) in thioglycollate-elicited wild-type peritoneal macrophages (PEM) (**a**), CD14^{+}CD16^{-} human monocytes (**b**) or wild-type BMDMs (**c**,**e**,**f**) left unstimulated (control (Ct)) or stimulated for 1.5 h (**a**–**c**,**e**) or for 0–18 h (horizontal axis; **f**) with *E. coli* or *S. enterica* Typhimurium (SL1344) (**c**); results are presented relative to those of untreated cells, set as 100%. (**d**) ATP synthesis in wild-type BMDMs left unstimulated or stimulated for 1.5 h with *E. coli*, in the presence of succinate; results presented relative to those of untreated cells, set as 100% (corresponding to a rate of 70.4 ± 18.1 nmol ATP per min per mg protein (mean ± s.e.m.)). (**g**–**i**) Activity of mG3PDH (**g**,**h**) or mG3PDH + CIII (**i**) in thioglycollate-elicited wild-type macrophages (**g**) or BMDMs (**h**,**i**) left unstimulated or stimulated for 1.5 h (**g**) or for 0–18 h (horizontal axis; **h**,**i**) with *E. coli* (presented as in **a**–**c**,**e**,**f**). $*P < 0.05$ and $**P < 0.001$ (two-tailed unpaired Student's *t*-test). Data are from one experiment with five mice per group (**a**) or three donors (**b**) and three technical replicates (mean ± s.e.m.) or three (**c**,**h**,**i**), four (**f**), six (**e**) or eight (**d**) independent experiments with three to five technical replicates (mean ± s.e.m.).

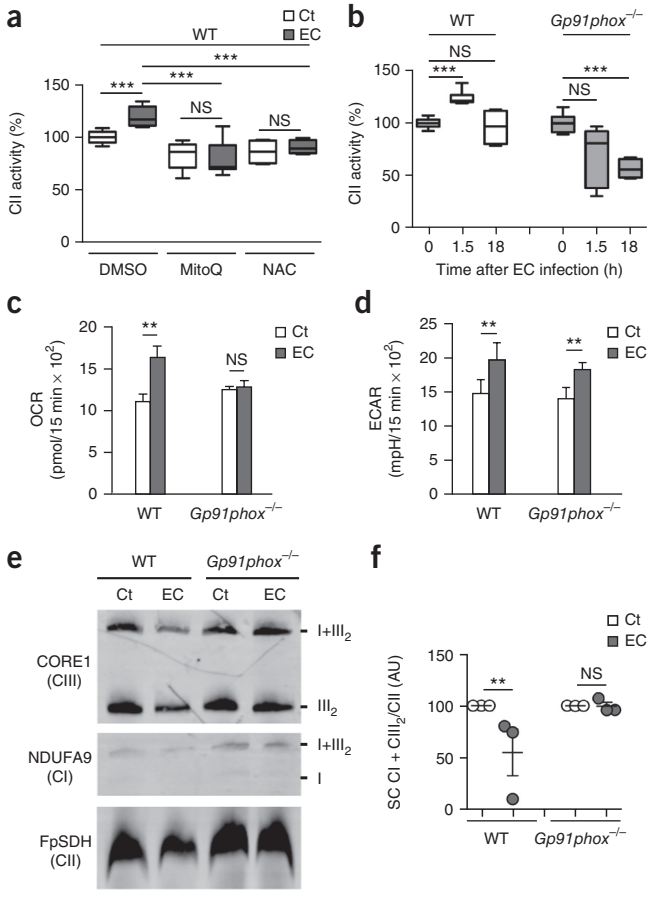

Figure 4 The induction of mitochondrial CII activity and decrease in SC abundance after detection of *E. coli* relies on phagosomal ROS. (**a**,**b**) CII activity in wild-type (WT) and *Gp91phox*$^{-/-}$ BMDMs left unstimulated or stimulated for 1.5 h (**a**) or for 0, 1,5 or 18 h (horizontal axis; **b**) with *E. coli* and treated with vehicle (DMSO) or the ROS inhibitors N-acetylcysteine (NAC) or mitoQ (**a**) or given no further treatment (**b**); results are presented relative to those of untreated cells, set as 100%. (**c**,**d**) SRC (assessed as OCR) (**c**) and ECAR (**d**) in wild-type and *Gp91phox*$^{-/-}$ BMDMs left unstimulated or stimulated for 2 h with *E. coli*. (**e**) BN-PAGE immunoblot analysis of mitochondria isolated from wild-type and *Gp91phox*$^{-/-}$ BMDMs left unstimulated or stimulated for 2 h with *E. coli*. (**f**) Densitometry of BN-PAGE, presented as the signal ratio of SC CI + $CIII_2$ to CII, relative to that of untreated cells, set as 100%. $^{*}P < 0.01$ and $^{**}P < 0.001$ (two-tailed unpaired Student's *t*-test). Data are from four (**a**) or three (**b**–**d**,**f**) independent experiments with two (**b**,**f**) or five (**c**,**d**) technical replicates (mean and s.e.m.) or one experiment representative of three independent experiments with similar results (**e**).

less secretion of IL-1β by *Fgr*$^{-/-}$ BMDMs than by wild-type BMDMs (**Supplementary Fig. 5o**). Together these results indicated that other kinases of the Src family might have compensated for the loss of Fgr in the expression of inflammatory cytokines[31].

CII activity contributes to anti-microbial responses

Because Fgr has other targets beyond CII, we used the succinate dehydrogenase (SDH)-specific inhibitor 3-nitropropionic acid (NPA)[32] to block CII activity. At the concentrations tested, NPA did not affect the survival or phagocytic activity of wild-type BMDMs (**Supplementary Fig. 6a**,**b**) but strongly repressed CII activity in resting and *E. coli*–stimulated BMDMs relative to its activity in untreated BMDMs (**Supplementary Fig. 6c**) without affecting bacterial SDH activity or growth (**Supplementary Fig. 6d**,**e**). Treatment of wild-type BMDMs with NPA did not prevent SC disassembly (**Supplementary Fig. 6f**) or the drop in CI-mediated ATP production induced by *E. coli* challenge but efficiently prevented the increase in CII-mediated ATP production induced similarly (**Supplementary Fig. 6g**), in contrast to results obtained for untreated BMDMs. NPA treatment also substantially diminished the MRR induced by *E. coli* (**Fig. 6a** and **Supplementary Fig. 6h**) and ablated the increase in SRC (**Fig. 6b**) without affecting induction of the ECAR (**Fig. 6c** and **Supplementary Fig. 6i**) or production of lactate (**Supplementary Fig. 6j**) in wild-type BMDMs. Similar results were obtained with the CII competitive inhibitors dimethyl-malonate[33] and thenoyltrifluoroacetone (**Supplementary Fig. 6k**–**o**).

We next investigated whether CII activity contributed to anti-microbial function. Mice treated with NPA were more susceptible to infection with *S. enterica* Typhimurium than were mice treated with vehicle (**Fig. 6d**) and had a greater splenic bacterial burden at 72 h after intra-peritoneal infection with viable *E. coli* than that of their counterparts treated with vehicle (**Fig. 6e**), despite normal recruitment of inflammatory cells to the peritoneal cavity (**Supplementary Fig. 7a**). The greater bacterial load in NPA-treated mice correlated with their lower serum concentrations of the pro-inflammatory cytokine IL-1β and higher concentrations of anti-inflammatory cytokine IL-10 than those of vehicle-treated mice, while their concentration of the cytokine TNF was not affected relative to that of vehicle-treated mice (**Fig. 6f**). We also found a greater number of viable *E.coli* in NPA-treated BMDMs than in vehicle-treated BMDMs (**Fig. 6g**,**h**), which indicated that inhibition of CII impaired macrophage bactericidal activity *in vitro*. In addition, NPA-treated BMDMs

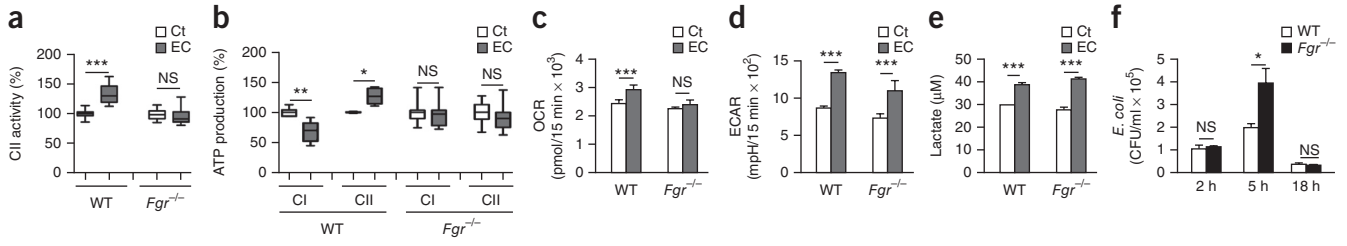

Figure 5 Fgr is required for the induction of CII activity after detection of *E. coli*. (**a**–**e**) CII activity (**a**), substrate-driven CI- or CII-mediated ATP synthesis (**b**), SRC (assessed as OCR) (**c**), ECAR (**d**) and extracellular lactate concentration (**e**) of wild-type and *Fgr*$^{-/-}$ BMDMs stimulated with *E. coli*; results in **a**,**b** are presented relative to those of untreated cells, set as 100% (corresponding (in **b**) to a rate of 72.1 nmol (CI; wild-type), 66.3 nmol (CI; *Fgr*$^{-/-}$), 21.2 nmol (CII; wild-type) or 17.8 nmol (CII; *Fgr*$^{-/-}$) ATP per min per mg protein). (**f**) Intracellular *E. coli* in wild-type and *Fgr*$^{-/-}$ BMDMs infected for 2, 5 or 18 h (horizontal axis) with *E. coli* at a multiplicity of infection of 5, presented as colony-forming units (CFU). $^{*}P < 0.05$, $^{**}P < 0.01$ and $^{***}P < 0.001$ (two-tailed unpaired Student's *t*-test). Data are from seven (**a**), three (**b**–**e**) or two (**f**) independent experiments with two (**a**), three (**b**,**f**) to five (**c**–**e**) technical replicates (mean and s.e.m.).

had lower *E. coli*–induced expression of IL-1β protein and *Il1b* and *Ifnb* mRNA than that of their untreated counterparts but had TNF expression similar to that of their untreated counterparts (**Supplementary Fig. 7b**,**c**), consistent with the relative insensitivity of TNF production to macrophage-metabolic fluctuations and oxygen availability[7,34]. Itaconic acid, which results from decarboxylation of the TCA-cycle intermediate *cis*-aconitate, has anti-bacterial properties[12]. We found that the TCA-cycle intermediate fumarate, which is produced by the oxidation of succinate by CII, strongly inhibited bacterial growth (**Supplementary Fig. 7d**) and induced bacterial death, while succinate had negligible effects relative to those of PBS (**Supplementary Fig. 7e**,**f**). To exclude the possibility that mere lowering of the pH accounted for the observed effects of fumarate on bacteria viability, we used ester forms of these TCA intermediates. Dimethyl fumarate impaired the growth of *E. coli* (**Fig. 6i**) and *S. enterica* Typhimurium *in vitro* (**Fig. 6j**), but dimethyl succinate did not. These data identified CII as an important contributor to the macrophage mitochondrial respiratory functions needed for anti-microbial responses.

Microbial viability drives ETC adaptations

In contrast to viable *E. coli*, heat-killed *E. coli* did not affect the assembly of CI or the CI + $CIII_2$ SC in BMDMs (**Fig. 7a** and **Supplementary Fig. 8a**,**b**). In contrast to viable *E. coli*, heat-killed *E. coli* did not impair the in-gel activity of CI within the CI + $CIII_2$ SC (**Fig. 7a**) and failed to increase mitochondrial MRR (**Supplementary Fig. 8c**) or SRC (**Fig. 7b**) in BMDMs. However, viable and heat-killed *E. coli* both efficiently induced ECAR (**Fig. 7c**), lactate release (**Supplementary Fig. 8d**) and mG3PDH activity (**Supplementary Fig. 8e**) in BMDMs, probably reflective of the ability of LPS to trigger a glycolytic switch in macrophages[5,7]. Unlike viable *E. coli*, heat-killed *E. coli* did not induce CII activity in BMDMs (**Fig. 7d**), human $CD14^+CD16^-$ monocytes (**Fig. 7e**) or peritoneal macrophages (**Supplementary Fig. 8f**). Notably, live *E. coli* were more efficient than heat-killed *E. coli* at inducing phagosomal ROS production by wild-type BMDMs (**Fig. 7f** and **Supplementary Fig. 8g**), which was required for the induction of CII and SRC in macrophages. These findings indicated that stimuli associated with viable bacteria triggered ETC adaptations in macrophages.

An association with bacterial viability has been suggested for several bacterial molecules[2,35], including bacterial RNA[19]. We found that CII activity in BMDMs was enhanced in response to RNA purified from *E. coli* and was unaffected when the RNA preparations were pre-treated with RNases (**Fig. 7g** and **Supplementary Fig. 8h**). The double-stranded RNA mimic polyinosinic:polycytidylic acid (poly(I:C)) and the single-stranded RNA mimic R848 (which trigger TLR3 and TLR7, respectively) also induced CII activity in BMDMs

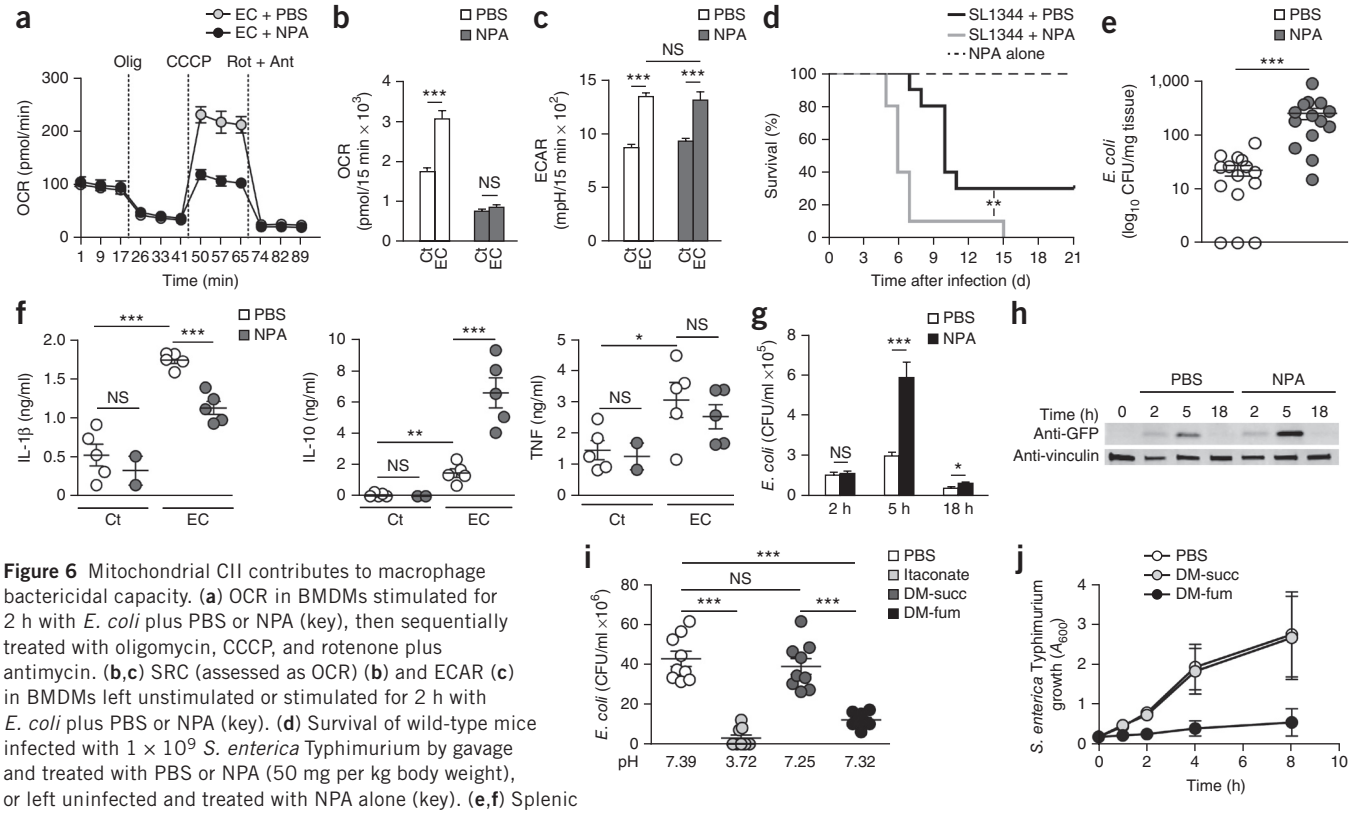

Figure 6 Mitochondrial CII contributes to macrophage bactericidal capacity. (**a**) OCR in BMDMs stimulated for 2 h with *E. coli* plus PBS or NPA (key), then sequentially treated with oligomycin, CCCP, and rotenone plus antimycin. (**b**,**c**) SRC (assessed as OCR) (**b**) and ECAR (**c**) in BMDMs left unstimulated or stimulated for 2 h with *E. coli* plus PBS or NPA (key). (**d**) Survival of wild-type mice infected with 1×10^9 *S. enterica* Typhimurium by gavage and treated with PBS or NPA (50 mg per kg body weight), or left uninfected and treated with NPA alone (key). (**e**,**f**) Splenic bacterial burden (**e**) and serum concentration of IL-1β, IL-10 and TNF (**f**) in PBS- or NPA-treated wild-type mice at 72 h (**e**) or 2 h (**f**) after no infection (Ct) or intraperitoneal injection of 1×10^8 *E. coli* (**e**) or 1×10^9 *E. coli* (**f**). (**g**) Intracellular *E. coli* in PBS- or NPA-treated wild-type BMDMs infected for 2, 5 or 18 h (horizontal axis) with *E. coli* at a multiplicity of infection of 5. (**h**) Immunoblot analysis of SDS-solubilized extracts of PBS- or NPA-treated wild-type BMDMs infected for 0, 2, 5 or 18 h (above lanes) with green-fluorescent-protein-expressing *E. coli* at a multiplicity of infection of 5, probed with antibody to (Anti-) green fluorescent protein (GFP) or antibody to vinculin (loading control). (**i**) Growth of 1×10^5 *E. coli* incubated for 3 h with unsupplemented PBS or PBS supplemented with itaconic acid (Itaconate), dimethyl succinate (DM succ) or dimethyl fumarate (DM fum); horizontal axis, pH of the resultant buffers. (**j**) Growth of *S. enterica* Typhimurium in presence of PBS, dimethyl succinate (10 mM) or dimethyl fumarate (10 mM), presented as absorbance at 600 nm (A_{600}). $^*P < 0.05$, $^{**}P < 0.01$ and $^{***}P < 0.001$ (Student's *t*-test (**b**,**c**,**e**–**g**,**i**,**j**) or log-rank (Mantel-Cox) test (**d**)). Data are from are from one experiment representative of three independent experiments with similar results (**a**,**h**; mean ± s.d. in **a**) or two (**d**,**f**,**g**) or three (**b**,**c**,**e**,**i**,**j**) independent experiments with three (**i**,**j**) or five (**b**,**c**) technical replicates or with two to five mice per group (**d**–**f**) (mean and s.e.m. in **b**,**c**,**e**–**g**,**i**,**j**).

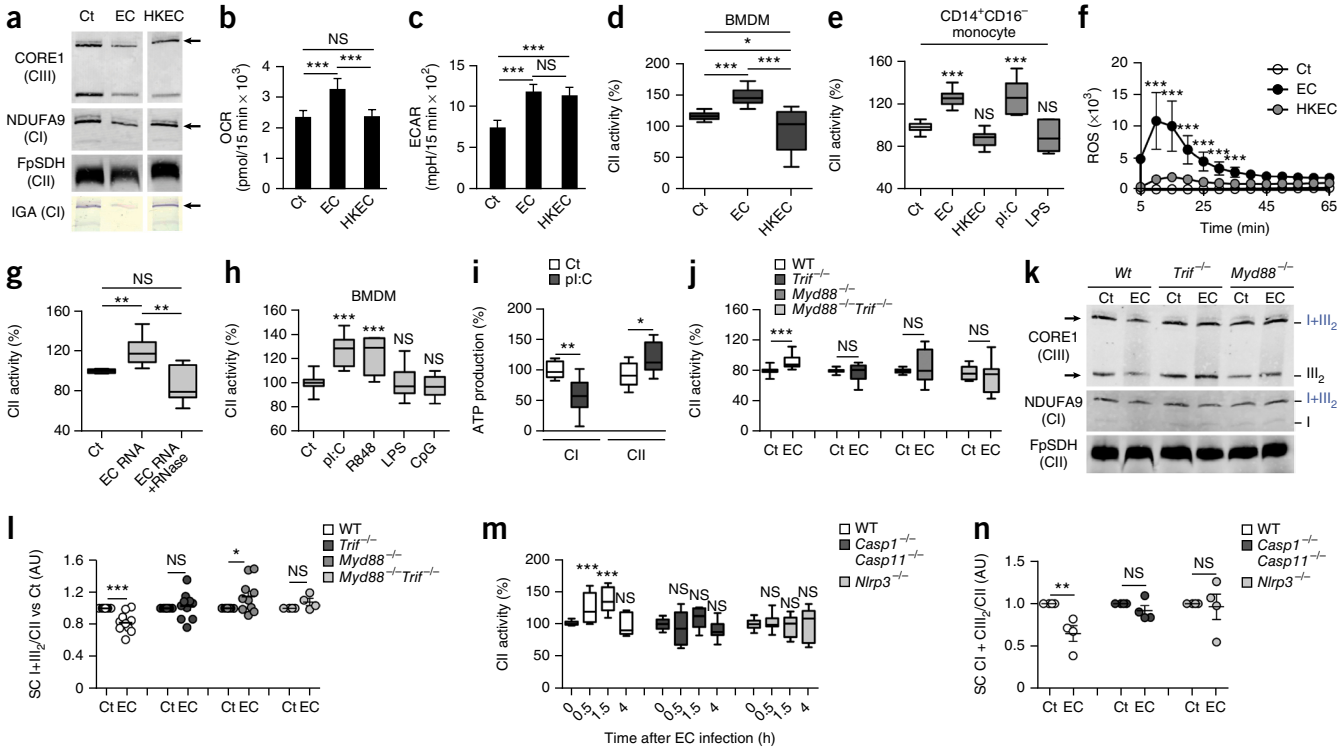

Figure 7 Sensing of bacterial viability induces a MyD88-and-TRIF- and NLRP3-inflammasome-dependent decrease in SC abundance and increase in CII activity. (**a**) BN-PAGE immunoblot analysis and CI in-gel activity assay in BMDMs left untreated (Ct) or treated with viable *E. coli* (EC) or heat-killed *E. coli* (HKEC). (**b**–**d**) SRC (assessed as OCR) (**b**), ECAR (**c**) and CII activity (**d**) in BMDMs treated as in **a**; results in **d** are presented relative to those of untreated cells, set as 100%. (**e**) CII activity in $CD14^+CD16^-$ human monocytes left unstimulated or stimulated with *E. coli* or heat-killed *E. coli* or treated with poly(I:C) (pI:C) or LPS (presented as in **d**). (**f**) ROS production by BMDMs treated as in **b**. (**g**,**h**) CII activity in wild-type BMDMs left unstimulated or stimulated for 1.5 h with *E. coli* RNA alone or in the presence of RNase (**g**) or with poly(I:C), R484, LPS or CpG (**h**) (presented as in **d**). (**i**) CI- or CII-mediated ATP synthesis in wild-type BMDMs left unstimulated or stimulated with poly(I:C); results are presented relative to those of untreated cells, set as 100% (corresponding to a rate of 25.1 nmol (CI) or 19.8 nmol (CII) ATP per min per mg protein). (**j**) CII activity in wild-type, *Trif*$^{-/-}$, *Myd88*$^{-/-}$ and *Trif*$^{-/-}$*Myd88*$^{-/-}$ BMDMs (key) treated left untreated or treated with *E. coli* (horizontal axis), presented as in **d**. (**k**) BN-PAGE immunoblot analysis of unstimulated and *E. coli*–stimulated wild-type, *Trif*$^{-/-}$ and *Myd88*$^{-/-}$ BMDMs; arrows (left margin) indicate the main SCs affected. (**l**,**n**) Densitometry analysis of a BN-PAGE immunoblot of wild-type, *Trif*$^{-/-}$, *Myd88*$^{-/-}$ and *Trif*$^{-/-}$*Myd88*$^{-/-}$ BMDMs (**l**) or wild-type, *Casp1*$^{-/-}$*Casp11*$^{-/-}$ and *Nlrp3*$^{-/-}$ BMDMs (**n**) left unstimulated or stimulated for 1.5 h with *E. coli*, presented as the signal ratio of SC CI + $CIII_2$ to CII, relative to that of untreated cells. (**m**) CII activity in wild-type, *Casp1*$^{-/-}$*Casp11*$^{-/-}$ and *Nlrp3*$^{-/-}$ BMDMs stimulated for various times (horizontal axis) with *E. coli*, presented as in **d**. $^*P < 0.05$, $^{**}P < 0.01$ and $^{***}P < 0.001$ (two-tailed unpaired Student's *t*-test). Data are from one experiment representative of four independent experiments (**a**,**k**) or are from three (**b**,**c**,**e**,**i**), four (**d**,**g**,**h**,**m**,**n**) or five (**f**,**j**,**l**) independent experiments with five (**b**,**c**), two (**d**,**e**,**g**,**h**,**j**) or three (**f**,**i**) technical replicate (mean and s.e.m. in **b**–**j**,**l**–**n**).

(**Fig. 7h**), whereas LPS (a TLR4 agonist) and the oligodeoxynucleotide CpG (a TLR9 agonist) did not (**Fig. 7h** and **Supplementary Fig. 8i**–**j**). This was also evident in human $CD14^+CD16^-$ monocytes (**Fig. 7e**). In addition, treatment with poly(I:C) decreased CI-mediated ATP production and promoted CII-mediated ATP production in permeabilized BMDMs relative to that in resting cells (**Fig. 7i**). These results indicated that recognition of microbial RNA controlled CII activity.

Because bacterial RNA triggers viability-specific immune responses through the adaptor TRIF[19], we evaluated the contribution of TLR adaptors to ETC changes induced by *E. coli*. In contrast to wild-type cells, BMDMs generated from mice deficient in TRIF (*Ticam1*$^{-/-}$; called '*Trif*$^{-/-}$' here) or the adaptor MyD88 (*Myd88*$^{-/-}$) or both (*Trif*$^{-/-}$*Myd88*$^{-/-}$) did not undergo induction of CII activity when exposed to bacteria (**Fig. 7j**). In contrast, the induction of CII activity after challenge with *E. coli* was unaffected in BMDMs deficient in STING or MAVS (**Supplementary Fig. 8k**), two adaptors that use mitochondria to mediate the sensing of nucleic acids and poly(I:C) by cytosolic receptors[14]. In addition, both TRIF and MyD88 were required for the initiation of changes in ETC composition after *E. coli* was sensed (**Fig. 7k**,**l** and **Supplementary Fig. 8l**). Thus, the adjustments to CII function in response to bacteria were probably regulated by phagosomal RNA-sensing TLRs rather than by cytosolic nucleic-acid-sensing innate immunological receptors[2]. Viability-specific immune responses and sensing of bacterial RNA also involve the NLRP3 inflammasome[2,19,36], the activation of which has been linked to mitochondria, phagosomal NADPH oxidase and ROS release[2,14,19,36,37]. Both the induction of CII (**Fig. 7m**) and the decrease in ETC supercomplex assembly (**Fig. 7n** and **Supplementary Fig. 8m**) were markedly impaired in *E. coli*–treated BMDMs deficient in NLRP3 (*Nlrp3*$^{-/-}$) or in caspase-1 and casepase-11 (*Casp1*$^{-/-}$*Casp11*$^{-/-}$) relative to that in *E. coli*–challenged wild-type cells, which would place CII activation at the center of viability-specific immune responses to bacteria. Consistent with that, treatment of *E. coli*–infected wild-type mice with the CII inhibitor dimethyl-malonate diminished the serum concentration of IL-1β and increased the serum concentration of IL-10 to their concentrations in mice treated with heat-killed *E. coli* without influencing serum concentration of the IL-6 (**Fig. 8**). Together these

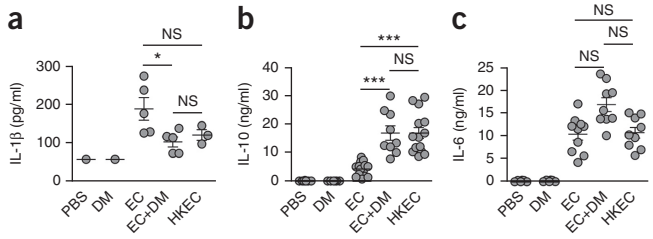

Figure 8 Inhibition of CII *in vivo* modulates cytokine production after challenge with viable *E. coli*. Serum concentration of IL-1β (**a**), IL-10 (**b**) and IL-6 (**c**) in wild-type mice treated with PBS alone (PBS) or with dimethyl malonate (600 mg per kg body weight) alone (DM) or together with intraperitoneal injection of 1×10^9 viable *E. coli* (EC + DM), or with intraperitoneal injection of 1×10^{10} heat-killed *E. coli* alone (HKEC). Each symbol represents an individual mouse; small horizontal lines indicate the mean (± s.e.m.). $^*P < 0.05$, $^{**}P < 0.01$ and $^{***}P < 0.001$ (two-tailed unpaired Student's *t*-test). Data are from one (**a**) or two (**b**,**c**) independent experiments with two to five mice per group.

data suggested that CII activity regulates cytokine production by macrophages during bacterial infection (**Supplementary Fig. 8n**).

DISCUSSION

Our study has described a mechanism by which macrophages adjusted their metabolism in response to viable bacteria by coupling TLR engagement, the NLRP3 inflammasome and ROS signaling to the mitochondrial ETC. This metabolic adjustment in turn contributed to pathogen-specific immune responses. The ETC architecture was altered in response to the detection of viable bacteria because of a decrease in the abundance of assembled CI. Several explanations can account for this. CI is an unstable ETC multiprotein complex composed of 44 different protein subunits, the assembly of which is influenced by the oxidative environment within the ETC[15] and/or by previous assembly of other ETC components, including CIII[38] or cytochrome *c* oxidase[39]. A switch in the substrate that fuels the TCA cycle modifies the NADH/$FADH_2$ ratio, which can saturate the oxidation capacity of the coenzyme Q pool and thereby induce a reverse electron transfer toward CI. This in turn increases superoxides that oxidize specific CI proteins and thereby leads to disassembly of the complex[23]. After engagement of surface TLRs, ROS expression within the ETC is increased[26] and this constitutes a potential source of CI-destabilizing ROS. In addition, a modulation of the NADH/$FADH_2$ ratio that induces reverse electron transfer is likely to occur here because activation of innate immunological receptors diverts pyruvate from entering the mitochondria and limits fatty-acid oxidation, while glutaminolysis ensures replenishment of the TCA cycle[5,40].

Unless an as-yet-to-be-determined bacterial viability–specific metabolic-flux adaptation further modulates the NADH/$FADH_2$ ratio, CI destabilization should occur in response to both heat-killed bacteria and viable bacteria. However, we observed alterations in the ETC only in response to the latter. In addition, the inhibition of CII in macrophage challenged with viable *E. coli* did not impair the decrease in the abundance of CI and CI-containing SCs, nor did it prevent the decrease in CI-mediated ATP synthesis. Phagosomal ROS might also account for the oxidative destabilization of CI. Indeed, we found that $gp91^{phox}$-deficient macrophages had preserved ETC architecture in response to viable *E. coli* and that phagosomal ROS concentrations in wild-type macrophages were substantially lower in response to heat-killed *E. coli* than in response to live bacteria. However, $gp91^{phox}$ deficiency also impaired the induction of CII activity and, as a consequence, might also prevent CI-destabilizing reverse electron transfer. Therefore, whether the changes in ETC architecture after challenge with viable bacteria were a consequence of the rapid increase in oxidative burst within the ETC due to innate immune signaling or resulted from a fuel switch remains to be determined. Nevertheless, our data indicated that recognition of *E. coli* induced a transient alteration in SCs in macrophages, which might make CIII available for electrons provided by $FADH_2$-dependent enzymes and thereby allow mitochondria to re-oxidize cytoplasmic NADH without the use of CI, as shown in other models[15,20].

Whether metabolic reprogramming directly contributes to macrophage effector function remains unclear. Itaconate, a non-amino organic acid, can exert antimicrobial functions at a concentration of about 10 mM (refs. 12,13). Consistent with that, we found that the CII enzymatic product fumarate prevented bacterial growth *in vitro* and decreased bacterial viability at a concentration of 10 mM, but its precursor succinate did not. At such concentrations, the pH is merely decreased and should therefore impair normal macrophage function. However, after macrophages encounter bacteria, mitochondria are juxtaposed to microbe-containing phagosomes[26,41]. This is mediated by the formation of a complex between the TLR signaling adaptor TRAF6 and the mitochondrial CI-assembly factor ECSIT[26], the interaction of which is regulated by the Mst1-Mst2-Rac signaling axis[41]. Such proximity between mitochondria and bacteria-containing phagosomes might permit the delivery of mROS or mitochondrial metabolites to contribute to the killing of bacteria[14]. Such model presents some advantages because it would allow those 'antimicrobial metabolites' to reach sufficient concentrations locally (i.e., within the phagosome) while sparing host cellular metabolism. Future work should provide additional insight into this issue.

The use of LPS to activate macrophages has generated a considerable amount of information on the metabolic pathways and reprogramming engaged during inflammation[8]. We found that challenge of macrophage with heat-killed bacteria recapitulated many aspects of LPS-mediated engagement of TLR4 on mitochondrial respiration, including induction of glycolytic flux (increased ECAR and lactate release) and decreased oxygen consumption in the mitochondria. However, we observed the induction of CII activity and destabilization of the ETC only in response to viable bacteria. Therefore, while the use of a single pathogen-associated molecular pattern certainly presents advantages, it offers only a partial view of the complexity of the innate immunological signals that might regulate metabolic adjustments after an encounter with a whole viable microorganism. This is not trivial, because macrophages tightly 'scale' their response to many features of bacteria, including viability-specific signals[2,35]. Most notably, we found that the inhibition of CII during challenge of mice with viable bacteria increased the concentration of IL-10 and decreased the concentration of IL-1β in the serum to the concentrations observed when heat-killed bacteria were used. Thus, the establishment of a functional link among pattern-recognition receptors, ETC organization and subsequent inflammatory immune responses might offer substantial benefits for vaccine design and provide valuable new targets for pharmacological intervention both during infection and in metabolic inflammatory disorders.

METHODS

Methods and any associated references are available in the online version of the paper.

Note: Any Supplementary Information and Source Data files are available in the online version of the paper.

ACKNOWLEDGMENTS

We thank A. Hidalgo for critical reading of the manuscript; S. Akira (Osaka University) for *Ips1*$^{-/-}$ mice; J. Magarian Blander (Mount Sinai School of Medicine) for *Myd88*$^{-/-}$, *Trif*$^{-/-}$ and *Trif*$^{-/-}$*Myd88*$^{-/-}$ mice; F. Norel-Bozouklian (Institut Pasteur) for *S. thyphimurium* SL1344; S. Trombetta (New York University) for the plasmid encoding GFP-OT; S. Bartlett for English editing; and M. Fernández-Monreal, M. Villalba, F. Ruperez-Pascualena and members of the Sancho and Enríquez laboratories for discussions and support. Supported by the European Community (FP7-Marie Curie-CIG#332881 to J.G.; ERC-2010-StG 260414 and 635122-PROCROP H2020 to D.S.; and UE0/MCA1108 and UE0/MCA1201 to J.A.E.), the French association 'La Ligue Contre le Cancer-comité du Gard' (CG/59-2013 to J.G.), the Spanish Ministry of Economy and Competitiveness (SAF-2013-42920R to D.S.; SAF2012-1207 to J.A.E.; and RyC2011-07826 to R.A.-P.), the Comunidad de Madrid (CAM/API1009 to J.A.E.), the German research council (DFG grant SA1940/2-1 and SFB-TR84 TP-C08 to L.E.S.). CNIC is supported by the MINECO and the Pro-CNIC Foundation, and is a Severo Ochoa Center of Excellence (SEV-2015-0505).

AUTHOR CONTRIBUTIONS

J.G. and R.A.-P. designed and performed all experiments; S.M.-C. and M.E. performed experiments measuring oxidative-phosphorylation enzymatic activity, prepared samples for BN-PAGE and immunoblot analysis and helped with experiments with mice; M.U. and L.E.S. performed experiments with human monocytes; E.N.-V. and S.H.-S. provided bone marrow progenitor cells from STING-deficient and MAVS-deficient mice and generated MAVS-deficient *Trif*$^{-/-}$ mice; P.P. provided *Nlrp3*$^{-/-}$ and *Casp1*$^{-/-}$*Casp11*$^{-/-}$ mice; and J.G., R.A.-P., J.A.E. and D.S. directed the study, analyzed the data and wrote the manuscript.

COMPETING FINANCIAL INTERESTS

The authors declare no competing financial interests.

1. Ginhoux, F. & Jung, S. Monocytes and macrophages: developmental pathways and tissue homeostasis. *Nat. Rev. Immunol.* **14**, 392–404 (2014).
2. Blander, J.M. & Sander, L.E. Beyond pattern recognition: five immune checkpoints for scaling the microbial threat. *Nat. Rev. Immunol.* **12**, 215–225 (2012).
3. Taylor, P.R. *et al.* Macrophage receptors and immune recognition. *Annu. Rev. Immunol.* **23**, 901–944 (2005).
4. Huang, S.C. *et al.* Cell-intrinsic lysosomal lipolysis is essential for alternative activation of macrophages. *Nat. Immunol.* **15**, 846–855 (2014).
5. Jha, A.K. *et al.* Network integration of parallel metabolic and transcriptional data reveals metabolic modules that regulate macrophage polarization. *Immunity* **42**, 419–430 (2015).
6. Rodríguez-Prados, J.C. *et al.* Substrate fate in activated macrophages: a comparison between innate, classic, and alternative activation. *J. Immunol.* **185**, 605–614 (2010).
7. Tannahill, G.M. *et al.* Succinate is an inflammatory signal that induces IL-1β through HIF-1α. *Nature* **496**, 238–242 (2013).
8. O'Neill, L.A. & Pearce, E.J. Immunometabolism governs dendritic cell and macrophage function. *J. Exp. Med.* **213**, 15–23 (2016).
9. Stanley, I.A., Ribeiro, S.M., Giménez-Cassina, A., Norberg, E. & Danial, N.N. Changing appetites: the adaptive advantages of fuel choice. *Trends Cell Biol.* **24**, 118–127 (2014).
10. Weinberg, S.E., Sena, L.A. & Chandel, N.S. Mitochondria in the regulation of innate and adaptive immunity. *Immunity* **42**, 406–417 (2015).
11. Moon, J.S. *et al.* mTORC1-induced HK1-dependent glycolysis regulates NLRP3 inflammasome activation. *Cell Rep.* **12**, 102–115 (2015).
12. Michelucci, A. *et al.* Immune-responsive gene 1 protein links metabolism to immunity by catalyzing itaconic acid production. *Proc. Natl. Acad. Sci. USA* **110**, 7820–7825 (2013).
13. Naujoks, J. *et al.* IFNs modify the proteome of legionella-containing vacuoles and restrict infection via IRG1-derived itaconic acid. *PLoS Pathog.* **12**, e1005408 (2016).
14. West, A.P., Shadel, G.S. & Ghosh, S. Mitochondria in innate immune responses. *Nat. Rev. Immunol.* **11**, 389–402 (2011).
15. Enríquez, J.A. Supramolecular organization of respiratory complexes. *Annu. Rev. Physiol.* **78**, 533–561 (2016).
16. Schägger, H. & Pfeiffer, K. Supercomplexes in the respiratory chains of yeast and mammalian mitochondria. *EMBO J.* **19**, 1777–1783 (2000).
17. Kelly, B., Tannahill, G.M., Murphy, M.P. & O'Neill, L.A. Metformin inhibits the production of reactive oxygen species from NADH:ubiquinone oxidoreductase to limit induction of interleukin-1β (IL-1β) and boosts interleukin-10 (IL-10) in lipopolysaccharide (LPS)-activated macrophages. *J. Biol. Chem.* **290**, 20348–20359 (2015).
18. Jin, Z., Wei, W., Yang, M., Du, Y. & Wan, Y. Mitochondrial complex I activity suppresses inflammation and enhances bone resorption by shifting macrophage-osteoclast polarization. *Cell Metab.* **20**, 483–498 (2014).
19. Sander, L.E. *et al.* Detection of prokaryotic mRNA signifies microbial viability and promotes immunity. *Nature* **474**, 385–389 (2011).
20. Lapuente-Brun, E. *et al.* Supercomplex assembly determines electron flux in the mitochondrial electron transport chain. *Science* **340**, 1567–1570 (2013).
21. Acín-Pérez, R., Fernández-Silva, P., Peleato, M.L., Pérez-Martos, A. & Enriquez, J.A. Respiratory active mitochondrial supercomplexes. *Mol. Cell* **32**, 529–539 (2008).
22. Speijer, D. Oxygen radicals shaping evolution: why fatty acid catabolism leads to peroxisomes while neurons do without it: FADH/NADH flux ratios determining mitochondrial radical formation were crucial for the eukaryotic invention of peroxisomes and catabolic tissue differentiation. *BioEssays* **33**, 88–94 (2011).
23. Guarás, A. *et al.* The CoQH2/CoQ ratio serves as a sensor of respiratory chain efficiency. *Cell Rep.* **15**, 197–209 (2016).
24. Benard, G. *et al.* Functional dynamic compartmentalization of respiratory chain intermediate substrates: implications for the control of energy production and mitochondrial diseases. *Int. J. Biochem. Cell Biol.* **40**, 1543–1554 (2008).
25. Mráček, T., Drahota, Z. & Houštěk, J. The function and the role of the mitochondrial glycerol-3-phosphate dehydrogenase in mammalian tissues. *Biochim. Biophys. Acta* **1827**, 401–410 (2013).
26. West, A.P. *et al.* TLR signalling augments macrophage bactericidal activity through mitochondrial ROS. *Nature* **472**, 476–480 (2011).
27. Kelso, G.F. *et al.* Selective targeting of a redox-active ubiquinone to mitochondria within cells: antioxidant and antiapoptotic properties. *J. Biol. Chem.* **276**, 4588–4596 (2001).
28. Nunes, P., Demaurex, N. & Dinauer, M.C. Regulation of the NADPH oxidase and associated ion fluxes during phagocytosis. *Traffic* **14**, 1118–1131 (2013).
29. Acín-Pérez, R. *et al.* ROS-triggered phosphorylation of complex II by Fgr kinase regulates cellular adaptation to fuel use. *Cell Metab.* **19**, 1020–1033 (2014).
30. Nath, A.K. *et al.* PTPMT1 inhibition lowers glucose through succinate dehydrogenase phosphorylation. *Cell Rep.* **10**, 694–701 (2015).
31. Lowell, C.A. Src-family kinases: rheostats of immune cell signaling. *Mol. Immunol.* **41**, 631–643 (2004).
32. Alston, T.A., Mela, L. & Bright, H.J. 3-Nitropropionate, the toxic substance of Indigofera, is a suicide inactivator of succinate dehydrogenase. *Proc. Natl. Acad. Sci. USA* **74**, 3767–3771 (1977).
33. Gutman, M. Modulation of mitochondrial succinate dehydrogenase activity, mechanism and function. *Mol. Cell. Biochem.* **20**, 41–60 (1978).
34. Pan, H. & Wu, X. Hypoxia attenuates inflammatory mediators production induced by Acanthamoeba via Toll-like receptor 4 signaling in human corneal epithelial cells. *Biochem. Biophys. Res. Commun.* **420**, 685–691 (2012).
35. Vance, R.E., Isberg, R.R. & Portnoy, D.A. Patterns of pathogenesis: discrimination of pathogenic and nonpathogenic microbes by the innate immune system. *Cell Host Microbe* **6**, 10–21 (2009).
36. Kanneganti, T.D. *et al.* Bacterial RNA and small antiviral compounds activate caspase-1 through cryopyrin/Nalp3. *Nature* **440**, 233–236 (2006).
37. Sokolovska, A. *et al.* Activation of caspase-1 by the NLRP3 inflammasome regulates the NADPH oxidase NOX2 to control phagosome function. *Nat. Immunol.* **14**, 543–553 (2013).
38. Acín-Pérez, R. *et al.* Respiratory complex III is required to maintain complex I in mammalian mitochondria. *Mol. Cell* **13**, 805–815 (2004).
39. Diaz, F., Fukui, H., Garcia, S. & Moraes, C.T. Cytochrome c oxidase is required for the assembly/stability of respiratory complex I in mouse fibroblasts. *Mol. Cell. Biol.* **26**, 4872–4881 (2006).
40. Huang, Y.L. *et al.* Toll-like receptor agonists promote prolonged triglyceride storage in macrophages. *J. Biol. Chem.* **289**, 3001–3012 (2014).
41. Geng, J. *et al.* Kinases Mst1 and Mst2 positively regulate phagocytic induction of reactive oxygen species and bactericidal activity. *Nat. Immunol.* **16**, 1142–1152 (2015).

ONLINE METHODS

Mouse strains. C57BL/6J and CD1 mice were purchased from Harlan Laboratories. *Myd88*$^{-/-}$ and *Trif*$^{-/-}$ mice were originally generated by S. Akira and bred to homozygosity to generate *Trif*$^{-/-}$*Myd88*$^{-/-}$ mice by R. Medzhitov. *Ips1*$^{-/-}$ mice were originally obtained from S. Akira and backcrossed with *Trif*$^{-/-}$ mice to obtain *Ips1*$^{-/-}$*Trif*$^{-/-}$ mice. C57BL/6J-Tmem173gt/J mice (called '*GT-Sting* mice' here) and *Gp91phox*$^{-/-}$ (B6.129S6-Cybb^{tm1Din}/J) mice were obtained from the Jackson Laboratory. *Nlrp3*$^{-/-}$ and *Casp1*$^{-/-}$*Casp11*$^{-/-}$ mice have been described previously[42,43]. We used 8- to 10-week-old animals (males or females) for all experiments. Experiments were repeated three times and three to five animals per group were used to reach statistical significance. No blinding or randomization strategy was used and no animal was excluded from analysis. All experimental procedures were approved by institutional care and use committees and performed in agreement with EU directive 86/609/EEC and recommendation 2007/526/EC regarding the protection of laboratory animals and enforced under Spanish law by Royal decree 1201/2005.

Reagents. Lipopolysaccharide, polyinosinic:polycytidylic acid (polyI:C), CpG ODN were purchased from Invivogen. 3-nitropropionic acid (NPA), succinate, succinate hexahydrate, glutamate, malate disodium-salt, fumarate, dimethyl-fumarate, dimethyl succinate, dimethyl malonate, itaconic acid, thenoyltrifluoroacetone, carbonilcyanide p-triflouromethoxyphenylhydrazone, CCCP, oligomycin, rotenone, antimycin A, ubiquinone, sn-glycerol 3-phosphate, oxidized cytochrome *c*, adenosine tri-phosphate (ATP), adenosine di-phosphate (ADP), phenazine methosulfate (PMS) and digitonin were all from Sigma. Luciferin and luciferase were from Promega and Roche, respectively.

Bacteria. *Escherichia coli* K12, strain DH5α, was purchased from Invitrogen. *Salmonella enterica* serovar Thyphimurium strain SL1344 was provided by F. Norel-Bozouklian. SL1344 bacteria were grown in LB broth supplemented with 50 μg/ml streptomycin (Sigma). For phagocytosis experiments, bacteria were grown overnight in Luria-Bertani (LB) broth with shaking, diluted 1/50, and grown until log-phase (optical density of 0.8–1.2 at 600 nm) without shaking. Bacteria were washed with phosphate-buffered saline (PBS) to remove LB salts before addition to cells. For heat killing, *E. coli* were grown to log phase, washed, re-suspended in PBS and subsequently incubated at 60 °C for 60–90 min. Aliquots of heat-killed bacteria were stored at −80 °C until use. Efficient killing was confirmed by overnight plating on LB-agar plates. Total RNA was isolated from *E. coli* using the e.z.n.a. Bacterial RNA kit (Omega Bio-Tek). *E. coli*-GFP were generated by transformation of BL21pLysS bacteria (Invitrogen) with a pET-28 vector encoding the GFP-OT fusion protein[44]. *E. coli*-GFP were grown in the presence of 50 μg/ml kanamycin and 50 μg/ml chloramphenicol. To induce GFP expression, bacteria grown overnight were diluted to an optical density of 0.8 at 600 nm and incubated for 4 h in the presence of 1 mM Isopropyl β-D-1-thiogalactopyranoside (IPTG).

Antimicrobial assay. The following bacteria strains were used: *Salmonella enterica* serovar Thyphimurium strain SL1344, *Escherichia coli* K12, strain DH5α (Invitrogen). Bacteria were cultured at 37 °C overnight in lysogeny broth (LB). Bacterial concentrations were measured by spectrophotometry at 600 nm and diluted to a concentration of 10^5 CFU/ml in PBS supplemented with 0.1, 1, or 10 mM of itaconate, fumarate, succinate, dimethyl fumarate or dimethyl succinate and incubate for 6 h at room temperature. Serial dilutions were then plated on LB-agar plates supplemented with 50 mM streptomycin (for SL1344) and grown overnight at 37 °C. Photographs were taken using a scanner. Alternatively, bacteria were diluted to a final optical density of 0.2 at 600 nm in LB supplemented as above and growth was measured every 2 h by spectrophotometry. For CFU enumeration, bacteria were diluted to a concentration of 10^5 CFU/ml in PBS supplemented as above, incubated for 6h and serial dilution were plated on LB-agar plates. The number of colonies formed after overnight incubation was counted. For analysis of cell death, bacteria were stained with 5 μM propidium iodide (to stain nucleic acids) and 5 μM of cell SYTO red dye (Life Technology) for 15 min, and analyzed by flow cytometry.

Macrophage preparation and treatment with *Escherichia coli*. Murine bone marrow-derived macrophages (BMDMs) were generated from C57BL/6J, CD1, *Fgr*$^{-/-}$, *Myd88*$^{-/-}$, *Trif*$^{-/-}$, *Trif*$^{-/-}$*Myd88*$^{-/-}$, *GT-sting*, *Ips-1*$^{-/-}$, *Trif*$^{-/-}$*Ips-1*$^{-/-}$, *Gp91phox*$^{-/-}$, *Nlrp3*$^{-/-}$ and *Casp1*$^{-/-}$*Casp11*$^{-/-}$ mice, as described previously[45], in RPMI 1640 supplemented with M-CSF (30% mycoplasma-free L929 cell supernatant, NCBI Biosample accession # SAMN00155972) and 10% FBS, plus 100 μg/ml penicillin, 100 μg/ml streptomycin, 10 mM HEPES, 1 nM sodium pyruvate and 50 mM 2-mercaptoethanol (all from Gibco). Peritoneal macrophages were harvested 72 h after intraperitoneal injection of 1 ml 3% thioglycollate medium (BD Bioscience). Human CD14$^+$CD16$^-$ monocytes were obtained from buffy coats using the EasySep Human Monocyte Enrichment Immunomagnetic kit (Stemcell Technologies). For treatment with viable *E. coli* and heat-killed *E. coli*, cells were plated at 1.5×10^6 cells/well in non-treated six-well cell culture plates (BD Bioscience) and left to adhere for at least 4 h. BMDMs were challenged with *E. coli* or heat-killed *E. coli* at a multiplicity of infection of 20 and plates were spun at 400*g* for 5 min. Cells were incubated for 1.5 h unless otherwise indicated. For longer time points, 50 μg/ml gentamicin sulfate (Gibco) was added after 1 h of incubation. Alternatively, cells were stimulated with soluble ligands as follows: 200 ng/ml LPS, 20 μg/ml poly(I:C) or 5 μg/ml CpG ODN. For treatment with metabolic inhibitors, 0.5 mM 3-nitropropionic acid (NPA), 0.5 mM dimethyl-fumarate or 0.5 mM thenoyltrifluoroacetone was added to the cells 30 min to 1 h before challenge. For stimulation of human cells, CD14$^+$CD16$^-$ monocytes were isolated from buffy coats. Cells were plated at 1×10^6 cells/ml in non-treated 12-well cell culture plates (BD Bioscience) and left to adhere for at least 2 h. Cells were challenged with *E. coli* and heat-killed *E. coli* at a multiplicity of infection of 10 and plates were spin at 2,500 r.p.m. for 1 min. Cells were incubated for 1.5 h. Alternatively, cells were stimulated with soluble ligands as follows: 250 ng/ml Ultrapure EK-LPS and 10 μg/ml LMW poly(I:C). For supernatant collection, cells were plated at 3×10^5 cells/well in a 48-well plate and stimulated as described above.

Oxygen consumption rate and glycolytic flux evaluation. Real-time oxygen-consumption rate (OCR) and extracellular acidification rate (ECAR) in BMDMs were determined with an XF-96 Extracellular Flux Analyzer (Seahorse Bioscience); 1×10^5 cells/well in five to six wells were used for each condition. The assay was performed in DMEM supplemented with 2 mM glutamine, 100 μg/ml penicillin, 100 μg/ml streptomycin, phenol red and 25 mM glucose + 1mM pyruvate or 5 mM L-carnitine + 50 μM palmitoyl-CoA. The pH was adjusted to 7.4 with KOH (seahorse medium). Three consecutive measurements were performed under basal conditions and after the sequential addition of the following ETC inhibitors: 1 μM oligomycin, 1 μM CCCP, 1 μM rotenone and 1 μM antimycin. Basal respiration rate (BRR) was defined as OCR in the absence of any inhibitor. Maximal respiration rate (MRR) was defined as the OCR after addition of oligomycin and carbonilcyanide p-triflouromethoxyphenylhydrazone. Spare respiration capacity (SRC) was defined as the difference between MRR and BRR. ECAR was measured in the absence of drug. Where indicated, cells were treated with 0.5 mM NPA for 30 min before stimulation. For lactate production measurement, cells (1×10^5/well) were plated on a 96-well plate and stimulated as indicated. Cells were washed 5 times with PBS and 100 μl of seahorse medium was added. Plates were incubated at 37 °C without CO_2 for 1h and supernatants were harvested. 25 μl of supernatant diluted five times was used to measure lactate production using a Lactate assay kit II (Sigma) according to manufacturer's instructions.

Isolation of mitochondria and BMDMs permeabilization. Mitochondria were isolated as described[46] with some modifications. 1×10^8 BMDMs were collected in PBS supplemented with 5 mM EDTA and washed with PBS. Cell pellets were frozen at −80 °C to increase cell breakage and were homogenized in a tightly fitting glass-teflon homogenizer with 10 volumes of buffer A (83 mM sucrose, 10 mM MOPS, pH 7.2). An equal volume of buffer B (250 mM sucrose, 30 mM MOPS, pH 7.2) was added and nuclei and unbroken cells were removed by centrifugation at 1,000*g* for 5 min. Supernatants were collected and centrifuged at 12,000*g* for 2 min. Mitochondria pellets were washed once with buffer C (320 mM sucrose, EDTA 1 mM, 10 mM Tris-HCl, pH 7.4). Mitochondria were then suspended in an appropriate volume of PBS for storage at −80 °C.

Blue-native PAGE (BN-PAGE), two-dimensional gel analysis, and in gel activity assay. For BMDM permeabilization, 3×10^6 macrophages were resuspended in 100 μl of PBS. 32.5 μl of digitonin (8 mg/ml) was added and

doi:10.1038/ni.3509

cells incubated on ice for 10 min. Cold PBS (1 ml) was added and cells were centrifuged for 5 min at 10,000*g*. The pellet was suspended in 100 µl of AA buffer (500 mM 6-aminohexanoic acid, 50 mM immidazole, 1 mM EDTA, pH 7) and 10 µl of a 10% digitonin solution was added. Cells were centrifuged for 30 min at 18,000*g*. Supernatant was harvested and 10 µl of sample buffer (5% Blue G-250, 5% glycerol in AA Buffer) was added. Samples were stored at −80 °C until use. BN-PAGE was performed as described[47]. For two-dimensional gel analysis, 50–75 µg of mitochondria were digitonin-permeabilized with 4 µg digitonin per µg of protein and loaded on a BN polyacrylamide gel. Each individual band on the BN-PAGE was cut out and incubated for 1 h in buffer containing 1% SDS and 1% 2-mercaptoethanol. The buffer was replaced with a 1% SDS solution and incubation was continued for 30 min. BN-PAGE bands were loaded on an SDS polyacrylamide gel composed of a 10% acrylamide/Bis-acrylamide (AB) stacking gel and a 16% AB resolving gel. Electrophoresis was performed overnight at 12–15 mA, and proteins were transferred to a PVDF membrane using a Trans-Blot Semi-Dry Transfer Cell (Bio-Rad). For in-gel OXPHOS complex activity assays, CI was revealed by incubating the BN gel for 1–3 h in 0.1M Tris-HCl, pH 7.5, containing 1 mg/ml NBT and 0.14 mM NADH. For densitometry analysis, the ImageJ64 software was used. Band limits were determined using low-exposure images to efficiently distinguish the different bands. Background correction was applied for each analysis.

Oxidative-phosphorylation function and enzyme activities. CII activity was measured spectrophotometrically from the reduction of 2,6-diclorophenol-indophenol (DCPIP) by tracking the absorbance at 600 nm over 3 min as described[48] with some modifications. 3×10^6 cells were suspended in 100 µl PBS on ice. Protein concentration was determined and the volume was adjusted to the lowest concentrated sample. Sample (20 µl) was suspended in 950 µl of buffer C1/C2 (25 mM potassium phosphate (K_2HPO_4) pH = 7.2, 5 mM $MgCl_2$, 3 mM KCN, 2.5 mg/ml BSA) supplemented with 100 mM succinate and 0.1% Triton X-100, and incubated 10 min at room temperature in a cuvette. After addition of 6 µl 5 mM DCPIP, 2 µl 1 mg/ml of antimycin A and 2 µl 1 mM rotenone, samples were incubated for 2 min. Then, 6 µl of 10 mM UQ_1 was added and absorbance was measured. CII activity was extrapolated using the following formula: [CII activity = ((rate/min)/19.1) / sample volume × 1000 × dilution factor], where 19.1 is the molar extinction coefficient at 30 °C ($mM^{-1}cm^{-1}$). For CII + CIII, UQ_1 was replaced with 1 mM oxidized cytochrome *c* (Sigma). For SDH activity, UQ_1 was replaced with phenazine methosulfate (PMS). For mitochondrial glycerol 3-phosphate dehydrogenase (mG3PDH) activity, succinate was replaced with 1 M glycerol-3-phosphate. For OXPHOS enzymatic activities in isolated mitochondria, individual and combined complex activities of isolated mitochondria were measured spectrophotometrically as described[48]. The CII-, CII-plus-CIII- and mG3PDH-specific activities corresponding to 100% activity measured in permeabilized untreated BMDMs are 0.0165 ± 0.005 IU/mg protein (N = 25), 0.020 ± 0.008 IU/mg protein (N = 4) and 0.0180 ± 0.006 IU/mg protein (N = 18), respectively.

ATP synthesis assay. ATP synthesis was measured in permeabilized cells by kinetic luminescence assay[49]. Cells (2×10^6) were suspended in 160 µl of buffer A (150 mM KCl, 25 mM Tris-HCl, 2 mM EDTA, 0.1% BSA FA, 10 mM K-phosphate, 0.1 mM $MgCl_2$, pH 7.4) at room temperature and 50 µg/ml digitonin was added. Samples were mixed gently for 1 min, and the reaction was stopped by addition of 1ml of buffer A. Cells were centrifuged at 3,000 r.p.m. for 2 min at room temperature, and pellets were suspended in 160 µl of buffer A and dispensed into the wells of a 96-well luminescence reading plate (Costar). Substrate cocktail (50 µl) and 20 µl of buffer B (0.5 M Tris-acetate, pH 7.75, 0.8 mM luciferine, 20 µg/ml luciferase) were added, and luminescence was measured over 1 min. Substrate cocktails were composed of 6 mM diadenosin pentaphosphate and 6 mM ADP supplemented with 1 M glutamate + 1 M malate for determination of CI activity or with 1 M succinate for CII activity. ATP production rate is presented as 'nmol of ATP/min/mg of protein.' All measurements were performed in triplicate.

Phagocytosis assay. Macrophages (3×10^5) were seeded in triplicate on an untreated 24-well plate (BD Biosciences). Cells were challenged with 6×10^6 3-µm Fluoresbrite microspheres (Polysciences) or 3×10^6 *E. coli*–GFP and centrifuged for 5 min at 400*g*. After 20 min incubation, cells were washed with PBS, harvested in PBS containing 5 mM EDTA, and analyzed by flow cytometry.

Cytokine enzyme-linked immunosorbent assay (ELISA). IL-1β, IL-10 and TNF-α ELISA kits were from BD Biosciences. Capture/detection antibodies for IL-6 were from BD Biosciences. Supernatants from BMDMs were collected at 24 h after stimulation. ELISA kits are used according to the manufacturer's instructions. Detection antibodies were biotinylated and labeled with streptavidin-conjugated horseradish peroxidase (HRP, from invitrogen) and visualized by incubation with 5,5′-tetramethylbenzidine solution (TMB, KPL). Color development was stopped with TMB-stop solution (KPL). Recombinant cytokines served as standards and were purchased from Peprotech. Absorbance at 450 nm was measured on a microplate reader (Benchmark Plus, Bio-Rad).

***In vitro* and *in vivo* infection and bactericidal activity experiments.** For *in vitro* experiments, BMDMs were plated at 2×10^5 cells/well in triplicate on a 24-well plate in an antibiotic-free complete medium. BMDMs were infected with DH5α or SL1344 at a multiplicity of infection of 5 and centrifuged for 5 min at 400*g*. After 30 min incubation, cells were washed and complete medium supplemented with 50 µg/ml gentamycin was added. At the indicated time point after infection, cells were washed with PBS and 1 ml of PBS containing 1% Triton X-100 was added. Plates were incubated at room temperature for 15 min and serial dilutions (1/10, 1/100, 1/1,000) were plated on an LB-agar plate, which in the case of SL1344 contained 50 µg/ml streptomycin. Plates were incubated at 37 °C and bacterial colonies were counted. When needed, cells were pretreated with 3-nitropropionic acid (NPA) 30 min before infection; the inhibitor concentration was maintained throughout the experiment. For *in vivo* experiments, mice were injected intraperitoneally (i.p.) with 50 mg/kg NPA 1 h before infection. Injection of inhibitor was repeated every second day over the course of the experiment. For *E. coli* infection, mice were injected i.p. with 1×10^8 DH5α and sacrificed at 72 h after infection. Spleens were harvested and homogenized in 5 ml PBS, and serial dilutions were plated on LB-agar plates for colony counting. For peritoneal cell analysis, mice were injected i.p. with 1×10^8 DH5α. 12 h later, mice were sacrificed and peritoneal cells were collected in 8 ml ice-cold PBS. Each experiment included four to five mice per group and was repeated three times with similar results. No specific blinding or randomization strategy was used. No animal was excluded from analysis.

Immunoblot analysis. For protein-extract collection, 1.5×10^6 cells were lysed in RIPA buffer supplemented with protease and phosphatase inhibitor cocktails (both from Roche) and subsequently sonicated and boiled for 5 min at 95 °C. Protein lysates were separated on 4–12% SDS-gradient gels (Bio-Rad). Proteins were transferred to PVDF membranes (Millipore). Membranes were blocked with 5% bovine serum albumin (BSA) in PBS and probed with antibodies sourced as follows: anti-CORE1 (1/5,000 dilution, ab110252, Abcam), anti-NDUSF3 (1/5,000 dilution, ab110246, Abcam), anti-ATP-B (1/2,000 dilution, ab43176, Abcam), and anti-NDUFA9 (1/5,000 dilution, ab14713, Abcam), anti-FpSDH (1/5,000 dilution, #459200, Invitrogen), anti-Cox5b (1/5,000 dilution, #11418-2-AP, Proteintech Europe), anti-vinculin (1/10,000 dilution, V9131, Sigma); and anti-β-actin (1/10,000 dilution, sc-91178, Santa Cruz Biotechnology).

Real-time PCR. Total RNA was isolated from macrophages using the RNeasy kit (Qiagen). Contaminating genomic DNA was removed by DNase digestion (Qiagen). Reverse transcription was performed using the High Capacity cDNA Reverse Transcriptase kit (Applied Biosystem), and cDNA was used for subsequent real-time PCR reactions. Quantitative real-time PCR was conducted on an 7900 HT Fast Real-Time PCR system (Lifetechnologies) using SYBR green qPCR Master Mix (Promega) with the following primer pairs: *Actb*, FW 5′-GAAGTCCCTCACCCTCCCAA-3′, RV 5′-GGCATGGACGCGACCA-3′; *Il1b*, FW 5′-AAAGACGGCACACCCACCCTGC-3′, RV 5′-TGTCCTGAC CACTGTTGTTTCC CAG-3′; *Ifnb*, FW 5′-TCAGAATGAGTGGTGGTTGC; RV 3′-GACCTTTCAAAT GCAGTAGATTCA; *Tnf* FW 5′-CCCCAAAGGG ATGAGAAGTT, RV 3′-TGGGC TACAGGCTTGTCACT.

Flow cytometry. Cells were stained with the appropriate antibody cocktails in ice-cold PBS supplemented with 2 mM EDTA, 1% FCS and 0.2% sodium azide for 15 min. Samples were processed by FACS canto-3L or LSR-Fortessa analyzers (BD Biosciences) and data were analyzed with FlowJo software. Antibodies used were anti-CD11b-APC-Cy7 (1/200 dilution, M1/70, #557657, BD Bioscience), anti-Ly6G-PE-Cy7 (1/200 dilution, 1A8, #560601, BD Bioscience), anti-F4/80-PE (1/400 dilution, BM8, eBioscience).

Gene microarray analysis. Affymetrix Microarray data from BMDMs were previously deposited with the NCBI Gene Expression Omnibus under accession code GSE27960 (ref. 19). Data for genes encoding ETC subunits were analyzed and plotted using Genesis software from Graz university of Technology (http://genome.tugraz.at/).

Statistical analysis. Statistical differences were analyzed with Prism software (version 5, GraphPad Software Inc.). Comparisons of two groups were calculated with two-tailed unpaired Student's *t*-test and, where indicated, with paired Student's *t*-test or one-way ANOVA followed by Tukey post-test analysis. For survival experiments, statistical significance was tested by a log-rank (Mantel-Cox) test. A *P* value of less than 0.05 was considered statistically significant. No randomization or exclusion of data points was used. Pilot *in vivo* studies were used for estimation of the sample size required to ensure adequate power.

42. Kuida, K. *et al.* Altered cytokine export and apoptosis in mice deficient in interleukin-1 beta converting enzyme. *Science* **267**, 2000–2003 (1995).
43. Martinon, F., Pétrilli, V., Mayor, A., Tardivel, A. & Tschopp, J. Gout-associated uric acid crystals activate the NALP3 inflammasome. *Nature* **440**, 237–241 (2006).
44. Drutman, S.B. & Trombetta, E.S. Dendritic cells continue to capture and present antigens after maturation in vivo. *J. Immunol.* **185**, 2140–2146 (2010).
45. Blander, J.M. & Medzhitov, R. Regulation of phagosome maturation by signals from toll-like receptors. *Science* **304**, 1014–1018 (2004).
46. Schägger, H. & von Jagow, G. Blue native electrophoresis for isolation of membrane protein complexes in enzymatically active form. *Anal. Biochem.* **199**, 223–231 (1991).
47. Wittig, I., Braun, H.P. & Schägger, H. Blue native PAGE. *Nat. Protoc.* **1**, 418–428 (2006).
48. Birch-Machin, M.A. & Turnbull, D.M. Assaying mitochondrial respiratory complex activity in mitochondria isolated from human cells and tissues. *Methods Cell Biol.* **65**, 97–117 (2001).
49. Vives-Bauza, C., Yang, L. & Manfredi, G. Assay of mitochondrial ATP synthesis in animal cells and tissues. *Methods Cell Biol.* **80**, 155–171 (2007).

doi:10.1038/ni.3509